CHARLES UNIVERSITY IN PRAGUE

FACULTY OF SCIENCE

DEPARTMENT OF GENETICS AND MICROBIOLOGY

Mgr. Anna Herrmannová

Complex structural and functional analysis of individual subunits of yeast translation initiation factor 3.

Komplexní strukturní a funkční analýza jednotlivých podjednotek kvasinkového translačního iniciačního faktoru 3.

Ph.D. Thesis

Supervisor: Leoš Valášek, Ph.D.

INSTITUTE OF MICROBIOLOGY AS CR

Prague, 2014

Declaration:

With this, I declare that I have written this work on my own, appropriately acknowledged citations, and used no other than the listed resources and aids.

Prague ..... **.....**

Mgr. Anna Herrmannová

ACKNOWLEDGEMENTS

I would like to thank to my supervisor Leoš Valášek, Ph.D., for his patient guidance and support throughout all the years of my studies and for the opportunity to be a part of a great collective of the Laboratory of Regulation of Gene Expression, Institute of Microbiology AS CR. I would also like to thank to all the current and former members of our lab for their help, advices and long discussions which helped me greatly during my studies.

Many thanks belongs also to the members of Libor Krásný, Ph.D., Doc. David Staněk, Ph.D. and Doc. Petr Svoboda, Ph.D. laboratories for their constructive criticism, great questions and suggestions, which helped me to gain perspective and to look at my projects from different angles.

Special thanks I dedicate to my family for their patience and support, emotional and financial, during my long studies and to my boyfriend Michal, who always encouraged and motivated me when I needed it.

This work was supported by the Wellcome Trust (grant number 076456/Z/05/Z and 090812/B/09/Z), National Institutes of Health research grant R01 TW007271 funded by Fogarty International Center, Howard Hughes Medical Institute, Fellowship of Jan E. Purkyně from Academy of Sciences of the Czech Republic, Institutional Research Concept AV0Z50200510 and Czech Science Foundation 305/10/0335.

LIST OF CONTENTS

ABBREVIATIONS

CTD	C-terminal domain
eIF	Eukaryotic initiation factor
HLD	HCR1-like domain
Met-tRNAi	Methionyl initiator tRNA
MFC	Multifactor complex
mRNA	Messenger RNA
NMR	Nuclear magnetic resonance
NTD	N-terminal domain
PIC	Pre-initiation complex
REI	Reinitiation
RPS	Ribosomal protein (small subunit)
RRM	RNA recognition motif
rRNA	Ribosomal RNA
TC	Ternary complex
uORF	Upstream open reading frame
UTR	Untranslated region
WT	Wild type

ABSTRACT

Translation initiation in eukaryotes is a complex process promoted by numerous proteins or protein complexes called eukaryotic initiation factors (eIFs). The eukaryotic initiation factor 3 (eIF3) is a multisubunit complex that has been implicated in several steps of the translation initiation pathway. In yeast *Saccharomyces cerevisiae*, eIF3 is composed of five essential subunits (a/TIF32, b/PRT1, c/NIP1, g/TIF35, i/TIF34) and one nonessential subunit (j/HCR1). It is our long-term goal to understand how eIF3 promotes different stages of translation initiation and which subunits or their domains play a critical role in this process as well as to map the binding sites of eIF3 on 40S ribosomal subunit and to create a structural model of eIF3 complex.

Here I present two structural studies showing interactions between the RNA recognition motif of eIF3b and a short peptide of eIF3j subunits of human eIF3 solved by NMR spectroscopy, and a crystal structure of the C-terminal fragment of yeast b/PRT1 in complex with the full length i/TIF34 subunit at 2.2 Å resolution. In the former study, me and my colleagues showed that the critical determinants mediating this eIF3b–eIF3j interaction are evolutionary conserved, since their mutations in yeast proteins reduced cellular growth rate, eliminated j/HCR1 association with b/PRT1 *in vitro* and *in vivo*, affected 40S-binding of the entire eIF3 complex, and finally produced a leaky scanning defect (skipping the AUG start codon) indicating impairment of the AUG selection process. In the latter study, I revealed that the b/PRT1-i/TIF34 interaction is mediated by two major contacts. Site-directed mutagenesis of these contacts eliminated association of i/TIF34 and g/TIF35 with the rest of eIF3 *in vivo*, affected 40S-binding of the remaining trimeric subcomplex of eIF3 and its binding partner eIF5, and, as a result, led to accumulation of aberrant preinitiation complexes containing only eIF1 and eIF2 causing a severe leaky scanning defect.

In other studies, we identified novel contacts between the a/TIF32 C-terminal domain (a/TIF32-CTD) and yeast small ribosomal proteins RPS2 and RPS3, and between j/HCR1 and RPS2 and RPS23, which place this mutually interacting eIF3 subunits in the vicinity of the mRNA entry channel, where they can contribute to regulation of the start codon recognition, and at least in case of the a/TIF32-CTD, also in mRNA recruitment, as we demonstrated. We also identified RPS3 and RPS20 as the

binding partners of g/TIF35, which places the g/TIF35-i/TIF34 subcomplex on the solvent side of the 40S subunit right above the mRNA entry channel, where it can contribute to the proper assembly of the 48S pre-initiation complex and influence subsequent scanning for AUG, as we showed. We also mapped the binding sites of two factors critically involved in AUG recognition within the c/NIP1 N-terminal domain, namely eIF1 and eIF5, and characterized how these contacts promote the ternary complex recruitment and modulate start codon selection.

Finally, in our functional genetic studies, we showed that a/TIF32 N-terminal domain and g/TIF35 play important roles in the process of gene-specific regulation called reinitiation, although by a different molecular mechanism.

ABSTRAKT

Eukaryotická iniciace translace je komplexní proces, který je ovlivněn mnoha proteiny a proteinovými komplexy, které nazýváme translační iniciační faktory. Eukaryotický translační iniciační faktor 3 (eIF3) je komplexem více podjednotek a hraje roli hned v několika fázích iniciace translace. Iniciační faktor eIF3 se v kvasince *Saccharomyces cerevisiae* skládá z pěti esenciálních podjednotek (a/TIF32, b/PRT1, c/NIP1, g/TIF35, i/TIF34) a jedné neesenciální podjednotky (j/HCR1). Naším dlouhodobým cílem je porozumět tomu, jak eIF3 působí v různých fázích iniciace translace, které podjednotky nebo jejich domény hrají při těchto proceses důležitou roli, a také zmapování jeho vazebných míst na malé ribosomální podjednotce a vytvoření strukturního modelu celého komplexu.

V této práci prezentuji výsledky dvou strukturních studií. První popisuje interakci objevenou pomocí NMR spektroskopie mezi RNA-rozpoznávajícím motivem lidského faktoru eIF3b a podjednotkou eIF3j. Druhá studie představuje krystalickou strukturu interakce mezi C-koncovým fragmentem kvasinkové podjednotky b/PRT1 a podjednotkou i/TIF34 v rozlišení 2,2 A. V první práci jsme ukázali, že kritické determinanty této interakce jsou konzervovány také v kvasinkách, a že jejich mutace způsobuje zpomalení růstu, eliminuje asociaci j/HCR1 s b/PRT1 *in vitro* a in *vivo*, má vliv na vazbu eIF3 na 40S podjednotku a vede k defektu zvanému „leaky scanning“, který indikuje narušení procesu výběru AUG kodonu. V druhé studii jsme odhalili, že interakce mezi b/PRT1 a i/TIF34 závisí na dvou hlavních kontaktech. Mutace těchto kontaktů způsobují eliminaci vazby i/TIF34 a g/TIF35 podjednotek na multifaktoriální komplex, snižují vazbu zbývajících podjednotek eIF3 a také iniciačního faktoru 5 na ribozóm a vedou k akumulaci aberantních preiniciačních komplexů, které způsobují „leaky scanning“.

V dalších studiích jsme identifikovali nové kontakty mezi C-koncovou doménou a/TIF32 a ribozomálními proteiny malé podjednotky RPS2 a RPS3, a mezi j/HCR1 a RPS2 a RPS23. Tyto kontakty vzájemně interagujících podjednotek eIF3 naznačují, že se tyto podjednotky váží na ribozóm v blízkosti vstupního kanálu pro mRNA, kde mohou regulovat výběr start kodonu, a v případě a/TIF32-CTD také usnadňovat vazbu mRNA na ribozóm. Dále jsme také zjistili, že se podjednotka g/TIF35 váže na

ribozomální proteiny RPS3 a RPS20, což naznačuje že subkomplex g/TIF35-i/TIF34 se nachází nad vstupním kanálem pro mRNA, kde může ovlivňovat skenování a také kriticky přispívat ke správnému sestavení 48S preiniciačního komplexu. Dále jsme také popsali, jak N-koncová doména c/NIP1 ovlivňuje působení faktorů eIF1 a eIF5 během vazby ternárního komplexu a během výběru iniciačního kodonu a zmapovali jsme vazebná místa těchto faktorů na podjednotce c/NIP1-NTD.

V dalších studiích jsme poté ukázali, že N-koncová doména a/TIF32 a podjednotka g/TIF35 hrají důležitou roli v procesu genově specifické regulace zvané reiniciace, ačkoli molekulární mechanismus působení obou podjednotek se liší.

1. INTRODUCTION

Gene expression is a complex process by which the information encoded in DNA of individual genes is first transcribed into a sequence of nucleotides of a messenger RNA and subsequently translated into a string of amino acids producing a new protein molecule. This principal – the flow of genetic information from DNA to RNA to protein is called the central dogma of molecular biology.

Gene expression is regulated at multiple levels, including the translation of mRNAs into proteins. Compared to transcriptional regulation, translational control of existing mRNA's allows for more rapid changes in concentration of the encoded proteins, which gives cells flexibility to adapt to a variable environment, external signals, damage to the cell etc.

Translation takes place in cytoplasm where the mRNA associates first with small and then with large ribosomal subunits. It can be divided into four steps: initiation, elongation, termination and ribosome recycling. Most regulation is exerted during the initiation phase making it the most critical step of the translation process. Thus it is not surprising that translation initiation has been studied extensively in the past two decades (reviewed in Hinnebusch and Lorsch, 2012; Valásek, 2012)

Translation initiation in eukaryotes requires the participation of numerous proteins and protein complexes that are called eukaryotic initiation factors (eIFs). At least a dozen eIFs are required to orchestrate assembly of elongation-competent 80S ribosomes, which is in sharp contrast to bacteria, where only three factors are required.

1.1 Translation initiation

Translation initiation in eukaryotes is a complex series of reactions leading to the formation of an 80S ribosomal complex containing initiator methionyl-tRNA (Met-tRNAi) base paired to the AUG start codon in the ribosomal P-site. The main initiation pathway in eukaryotes is cap-dependent. The 40S ribosome binds near the 7-methyl

guanosine cap at the 5‘ end of mRNA and then scans the mRNA’s leader in the 5‘ to 3‘ direction until it encounters the AUG start codon (Kozak, 1978).

The conventional view of the translation initiation pathway is presented in Figure 1. It starts with the recruitment of the ternary complex (TC) consisting of Met-tRNAi and GTP-bound form of eIF2 (Erickson and Hannig, 1996; Kapp and Lorsch, 2004) to the 40S ribosomal subunit to form the 43S preinitiation complex (PIC). The binding of TC to the 40S subunit is promoted by eIFs 1, 1A, 5 and the eIF3 complex (reviewed in Hinnebusch et al., 2007; Lorsch and Dever, 2010; Pestova et al., 2007). With the exception of eIF1A, all of these factors are components of the so called Multifactor complex (MFC), which occurs in yeast (Asano et al., 2000), plants (Dennis et al., 2009) and also mammals (Sokabe et al., 2012). In depth studies in yeast showed that it enhances the formation and stability of the 43S PICs (Asano et al., 2000; Singh et al., 2004; Valášek et al., 2002). The 43S PIC then binds to the capped 5‘ end of mRNA, with the help of eIF4F, eIF4B, PABP, and eIF3 (Mitchell et al., 2010), thus forming 48S PIC. For the sake of completeness, the eIF4F complex is comprised of the cap-binding protein eIF4E, scaffolding protein eIF4G, and the RNA helicase eIF4A.

Once bound near the cap, the resulting 48S PIC scans the mRNA’s leader until the AUG start codon in optimal context is recognized (Kozak, 1986). Scanning is accompanied by unwinding of secondary structures in an ATP-dependent reaction stimulated by helicases eIF4A (Rogers Jr. et al., 1999), DHX29 (Pisareva et al., 2008) and DED1 (Iost et al., 1999). The mRNA slides through a tunnel, formed by the ribosomal proteins, eIF1A and eIF1, which ensures scanning processivity by keeping the mRNA unstructured and properly oriented for the inspection of the nucleotide sequence in the P site by Met-tRNAi.

In mammalian reconstituted systems, eIFs 1, 1A, and 3 sufficiently promoted location of the AUG start codon on mRNAs with unstructured 5’ UTRs and insertion of even a weak secondary structure in the leader imposes a need for the eIF4F complex (Pestova and Kolupaeva, 2002). Yeast genetic data then indicate that in addition to these, eIF5 is also required *in vivo* (Cuchalová et al., 2010; Nielsen et al., 2004; Yamamoto et al., 2005).

During scanning, 40S ribosome is in the open/scanning conducive conformation, which is believed to be induced by 40S-association of eIF1 and eIF1A (Passmore et al., 2007). In the open state, helix h16 of 18S rRNA and small ribosomal protein 3 (RPS3) are forming a connection between the head and the body of the 40S (Passmore et al., 2007).

The anticodon of Met-tRNAi is not fully engaged in the ribosomal P-site in order to prevent premature engagement with putative start codons, hence it occurs in the so called P^{out} state (Saini et al., 2010; Yu et al., 2009). eIF5 stimulates partial GTP hydrolysis by eIF2 to GDP and Pi, but the Pi is not released from the scanning complex until the anticodon of Met-tRNAi base-pairs with the AUG start codon, which induces dissociation or displacement of eIF1 (Algire et al., 2005; Cheung et al., 2007; Karásková et al., 2012). The Met-tRNAi is then fully accommodated in the P-site, in the so called P^{in} state, and the 48S PIC switches its conformation to the closed/scanning arrested form (Cheung et al., 2007). This conformation is characterized by the formation of the helix18–helix34-RPS3 connection designated as the latch on the mRNA entry channel (Passmore et al., 2007).

Recently, this model was challenged by two structural studies (Lomakin and Steitz, 2013; Weisser et al., 2013). They proposed that the 40S ribosome adopts the open conformation only during mRNA loading and that the closure of the latch is a necessary prerequisite for the actual onset of scanning rather than for the arrest of scanning upon AUG recognition. Hence, in this new model the base-pairing of the anticodon with the AUG start codon is not accompanied by any large conformational change of the ribosome, yet it also triggers dissociation or displacement of eIF1.

Subsequently, after AUG start codon was recognized, GTP-bound eIF5B stimulates joining of the 60S ribosomal subunit (Pestova et al., 2000). Upon subunit joining, most eIFs are ejected with exception of eIF1A (Unbehaun et al., 2004), and possibly also eIF3 (Munzarová et al., 2011; Szamecz et al., 2008) and eIF4F (Pöyry et al., 2004). Finally, GTP-hydrolysis on eIF5B stimulated by the GTP-ase activating center of the 60S subunit triggers the release of eIF1A and eIF5B itself producing an elongation-competent 80S ribosome. For a new round of initiation, the ejected eIF2-GDP must be recycled to eIF2-GTP by the guanine nucleotide exchange factor eIF2B (Pavitt et al., 1998).

Experiments with the yeast *Saccharomyces cerevisiae* revealed that translation initiation in this lower eukaryote strongly resembles cap-dependent initiation in mammals. This is perhaps most convincingly demonstrated by finding that some mammalian initiation factors can substitute for yeast factors *in vivo* (Schwelberger et al., 1993). Numerous key studies that were conducted with this model organism since early 80s have contributed by a great deal to our understanding of this fundamental process.

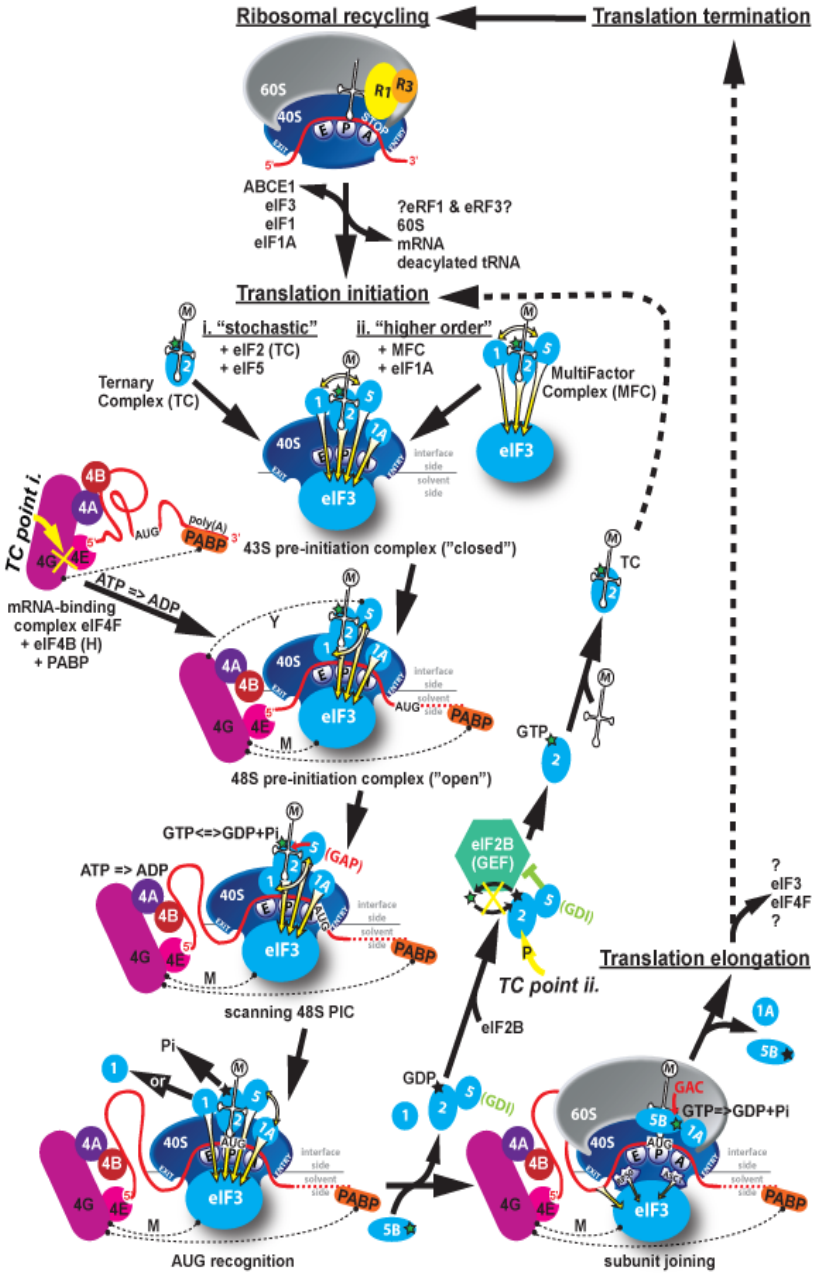

Figure 1. Schematic of the canonical translation pathway in eukaryotes with the ribosomal recycling and initiation phases shown in detail (adapted from Valášek, 2012). This figure combines findings from both yeast and mammals and indicates potential differences. The terminating 80S ribosome is split into individual subunits with help of ABCE1/RLI1 and eIFs 1, 1A and 3. The former eIFs either remain bound to the 40S subunit or dissociate prior to the initiation phase. In the former case, the ternary complex (TC) and eIF5 join the existing 40S-eIF1-eIF1A-eIF3 post-recycling complex in a "stochastic" way (i) to form the 43S pre-initiation complex (PIC). In the latter case, the 43S PIC is formed in the "higher order" manner via simultaneous binding of all components of the Multifactor complex (eIFs 1, 3, 5 and the TC) and eIF1A. mRNA is delivered to the 43S PIC in a complex with eIF4F, eIF4B (and/or eIF4H in mammals) and PABP in an ATP-dependent reaction creating a "landing pad" close to the mRNA's cap structure that is bound by eIF4E (the interaction between eIF4G and PABP is shown as a dotted line for simplicity). As a result, the 48S PIC is formed and scanning for AUG commences. The actual attachment of mRNA to the ribosome is believed to be

mediated via the eIF4G – eIF3 interaction in mammals (dotted line "M") that seems to be bridged via eIF5 in yeast (dotted line "Y"; this line is not shown in all cartoons for simplicity). During scanning, all secondary structures that could impede the movement of the PIC in the 5' to 3' direction are melted with help of helicase eIF4A and its co-factors eIF4B or eIF4H at the expense of ATP. Also, eIF5 stimulates GTP hydrolysis on eIF2 (GAP activity), however, the resulting Pi is not released until the AUG is located. Upon AUG recognition, eIF1 as a gatekeeper is either ejected from the ribosome or could move back to eIF3 to allow Pi release. eIF5B then promotes subunit joining that kicks out all interface-side-bound eIFs with the exception of eIF1A, and the solvent-side-bound eIF3 and eIF4F (interactions between eIF3 and two "solvent-side" ribosomal proteins RPS0 and RACK1/ASC1, are indicated). GTP hydrolysis on eIF5B stimulated by the GTPase activating center (GAC) of the large subunit triggers coupled release of eIF5B and eIF1A rendering the resulting 80 initiation complex ready to elongate. It is believed that eIF3 and eIF4F can stay 80S-bound for at least a few elongation cycles thanks to their location on the back of the 40S subunit. eIF2•GDP is released in a binary complex with eIF5 that competes with and thus partially inhibits the action of the GEF eIF2B to exchange GDP for GTP on eIF2 (GDI activity). Upon this exchange, eIF2•GTP is ready to form a new TC that can enter the entire cycle all over again. Two "Translational control (TC) points" are indicated by yellow arrows and the mechanism of their action by yellow cross lines; the first targets the eIF4E–eIF4G interaction and the other the GTP/GDP exchange on eIF2 by phosphorylating its α subunit.

1.2 The eIF3 complex

Eukaryotic translation initiation factor 3 was one of the first initiation factors to be identified in the 1970s, but it is only in the past two decades that much of our knowledge about eIF3 structure and function at the molecular level has been gained. Evidence now indicate that eIF3 participates in nearly every step of the translation initiation pathway (Valásek, 2012).

Yeast eIF3 is a large multisubunit protein complex (about 360kD) that promotes binding of Met-tRNAi and mRNA to the 40S ribosomal subunit (Jivotovskaya et al., 2006; Nielsen et al., 2006), plays an important role in the subsequent scanning and AUG recognition (Chiu et al., 2010), facilitates the process of reinitiation (Szamecz et al., 2008), and even participates in translation termination *in vivo* (Beznosková et al., 2013) and in ribosomal recycling *in vitro* (Pisarev et al., 2007; Pisarev et al., 2010).

eIF3 from the yeast *Saccharomyces cerevisiae* is composed of five core essential subunits: a/TIF32, b/PRT1, c/NIP1, i/TIF34 and g/TIF35 (Asano et al., 1998) and one

non-essential substoichiometric subunit j/HCR1 (Valásek et al., 1999). All of them have corresponding orthologs in the mammalian eIF3 complex that contains 13 non-identical subunits designated eIF3a – eIF3m. Interestingly, one study based on tandem mass spectrometry identified three stable modules of human eIF3, one of which, composed of a, b, g and i subunits, closely resembled the yeast eIF3 core (Zhou et al., 2008).

The web of subunit-subunit interactions of yeast eIF3 has been mapped in great detail (Asano et al., 1998; Asano et al., 2000; Elantak et al., 2010; Herrmannová et al., 2011; Phan et al., 2001; Valásek et al., 2001a; Valášek et al., 2002; Valášek et al., 2003), whereas there is only limited information about the mutual contacts of mammalian eIF3 (Querol-Audi et al., 2013; Zhou et al., 2008). The individual interactions within the yeast eIF3 and its associated eIFs will be described later in chapters devoted to each eIF3 subunit; for the summary of these contacts please see Figure 2.

Systematic effort was also devoted to mapping the binding sites of eIF3 subunits on the 40S ribosome. There is accumulating evidence that the major eIF3 body binds to the solvent-exposed side of the 40S ribosome (Cuchalová et al., 2010; Elantak et al., 2010; Chiu et al., 2010; Kouba et al., 2012a; Kouba et al., 2012b; Valášek et al., 2003), while just a few of its domains protrude to the subunit interface side (Karásková et al., 2012; Valášek et al., 2003; Valášek et al., 2004). The individual contacts of eIF3 with the 40S ribosomal subunit will be described in detail further in chapters describing each eIF3 subunit at a time; for their summary and a hypothetical location of eIF3 on the 40S ribosome please see Figure 3.

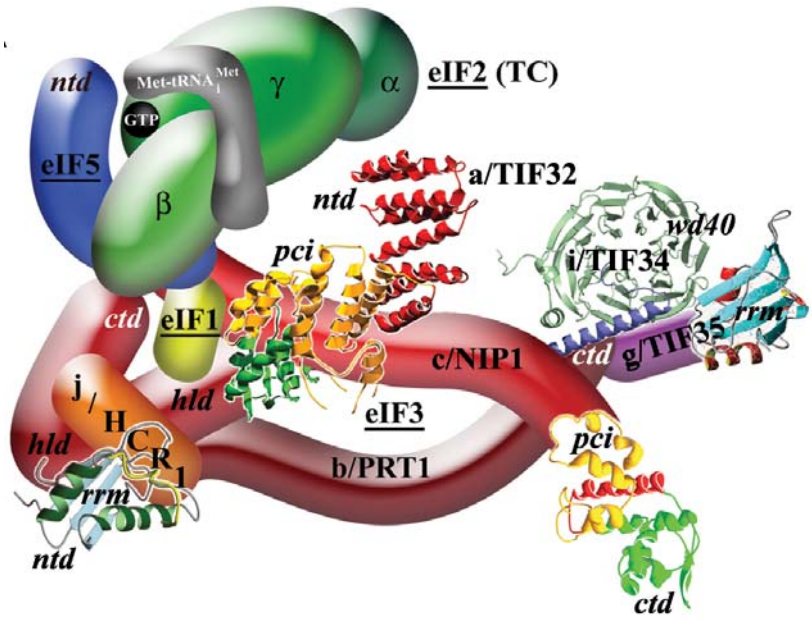

Figure 2. A 3D model of eIF3 and its associated eIFs in the MFC (Valášek et al., unpublished data). ntd, N-terminal domain; ctd, C-terminal domain; hld, HCR1-like domain; rrm, RNA recognition motif; pci, PCI domain; TC, ternary complex. The NMR structure of the interaction between the RRM of human eIF3b (green and light blue) and the N-terminal peptide of human eIF3j (yellow) (Elantak et al., 2010), the NMR structure of the C-terminal RRM of human eIF3g (red and sky-blue, PDB accession code 2CQ0) (Cuchalová et al., 2010), the X-ray structure of the yeast i/TIF34 – b/PRT1-CTD complex (Herrmannová et al., 2011), the 3D homology model of the c/NIP1-CTD (Kouba et al., 2012b) and the crystal structure of the a/TIF32-NTD (residues 276-494) extended by a homology-based prediction of residues 1-275 (S. Khoshnevis unpublished data) were used to replace the original schematic representations of the corresponding molecules.

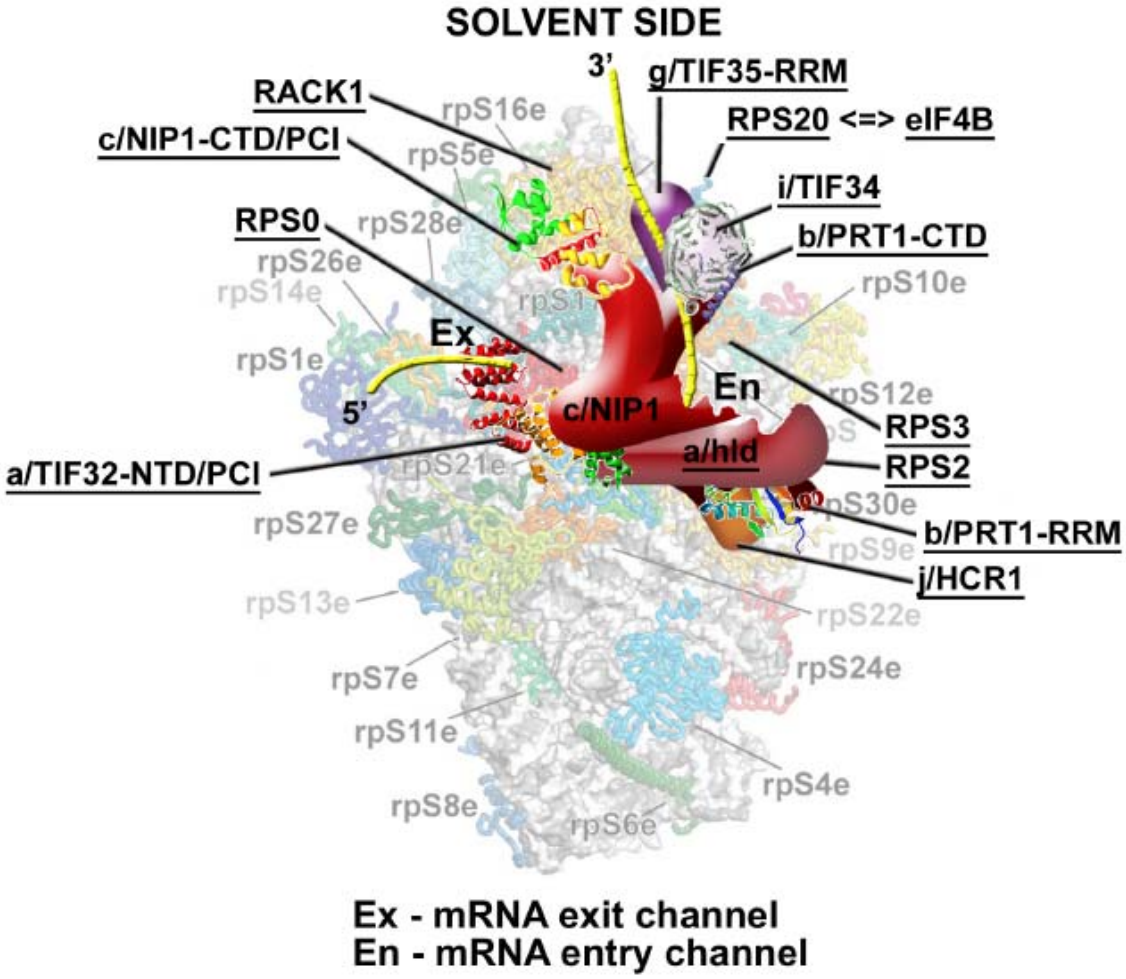

Figure 3. A model of eIF3 on the 40S ribosome spanning the mRNA exit and entry channels. The crystal structure of the 40S subunit is shown from the solvent side with ribosomal proteins shown as cartoons in individual colors; rRNA is shown as gray surface (adapted from (Rabl et al., 2011)). A hypothetical location of *S. cerevisiae* eIF3 on the back side of the 40S subunit is based on the published interactions between RACK1 and the c/NIP1-CTD/PCI (Kouba et al., 2012b); RPS0 and the a/TIF32-NTD/PCI (Szamecz et al., 2008; Valášek et al., 2003); RPS2 and j/HCR1 (Elantak et al., 2010); RPS2 and 3 and the a/TIF32-CTD (Chiu et al., 2010); helices 16-18 of 18S rRNA and the a/TIF32-CTD (Valášek et al., 2003); and RPS3 and 20 and g/TIF35 (Cuchalová et al., 2010). The extreme N-terminal and C-terminal domains of c/NIP1 and a/TIF32, respectively, are predicted to interact with the interface side of the 40S subunit (Valášek et al., 2003), as hinted. The recently published interaction between RPS20 and eIF4B is indicated by a double-headed arrow (Walker et al., 2013). Positions of all eIF3 subunits as well as RACK1, RPS0, 2, 3 and 20 are highlighted in bold. Schematic representations of i/TIF34 bound to the b/PRT1-CTD, the b/PRT1-RRM, the a/TIF32-NTD/PCI, and the c/NIP1-CTD/PCI were replaced with the X-ray structures (Herrmannová et al., 2011; Khoshnevis et al., 2010a) or the 3D structural model (Kouba et al., 2012b), respectively. The yellow lines represent mRNA.

1.2.1 The a/TIF32 subunit

a/TIF32 is, with calculated molecular mass of approximately 110kDa, the largest subunit of yeast eIF3. This sequential and functional homologue of the mammalian p170 subunit (Valášek et al., 1998) was originally described as an essential protein being required for passage through the G1 phase of the cell cycle (Kovarik et al., 1998).

The N-terminal half of a/TIF32 harbors a PCI domain, which spans residues 276-494 and is most probably preceded by the bundle of alpha helices (S. Khosnevish et al., under review in Nucleic Acid Res.). As shown previously, this part of a/TIF32 binds the small ribosomal protein RPS0A (Kouba et al., 2012a; Valášek et al., 2003) (Fig. 3) and the C-terminal domain (CTD) of c/NIP1 (Khoshnevis et al., 2012; Valášek et al., 2002) (Fig. 2). The interaction with RPS0A creates an important intermolecular bridge between eIF3 and the 40S subunit, as the truncation of the first 200 aminoacid residues severely reduced association of the whole MFC with small ribosomal subunits *in vivo* (Valášek et al., 2003). In addition to that, the extreme N-terminal domain (NTD) of a/TIF32 contains two regions that promote a gene-specific regulatory mechanism called reinitiation (REI) by interacting with specific sequences in the 5' untranslated region (UTR) of specific mRNAs (Munzarová et al., 2011; Szamecz et al., 2008). Since RPS0A is located near the mRNA exit pore on the solvent side of the 40S subunit (Ben-Shem et al., 2011) (Fig. 3), it suggests that also the N-terminus of a/TIF32 resides in this area, where it was proposed to create an extension of the mRNA exit channel (Munzarová et al., 2011). Consistently, also mammalian eIF3a was shown to interact with mRNA in the 48S PIC in a way extending the mRNA binding channel beyond the exit site (Pisarev et al., 2008)

The C-terminal half of a/TIF32 contains the HCR1-like domain (HLD) that shares 25% identity with j/HCR1 subunit and interacts with b/PRT1, j/HCR1 and eIF1(Valášek et al., 2002) (Fig 2.). The extreme a/TIF32-CTD interacts with eIF2 (Valášek et al., 2002) (Fig. 2), with helices 16-18 of the 18S rRNA (Valášek et al., 2003) and with ribosomal proteins RPS2 and RPS3 (Chiu et al., 2010) (Fig. 3). Interestingly, the a/TIF32-CTD was shown to promote mRNA recruitment to the 43S PICs, scanning, and together with b/PRT1 and j/HCR1, also to influence the selection of AUG start codon (Chiu et al., 2010). This is not surprising, as helices 16–18 are a part of the ribosome

shoulder and together with RPS2 and RPS3 form the mRNA entry channel (Ben-Shem et al., 2011), thus all these functions can be directly accounted to these contacts.

As can be seen from the multiple contacts with ribosome, and as mentioned above, a/TIF32 as a whole has a critical role in anchoring the entire eIF3 complex to the 40S ribosome.

1.2.2 The b/PRT1 subunit

b/PRT1 is a 90kDa subunit of eIF3 homologous to the mammalian p116 subunit. Yeast b/PRT1 was identified by complementation of one of the original Hartwell's temperature sensitive CDC mutants, *cdc63/prt1-1*, and it was the first gene encoding a protein involved in the initiation of protein synthesis in any eukaryotic organism to be isolated (Keierleber et al., 1986). The b/PRT1 subunit serves as a major scaffolding subunit making contacts with all other subunits of yeast eIF3 (Asano et al., 1998).

The N-terminal domain contains a conserved RNA recognition motif (RRM), which mediates its interaction with the a/TIF32-HLD and the j/HCR1-NTD (Fig 2.) that is important for proper AUG recognition. The b/PRT1-RRM also critically contributes to the eIF3 affinity for the 40S subunit although its binding partner remains to be identified (ElAntak et al., 2007; Elantak et al., 2010; Chiu et al., 2010; Valásek et al., 2001a). The middle domain of b/PRT1 is predicted to fold into two beta-propeller structures formed by WD40 motif repeats (Marintchev and Wagner, 2005), the second of which contains a binding site for c/NIP1 (Valášek et al., 2002) (Fig 2.). Interestingly, a binary complex of b/PRT1-c/NIP1 was never observed (Khoshnevis et al., 2012; Phan et al., 2001), but a subcomplex of c/NIP1-b/PRT1-g/TIF35-i/TIF34 was identified *in vitro* (Khoshnevis et al., 2012)

Finally, the extreme C-terminal domain, which adopts a long alpha-helical structure with unstructured C-terminal tail, is required for association of i/TIF34 and g/TIF35 with the rest of eIF3 and for proper and stable assembly of the PICs (Asano et al., 1998; Herrmannová et al., 2011). Mutating the residues that mediate the interaction with i/TIF34 eliminates both small subunits from MFC *in vivo* and leads to accumulation of aberrant PIC that display severe leaky scanning phenotype (Herrmannová et al., 2011).

Taken together, b/PRT1 is important for eIF3 and MFC integrity, and by interacting with other eIF3 subunits also influences proper selection of the AUG start codon.

1.2.3 The c/NIP1 subunit

The c/NIP1 is a 93kDa subunit of eIF3, first identified in a screen for temperature conditional mutants exhibiting defects in nuclear import, hence its name **N**uclear **I**m**P**ort **1** (Gu et al., 1992). c/NIP1 was shown to regulate AUG recognition via its direct contacts with eIFs 1 and 5 (Karásková et al., 2012; Valášek et al., 2004) and to promote association of eIF3 and the whole MFC with 40S subunits (Greenberg et al., 1998; Kouba et al., 2012b; Valášek et al., 2003).

The contacts of the N-terminal domain of c/NIP1 with eIF1 and eIF5, and via eIF5 also with the TC (Asano et al., 2000; Valášek et al., 2002) (Fig. 3), serve as an important nucleation center for the MFC as well as 43S PIC formation. As such, mutations in the N-terminus of c/NIP1 impairing its contact with eIF1 produce so called Sui- phenotype by allowing selection of near cognate codons in place of AUG as a start codon. In addition, mutations in the extreme N-terminus of c/NIP1, where eIF5 binding site is located, lead to defects in the TC recruitment (Karásková et al., 2012). These findings thus provide strong support for the importance of c/NIP1 interactions with eIF1 or eIF5 in the PIC formation as well as in stringent selection of the AUG start codon.

The immediately following domain then mediates a key contact of c/NIP1 with the PCI domain of a/TIF32 (Khoshnevis et al., 2012; Valášek et al., 2002). Indeed, a mutant form of c/NIP1 lacking the a/TIF32 binding domain failed to co-purify with other core eIF3 subunits but retained strong association with eIFs 1, 2 and 5 (Valášek et al., 2002).

The middle domain (residues 371-570) contain a binding site for b/PRT1 (Valášek et al., 2002) (Fig. 2), which was confirmed recently by isolation of a stable NIP1-PRT1-TIF34-TIF35 subcomplex (Khoshnevis et al., 2012).

Finally, the C-terminus forms a canonical PCI domain (Hofmann and Bucher, 1998); a PIC domain is in general known to serve as the principal scaffold for the 26S proteasome lid, COP9 signalosome (CSN) and mammalian eIF3 (rewieved in Pick et al., 2009). Besides c/NIP1, yeast eIF3 contains only one additional PCI subunit in

a/TIF32, whereas mammalian eIF3 is composed of 6 PCI subunits (a, c, e, k, l, m). Most probably due to the insufficiency of subunits with PCI domains, yeast eIF3 does not manifest the typical PCI complex structure. Furthermore, it was shown that deletion of the PCI domain in c/NIP1 did not influence the integrity of eIF3 and also the direct interaction between the PCI domains of c/NIP1 and a/TIF32 was never observed (Khoshnevis et al., 2012). Instead, the c/NIP1-PCI shows strong but unspecific binding to RNA and directly interacts with blades 1-3 of the small ribosomal protein RACK1/ASC1 (Kouba et al., 2012b), thus linking the eIF3 with the solvent-exposed head region of the small ribosomal subunit (Fig. 3).

Together the three largest subunits (a/TIF32, b/PRT1 and c/NIP1) make a triangle-like complex that is crucial for the eIF3 integrity.

1.2.4 The g/TIF35 and i/TIF34 subunits

The g/TIF35 is a small 30,5kDa subunit of eIF3. It was predicted to contain a Zn-finger domain in its N-terminus that is responsible for binding to i/TIF34 and b/PRT1 (Asano et al., 1998). The g/TIF35 interaction with i/TIF34 is much stronger than that with b/PRT1, but the latter can be markedly stabilized by a concurrent association with i/TIF34 to form a trimeric complex (Herrmannová et al., 2011; Khoshnevis et al., 2012). The C-terminal domain of g/TIF35 harbors the RNA recognition motif (RRM) that can non-specifically bind both mRNA as well as rRNA fragments. Interestingly, it was shown to be nonessential (Hanachi et al., 1999). The structure of human eIF3g-RRM was solved by NMR (Figure 2., K. Tsuda et al. unpublished, Protein Data Bank accession code 2CQ0) and as the human and yeast g/TIF35-RRM are homologous (Cuchalová et al., 2010), we can presume that they also share a common structure. Finally, g/TIF35 was also showed to interact with small ribosomal proteins RPS3 and RPS20 located near the ribosomal mRNA entry channel (Cuchalová et al., 2010) (Fig. 3).

i/TIF34 is a 39kDa subunit of eIF3 identified as a protein required for cell cycle progression and for mating, playing an important role in translation initiation (Naranda et al., 1997; Verlhac et al., 1997). It folds into a canonical seven-bladed beta-propeller structure with a bent alpha-helix at the C-terminus and interacts with b/PRT1 via two

contacts in blades 5 and 6 (Herrmannová et al., 2011). i/TIF34 also binds to the NTD of g/TIF35 but the specific binding site is yet to be determined (Asano et al., 1998).

The role of both small subunits in translation initiation was mysterious until recently, when we showed that they are required for a stable and proper assembly of the 48S PICs, which is a necessary prerequisite for scanning and stringent selection of the AUG start codon (Herrmannová et al., 2011). In particular, g/TIF34 affects the scanning rate, as the mutation in this subunit mapping into the blade 6 provoked a slow scanning phenotype while having no effect on eIF3 integrity, and g/TIF35 influences processivity of scanning through stable secondary structures and also promotes reinitiation, although by different molecular mechanism than the a/TIF32-NTD (Cuchalová et al., 2010).

1.2.5 The j/HCR1 subunit

The j/HCR1 29,5 kDA protein was originally isolated as a high copy suppressor of temperature sensitive phenotype of the *rpg1-1* allele of a/*TIF32* (Valásek et al., 1999). j/HCR1 is a nonessential substoichiometric subunit of eIF3 with dual function in translation initiation and in processing of 20S pre-rRNA (Valásek et al., 2001b). It can bind to 40S ribosomes independently of eIF3 and other components of the MFC (Phan et al., 2001) and modestly stimulate 40S binding of eIF3 (Elantak et al., 2010; Nielsen et al., 2006)

j/HCR1 can be functionally divided into two halves. Its N-terminal half is indispensable for the otherwise non-essential, stimulatory functions of j/HCR1. It was also showed to interact with the b/PRT1-RRM through its N-terminal acidic motif (NTA). Its deletion caused a leaky scanning phenotype, which can be suppressed by overexpression of eIF1A, suggesting its role in proper selection of AUG start codon (Elantak et al., 2010).

The C-terminal of j/HCR1 interacts with small ribosomal proteins RPS2 and RPS23 located in the vicinity of the mRNA entry channel (Fig 3.) and with a/TIF32. Although normally dispensable, the j/HCR1-CTD is required together with the j/HCR1-NTD for tight association with eIF3, as neither half of j/HCR1 co-purifies independently with eIF3 *in vivo*. The tight binding to eIF3 becomes especially important when the binding partner of j/HCR1, the a/TIF32-HLD, is compromised by mutations causing deregulation of AUG selection (Chiu et al., 2010).

Strikingly, only recently we revealed that j/HCR1 plays an important role also in translation termination. j/HCR1 was previously showed to interact with RLI1 protein, which critically promotes translation termination and ribosomal recycling (Barthelme et al., 2011; Khoshnevis et al., 2010b; Pisarev et al., 2010; Shoemaker and Green, 2011). We showed that deletion of j/HCR1 caused increased termination codon read-through fully suppressible by overexpression of RLI1. Moreover, RLI1 also fully suppressed the slow growth phenotype of the j/hcr1Δ strain. Taken together we proposed that the major contributor to the slow growth phenotype of hcr1 deletion is not an initiation defect, as previously believed, but a defect in translation termination (Beznosková et al., 2013). This suggests that j/HCR1 probably should not be considered a *bona fide* eIF3 subunit anymore.

2. AIMS OF THE STUDY

The aim of this study was to investigate and describe the roles of individual subunits of eIF3 in translation initiation to better understand their functions and interactions among themselves and with the 40S ribosome on the molecular level. The ultimate goal of our laboratory, to which this work significantly contributed to, is to solve the 3D structure of eIF3 alone and in complex with other eIFs on the 40S ribosome.

In particular, I aimed to:

1. solve the structure of the interaction between the C-terminus of b/PRT1 and i/TIF34, to pinpoint the specific residues responsible for this interaction, to confirm the importance of these residues by targeted mutational analysis in yeast, and to examine the functional consequences of these mutations;

2. solve the structure of the interaction between human eIF3b-RRM and eIF3j, to determine if the mode of this interaction is conserved in their yeast orthologues, and if true, to test the importance of the contact points by targeted mutational analysis and examine functional consequences of their mutations; in addition, to characterize the contributions of individual halves of j/HCR1 to the translation initiation process.

3. characterize the function of the a/TIF32-CTD, mainly of the HCR1-like domain and the evolutionarily conserved KERR motif within this domain, in translation initiation by the means of targeted mutational analysis; in addition, to identify the binding partners of the a/TIF32-CTD among small ribosomal proteins to map its location on the ribosome;

4. assign functions to the two small, previously functionally uncharacterized subunits of eIF3 in i/TIF34 and g/TIF35; in particular, to isolate mutations in these two subunits that do not interfere with the eIF3 integrity yet produce

severe growth phenotypes, which would help us to reveal the molecular roles of these two small subunits for translation initiation; in addition, to identify their binding partners among small ribosomal proteins to map their location on the ribosome;

5. further characterize the role of the N-terminal domain of c/NIP1 in AUG recognition and TC binding to 40S subunits by means of semi-random mutagenesis in order to identify specific residues responsible for these functions, and if possible, to identify individual binding sites for eIF1 and eIF5 in the c/NIP1-NTD.

3. MATERIALS AND METHODS

All experiments were carried out on a model organism of budding yeast *Saccharomyces cerevisiae* with exception of the structural study of interaction between b/PRT1-RRM and j/HCR1, where human proteins were used.

List of methods:

1% or 2% HCHO-crosslinking, WCE preparation, and fractionation of extracts for analysis of preinitiation complexes
48S PIC analysis (mRNA recruitment assay)
Beta-galactosidase assay
Crystallization
Diffraction data collection and structure determination
Gel mobility shift assay
Glutathione S-transferase (GST) pull-down experiments
Isothermal titration calorimetry (ITC) experiments
Luciferase assay
Ni2+ chelation chromatography
NMR spectroscopy
mRNA binding assay
Polysome profile analysis
Preparation of antibodies
Protein purifications
Resedimentation analysis of preinitiation complexes
Western blot analysis

4. RESULTS

List of publications in chronological order:

eIF3a cooperates with sequences 5' of uORF1 to promote resumption of scanning by post-termination ribosomes for reinitiation on GCN4 mRNA

Szamecz B., Rutkai E., Cuchalová L., Munzarová V., Herrmannová A., Nielsen K.H., Hinnebusch A.G., Valášek L.

Genes Dev. 2008 Sep 1;22(17):2414-25.

PMID: 18765792

The indispensable N-terminal half of eIF3j/HCR1 cooperates with its structurally conserved binding partner eIF3b/PRT1-RRM and with eIF1A in stringent AUG selection.

Elantak L.*, Wagner S.*, Herrmannová A.*, Karásková M., Rutkai E., Lukavsky P.J., Valášek L.

J Mol Biol. 2010 Mar 5;396(4):1097-116.

PMID: 20060839

*These authors contributed equally to this work

The C-terminal region of eukaryotic translation initiation factor 3a (eIF3a) promotes mRNA recruitment, scanning, and, together with eIF3j and the eIF3b RNA recognition motif, selection of AUG start codons.

Chiu W.L., Wagner S., Herrmannová A., Burela L., Zhang F., Saini A.K., Valášek L., Hinnebusch A.G.

Mol Cell Biol. 2010 Sep;30(18):4415-34.

PMID: 20584985

The RNA recognition motif of eukaryotic translation initiation factor 3g (eIF3g) is required for resumption of scanning of posttermination ribosomes for reinitiation on GCN4 and together with eIF3i stimulates linear scanning.

Cuchalová L., Kouba T., Herrmannová A., Dányi I., Chiu W.L., Valášek L.

Mol Cell Biol. 2010 Oct;30(19):4671-86.

PMID: 20679478

Structural analysis of an eIF3 subcomplex reveals conserved interactions required for a stable and proper translation pre-initiation complex assembly.

Herrmannová A.*, Daujotyte D.*, Yang J.C., Cuchalová L., Gorrec F., Wagner S., Dányi I., Lukavsky P.J., Valášek L.

Nucleic Acids Res. 2012 Mar;40(5):2294-311.

PMID: 22090426

*These authors contributed equally to this work

Functional characterization of the role of the N-terminal domain of the c/Nip1 subunit of eukaryotic initiation factor 3 (eIF3) in AUG recognition.

Karásková M.*, Gunišová S.*, Herrmannová A.*, Wagner S., Munzarová V., Valášek L.

J Biol Chem. 2012 Aug 17;287(34):28420-34.

PMID: 22718758

*These authors contributed equally to this work

eIF3a cooperates with sequences 5' of uORF1 to promote resumption of scanning by post-termination ribosomes for reinitiation on GCN4 mRNA

Szamecz B., Rutkai E., Cuchalová L., Munzarová V., Herrmannová A., Nielsen K.H., Hinnebusch A.G., Valášek L.

Genes Dev. 2008 Sep 1;22(17):2414-25.
PMID: 18765792

The major part of this study was driven by our effort to elucidate the molecular mechanism that makes short upstream uORF1 of the *GCN4* mRNA leader reinitiation-permissive. uORF1 is a key component of a very sophisticated translation control mechanism that controls expression of a transcriptional activator *GCN4* and relies on reinitiation of translation on the same mRNA molecule. In particular, when uORF1 gets translated, it allows small ribosomal subunit to stay bound to mRNA post-termination (it does not undergo recycling) in order to resume scanning for reinitiation downstream.

In this article we showed that the N-terminal domain of a/TIF32 forms an important intermolecular bridge between eIF3 and 40S ribosome. We demonstrated this by generating a partial deletion of the RPS0A binding site in the a/tif32-Δ8 mutant that not only reduced amount of 40S-associated MFC components *in vivo*, but also severely blocked the induction of the *GCN4* expression. Detailed examination revealed that a/TIF32-NTD binds to specific sequences lying upstream of uORF1 and by doing so it stabilizes post-termination 40S on the mRNA to resume scanning.

We described this interaction between the a/TIF32-NTD and sequences upstream of uORF1 in great detail and showed that these uORF1 reinitiation enhancing sequences must be properly placed relative to the 40S mRNA exit channel for efficient reinitiation. This work also provided the first *in vivo* evidence that eIF3 stays bound to the ribosome after subunit joining and travels with elongating 80S ribosomes at least for several elongation cycles before it progressively dissociates.

eIF3a cooperates with sequences 5′ of uORF1 to promote resumption of scanning by post-termination ribosomes for reinitiation on *GCN4* mRNA

Béla Szamecz,[1] Edit Rutkai,[1] Lucie Cuchalová,[1] Vanda Munzarová,[1] Anna Herrmannová,[1] Klaus H. Nielsen,[2] Laxminarayana Burela,[3] Alan G. Hinnebusch,[3] and Leoš Valášek[1,4]

[1]Laboratory of Regulation of Gene Expression, Institute of Microbiology AVCR, Prague, Videnska 1083, 142 20, The Czech Republic; [2]Centre for mRNP Biogenesis and Metabolism, Department of Molecular Biology, University of Aarhus, 8000 Århus C, Denmark; [3]Laboratory of Gene Regulation and Development, National Institute of Child Health and Human Development, Bethesda, Maryland 20892, USA

Yeast initiation factor eIF3 (eukaryotic initiation factor 3) has been implicated in multiple steps of translation initiation. Previously, we showed that the N-terminal domain (NTD) of eIF3a interacts with the small ribosomal protein RPS0A located near the mRNA exit channel, where eIF3 is proposed to reside. Here, we demonstrate that a partial deletion of the RPS0A-binding domain of eIF3a impairs translation initiation and reduces binding of eIF3 and associated eIFs to native preinitiation complexes in vivo. Strikingly, it also severely blocks the induction of *GCN4* translation that occurs via reinitiation. Detailed examination unveiled a novel reinitiation defect resulting from an inability of 40S ribosomes to resume scanning after terminating at the first upstream ORF (uORF1). Genetic analysis reveals a functional interaction between the eIF3a-NTD and sequences 5′ of uORF1 that is critically required to enhance reinitiation. We further demonstrate that these stimulatory sequences must be positioned precisely relative to the uORF1 stop codon and that reinitiation efficiency after uORF1 declines with its increasing length. Together, our results suggest that eIF3 is retained on ribosomes throughout uORF1 translation and, upon termination, interacts with its 5′ enhancer at the mRNA exit channel to stabilize mRNA association with post-termination 40S subunits and enable resumption of scanning for reinitiation downstream.

[*Keywords*: Translation initiation; reinitiation; eIF3; 40S ribosomal subunit; *GCN4*; short uORF]

Supplemental material is available at http://www.genesdev.org.

Received March 20, 2008; revised version accepted July 8, 2008.

General translation initiation (GTI) in eukaryotes consists of several steps that ultimately lead to formation of the 80S ribosome with the anti-codon of methionyl initiator tRNA (Met-tRNA$_i^{Met}$) base-paired to the AUG start codon in the ribosomal P-site. In the first step, Met-tRNA$_i^{Met}$ is bound by eukaryotic initiation factor 2 (eIF2) in its GTP form to produce the ternary complex (TC). The TC is subsequently recruited to the small ribosomal subunit with the help of eIF3, eIF1, eIF5, and eIF1A, forming the 43S preinitiation complex (PIC). The 43S PIC then interacts with the 5′ end of mRNA in a reaction stimulated by eIF4F, eIF4B, PABP, and eIF3. The 48S PIC thus formed scans the mRNA leader until the AUG start codon is recognized (for review, see Marintchev and Wagner 2005). Scanning is promoted by eIF1, eIF1A, and eIF4F in a mammalian reconstituted system (Pestova and Kolupaeva 2002), whereas yeast genetic data indicate that eIF3 and eIF5 also participate in vivo (Nielsen et al. 2004; Yamamoto et al. 2005). The GTP bound to eIF2 is partially hydrolyzed to GDP and P_i, dependent on the GAP eIF5, but the P_i is not released from the scanning complex until initiation codon–anticodon base-pairing induces dissociation or displacement of eIF1 (Algire et al. 2005; Cheung et al. 2007). Met-tRNA$_i^{Met}$ is then released into the P-site, and the 60S subunit can join the 40S-mRNA-Met-tRNA$_i^{Met}$ PIC in a reaction stimulated by GTP-bound eIF5B (Pestova et al. 2000). Subunit joining is thought to facilitate ejection of all eIFs but eIF1A (Unbehaun et al. 2004). Finally, GTP-hydrolysis on eIF5B triggers its dissociation, producing an active 80S ribosome poised for elongation (summarized in Fig. 6, below).

Various alternative mechanisms to the GTI pathway exist that are mostly utilized by viruses or function in

[4]Corresponding author.
E-MAIL valasekl@biomed.cas.cz; FAX 420-241-062-665.
Article is online at http://www.genesdev.org/cgi/doi/10.1101/gad.480508.

gene-specific translational control. They rely on *cis*-acting mRNA features and exhibit distinct factor requirements. Reinitiation (REI) is one such mechanism utilized to down- or up-regulate translation of regulatory proteins such as transcription factors and proto-oncogenes in response to various environmental stimuli (Kozak 2005). Ribosomes initiate in the normal way at the first AUG codon; however, at the termination codon, the 40S subunit (40S) remains bound to the mRNA, resumes scanning, and initiates again at a downstream start site. REI depends on de novo recruitment of the TC that is required to recognize the next AUG codon; therefore, it can be delicately regulated by manipulating the eIF2·GTP levels (for review, see Hinnebusch 2005).

Except for a few features in mRNA structure, we know very little about the molecular mechanisms underlying REI. It was shown that the ability of the 40S to reinitiate is limited by the size of the upstream ORF (uORF); however, the critical parameter that determines whether the 40S resumes scanning seems to be the time taken to translate the uORF, rather than its length (Kozak 2001; Rajkowitsch et al. 2004). REI is usually inefficient owing to excessive length or other features of the uORF that prevent retention of post-termination 40S ribosomes on mRNA. Hence, short uORFs generally serve to reduce protein production from a major ORF downstream (Kozak 2005). There are, however, a few examples where uORFs bear special characteristics that render them highly permissive for REI (REI-permissive), such as the mRNAs encoding the yeast transcription factors *YAP1* (Vilela et al. 1998), *GCN4* (Hinnebusch 2005) and its mammalian ortholog *ATF4* (Vattem and Wek 2004), and bZIP transcriptional regulator *ATF5* (Zhou et al. 2008).

GCN4 is a transcriptional activator of a large number of biosynthetic genes (Hinnebusch 2005). Although *GCN4* mRNA is synthesized constitutively, its translation is repressed under nutrient-rich conditions through a REI mechanism involving four upstream open reading frames (uORFs 1–4) that is very sensitive to the TC levels in cells. After translating the first and only REI-permissive uORF1, small ribosomal subunits remain attached to the mRNA, resume scanning, and reinitiate downstream. Under nonstarvation conditions, characterized by high levels of the TC, nearly all of the rescanning 40S ribosomes will rebind the TC before reaching uORFs 2–4, translate one of them, and dissociate from the mRNA. Amino acid starvation leads to phosphorylation of eIF2α by kinase GCN2, converting eIF2.GDP from a substrate to a competitive inhibitor of its GEF, eIF2B, thus reducing the concentration of TC. Low TC levels derepress *GCN4* translation by allowing ~50% of rescanning 40S ribosomes to rebind TC after bypassing uORF4 and reinitiate at *GCN4* instead. Failure to induce expression of *GCN4* in response to a shortage of amino acids in various mutant cells confers increased sensitivity to inhibitors of amino acid biosynthetic enzymes, and is designated the Gcn$^-$ phenotype. Conversely, constitutive expression of *GCN4* independent of amino acid levels due to a defect in TC assembly or recruitment overcomes sensitivity to the latter inhibitors in *gcn2*Δ cells and is called the Gcd$^-$ phenotype. A related but not identical mechanism has been shown to govern translation of the mammalian *ATF4* and *ATF5* transcription factors, indicating that at least basic principles of this regulatory system have been evolutionarily conserved (Vattem and Wek 2004).

A crucial but vaguely understood feature of *GCN4* translational control is the highly disparate capacities of uORF1 and uORF4 to permit efficient resumption of scanning following translation termination. Mutational analyses revealed that AU-rich sequences surrounding the stop codon of uORF1 favor resumption of scanning and REI, whereas GC-rich sequences flanking the uORF4 stop codon likely trigger ribosome release (Grant and Hinnebusch 1994). Sequences 5′ of uORF1 were also shown to be critical for efficient REI (Grant et al. 1995). Virtually nothing is known about what *trans*-acting factors, if any, function in concert with these mRNA features to promote REI. Mutations in eIF3 subunits b and c, and in eIF1, eIF5, eIF1A, and eIF5B, respectively, were shown to deregulate translational control of *GCN4* through their defects in TC recruitment, scanning, AUG selection, or subunit joining (for review, see Hinnebusch 2005); however, no mutations have been isolated that impair retention of post-termination ribosomes at the uORF1 stop codon and the resumption of scanning that is required for REI.

Our previous studies of yeast *Saccharomyces cerevisiae* eIF3 demonstrated that it plays a stimulatory role in nearly all steps of GTI (for review, see Hinnebusch 2006). It is composed of six subunits (a, b, c, i, g, and j), all of which have corresponding orthologs in mammalian eIF3 (meIF3). In *S. cerevisiae*, the TC and eIF1, eIF3, and eIF5 can be found in the higher-order ribosome-free assembly called the Multifactor Complex (MFC), and we and others previously demonstrated that there is a substantial cooperation among the eIFs assembled in the MFC in their binding to the 40S as well as their ribosome-associated functions in scanning and AUG recognition (Valášek et al. 2002, 2004; Nielsen et al. 2004, 2006; Yamamoto et al. 2005; Jivotovskaya et al. 2006). An important task is to elucidate the molecular mechanism underlying this extensive cooperation within the MFC.

We began addressing this issue by mapping the positions of individual components of the MFC on the 40S (Valášek et al. 2003). We found that deleting the N- and C-terminal domains (NTD and CTD) of eIF3c or the NTD of eIF3a impaired association of otherwise intact eIF3 complexes with the 40S, and, in addition, deleting the eIF3a-CTD reduced 40S association of the MFC when the connection between eIF3 and eIF5/TIF5 in the MFC was impaired by the *tif5-7A* mutation. In a separate study, the RNA recognition motif (RRM) of the eIF3b-NTD that mediates its interactions with eIF3j and eIF3a was implicated in the ability of eIF3j to stimulate 40S binding by eIF3 (Nielsen et al. 2006). This RRM-eIF3j network is conserved in mammals (ElAntak et al. 2007). Importantly, our findings that the eIF3a-CTD interacts with helices 16–18 of 18S rRNA and that eIF3a-NTD binds to ribosomal proteins RPS0A and RPS10A (Valášek

et al. 2003) suggested that yeast eIF3 associates with the solvent-exposed side of the 40S (Fig. 1A), as suggested by others for meIF3 (Srivastava et al. 1992; Siridechadilok et al. 2005).

In this study, we focused on the role of the NTD of eIF3a, known as *TIF32* in yeast, in promoting association of eIF3 and other MFC components with the 40S. We found that a partial deletion of the RPS0A-binding site in the a/*tif32-NTD* (Δ8) is not lethal but reduces the amounts of 40S-bound MFC components in vivo, consistent with the idea that the eIF3a-NTD forms a crucial intermolecular bridge between eIF3 and the 40S. Strikingly, the *a/tif32-Δ8* truncation imparted a severe Gcn$^-$ phenotype with novel characteristics, providing the first in vivo evidence that eIF3 is required for post-termination retention of 40S ribosomes at the uORF1 stop codon. Genetic epistasis interactions between mutations in the stimulatory sequences upstream of uORF1 and *a/tif32-Δ8* strongly indicate that eIF3a interacts with this REI-enhancing element that we named eIF3a-NTD-responsive site (eIF3a-RS). Thus, we propose that establishment of the interaction between eIF3a-NTD and the specific eIF3a-RS 5′ of uORF1 at or near the mRNA exit channel of the post-termination 40S subunit stabilizes its association with mRNA and promotes the resumption of scanning for efficient REI at the downstream ORF.

Results

The eIF3a-NTD constitutes a critical link between eIF3 and the 40S subunit

We recently identified several important domains of eIF3 subunits and eIF5 mediating interaction of the MFC with the 40S that allowed us to predict certain aspects of the organization of the 43S PIC (Fig. 1A; Valášek et al. 2003). Among them, the eIF3a-NTD was found to interact in vivo and in vitro with the CTD of small ribosomal protein RPS0A, which has been located beneath the mRNA exit channel on the solvent side of the 40S (Spahn et al. 2001). Consistently, a partial deletion of the RPS0A-binding domain (R0BD) in *a/tif32-Δ8* (Fig. 1B) that did not interfere with the integrity of the MFC (Valášek et al. 2002) completely eliminated binding of the mutant form of the complex (MFC-Δ8) to the 40S in vivo when competing with the wild-type MFC (Valášek et al. 2003). Our previous finding that *a/tif32-Δ8* partially complemented the temperature sensitive (Ts$^-$) phenotype of the *a/tif32-R731I/rpg1-1* mutant strain (Valášek et al. 2002) prompted us to inquire whether *a/tif32-Δ8* can support viability in cells lacking wild-type *a/TIF32*. If so, we could eliminate the effect of competition and examine the phenotypes of *a/tif32-Δ8* in cells lacking wild-type *a/TIF32*. Thus, we constructed a YAH01 strain in which wild-type *a/TIF32* is expressed under control of the *MET3* promoter that can be turned off by addition of methionine to the medium. Indeed, plasmid-borne *a/tif32-Δ8* supported growth of YAH01 cells in the presence of methionine, albeit producing a slow-growth phenotype (Slg$^-$) with a doubling time (dt) of 2.8 h compared with 1.6 h for the wild-type strain (Fig. 1C, row 3 vs. 2). By contrast, *a/tif32-Δ7*, with a nearly complete deletion of the R0BD (Fig. 1B), did not complement depletion of wild-type eIF3a (Fig. 1C, row 4), even when expressed from a high-copy plasmid (data not shown).

We next wished to confirm that Slg$^-$ of the *a/tif32-Δ8* cells is associated with a defect in GTI. To that end, we analyzed the polysome content in *a/tif32-Δ8* cells pre-

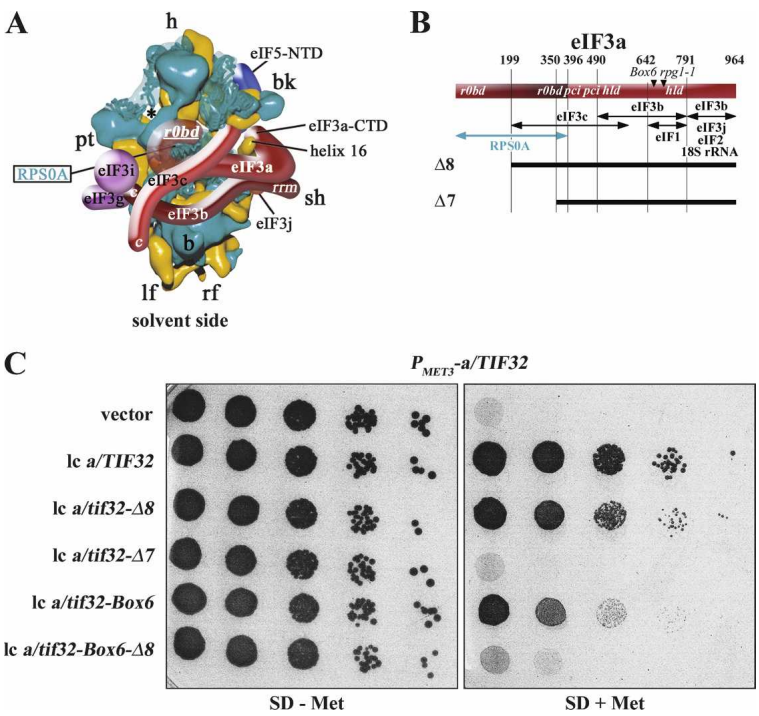

Figure 1. Genetic evidence that a partial deletion of the RPS0A-binding domain in the eIF3a-NTD affects cell growth. (*A*) Hypothetical location of the eIF3 complex on the *S. cerevisiae* 40S subunit based on Cryo-EM reconstruction adapted from Valášek et al. (2003). The 40S subunit is shown from the solvent side, with RNA segments in yellow and proteins in green. Positions of RPS0A and the RPS0A-binding domain (R0BD) of eIF3a are indicated. The mRNA exit channel is designated by an asterisk. (*B*) Schematic of eIF3a with arrows delimiting the minimal binding domains for the indicated proteins identified previously. The lines beneath the schematic depict two N-terminally truncated eIF3a-His proteins that were analyzed in this study. The locations of the RPS0A-binding domain (*r0bd*), the PCI homology domain (*pci*), the eIF3j/HCR1-like domain (*hld*), and two mutations are indicated in the colored rectangle. (*C*) Partial deletion of the R0BD in the eIF3a-NTD (*a/tif32-Δ8*) produces the Slg$^-$ phenotype. Transformants of strain YAH01 bearing the *a/TIF32* wild-type allele under control of the *MET3* promoter containing empty vector; lc pRSeIF3a-His; lc pRSeIF3a-Δ8-His; lc pRSeIF3a-Δ7-His; lc pRSeIF3a-Box6; and lc pRSeIF3a-Δ8-Box6-His, respectively, were spotted in five serial dilutions on SD medium in the absence (*left* panel) or presence (*right* panel) of 2 mM methionine and incubated for 2 d at 30°C.

treated with formaldehyde to cross-link ribosomes on mRNA, by resolving whole-cell extracts (WCEs) by velocity sedimentation through 5%–45% sucrose gradients (Valášek et al. 2007). The *a/tif32-Δ8* extracts showed polysomal run-off and an increased amount of 80S monosomes, leading to a ~2.5-fold decrease in the polysome to monosome (P/M) ratio, which indicates a reduced rate of GTI (Fig. 2A).

To provide evidence that the eIF3a-NTD represents an important link between the MFC and the 40S, we measured binding of eIF3 subunits and other MFC components to 40S subunits in WCEs of mutant *a/tif32-Δ8* cells treated with 1% formaldehyde. This treatment cross-links eIFs to 40S ribosomes in vivo, minimizing dissociation of PICs during sedimentation and thus provides the best available approximation of the native 43S/48S PICs composition in vivo (Valášek et al. 2007). As shown in Figure 2, B and C, we observed ~40% decreases in the amounts of selected eIF3 subunits sedimenting in the 40S-containing fractions (10–12) with commensurate increases in their levels in fractions 4–7 containing free MFC in the *a/tif32-Δ8* cells versus the wild-type control. Similar, but less pronounced, reductions in 40S binding (~25%) were also observed for eIF5 and the TC component eIF2γ. These results demonstrate that partial deletion of the R0BD of eIF3a reduces stable association of eIF3 and, to a lesser extent, eIF2 and eIF5 with the 40S in vivo.

Further support for the role of the eIF3a-NTD in anchoring eIF3 to the 40S arose from combining *a/tif32-Δ8* with a 10-alanine substitution of amino acids 692–701 in the eIF3j/HCR1-like domain (HLD) of eIF3a designated *a/tif32-Box6*. The *a/tif32-Box6* mutation also imparts a Slg⁻ phenotype (dt ~3.6 h) and reduces association of eIF3 and other MFC constituents with the 40S, suggesting that the HLD also promotes 40S binding of the MFC (L. Burela, L. Valášek, and A.G. Hinnebusch, unpubl.). As shown in Figure 1C, rows 5 and 6, combining the *Δ8* and *Box6* mutations in the same *a/TIF32* allele results in synthetic lethality, consistent with the idea that these mutations disrupt independent contacts of eIF3 with the 40S.

Evidence that a/tif32-Δ8 severely interferes with reinitiation by preventing retention of post-termination ribosomes on mRNA at uORF1

We next wished to confirm our observation that *a/tif32-Δ8* reduces association of the TC with the 40S by examining translational regulation of *GCN4* expression, which is very sensitive to decreases in the rate of TC loading on 40S subunits in living cells. Based on our biochemical data, we expected that the *a/tif32-Δ8* mutation would impart a Gcd⁻ phenotype and allow *gcn2Δ* cells to grow on 3-aminotriazole (3-AT), an inhibitor of histidine biosynthetic genes. However, this was not observed (data not shown), suggesting that the derepression of *GCN4* translation expected from a defect in TC recruitment is being suppressed by another stronger defect in the REI process in this mutant.

In fact, we found that *a/tif32-Δ8 GCN2⁺* cells exhibit a severe Gcn⁻ phenotype, displaying sensitivity to 3-AT nearly as strong as that of the *a/TIF32⁺ gcn2Δ* strain where eIF2α cannot be phosphorylated (Fig. 3A). Consistently, derepression of the *GCN4-lacZ* reporter contain-

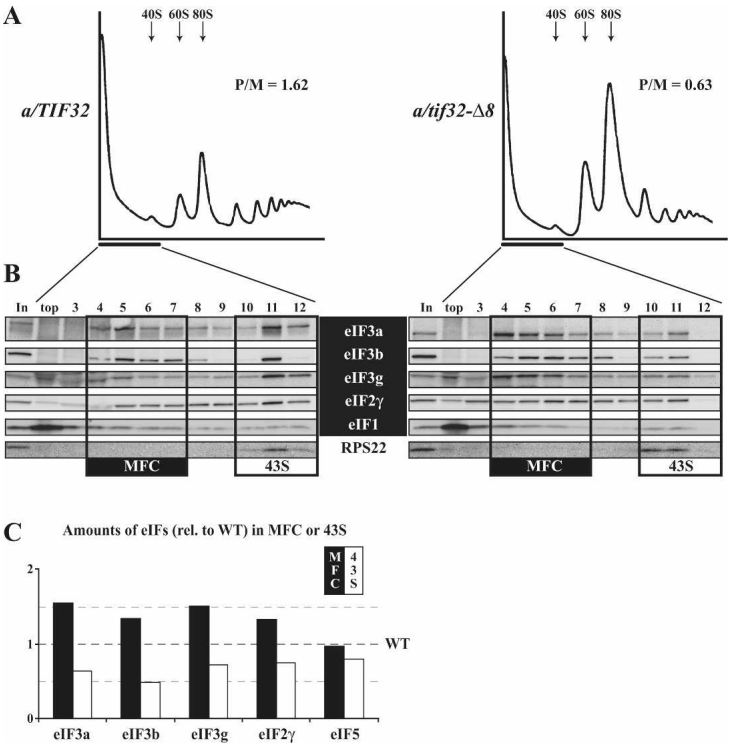

Figure 2. The eIF3a-NTD constitutes a critical link between eIF3 and the 40S ribosome. (*A*) Isogenic strains YBS47 (*GCN2 a/tif32*Δ pRSeIF3a-His) and YBS53 (*GCN2 a/tif32*Δ pRSeIF3a-Δ8-His) were grown in YPD medium at 30°C to an OD_{600} of ~1.5 and cross-linked with 1% HCHO prior to harvesting. WCEs were prepared and subsequently separated on a 5%–45% sucrose gradient by centrifugation at 39,000 rpm for 2.5 h. The gradients were collected and scanned at 254 nm to visualize the ribosomal species. Positions of 40S, 60S and 80S species are indicated by arrows and P/M ratios are given above the profiles. (*B*) The same as in *A*, except that WCEs were separated on a 7.5%–30% sucrose gradient by centrifugation at 41,000 rpm for 5 h. Proteins from the collected fractions were subjected to Western analysis using antibodies against the proteins listed between the blots. An aliquot of each WCE was analyzed in parallel (In, input), and the first two fractions were combined (top). Rectangles indicate fractions where the Multifactor complex (MFC) constituents (highlighted in black) or the 43S PICs (43S), respectively, sediment. (*C*) Amounts of the each individual factor in all fractions from three independent experiments were quantified by fluorescence imaging, combined, and the percentage representation of the signal corresponding to the MFC (4–7) or 43S (10–12) fractions was calculated. Values obtained for the *a/TIF32* wild-type strain were set to 100%, and relative distribution of individual factors in the MFC and 43S fractions in the *a/tif32-Δ8* mutant cells was plotted.

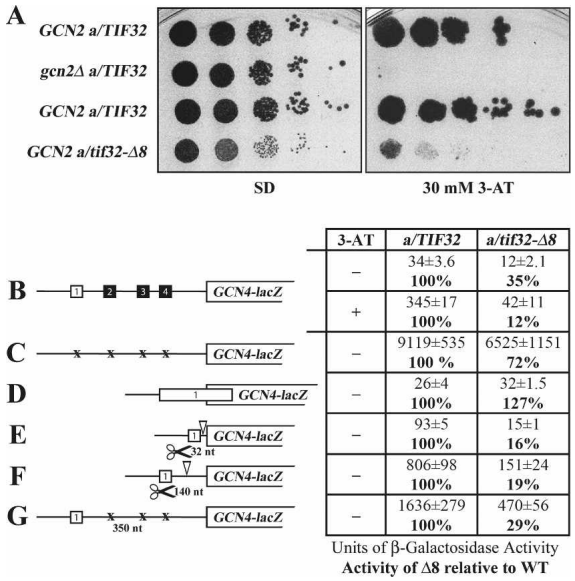

3-AT	a/TIF32	a/tif32-Δ8
–	34±3.6 **100%**	12±2.1 **35%**
+	345±17 **100%**	42±11 **12%**
–	9119±535 **100 %**	6525±1151 **72%**
–	26±4 **100%**	32±1.5 **127%**
–	93±5 **100%**	15±1 **16%**
–	806±98 **100%**	151±24 **19%**
–	1636±279 **100%**	470±56 **29%**

Units of β-Galactosidase Activity
Activity of Δ8 relative to WT

Figure 3. Evidence that *a/tif32-Δ8* severely interferes with the reinitiation process by preventing post-termination retention of the 40S ribosome on mRNA. (*A*) *a/tif32-Δ8* imparts a severe Gcn⁻ phenotype implicating eIF3 in regulation of translational control of *GCN4* expression that occurs via REI. Isogenic strains H2880 (*GCN2 a/TIF32*; row 1), and H2881 (*gcn2Δ a/TIF32*; row 2), YBS47 (*GCN2 a/tif32Δ* pRSeIF3a-His; row 3), YBS53 (*GCN2 a/tif32Δ* pRSeIF3a-Δ8-His; row 4), respectively, were spotted in five serial dilutions on SD (*left* panel) or SD containing 30 mM 3-AT (*right* panel) and then incubated for 3 and 7 d at 30°C, respectively. (*B*) *a/tif32-Δ8* reduces basal expression of *GCN4-lacZ* and prevents its full derepression upon starvation. Isogenic strains YBS47 (*a/TIF32*) and YBS53 (*a/tif32-Δ8*) were transformed with p180, grown in minimal media for 6 and 8 h, respectively, and the β-galactosidase activities were measured in the WCEs and expressed in units of nanomoles of o-nitrophenyl-b-D-galactopyranoside hydrolyzed per minute per milligram of protein. To induce *GCN4-lacZ* expression, *a/TIF32* and *a/tif32-Δ8* transformants grown at the minimal media for 2 h were treated with 10 mM 3-AT for 6 or 16 h, respectively. The mean values and standard deviations obtained from at least six independent measurements with three independent transformants, and activity in *a/tif32-Δ8* relative to wild type, respectively, are given in the table to the *left* of schematics. (*C*,*D*) The failure of *a/tif32-Δ8* to derepress *GCN4-lacZ* is not caused by leaky scanning. YBS47 and YBS53 were transformed with p227 (*C*) and pM226 (*D*), respectively, and analyzed as in *B*, except that they were not treated with 3-AT. (*E–G*) The failure of *a/tif32-Δ8* to derepress *GCN4-lacZ* is not caused by slow or defective scanning. YBS47 and YBS53 were transformed with pG67 (*E*), pM199 (*F*), or p209 (*G*), respectively, and analyzed as in *C* and *D*.

ing all four uORFs in response to 3-AT was reduced by a factor of about nine compared with the wild-type *a/TIF32* strain (Fig. 3B, "+"), fully accounting for the severe 3-AT^S phenotype of the *a/tif32-Δ8* mutant. This derepression defect resulted partly from a decrease in the induction ratio by a factor of about three and partly from a decrease in the basal level of *GCN4-lacZ* expression by a factor of about three (Fig. 3B, "–"). The fact that expression from the uORF-less *GCN4-lacZ* construct was reduced only by a factor of ~1.3 in *a/tif32-Δ8* cells (Fig. 3C) suggests that neither decreased *GCN4-lacZ* mRNA production nor a general decrease in translation efficiency owing to the 40S binding defect of *a/tif32-Δ8* can account for its severe derepression defect. In addition, phosphorylation of eIF2α by GCN2 upon starvation was found to be unaffected in *a/tif32-Δ8* cells (data not shown), ruling out this possible mechanism for the Gcn⁻ phenotype. Thus, these results strongly indicate that the eIF3a-NTD plays a critical role in the REI mechanism on *GCN4* mRNA, however, by a mechanism distinct from a simple reduction in TC recruitment to the rescanning ribosomes.

The reinitiation process can be divided into two phases: the initial REI-specific phase and the following GTI-like phase. The REI-specific steps occur following translation of uORF1 and include (1) 80S ribosome recycling after polypeptide termination, (2) post-termination retention of the 40S subunit, and (3) recruitment of factors required for resumption of scanning. The GTI-like phase is represented by (1) scanning, (2) TC recruitment, (3) GTP-hydrolysis by TC, (4) AUG recognition, and (5) subunit joining. To determine what step is perturbed by *a/tif32-Δ8* and leads to impairment of *GCN4* derepression, we analyzed a series of *GCN4-lacZ* reporters varying in their *GCN4* mRNA leader sequences. It should be noted here that the *GCN4-lacZ* mRNA levels for all constructs used throughout this study were found to be indistinguishable between the wild-type and *a/tif32-Δ8* cells (Supplemental Fig. 1). Defects in recognition of the AUG start codon or subunit joining could result in the bypass of uORF1 by scanning PICs (leaky scanning) with initiation at REI-nonpermissive uORFs 2–4 instead. To examine this possibility, the β-galactosidase activity was measured in WCEs from wild-type and mutant cells bearing a reporter plasmid in which uORF1 is elongated and overlaps the beginning of *GCN4*. The *a/tif32-Δ8* mutation produced only a small increase in expression from this construct (Fig. 3D), which cannot account for the strong derepression of wild-type *GCN4-lacZ* for the following reason: By comparing the results in panels C and D, it can be deduced that only a negligible amount of 40S ribosomes (<1%) that scan from the 5′ end leaky scan the uORF1 AUG, in both mutant and wild-type cells.

Another way to explain the derepression defect in *a/tif32-Δ8* cells is to propose that rescanning ribosomes progress more slowly from uORF1 to uORF4 in the mutant cells. This slower rate of scanning would compensate for the reduction in TC recruitment that we observed by providing the scanning 40Ss sufficient time to rebind TC before reaching uORF4. To test that, we analyzed constructs carrying only uORF1 at three different positions relative to *GCN4-lacZ* (Fig. 3E–G). As observed previously for *prt1-1* (eIF3b) (Nielsen et al. 2004), slow scanning would be expected to increase *GCN4-lacZ* expression from these constructs, particularly those in which uORF1 is closer than normal to the *GCN4* AUG start codon (Fig. 3E,F). Importantly, *a/tif32-Δ8* strongly decreases, not increases, expression from all three constructs (Fig. 3E–G), arguing against the slow scanning mechanism. It is noteworthy that *a/tif32-Δ8* reduces ex-

pression from all three constructs by nearly the same factor (71%–84%), despite the fact that the uORF1–*GCN4* interval varies dramatically from 32 nucleotides (nt) to 350 nt. This phenotype is also inconsistent with less processive scanning, leading to dissociation of 40S reinitiation complexes (RICs) as they travel downstream from uORF1. Reduced processivity would elicit a much greater reduction in REI efficiency for the construct with the 350-nt spacer (Fig. 3G) versus that with the 32-nt spacer (Fig. 3E), which is not the case.

Hence, we propose that *a/tif32-Δ8* impairs the ability of the 40S to either remain attached to *GCN4* mRNA following peptide termination at uORF1 or to acquire factors, such as eIF1 and eIF1A, which promote scanning. Either defect would reduce the number of 40Ss that resume scanning and reinitiate at *GCN4*. This model readily explains why the REI efficiency is reduced by nearly the same factor for the constructs in Figure 3, E–G, in *a/tif32-Δ8* mutant cells. The implication of this model is that the specialized ability of uORF1 to promote efficient REI depends on the eIF3a-NTD and, hence, on the presence of eIF3 on the terminating ribosome at the uORF1 stop codon. The *a/tif32-Δ8* mutation thus establishes a novel class of Gcn$^-$ mutants affecting translational control of *GCN4* by impairing the initial specific steps of REI.

A functional interaction between the eIF3a-NTD and sequences 5′ of uORF1 promotes resumption of scanning by post-termination 40S subunits

It was shown previously that the high propensity of uORF1 for REI requires sequences upstream of its start codon as well as its last codon and 6 nt following the stop codon (Grant and Hinnebusch 1994; Grant et al. 1995); however, the molecular mechanism of their function(s) is unknown. Having established that the eIF3a-NTD promotes association of eIF3 with the 40S and is critical for REI, we wished to examine whether the eIF3a-NTD acts together with specialized sequences that impart the high REI potential of uORF1. Based on its interaction with RPS0A, the eIF3a-NTD is expected to bind in the vicinity of the mRNA exit channel on the solvent side of the 40S (Spahn et al. 2001; Valášek et al. 2003). Whereas the 3′ 12-nt sequence feature surrounding the stop codon of uORF1 should be buried in the mRNA-binding cleft of the terminating 80S ribosome, sequences beginning at nucleotide –10 upstream of the uORF1 AUG would most likely have emerged from the mRNA exit channel and be accessible to the eIF3a-NTD (Fig. 4A; Wang and Sachs 1997). Hence, it is conceivable that interaction of the eIF3a-NTD with sequences upstream of –9 would stabilize binding of the 40S to the mRNA following termination at uORF1 and thereby promote its ability to resume scanning.

It was demonstrated that deletion of 40 nt from nucleotide –21 upstream of the 5′ sequences of uORF1 (*Δ40*) dramatically reduced (by ~65%) the induction of *GCN4-lacZ* expression in wild-type cells (Fig. 4D), whereas replacing the –15 to –1 region 5′ of ORF1 ("linker" and "buried" sequences in Fig. 4A) with the corresponding region upstream of uORF4 had no effect (Miller and Hinnebusch 1989; Grant et al. 1995). Nearly complete elimination of the 5′ sequences in *Δ160* then further diminished *GCN4-lacZ* expression, showing only 15% of the wild-type activity derived most probably from the intact 3′ feature (Fig. 4F; Grant et al. 1995). We found, in addition, that replacement of the –21 AAAATT –16 stretch with CCCCGG [$(C)_4GG$] also significantly reduced β-galactosidase activity by ~40% in wild-type cells (Fig. 4C). Combining the latter mutation with *Δ40* in the *Δ46* construct carrying deletion of 46 nt from nucleotide –61 to –15 resulted in an additive effect (~75% reduction; Fig. 4E). Thus, we reasoned that if the region upstream of nucleotide –15 contains the eIF3a-NTD-binding site, then all these mutations should have a smaller to no effect on REI in *a/tif32-Δ8* versus wild-type cells because the interaction would be already disrupted by *a/tif32-Δ8*. Accordingly, $(C)_4GG$, *Δ40*, and *Δ46* mutations conferred significantly smaller reductions of

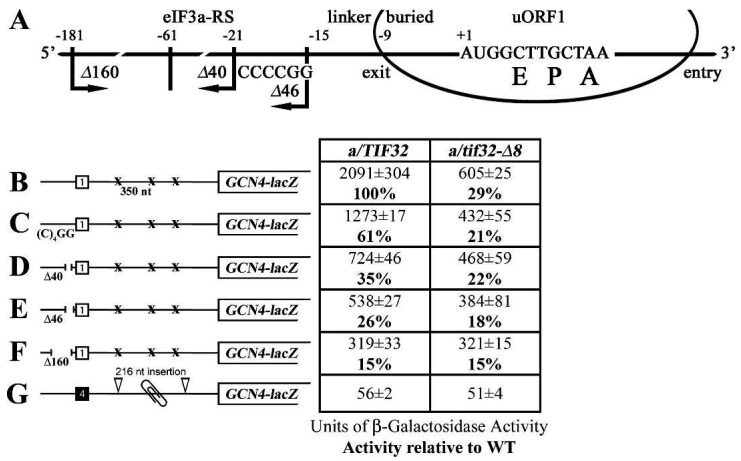

Figure 4. The eIF3a-NTD functionally interacts with the 5′ sequences of uORF1 to ensure efficient resumption of scanning. (*A*) Schematic showing predicted position of the 40S ribosome terminating at the stop codon of uORF1 from the *GCN4* mRNA leader (data adapted from Wang and Sachs 1997). E, P, and A sites of the 40S ribosomes are aligned with the last two coding triplets and the TAA stop codon. Location of the eIF3a-NTD-responsive site (eIF3a-RS), linker, and buried parts of the sequences upstream of uORF1 are indicated at the *top*; 3′ boundary of the *Δ40* deletion (identical to *Δ160*), *Δ46* deletion, and the $(C)_4GG$ multiple substitution are shown *below* the line depicting mRNA. (*B–F*) Same as in Figure 3B, except that YBS47 and YBS53 were transformed with p209, pBS64, pBS62, pVM11, and pBS63, respectively, and analyzed without 3-AT treatment. Activities relative to wild type are given in bold in the table to the *left* of schematics. (*G*) *a/tif32-Δ8* does not affect *GCN4-lacZ* expression after translating the REI-nonpermissive uORF4. YBS47 and YBS53 were transformed with pA80z and analyzed as in Figure 3B.

GCN4-lacZ expression in *a/tif32-Δ8* cells, whereas the most destructive *Δ160* mutation completely eliminated the negative impact of *a/tif32-Δ8* on REI efficiency, producing identical residual activities in both wild-type and *a/tif32-Δ8* cells (Fig. 4C–F). These findings of genetic epistasis strongly suggest that the 5′ sequences from nucleotides −181 to −16 constitute an eIF3a-NTD-responsive site (eIF3a-RS), perhaps a direct binding domain, which is required for efficient REI.

To further underscore this point, we analyzed a construct containing solitary uORF4 with its 5′ and 3′ flanking sequences that was placed precisely at the normal position of uORF1 (Fig. 4G). Since it was previously shown that sequences functionally equivalent to the eIF3a-RS of uORF1 are lacking upstream of uORF4, and thus this short uORF allows only a negligible level of REI (Grant and Hinnebusch 1994), we predicted that *a/tif32-Δ8* should not affect *GCN4-lacZ* expression from the latter construct when compared with wild type. Indeed, Figure 4G clearly demonstrates that the deletion of eIF3a-NTD has no impact on REI in the absence of the eIF3a-RS of uORF1.

Proper placement of the eIF3a-RS of uORF1 relative to the 40S mRNA exit channel is critical for efficient reinitiation

Reinitiation was found to decrease as the uORF was lengthened up to 35 codons, or the rate of translation elongation was slowed down (Kozak 2001; Rajkowitsch et al. 2004). To explain this phenomenon, it was proposed that REI depends on retention of certain initiation factors that gradually dissociate from 80S ribosomes during the course of elongation, thereby reducing the efficiency of REI (Kozak 2005). The results presented so far allow us to propose that eIF3 is a factor that stays bound temporarily to the elongating ribosome, owing to its strategic position on the solvent-exposed "back" side of the 40S subunit. Furthermore, our finding of the specific eIF3a-RS 5′ of uORF1 that promotes REI suggested to us that lengthening uORF1 could decrease REI efficiency by a combination of two effects: (1) displacing this potential eIF3a-NTD-binding site from the mRNA exit channel when the ribosome reaches the stop codon, and (2) by progressive reduction of the eIF3 occupancy on elongating ribosomes.

Since the effect of progressive lengthening of uORF1 has not been investigated before, we analyzed the effect of adding an increasing number of alanine codons to uORF1 on *GCN4-lacZ* expression in wild-type *a/TIF32* cells. As expected, extending the MAC coding sequence of uORF1 with additional Ala codons led to a gradual decrease in β-galactosidase activity (Fig. 5E–I, left column). Addition of two Ala codons [Fig. 5B,G, MA(A)$_2$C] reduced activity by 14%, whereas addition of 10 Ala codons resulted in a ~72% reduction (Fig. 5I; MA(A)$_{10}$C). Assuming that spacing between the eIF3a-RS of uORF1 and its stop codon affects REI efficiency and that the two-Ala extension will reduce eIF3 occupancy on the elongating ribosomes only by a small margin, we should

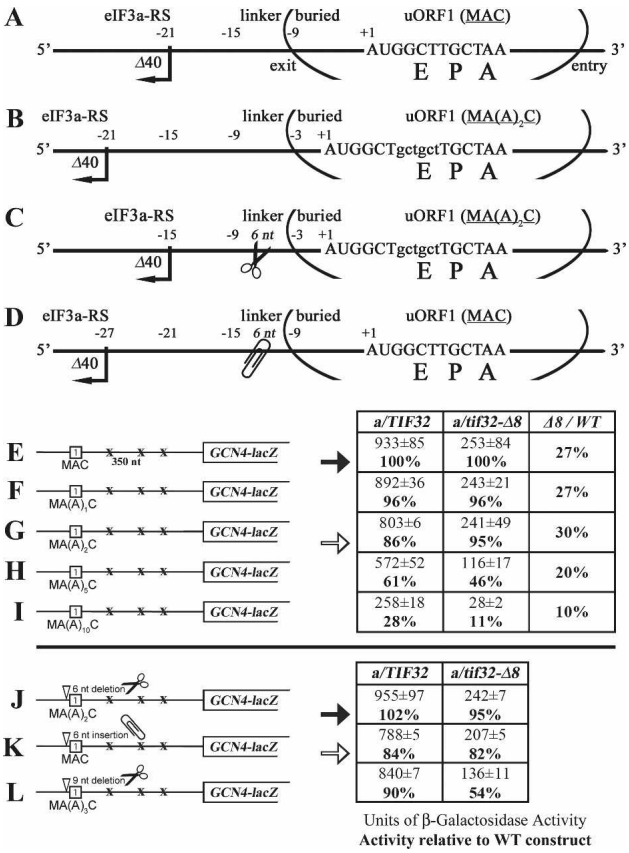

Figure 5. Proper placement of the eIF3a-NTD-responsive site (eIF3a-RS) in 5′ of ORF1 relative to the mRNA exit channel is a critical requirement for efficient REI. (*A–D*) Schematics as in Figure 4A except that the change in a position of the 40S ribosome on the mRNA of uORF1 extended by two codons (*B*), extended by two codons and at the same time shortened by 6 nt in the linker region (*C*), and shortened by 6 nt in the linker only (*D*) are shown. (*E–I*) Progressive extension of the uORF1 reading frame results in a gradual decrease in the *GCN4-lacZ* expression in the wild-type but not in *a/tif32-Δ8* strains. Same as in Figure 4, B–F, except that YBS47 and YBS53 transformed with pM128 or pBS71 through pBS74, respectively, were examined. In addition, activities in *a/tif32-Δ8* relative to wild type, respectively, are given in the *right* column of the table. (*J–L*) Spacing between the eIF3a-RS and the uORF1 stop codon is a critical determinant of REI. Same as above, except that the strains were transformed with pBS75, pBS77, and pBS94, respectively. Closed and open arrows highlight β-galactosidase activities obtained with constructs with the eIF3a-RS in its native position or shifted by 6 nt upstream, respectively.

be able to restore the REI activity of the MA(A)$_2$C construct at least partially by shortening the linker sequence by 6 nt (Fig. 5C). Indeed, the 6-nt linker deletion in MA(A)$_2$C produced 102% of wild-type activity (Fig. 5, J vs. E, closed arrows). Consistently, moving the eIF3a-RS further upstream by extending the linker by 6 nt in the MAC construct (Fig. 5D) decreased *GCN4-lacZ* expression to a level comparable with the MA(A$_2$)C construct (Fig. 5, K vs. G, open arrows). In contrast, correcting the spacing in MA(A)$_3$C by the deletion of 9 nt no longer

restored the wild-type activity (Fig. 5L), most probably due to the more pronounced reduction in eIF3 occupancy on the elongating 80S as judged from a more dramatic impact on REI activity in *a/tif32-Δ8* cells (see also below). The fact that similar results were obtained by testing some of these uORF1 extensions and deletions in a construct containing uORF1 and uORF4 that suffice for wild-type regulation of *GCN4* expression (Supplemental Fig. 2) further support our aforementioned suggestion of the compound effect of lengthening of uORF1 on efficiency of REI.

Addition of two Ala codons to uORF1 did not reduce *GCN4-lacZ* expression as much in *a/tif32-Δ8* cells as in the wild type; however, the longer extensions of five or 10 Ala codons produced a larger decrease in β-galactosidase activity in the mutant versus wild-type strains (Fig. 5E–I; middle and far right columns). This ostensibly paradoxical result can be understood by recalling that *a/tif32-Δ8* is expected to reduce REI by two distinct mechanisms: (1) impairing functional interaction of eIF3 with the eIF3a-RS 5′ of uORF1 and (2) decreasing retention of eIF3 by elongating ribosomes translating uORF1 by reducing the binding of eIF3 to 40S subunits. We observed that addition of five Ala codons was required to detect a marked decrease in *GCN4-lacZ* activity from a construct containing REI-nonpermissive uORF4 only (B. Szamecz and L. Valášek, unpubl.). Hence, we can stipulate that the retention of eIF3 is not significantly reduced by increasing the length of uORF1 by only one or two Ala codons. This would mean that the attenuation in *GCN4-lacZ* expression from the $MA(A)_1C$ and $MA(A)_2C$ constructs in wild-type cells results primarily from displacement of the 5′ sequence feature away from the mRNA exit site of a post-termination ribosome. We showed above that the *a/tif32-Δ8* mutation diminishes the effect of disrupting the 5′ eIF3a-RS by the $(C)_4GG$, *Δ40*, and *Δ46* mutations; hence, *a/tif32-Δ8* should likewise blunt the effects of the $MA(A)_1C$ and $MA(A)_2C$ mutations on REI, as we observed in Figure 5G. We further stipulate that the larger increases in uORF1 length of five or 10 codons lead to a significant reduction in eIF3 occupancy by post-termination 40S subunits. Because *a/tif32-Δ8* weakens binding of eIF3 to the 40S subunit, it can be expected that this mutation would exacerbate the effect of lengthening uORF1, as observed in Figure 5, H and I, for the $MA(A)_5C$ and $MA(A)_{10}C$ mutations. Taken together, these findings strongly support the idea that, at least for REI-permissive uORF1, it is not only the length of the coding region but also a proper placement of the 5′ eIF3a-RS relative to the mRNA exit channel on the post-termination 40S ribosome that represent two critical parameters for efficient REI.

Discussion

The major part of this study was driven by our efforts to address the longstanding question of what endows uORF1 from the *GCN4* mRNA leader with its unique ability to allow highly efficient REI. We began by demonstrating that the N-terminal domain of eIF3a forms an important intermolecular bridge between eIF3 and the 40S ribosomal subunit, most probably by its previously reported interaction with RPS0A (Valášek et al. 2003). The *a/tif32-Δ8* mutation also reduced 40S association of TC and eIF5, consistent with the role of eIF3 in stimulating 40S binding of other MFC components. We observed a mild defect in 40S biogenesis in *a/tif32-Δ8* cells, evident from the increased ratio of free 60S to 40S subunits (Fig. 2A; B. Szamecz and L. Valášek, unpubl.), which might contribute to the Slg^- phenotype. However, the fact that combining *a/tif32-Δ8* with *a/tif32-Box6*, which is known to affect 40S binding of eIF3 but not ribosome biogenesis (L. Burela, L. Valášek, and A.G. Hinnebusch, unpubl.), resulted in synthetic lethality supports our conclusion that the eIF3a-NTD is required primarily for an important contact between eIF3 and the 40S. Previously, mutations in eIF3b and eIF3c were shown to affect binding of eIF3 to the 40S (Valášek et al. 2001, 2004; Nielsen et al. 2006). Unlike *a/tif32-Δ8*, however, these mutations destabilized the MFC and thus might impair 40S binding indirectly. Hence, our results provide the first in vivo evidence implicating a particular domain of a core subunit of eIF3 in its 40S-binding activity.

Although *a/tif32-Δ8* decreases the efficiency of TC recruitment to 40S subunits in vivo, it does not constitutively derepress *GCN4* translation manifested by the Gcd^- phenotype. Rather, *a/tif32-Δ8* strongly impairs derepression of *GCN4* translation in starved cells. Our genetic analysis ruled out several mechanisms to explain this Gcn^- phenotype that were established previously for mutations in other eIFs, including leaky scanning of uORF1, a slow rate of scanning, and less processive scanning (Fig. 3). The simplest explanation of our results is that *a/tif32-Δ8* reduces the ability of 40S subunits to resume scanning after terminating at uORF1, neutralizing the specialized features that optimize uORF1 for this key first step in REI and that are lacking at uORF4. These are the first results directly implicating eIF3 in this critical aspect of the canonical REI mechanism involving short uORFs.

There is previous evidence that REI diminishes with increasing uORF length or in response to other perturbations that increase the time required to translate the uORF (Kozak 2001; Rajkowitsch et al. 2004). Accordingly, Kozak (2001) proposed that contacts between one or more eIFs and the 40S established in the PIC are not disrupted at subunit joining and, instead, decay stochastically during elongation. This would allow persistence of an eIF in association with post-termination 40S subunits following translation of a short uORF and thereby facilitate the resumption of scanning and REI. We found that elongating uORF1 by one or two Ala codons has only a small effect, whereas addition of five or 10 Ala codons produces a marked reduction in REI efficiency. Importantly, *a/tif32-Δ8* exacerbates the reduction in REI produced by lengthening uORF1 by five or 10 codons. Considering that *a/tif32-Δ8* impairs 40S binding of eIF3, these last data provide strong genetic evidence that eIF3 is a factor that remains bound to the 40S subunits of elongating 80S ribosomes as they translate uORF1, and

that this interaction is crucial for REI by post-termination ribosomes.

Based on structural (Srivastava et al. 1992; Siridechadilok et al. 2005) and biochemical data (Valášek et al. 2003), it appears that both mammalian and yeast eIF3 bind primarily to the solvent-exposed side of the 40S (Figs. 1A, 6A). Hence, it is plausible to suggest that eIF3 remains associated with the 40S, at least temporarily, after subunit joining (Fig. 6B–D). The interaction should be relatively weak, however, owing to the absence of supporting contacts that eIF3 makes with several eIFs that are ejected at subunit joining (summarized in Hinnebusch 2006). Presumably, eIF3 relies on direct interactions with 40S components—e.g., the eIF3a-NTD binding to RPS0A—and possibly also on contacts with mRNA residues near the entry and exit sites on the solvent side of the 40S subunit. Indeed, meIF3 and mRNA were shown to mutually stabilize their 40S interactions in vitro (Kolupaeva et al. 2005). Moreover, UV-cross-linking of 48S complexes revealed that human eIF3a specifically interacted with mRNA positions –14 and –17 and eIF3d cross-linked to positions –8 through –17, sug-

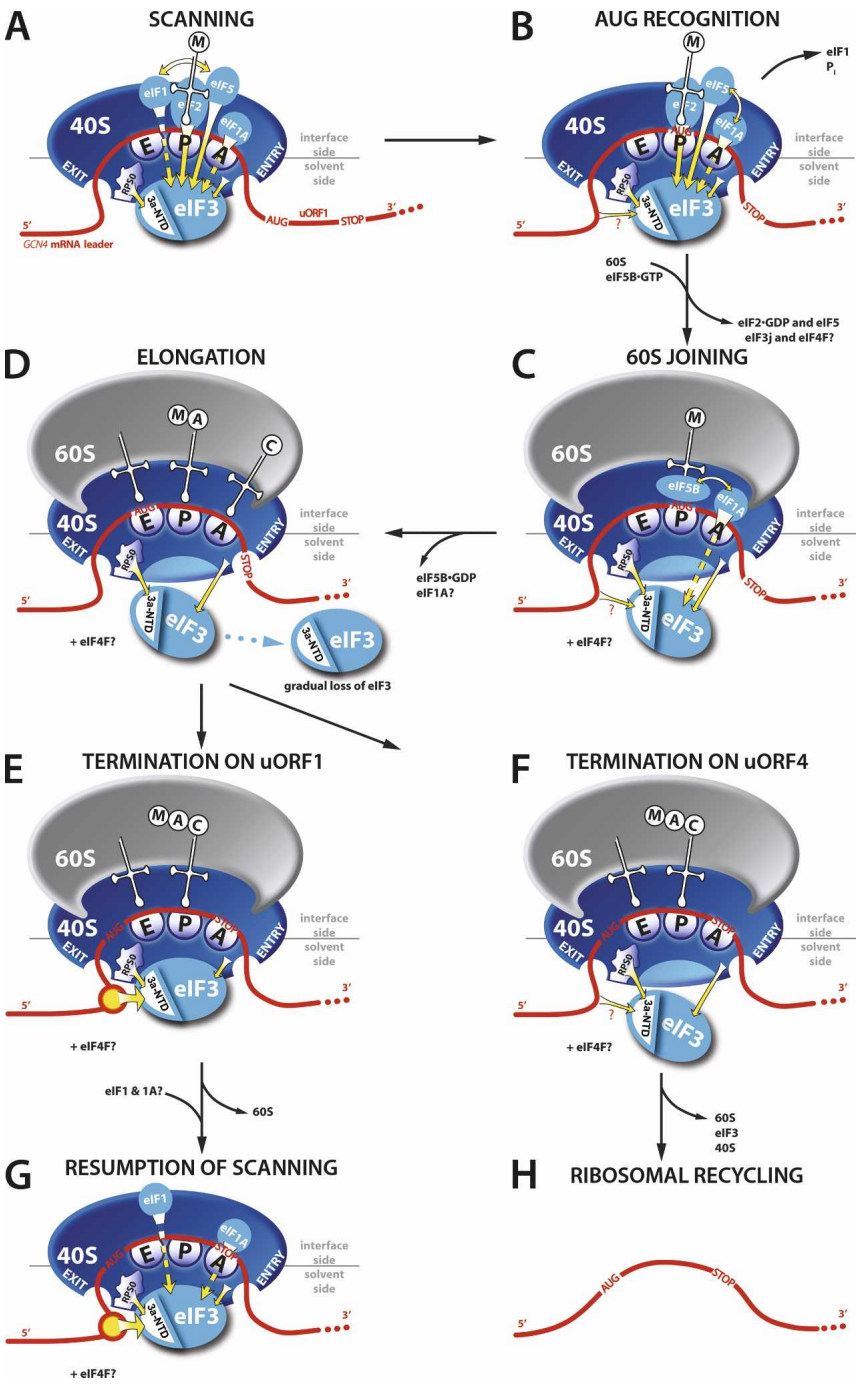

Figure 6. A yeast model for eukaryotic reinitiation following translation of a short uORF. (*A*,*B*) eIF3 association with the scanning 48S PIC is stabilized by supporting contacts with eIF1, eIF1A, eIF5, and the TC. (*C*) Upon subunit joining, eIF3 (and possibly also eIF4F) remains bound to the 80S ribosomes owing to its strategic position on the solvent-exposed side of the 40S ribosome and the contacts that it makes with 40S ribosomal components (e.g., eIF3a-NTD with RPS0A) and presumably also with mRNA. (*D*) During the first few rounds of elongation, weakly associated eIF3 gradually dissociates from the 80S as a function of length and complexity of the translated region. (*E*,*F*) After translation of a short uORF, a certain proportion of 80S ribosomes terminating at its stop codon still contains eIF3, the presence of which is required for resumption of scanning. (*E*,*G*) Binding of the eIF3a-NTD directly to the specific eIF3a-RS 5′ of uORF1 greatly stabilizes association of the post-termination 40S subunit with mRNA following dissociation of the 60S subunit in the first stage of the ribosome recycling reaction and thereby promotes efficient resumption of scanning and REI downstream. (*F*,*H*) Absence of the stimulatory eIF3a-RS, for example at uORF4, results in completion of ribosomal recycling by the majority of terminating 80S ribosomes.

gesting that eIF3 forms an extension of the mRNA-binding channel (Pisarev et al. 2008).

It is noteworthy, however, that *a/tif32-Δ8* does not exacerbate the small reductions in REI produced by lengthening uORF1 by only one or two codons. Likewise, *a/tif32-Δ8* does not diminish the minimal level of REI that wild-type uORF4 (also three codons in length) allows despite lacking stimulatory sequences of uORF1 (Fig. 4G). These results make it unlikely that *a/tif32-Δ8* reduces REI by decreasing eIF3 association with elongating ribosomes during translation of wild-type, three-codon uORF1. Presumably, the effect of *a/tif32-Δ8* in weakening eIF3 binding to the 40S is not great enough to significantly reduce eIF3 occupancy on elongating ribosomes until they have translated more than five codons, as with the elongated versions of uORF1. Hence, we conclude that *a/tif32-Δ8* interferes with a step in REI after termination at the stop codon of wild-type uORF1.

It was shown previously that sequences located upstream of uORF1, and also the last codon and sequences immediately 3′ to the uORF1 stop codon, stimulate REI. The absence of such sequences at uORF4 (Supplemental Fig. 3) contributes to the much lower REI frequency of uORF4 versus uORF1. The fact that *a/tif32-Δ8* has no effect on the low level of REI after uORF4 translation indicates that *a/tif32-Δ8* neutralizes one or more of the features of uORF1 that confer a high REI potential and are absent at uORF4. Importantly, we detected a genetic interaction between *a/tif32-Δ8* and mutations in sequences 5′ of uORF1, wherein the deleterious effect of *a/tif32-Δ8* on REI is blunted or even eliminated by mutations upstream of uORF1 (Fig. 4). These epistatic interactions strongly suggest that the eIF3a-NTD promotes REI by mediating the stimulatory function of the 5′ sequences of uORF1, which we thus refer to as the eIF3a-NTD-responsive site (eIF3a-RS).

We also presented genetic data supporting the idea that the eIF3a-RS of uORF1 must be located at a specific distance upstream of the uORF1 stop codon (Fig. 5). This finding strongly suggests that the efficiency of REI conferred by the eIF3a-RS strictly depends on its proper positioning relative to the 40S mRNA exit channel. Our previous observation that the eIF3a-NTD interacts directly with RPS0A, and the fact that RPS0A occurs near the 40S mRNA exit channel (Spahn et al. 2001), lead us to propose that the eIF3a-NTD binds directly to the stimulatory eIF3a-RS, present at uORF1 but lacking at uORF4, on the solvent side of the 40S when the ribosome is positioned at the uORF1 stop codon (Fig. 6, E vs. F). This interaction would help stabilize association of the 40S subunit with mRNA following dissociation of the 60S subunit in the first stage of the ribosome recycling reaction (Pisarev et al. 2007) and thereby promote efficient resumption of scanning and REI downstream from uORF1 (Fig. 6, G vs. H).

Why is this mechanism so sensitive to the proper placement of the eIF3a-RS? Perhaps the eIF3a-NTD binds to a special mRNA structure whose proper assembly and orientation is critical because the eIF3a-NTD attachment with the 40S is not flexible enough to accommodate even minor alterations. Thus far, we were unable to detect direct binding between purified eIF3a-NTD and the sequences 5′ of uORF1 using conventional UV-cross-linking assays. However, it seems reasonable to suppose that this interaction would be stabilized by simultaneous binding of eIF3 to the back side of the 40S and of mRNA to the mRNA-binding cleft of the 40S (Fig. 6E), making it impossible to detect with eIF3a and mRNA alone. Moreover, the proposed interaction should not be so strong as to impede the rapid resumption of scanning by the post-termination 40S·eIF3 complex.

Alternatively, it is conceivable that eIF3 bound to the post-termination 40S subunit recruits another factor that interacts with the sequences 5′ of uORF1 and possibly even with the eIF3a-NTD itself. Weakening this interaction by *a/tif32-Δ8* that also impairs 40S binding of eIF3 would reduce the recruitment of this hypothetical factor and still diminish the effect on REI of mutating these sequences, as we observed. Interestingly, it was reported that eIF4G/eIF4A must be involved in translating a short uORF to observe efficient REI at a downstream ORF in rabbit reticulocyte lysates (Pöyry et al. 2004). Since eIF3 mediates interaction of eIF4G with the 40S in mammals (Korneeva et al. 2000), eIF3 attachment to the back side of the 40S could allow eIF4G to remain bound temporarily to the ribosome during elongation of a short uORF. As eIF4G has mRNA-binding activity (Lomakin et al. 2000), it could help stabilize the binding of post-termination 40S subunits to the mRNA, as proposed for eIF3; however, eIF4G could also facilitate scanning to the downstream start codon based on its role in ribosomal scanning (Pestova and Kolupaeva 2002). It is true that a direct eIF3–eIF4G interaction has not been observed in yeast; however, this does not exclude a possibility that it occurs only in the ribosomal context, and the hypothetical involvement of eIF4G in translational control of *GCN4* expression has never been systematically investigated.

Our finding that eIF3 is critical for resumption of scanning by post-termination ribosomes and our identification of the eIF3a-RS upstream of the uORF1 stop codon that promotes REI resonate with recent findings on the mechanism of REI after translation of a long ORF. Only recently, Jackson and colleagues (Pöyry et al. 2007) identified eIF3 as a key factor required for REI after translation of a long ORF2 that overlaps the beginning of a downstream ORF3 on polycistronic subgenomic mRNA of feline calicivirus. They found that REI is enhanced by an 87-nt element at the 3′ end of ORF2 that functions at least partly as a binding site for eIF3 (Pöyry et al. 2007). Considering that eIF3 has been implicated in releasing eukaryotic ribosomes from the mRNA after termination of translation at stop codons (Pisarev et al. 2007), it was suggested that the resulting post-termination eIF3/40S complexes at the ORF2 stop codon do not dissociate from the mRNA, but instead get transferred to the 87-nt element by virtue of the eIF3-mRNA contact. This interaction would stabilize mRNA-40S binding and also position the AUG codon of ORF3 in the ribosomal P-site for efficient REI (Pöyry et al. 2007). This mechanism dif-

fers considerably from the canonical REI after a short uORF studied here in that (1) ORF2 is too long to retain eIF3 during translation; (2) eIF3 must be acquired de novo; and (3) there appears to be no scanning after termination of ORF2 before REI at ORF3. Nevertheless, it resembles the model we propose for *GCN4* uORF1 by involving a *cis*-acting enhancer of REI located upstream of the stop codon of the first ORF, which interacts with eIF3 to prevent dissociation of post-termination 40S subunits and stimulate REI.

The fact that translation in general is a rather conserved process in both lower and higher eukaryotes may suggest that our yeast model of REI illustrated in Figure 6 also applies to mammals. However, there are certain aspects by which yeast and mammals differ that ought to be mentioned here: (1) meIF3 contains seven subunits in addition to the yeast six that are conserved (Hinnebusch 2006). Moreover, meIF3a has an extended C terminus compared with its yeast counterpart, though, interestingly, the N termini show the highest degree of similarity. (2) Yeast ribosomes are less sensitive to the start codon context and more sensitive to inhibition by secondary structures (Kozak 2005). (3) REI efficiency in mammalian systems seems to fall off less drastically as the uORF is lengthened in the three to 13 codon range than in yeast (Fig. 5; Kozak 2001). This last fact might indicate that the interaction between eIF3 and the 40S subunit in mammals is stronger and persists longer after initiation at a short uORF, presumably owing to additional contacts that the seven extra mammalian subunits make with the 40S. (4) To our knowledge, there is virtually no information regarding the importance of 5′ and 3′ sequences flanking short uORFs for REI in mammals. Our attempt to compare sequences 5′ of uORF1 of yeast *GCN4* and mammalian *ATF4* and *ATF5* mRNAs, respectively, also did not yield evidence suggesting that the nature of the uORF1-specific post-termination 40S retention on the latter mammalian mRNAs is mechanistically similar to that described for *GCN4*. Thus, whereas it seems fair to propose that at least the basic principles drawn in Figure 6 are shared between the yeast and mammals, the REI mechanism in both systems will likely differ in numerous details.

Our conclusion that eIF3 allows post-termination 40S subunits to remain attached to the mRNA and resume scanning after translation of uORF1 seems at odds with the function of eIF3 in dissociating post-termination ribosomes identified by Pestova and colleagues in a reconstituted system (Pisarev et al. 2007). Moreover, if eIF3 is recruited to all post-termination 80S subunits to participate in ribosome recycling, then why isn't REI efficient after translation of any ORF, regardless of length? Assuming that eIF3 functions in ribosome recycling in vivo, it could be proposed that eIF3 that is acquired de novo from the cytoplasmic pool by post-termination 80S ribosomes at long ORFs differs functionally from eIF3 that is transferred from initiation complexes to elongating ribosomes during translation of a short uORF. In particular, the j-subunit of eIF3 and mRNA are mutually antagonistic for binding to 40S subunits (Unbehaun et al. 2004; Fraser et al. 2007), which might indicate that eIF3j dissociates from eIF3 prior to subunit joining (Fig. 6B). Moreover, eIF3j was shown to promote release of post-termination eIF3·40S complexes from mRNA in the last step of ribosome recycling (Pisarev et al. 2007). Hence, if the eIF3 transferred from the initiation complex to translating ribosomes lacks eIF3j, it would be defective for the last step of ribosome recycling. The persistence of this eIF3j-depleted eIF3 on 80S ribosomes terminating at uORF1 could still promote the eIF3-dependent release of the 60S subunit from the post-termination 80S ribosome (Pisarev et al. 2007), but not dissociation of the 40S from mRNA. Instead, it would stabilize the 40S·mRNA complex (by virtue of eIF3's interaction with eIF3a-RS of uORF1) and promote scanning and reassembly of the 48S PIC for REI downstream.

Materials and methods

Yeast strains and plasmids

Lists of strains and plasmids used in this study and details of their construction can be found in the Supplemental Material.

Biochemical methods

Polysome profile analysis, 1% HCHO-cross-linking, WCE preparation, and fractionation of extracts for analysis of preinitiation complexes were carried out as described by Valášek et al. (2007). β-galactosidase assays were conducted as described previously (Grant and Hinnebusch 1994).

Acknowledgments

We are thankful to Libor Krásný for critical reading of the manuscript, to the members of the Valášek and Krásný laboratories for helpful suggestions, and to Olga Krýdová, Anna Delijannisová, and Ilona Krupičková for technical and administrative assistance. This research was supported for the most part by The Wellcome Trusts Grant 076456/Z/05/Z, and partly also by the Howard Hughes Medical Institute, by NIH Research Grant R01 TW007271 funded by the Fogarty International Center, by the Fellowship of Jan E. Purkyne from the Academy of Sciences of the Czech Republic, by the Institute Research Concept AV0Z50200510, and by the Intramural Research Program of the National Institutes of Health.

References

Algire, M.A., Maag, D., and Lorsch, J.R. 2005. Pi release from eIF2, not GTP hydrolysis, is the step controlled by start-site selection during eukaryotic translation initiation. *Mol. Cell* **20:** 251–262.

Cheung, Y.N., Maag, D., Mitchell, S.F., Fekete, C.A., Algire, M.A., Takacs, J.E., Shirokikh, N., Pestova, T., Lorsch, J.R., and Hinnebusch, A.G. 2007. Dissociation of eIF1 from the 40S ribosomal subunit is a key step in start codon selection in vivo. *Genes & Dev.* **21:** 1217–1230.

ElAntak, L., Tzakos, A.G., Locker, N., and Lukavsky, P.J. 2007. Structure of eIF3b RNA recognition motif and its interaction with eIF3j: Structural insights into the recruitment of eIF3b to the 40 S ribosomal subunit. *J. Biol. Chem.* **282:** 8165–8174.

Fraser, C.S., Berry, K.E., Hershey, J.W., and Doudna, J.A. 2007. 3j is located in the decoding center of the human 40S ribosomal

subunit. *Mol. Cell* **26:** 811–819.
Grant, C.M. and Hinnebusch, A.G. 1994. Effect of sequence context at stop codons on efficiency of reinitiation in *GCN4* translational control. *Mol. Cell. Biol.* **14:** 606–618.
Grant, C.M., Miller, P.F., and Hinnebusch, A.G. 1995. Sequences 5′ of the first upstream open reading frame in *GCN4* mRNA are required for efficient translational reinitiation. *Nucleic Acids Res.* **23:** 3980–3988.
Hinnebusch, A.G. 2005. Translational regulation of GCN4 and the general amino acid control of yeast. *Annu. Rev. Microbiol.* **59:** 407–450.
Hinnebusch, A.G. 2006. eIF3: A versatile scaffold for translation initiation complexes. *Trends Biochem. Sci.* **31:** 553–562.
Jivotovskaya, A., Valášek, L., Hinnebusch, A.G., and Nielsen, K.H. 2006. Eukaryotic translation initiation factor 3 (eIF3) and eIF2 can promote mRNA binding to 40S subunits independently of eIF4G in yeast. *Mol. Cell. Biol.* **26:** 1355–1372.
Kolupaeva, V.G., Unbehaun, A., Lomakin, I.B., Hellen, C.U., and Pestova, T.V. 2005. Binding of eukaryotic initiation factor 3 to ribosomal 40S subunits and its role in ribosomal dissociation and anti-association. *RNA* **11:** 470–486.
Korneeva, N.L., Lamphear, B.J., Hennigan, F.L., and Rhoads, R.E. 2000. Mutually cooperative binding of eukaryotic translation initiation factor (eIF) 3 and eIF4A to human eIF4G-1. *J. Biol. Chem.* **275:** 41369–41376.
Kozak, M. 2001. Constraints on reinitiation of translation in mammals. *Nucleic Acids Res.* **29:** 5226–5232.
Kozak, M. 2005. Regulation of translation via mRNA structure in prokaryotes and eukaryotes. *Gene* **361:** 13–37.
Lomakin, I.B., Hellen, C.U., and Pestova, T.V. 2000. Physical association of eukaryotic initiation factor 4G (eIF4G) with eIF4A strongly enhances binding of eIF4G to the internal ribosomal entry site of encephalomyocarditis virus and is required for internal initiation of translation. *Mol. Cell. Biol.* **20:** 6019–6029.
Marintchev, A. and Wagner, G. 2005. Translation initiation: Structures, mechanisms and evolution. *Q. Rev. Biophys.* **37:** 197–284.
Miller, P.F. and Hinnebusch, A.G. 1989. Sequences that surround the stop codons of upstream open reading frames in *GCN4* mRNA determine their distinct functions in translational control. *Genes & Dev.* **3:** 1217–1225.
Nielsen, K.H., Szamecz, B., Valášek, L.J., Shin, B.S., and Hinnebusch, A.G. 2004. Functions of eIF3 downstream of 48S assembly impact AUG recognition and GCN4 translational control. *EMBO J.* **23:** 1166–1177.
Nielsen, K.H., Valášek, L., Sykes, C., Jivotovskaya, A., and Hinnebusch, A.G. 2006. Interaction of the RNP1 motif in PRT1 with HCR1 promotes 40S binding of eukaryotic initiation factor 3 in yeast. *Mol. Cell. Biol.* **26:** 2984–2998.
Pestova, T.V. and Kolupaeva, V.G. 2002. The roles of individual eukaryotic translation initiation factors in ribosomal scanning and initiation codon selection. *Genes & Dev.* **16:** 2906–2922.
Pestova, T.V., Lomakin, I.B., Lee, J.H., Choi, S.K., Dever, T.E., and Hellen, C.U.T. 2000. The joining of ribosomal subunits in eukaryotes requires eIF5B. *Nature* **403:** 332–335.
Pisarev, A.V., Hellen, C.U.T., and Pestova, T.V. 2007. Recycling of eukaryotic posttermination ribosomal complexes. *Cell* **131:** 286–299.
Pisarev, A.V., Kolupaeva, V.G., Yusupov, M.M., Hellen, C.U.T., and Pestova, T.V. 2008. Ribosomal position and contacts of mRNA in eukaryotic translation initiation complexes. *EMBO J.* **27:** 1609–1621.
Pöyry, T.A., Kaminski, A., and Jackson, R.J. 2004. What determines whether mammalian ribosomes resume scanning after translation of a short upstream open reading frame? *Genes & Dev.* **18:** 62–75.
Pöyry, T.A., Kaminski, A., Connell, E.J., Fraser, C.S., and Jackson, R.J. 2007. The mechanism of an exceptional case of reinitiation after translation of a long ORF reveals why such events do not generally occur in mammalian mRNA translation. *Genes & Dev.* **21:** 3149–3162.
Rajkowitsch, L., Vilela, C., Berthelot, K., Ramirez, C.V., and McCarthy, J.E. 2004. Reinitiation and recycling are distinct processes occurring downstream of translation termination in yeast. *J. Mol. Biol.* **335:** 71–85.
Siridechadilok, B., Fraser, C.S., Hall, R.J., Doudna, J.A., and Nogales, E. 2005. Structural roles for human translation factor eIF3 in initiation of protein synthesis. *Science* **310:** 1513–1515.
Spahn, C.M., Beckmann, R., Eswar, N., Penczek, P.A., Sali, A., Blobel, G., and Frank, J. 2001. Structure of the 80S ribosome from *Saccharomyces cerevisiae*—tRNA–ribosome and subunit–subunit interactions. *Cell* **107:** 373–386.
Srivastava, S., Verschoor, A., and Frank, J. 1992. Eukaryotic initiation factor 3 does not prevent association through physical blockage of the ribosomal subunit–subunit interface. *J. Mol. Biol.* **220:** 301–304.
Unbehaun, A., Borukhov, S.I., Hellen, C.U., and Pestova, T.V. 2004. Release of initiation factors from 48S complexes during ribosomal subunit joining and the link between establishment of codon–anticodon base-pairing and hydrolysis of eIF2-bound GTP. *Genes & Dev.* **18:** 3078–3093.
Valášek, L., Phan, L., Schoenfeld, L.W., Valášková, V., and Hinnebusch, A.G. 2001. Related eIF3 subunits TIF32 and HCR1 interact with an RNA recoginition motif in PRT1 required for eIF3 integrity and ribosome binding. *EMBO J.* **20:** 891–904.
Valášek, L., Nielsen, K.H., and Hinnebusch, A.G. 2002. Direct eIF2–eIF3 contact in the multifactor complex is important for translation initiation in vivo. *EMBO J.* **21:** 5886–5898.
Valášek, L., Mathew, A., Shin, B.S., Nielsen, K.H., Szamecz, B., and Hinnebusch, A.G. 2003. The yeast eIF3 subunits TIF32/a and NIP1/c and eIF5 make critical connections with the 40S ribosome in vivo. *Genes & Dev.* **17:** 786–799.
Valášek, L., Nielsen, K.H., Zhang, F., Fekete, C.A., and Hinnebusch, A.G. 2004. Interactions of eukaryotic translation initiation factor 3 (eIF3) subunit NIP1/c with eIF1 and eIF5 promote preinitiation complex assembly and regulate start codon selection. *Mol. Cell. Biol.* **24:** 9437–9455.
Valášek, L., Szamecz, B., Hinnebusch, A.G., and Nielsen, K.H. 2007. In vivo stabilization of preinitiation complexes by formaldehyde cross-linking. *Methods Enzymol.* **429:** 163–183.
Vattem, K.M. and Wek, R.C. 2004. Reinitiation involving upstream ORFs regulates ATF4 mRNA translation in mammalian cells. *Proc. Natl. Acad. Sci.* **101:** 11269–11274.
Vilela, C., Linz, B., Rodrigues-Pousada, C., and McCarthy, J.E. 1998. The yeast transcription factor genes YAP1 and YAP2 are subject to differential control at the levels of both translation and mRNA stability. *Nucleic Acids Res.* **26:** 1150–1159.
Wang, Z. and Sachs, M. 1997. Ribosome stalling is responsible for arginine-specific translational attenuation in *Neurospora crassa*. *Mol. Cell. Biol.* **17:** 4904–4913.
Yamamoto, Y., Singh, C.R., Marintchev, A., Hall, N.S., Hannig, E.M., Wagner, G., and Asano, K. 2005. The eukaryotic initiation factor (eIF) 5 HEAT domain mediates multifactor assembly and scanning with distinct interfaces to eIF1, eIF2, eIF3, and eIF4G. *Proc. Natl. Acad. Sci.* **102:** 16164–16169.
Zhou, D., Pallam, L.R., Jiang, L., Narasimhan, J., Staschke, K.A., and Wek, R.C. 2008. Phosphorylation of eIF2 directs ATF5 translational control in response to diverse stress conditions. *J. Biol. Chem.* **283:** 7064–7073.

The indispensable N-terminal half of eIF3j/HCR1 cooperates with its structurally conserved binding partner eIF3b/PRT1-RRM and with eIF1A in stringent AUG selection.

Elantak L.*, Wagner S.*, Herrmannová A.*, Karásková M., Rutkai E., Lukavsky P.J., Valášek L.

J Mol Biol. 2010 Mar 5;396(4):1097-116.

PMID: 20060839

*These authors contributed equally to this work

This study focused on characterizing the function of j/HCR1 and its interaction with the b/PRT1 RNA recognition motif (RRM). We showed that the C-terminal half of j/HCR1 is dispensable for all known j/HCR1 functions and that the N-terminal half of j/HCR1 is sufficient for efficient translation in yeast. In addition, we presented genetic evidence that j/HCR1-NTD promotes proper selection of the AUG start codon in cooperation with eIF1A and with the b/PRT1-RRM.

We also identified novel specific interactions between j/HCR1 and small ribosomal proteins RPS2 and RPS23 that are located near the mRNA entry channel.

Using NMR spectroscopy we determined the first solution structure of an interaction between two human eIF3 subunits. We revealed that a conserved tryptophan residue in the j/HCR1-NTD is held in the helix 1 and loop 5 hydrophobic pocket of the b/PRT1-RRM. Mutating the corresponding residues in yeast b/PRT1-RRM resulted in strong growth phenotypes and eliminated association of j/HCR1 with b/PRT1 *in vitro* and with MFC *in vivo*. Furthermore, the b/PRT1-RRM mutation also strongly reduced association of the whole eIF3 with 40S ribosome and produced a leaky scanning defect suggesting, that b/PRT1-RRM interacts with small ribosomal subunit with yet not identified binding partner and that it plays role in AUG selection process by its interaction with j/HCR1.

Here it should be noted that part of this study, namely the mutational analysis of the b/PRT1-RRM, was already published in my diploma thesis.

doi:10.1016/j.jmb.2009.12.047 J. Mol. Biol. (2010) 396, 1097–1116

JMB

Available online at www.sciencedirect.com

ScienceDirect

ELSEVIER

The Indispensable N-Terminal Half of eIF3j/HCR1 Cooperates with its Structurally Conserved Binding Partner eIF3b/PRT1-RRM and with eIF1A in Stringent AUG Selection

Latifa ElAntak[1]†, Susan Wagner[2]†, Anna Herrmannová[2]†, Martina Karásková[2], Edit Rutkai[2], Peter J. Lukavsky[1]* and Leoš Valášek[2]*

[1]*Structural Studies Division, MRC-Laboratory of Molecular Biology, Hills Road, Cambridge CB2 2QH, England, UK*

[2]*Laboratory of Regulation of Gene Expression, Institute of Microbiology AVCR, v.v.i., Videnska 1083, Prague 142 20, Czech Republic*

Received 16 October 2009; received in revised form 17 December 2009; accepted 22 December 2009
Available online 11 January 2010

Despite recent progress in our understanding of the numerous functions of individual subunits of eukaryotic translation initiation factor (eIF) 3, little is known on the molecular level. Using NMR spectroscopy, we determined the first solution structure of an interaction between eIF3 subunits. We revealed that a conserved tryptophan residue in the human eIF3j N-terminal acidic motif (NTA) is held in the helix α1 and loop 5 hydrophobic pocket of the human eIF3b RNA recognition motif (RRM). Mutating the corresponding "pocket" residues in its yeast orthologue reduces cellular growth rate, eliminates eIF3j/HCR1 association with eIF3b/PRT1 *in vitro* and *in vivo*, affects 40S occupancy of eIF3, and produces a leaky scanning defect indicative of a deregulation of the AUG selection process. Unexpectedly, we found that the N-terminal half of eIF3j/HCR1 containing the NTA is indispensable and sufficient for wild-type growth of yeast cells. Furthermore, we demonstrate that deletion of either j/HCR1 or its N-terminal half only, or mutation of the key tryptophan residues results in the severe leaky scanning phenotype partially suppressible by overexpressed eIF1A, which is thought to stabilize properly formed preinitiation complexes at the correct start codon. These findings indicate that eIF3j/HCR1 remains associated with the scanning preinitiation complexes and does not dissociate from the small ribosomal subunit upon mRNA recruitment, as previously believed. Finally, we provide further support for earlier mapping of the ribosomal binding site for human eIF3j by identifying specific interactions of eIF3j/HCR1 with small ribosomal proteins RPS2 and RPS23 located in the vicinity of the mRNA entry channel. Taken together, we propose that eIF3j/HCR1 closely cooperates with the eIF3b/PRT1 RRM and eIF1A on the ribosome to ensure proper formation of the scanning-arrested conformation required for stringent AUG recognition.

Edited by M. F. Summers

Keywords: translation initiation; AUG recognition; eIF3; eIF1A; NMR

**Corresponding authors.* E-mail addresses: pjl@mrc-lmb.cam.ac.uk; valasekl@biomed.cas.cz.

† L.E., S.W., and A.H. contributed equally to this work.

Present address: L. ElAntak, CNRS-IBSM, Laboratoire Interactions et Modulateurs de réponses, 31, Chemin Joseph Aiguier, 13402 Marseille Cedex 20, France.

Abbreviations used: eIF, eukaryotic translation initiation factor; NTA, N-terminal acidic motif; GTP, guanosine-5′-triphosphate; Met-tRNA$_i^{Met}$, methionyl initiator tRNA; TC, ternary complex; MFC, multifactor complex; NTD, N-terminal domain; CTD, C-terminal domain; RRM, RNA recognition motif; cryo-EM, cryo-electron microscopy; heIF3b, human eIF3b; heIF3j, human eIF3j; RNP, ribonucleoprotein; wt, wild type; L5, loop 5; GST, glutathione *S*-transferase; Slg$^-$, slow growth; ORF, open reading frame; Gcn$^-$, general control nonderepressible; 3-AT, 3-aminotriazole; NOE, nuclear Overhauser enhancement; ITC, isothermal titration calorimetry; WCE, whole-cell extract; 3D, three-dimensional; 2D, two-dimensional; NOESY, NOE spectroscopy.

Introduction

Translation captures the transfer of genetic information stored in DNA into effector molecules (polypeptides). The efficiency and accuracy of the initiation phase of translation are masterminded by numerous proteins called eukaryotic translation initiation factors (eIFs). Among them, eIF2 associates in its guanosine-5′-triphosphate (GTP)-bound state with methionyl initiator tRNA (Met-tRNA$_i^{Met}$) to form a ternary complex (TC; eIF2/GTP/Met-tRNA$_i^{Met}$), which is subsequently recruited to the 40S small ribosomal subunit with the help of eIF1, eIF1A, eIF3, and eIF5, producing the 43S preinitiation complex (reviewed by Hinnebusch *et al.*[1] and Pestova *et al.*[2]). eIF1 and eIF1A serve to stabilize a conformation that opens the 40S-mRNA binding channel[3] required for recruitment of mRNA, bound by the cap-binding complex eIF4F and poly(A) binding protein, in a reaction that is, at least in yeast, critically stimulated by eIF3.[4] In the thus formed 48S preinitiation complex, the 40S subunit is believed to adopt an open/scanning-conducive conformation that enables inspection of successive triplets in the mRNA leader in an ATP-dependent process called scanning, which is relatively poorly understood. During this process, eIF5 stimulates partial GTP hydrolysis on eIF2, but the resultant P_i is not released until initiation codon–anti-codon base-pairing has induced a conformational switch to the closed/scanning-arrested form, accompanied by displacement of eIF1 (reviewed by Mitchell and Lorsch[5]). This irreversible reaction serves as the decisive rate-limiting step stalling the entire machinery, with the AUG start codon placed in the decoding center (P site) of the 40S subunit. eIF1 is responsible for preventing premature engagement with putative start codons, whereas eIF1A is believed to stabilize properly formed preinitiation complexes at the correct start codon. eIF3 also contributes to the latter process via its contacts with eIF1, eIF2, and eIF5; however, molecular details of its participation are not known.[6] After eIF2 guanosine 5′-diphosphate release, the 60S large ribosomal subunit can join the 40S-mRNA–Met-tRNA$_i^{Met}$ preinitiation complex in a reaction stimulated by a second GTPase, eIF5B. Subunit joining is thought to facilitate ejection of all eIFs, except for eIF1A[7] and eIF3.[8] When eIF5B guanosine 5′-diphosphate dissociates, the 80S initiation complex is ready for elongation.

eIF3 is the most complex initiation factor composed of six subunits in yeast *Saccharomyces cerevisiae* (a/TIF32, b/PRT1, c/NIP1, i/TIF34, g/TIF35, and j/HCR1), all of which have corresponding orthologues in mammalian eIF3 containing additional seven subunits (d, e, f, h, k, l, and m).[9] Given such complexity, it is not surprising that eIF3 was demonstrated to promote nearly all initiation steps, including binding of TC and other eIFs to the 40S subunit, subsequent mRNA recruitment, and scanning for AUG recognition (reviewed by Hinnebusch[9]). These activities are facilitated by other eIFs such as eIF2, eIF1, and eIF5, which make direct contacts with eIF3 and, at least in yeast, occur in the ribosome-free assembly called the multifactor complex (MFC).[4,6,10–13] We previously pinpointed several eIF3 domains that could play a critical role in MFC association with the 40S subunit, including the N-terminal domain (NTD) and the C-terminal domain (CTD) of c/NIP1 and a/TIF32, and the RNA recognition motif (RRM) in the NTD of b/PRT1.[12,14] Identification of direct interactions between the NTD of a/TIF32 and the small ribosomal protein RPS0A, and the CTD of a/TIF32 and helices 16–18 of 18S rRNA allowed us to propose that eIF3 associates with the solvent-exposed side of the small subunit[14] (Fig. 1a), as suggested by others for mammalian eIF3.[17,18] In support, we have recently demonstrated that a partial nonlethal deletion of the NTD of a/TIF32 significantly reduced the amounts of 40S-bound MFC components *in vivo*, implicating this domain in the formation of a critical intermolecular bridge between eIF3 and the 40S subunit.[8]

Whereas there is no structural information available on yeast eIF3, whose detailed subunit interaction map is well defined,[10] the recent cryo-electron microscopy (cryo-EM) study of human eIF3 revealed a low-resolution particle with a five-lobed architecture.[18] The first attempt to unveil details of the spatial arrangement of its subunits and interactions between them suggested that human eIF3 is composed of three relatively stable modules, one of which bears resemblance to the yeast eIF3 core complex.[19] Both yeast and mammalian eIF3 were suggested to associate with the 40S subunit via its solvent-exposed side (Fig. 1a).[8,14,18] We recently provided the first insight into the molecular nature of eIF3 subdomains by resolving the NMR solution structure of the RRM of human eIF3b (heIF3b).[20] We reported a noncanonical RRM with a negatively charged surface in the β-sheet area, contradictory to the potential RNA binding activity of typical RRMs. Instead, we found that human eIF3j (heIF3j) interacts with the basic area of heIF3b-RRM, opposite to its β-sheet surface, via its N-terminal 69-amino-acid peptide, and that this interaction promotes heIF3b-RRM recruitment to the 40S subunit.

eIF3b is considered to serve as the major scaffolding eIF3 subunit shown to interact with a, c, g, i, and j in both mammals and yeast,[10,19,21–25] clearly illustrating a high evolutionary conservation of its structure-organizing role. Indeed, we previously demonstrated that b/PRT1 also interacts with j/HCR1 via its N-terminal RRM domain,[25] and this contact was later implicated in the ability of j/HCR1 to stimulate 40S binding by eIF3. Remarkably, mutating the ribonucleoprotein (RNP) 1 motif of b/PRT1-RRM in *b/prt1-rnp1* was shown to modestly increase leaky scanning, suggesting that the RRM of b/PRT1 also contributes to the efficiency of AUG recognition.

j/HCR1 is the only nonessential subunit in yeast[26] that is believed to stimulate eIF3 binding to the 40S subunit[12] and to promote 40S ribosome biogenesis.[27] Consistently, *in vitro* experiments revealed that heIF3j can bind to the 40S subunit by itself and is required for

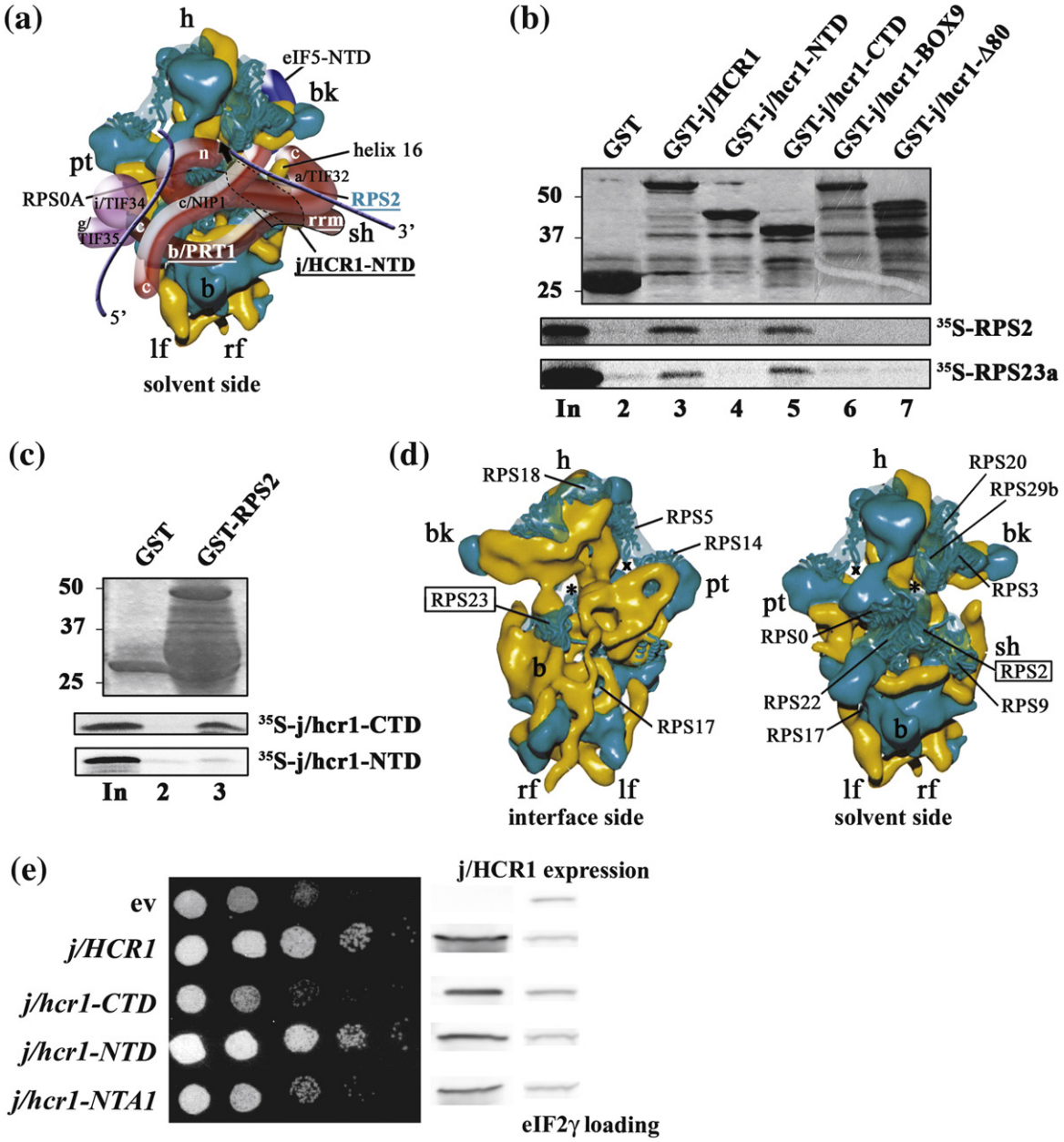

Fig. 1. The CTD of j/HCR1 interacts with RPS2 and RPS23a situated near the 40S mRNA entry channel, but is dispensable for efficient translation in yeast, as opposed to its NTD. (a) Hypothetical location of eIF3 on the solvent side of the *S. cerevisiae* 40S subunit based on cryo-EM reconstruction (adapted from Valášek *et al.*[14]). Protrusion of the CTD of eIF3j into the mRNA entry channel based on Fraser *et al.* is symbolized by a green arrow.[15] Blue lines represent mRNA. (b and c) j/hcr1-CTD interacts with RPS2 and RPS23a via its KERR motif. (b) Full-length j/HCR1 (lane 3), its N-terminal half (lane 4) or C-terminal half (lane 5), various mutants (lanes 6 and 7) defined in Fig. 2b fused to GST, and GST alone (lane 2) were tested for binding against ^{35}S-labeled wt RPS2 and RPS23a; 10% of input amounts added to each reaction are shown in lane 1 (In). (c) RPS2 fused to GST (lane 3) and GST alone (lane 2) were tested for binding to ^{35}S-labeled j/hcr1-CTD and NTD essentially in the same manner as in (b). (d) Cryo-EM reconstruction of the *S. cerevisiae* 40S subunit (adapted from Spahn *et al.*[16]). The 40S subunit is shown from the interface side (left) or the solvent side (right), with RNA segments in yellow and with proteins in green. The mRNA entry and exit channels are designated by (*) and (X), respectively. (e) j/hcr1-NTD is required for wt growth dependent on its intact NTA. Transformants of H428 (*j/hcr1*Δ) bearing an empty vector, YEp-j/HCR1-DS, YEp-j/hcr1-CTD, YEp-j/hcr1-NTD, and YEp-j/hcr1-NTA1, respectively, were spotted in five serial 10-fold dilutions on SD medium and incubated at 30 °C for 1.5 days. The far-right columns contain the results of Western blot analysis of WCEs from the very same strains using anti-j/HCR1 (j/HCR1 expression) and anti-GCD11 (eIF2γ loading) antibodies, respectively.

the stable 40S association of purified eIF3.[7,22,28] Intriguingly, heIF3j, in the absence of other factors, was also demonstrated to be mutually antagonistic for binding to the 40S subunit with mRNA.[7,15] Furthermore, mutual exclusivity for heIF3j in 40S subunit binding was also observed with eIF1A.[15]

These results, together with determination of the position of heIF3j-CTD in the 40S mRNA entry channel and in the ribosomal A site by hydroxyl radical probing,[15] suggested that eIF3j may coordinate binding of mRNA and eIFs within the decoding center and thus perhaps influence transitions between scanning-conducive and scanning-arrested conformations. To gain a full understanding of the physiological roles of eIF3j, we obtained detailed biochemical and structural information of its interactions and examined their importance in living cells.

Unexpectedly, here we show that the NTD of j/HCR1 is indispensable and sufficient for wild-type (wt) growth. Strikingly, we also found that deletion of j/HCR1 (or its NTD only) leads to a strong leaky scanning phenotype indicative of a defect in AUG recognition, partially suppressible by increased gene dosage of eIF1A. These novel results strongly suggest that eIF3j remains bound to scanning ribosomes even after mRNA recruitment. NMR spectroscopic analysis revealed that heIF3j is held via its N-terminal acidic motif (NTA) centered by the conserved tryptophan (Trp52) in a hydrophobic pocket formed by helix α1 and loop 5 (L5) of heIF3b-RRM. To our knowledge, this is the first structural insight into molecular interactions within eIF3 from any organism. Mutating these evolutionary conserved determinants in yeast j/HCR1 and b/PRT1 subunits disrupted their direct binding *in vitro*, as well as j/HCR1 association with MFC, but not with 40S subunits *in vivo*. Both j/HCR1 and b/PRT1 mutations resulted in growth phenotypes and imparted severe leaky scanning defects. The b/PRT1-RRM mutation then, in addition, strongly reduced the association of the core eIF3 with 40S subunits, suggesting that it forms, either directly or indirectly, an important intermolecular bridge between eIF3 and the small ribosomal subunit. We conclude that the key function of the NTD of j/HCR1 is to cooperate with the RRM of b/PRT1 and eIF1A on the 40S subunit to ensure proper establishment of the scanning-arrested conformation required for stringent AUG recognition.

Results

The N-terminal half of j/HCR1 is indispensable and sufficient for efficient translation in yeast

Recent observations made with glutathione *S*-transferase (GST) pull-down experiments showed that the last 16 amino acids of heIF3j are required for the stable binding of eIF3 to the 40S subunit,[22] and that binding of heIF3j-CTD occurs in the 40S mRNA entry channel.[15] Consistent with the latter, using GST pull-downs, we reproducibly detected weaker but highly specific interactions between the purified j/hcr1-CTD and small ribosomal proteins RPS2 and RPS23 (Fig. 1b, lane 5; Fig. 1c, middle panel) dependent on the last 80 amino acid residues of j/HCR1 and the intact KERR motif (K^{205}-x_5-$E^{211}R^{212}$-x_2-R^{215}) (Fig. 1b, lanes 6 and 7), which is conserved between eIF3j and the HCR1-like domain of eIF3a across species (see the text below).[25] (None of the remaining small ribosomal proteins, whose location on the ribosome was predicted based on homology modeling with bacterial proteins, interacted with j/HCR1 in this assay.) RPS2 and RPS23 were previously shown to occur on the solvent and interface sides of the mRNA entry channel, respectively[16] (Fig. 1d). Together, these findings suggest that the ribosomal binding site of the CTD of eIF3j might have remained evolutionary conserved and that it thus represents an important functional domain of eIF3j.

To examine this possibility, we first expressed the NTD and CTD of j/HCR1 (defined in Fig. 6b) in the *j/hcr1*Δ strain and tested the resulting transformants for the suppression of its slow-growth (Slg^-) phenotype. Surprisingly, we found that the CTD of j/HCR1 is dispensable for the wt growth of yeast cells in contrast to its NTD, the deletion of which phenocopied the Slg^- phenotype of *j/HCR1* deletion (Fig. 1e, fourth row *versus* third row). [Both truncated proteins, as well as other j/HCR1 mutants mentioned below, had to be tested from high-copy vectors due to their decreased stability. In this arrangement, their expression levels were about 3-fold higher than the physiological level and similar to the level of overexpressed wt j/HCR1, which does not produce any phenotype (Fig. 1e; data not shown).] This finding implies that the NTD of j/HCR1 should be able to associate with the 40S subunit independently of its CTD. To test this, we employed a formaldehyde cross-linking method, followed by resedimentation of the 40S fractions on a second gradient, to minimize the trailing of non-cross-linked factors into 40S fractions. It is worth mentioning that this method provides the best available approximation of the native 43S/48S preinitiation complexes composition *in vivo*.[29] As shown in Fig. 2a–c, both j/hcr1-NTD and j/hcr1-CTD retained ~20% of wt affinity for the 40S subunit. (Bands in the upper fractions after resedimentation most likely represent j/HCR1 proteins not properly cross-linked to preinitiation complexes *in vivo* that dropped off during two consecutive high-velocity centrifugations.) When the nonequilibrium character of this assay is taken into account, the given percentages are only relative numbers and, in principle, suggest that both j/HCR1 halves show less stable binding to 40S subunits under these conditions than the full-length protein. In fact, since j/hcr1-NTD fully supports the growth of *j/hcr1*Δ cells, it seems likely that in living cells, it associates with 40S subunits more efficiently. To learn whether the j/hcr1-NTD–40S interaction is bridged by eIF3, we examined the 40S binding of j/hcr1-NTD bearing a specific *NTA1* mutation, which, as described in detail below, destroys direct j/HCR1–b/PRT1 interaction and completely diminishes j/HCR1 association with MFC *in vivo* (Figs. 6c and 7b). As shown in Fig. 2d, the j/hcr1-NTD-NTA1 mutant still associated with 40S subunits, albeit with an affinity reduced by ~30% compared to j/hcr1-NTD.

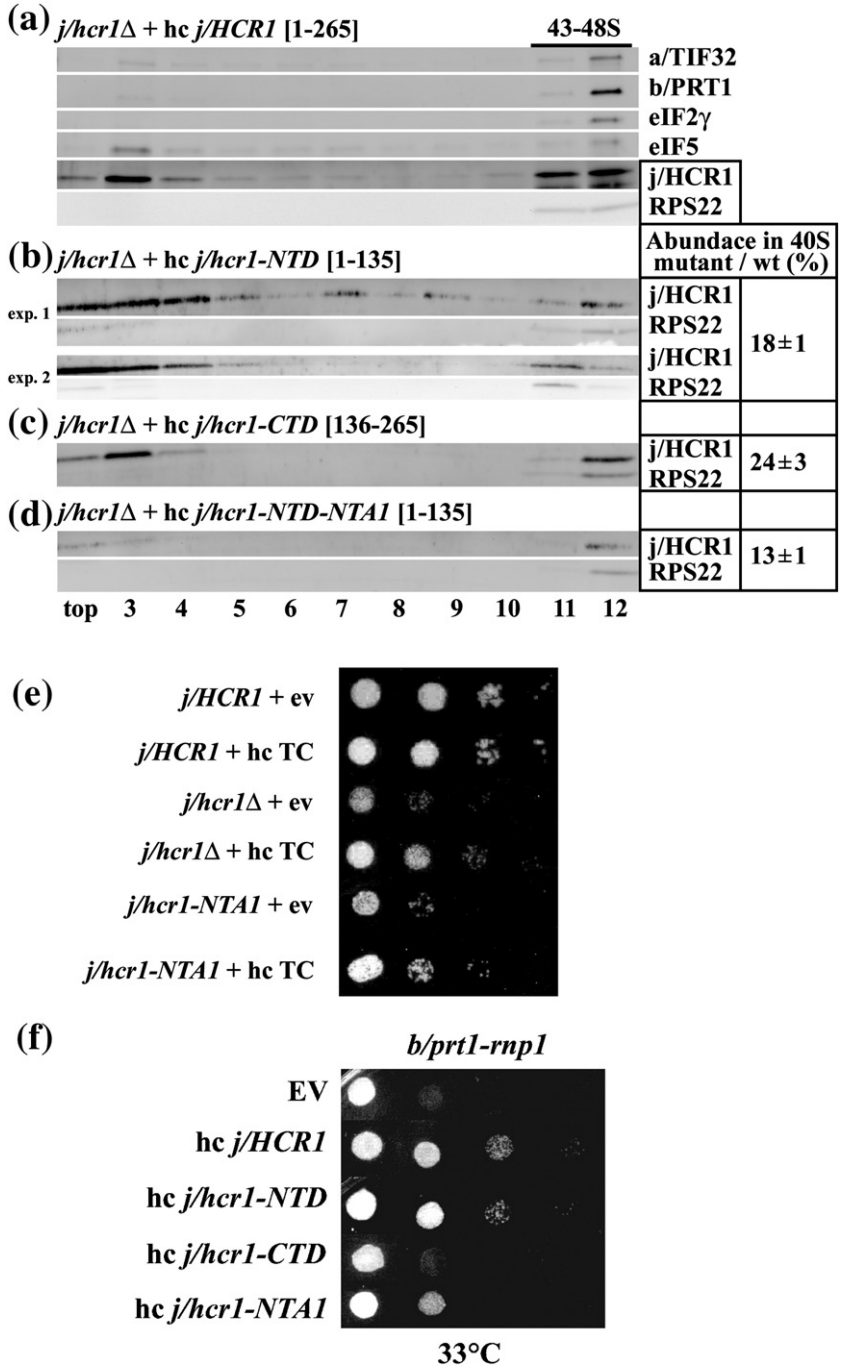

Fig. 2. Both the NTD and the CTD of j/HCR1 retain intrinsic 40S binding affinity. (a–d) Transformants of strain H428 (*j/hcr1*Δ) bearing YEp-j/HCR1-DS, YEp-j/hcr1-NTD, YEp-j/hcr1-CTD, and YEp-j/hcr1-NTD-NTA1, respectively, were grown in SD medium at 30 °C to an OD_{600} of ~1.5 and cross-linked with 2% HCHO prior to harvesting. WCEs were prepared and subsequently separated on a 7.5–30% sucrose gradient by centrifugation at 41,000 rpm for 5 h. The 40S fractions were pooled, resolved on a second gradient, and subjected to Western blot analysis. The first two fractions were combined (top). Proportions of the 40S-bound j/HCR1 proteins relative to the amount of 40S subunits were calculated, using NIH ImageJ, from two independent experiments. The resulting values obtained with the wt strain were set to 100%, and those obtained with mutant strains were expressed as percentages of wt (SD given). (e–f) Genetic evidence that j/HCR1 with intact NTA (or only its NTD) stimulates 40S binding by eIF3. (e) Overexpression of TC partially suppresses the Slg^- phenotype of *j/hcr1*Δ and *j/hcr1-NTA1* mutants. H416 (*j/HCR1*; rows 1 and 2), H428 (*j/hcr1*Δ YEplac181; rows 3 and 4), and SY73 (*j/hcr1*Δ YEp-j/hcr1-NTA1; rows 5 and 6) were transformed with either the empty vector (rows 1, 3, and 5) or the TC-overexpressing vector (rows 2, 4, and 6), and the resulting transformants were spotted in four serial 10-fold dilutions on SD medium and incubated at 30 °C for 2 days. (f) j/HCR1 with intact NTA (or only its NTD) partially suppresses the temperature-sensitive (Ts^-) phenotype of *b/prt1-rnp1*. Transformants of the strain H3674 (*b/prt1-rnp1*)[12] bearing the empty vector, YEp-j/HCR1-DS, YEp-j/hcr1-NTD, YEp-j/hcr1-CTD, and YEp-j/hcr1-NTA1, respectively, were spotted in four serial 10-fold dilutions on SD medium and incubated at 33 °C for 3 days.

Together, these experiments indicate that both halves of j/HCR1 possess an intrinsic 40S binding affinity that is additive and further strengthened by j/HCR1 contacts with 40S-bound eIF3.

Deletion of *j/HCR1* was previously shown to reduce the amounts of 40S-bound eIF3.[12] We next wished to show that the wt-like-behaving j/hcr1-NTD is also fully capable of supporting eIF3 loading onto the 40S subunit. However, the differences in the amounts of eIFs associated with 40S subunits between wt and *j/hcr1*Δ cells were somewhat smaller in our hands than those observed in the previous study. Because this discrepancy is still under examination, we could not conclusively address this question here. Nevertheless, we made two genetic observations supporting the idea that at least part of the *j/hcr1*Δ growth defect could be associated with the reduced eIF3 binding to the 40S subunit and that j/hcr1-NTD can fully substitute for full-length j/HCR1 in this respect: (i) overexpression of all three eIF2 subunits and $tRNA_i^{Met}$ (hc TC), previously shown to stimulate j/HCR1-independent 40S binding of eIF3,[4,12] partially suppressed the Slg^- phenotype of *j/hcr1*Δ cells (Fig. 2e, fourth row *versus* third row); and (ii) overexpression of j/hcr1-NTD, but not j/hcr1-CTD, suppressed the Slg^- phenotype of the *b/prt1-rnp1* mutant to the same degree as full-length wt j/HCR1 (Fig. 2f, rows 3 and 4). *b/prt1-rnp1* mutation was previously shown to affect eIF3 binding to the 40S subunit in a manner that is partially suppressible by high-copy j/HCR1 (see also the text below).[12] Interestingly, J. Lorsch and colleagues also did not observe any effect of an increased binding of eIF3 (containing only trace amounts of endogenous j/HCR1) to 43S complexes by addition of saturating amounts of separately purified j/HCR1 *in vitro* (J. Lorsch, personal communication, 2009). Taken together, this suggests that, in yeast, the effect of j/HCR1 on the binding of the rest of eIF3 to 40S subunits may be more subtle than was believed.

Genetic evidence that the NTD of j/HCR1 promotes proper selection of the AUG start codon in cooperation with eIF1A

The fact that heIF3j was suggested to govern access to the mRNA entry channel and to influence mRNA–40S subunit association during scanning and AUG recognition[15] prompted us to examine the stringency of AUG selection in *j/hcr1*Δ cells. We were interested mainly in assaying a leaky scanning defect that might suggest that the scanning preinitiation complexes have a reduced ability to switch from scanning-conducive conformation to scanning-arrested conformation when the start codon enters the P site.[30]

To investigate this, we took advantage of a reinitiation mechanism of *GCN4* translational control that can be used as an experimental tool to monitor various translational steps. Translation of *GCN4* mRNA is repressed in nutrient-replete cells by the last three of a total of four short upstream open reading frames (ORFs) in its leader. Under starvation conditions, the concentration of TC is reduced; as a result, a fraction of 40S subunits scanning downstream after terminating at the first reinitiation-permissive uORF1 rebinds TC only after bypassing inhibitory uORF2–uORF4 and then reinitiates at *GCN4*.[31] Leaky scanning leads to skipping over the AUG of uORF1 by scanning ribosomes, which subsequently initiate at downstream-inhibitory uORFs, preventing cells from derepressing *GCN4* translation under starvation conditions. This is called the general control nonderepressible (Gcn^-) phenotype and is characterized by the sensitivity of mutant cells to 3-aminotriazole (3-AT), an inhibitor of the *HIS3* product.

We found that *j/hcr1*Δ $GCN2^+$ cells exhibit significant sensitivity to 3-AT (Fig. 3a, row 3), which was further illustrated by an ~50% reduction in the derepression of the wt *GCN4-lacZ* reporter in response to 3-AT compared to wt $j/HCR1^+$ (Fig. 3b, "+"). Strikingly, examination of a *GCN4-lacZ* construct in which uORF1 is elongated and overlaps the beginning of *GCN4* revealed an ~8-fold increase in *GCN4-lacZ* expression in *j/hcr1*Δ cells (Fig. 3c, column 2). Similarly, an ~6-fold increase in *GCN4-lacZ* expression was also detected from a construct containing solitary uORF4 (Fig. 3d, column 2) that allows only a negligible level of reinitiation.[8,32] These results thus strongly suggest that deletion of *j/HCR1* impairs *GCN4* translational control by allowing a large fraction of preinitiation complexes scanning from the cap to leaky scan at the AUG of uORF1. Furthermore, the cells expressing the NTD-less j/hcr1-CTD also displayed 3-AT sensitivity (Fig. 3a, row 5) and increased *GCN4-lacZ* expression with constructs monitoring leaky scanning (Fig. 3c and d, column 3) by ~7-fold, as opposed to those expressing the CTD-less j/hcr1-NTD that increased leaky scanning only by a small margin (Fig. 3d, column 4). Hence, these results clearly suggest that the NTD is, for the most part, responsible for the j/HCR1 contribution to the stringent AUG selection.

eIF1A was shown to functionally interact with heIF3j[15] and is thought to facilitate pausing of the scanning preinitiation complexes at the correct start codon long enough to proceed with downstream initiation events—in other words, to prevent leaky scanning.[5,30] Accordingly, we observed that overexpression of eIF1A partially suppressed both Slg^- and Gcn^- phenotypes of *j/hcr1*Δ (Fig. 3f, row 2) and, most importantly, reduced leaky scanning over uORF4 by ~50% (Fig. 3e, last column). Taken together, we propose that the NTD of j/HCR1 communicates with eIF1A during scanning and promotes the eIF1A role in inducing smooth transition to closed/scanning-arrested conformation upon AUG recognition.

The overall structure of the heIF3b-$RRM_{170–274}$–heIF3$j_{35–69}$ complex

To gain a deeper insight into the collaboration between the j subunit and the b subunit of eIF3, we determined the solution structure of heIF3b-

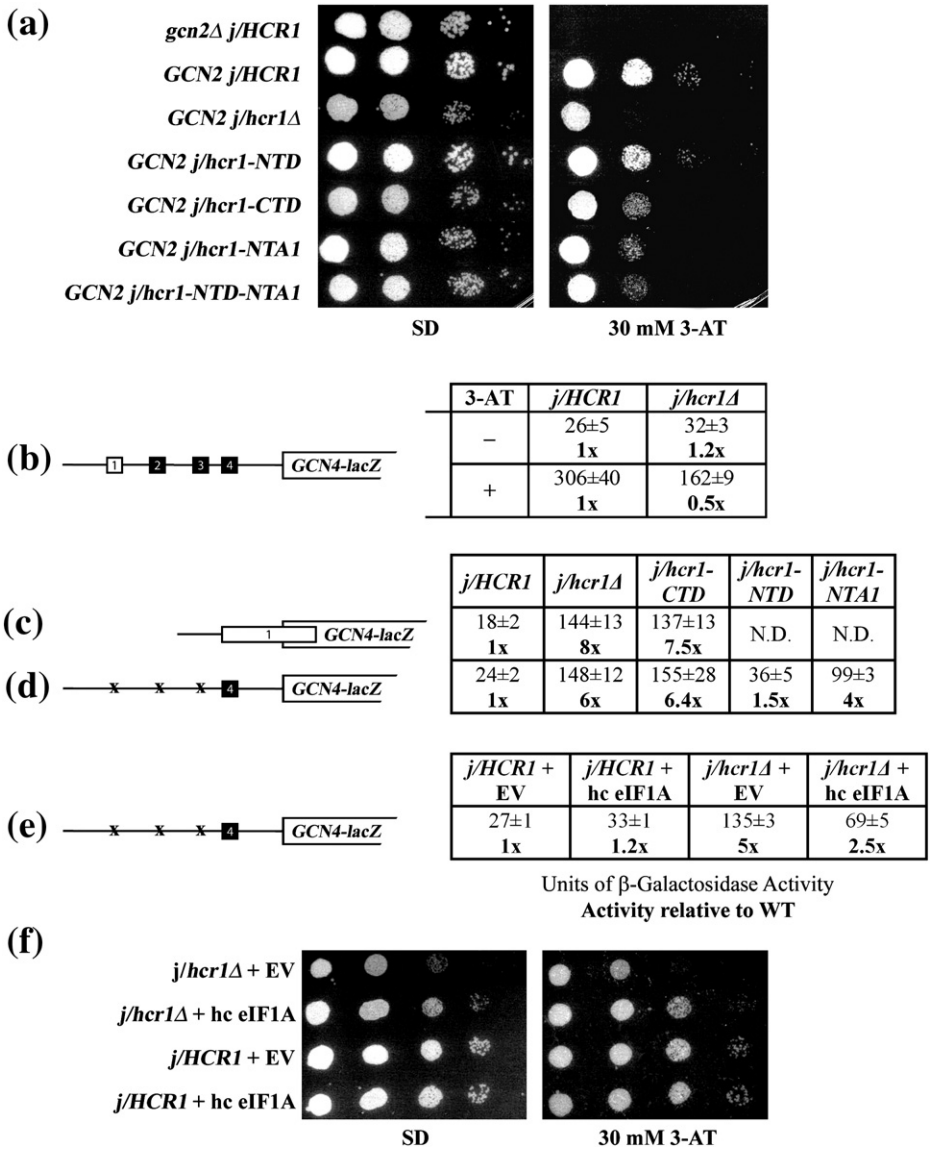

3-AT	*j/HCR1*	*j/hcr1Δ*
–	26±5 **1x**	32±3 **1.2x**
+	306±40 **1x**	162±9 **0.5x**

j/HCR1	*j/hcr1Δ*	*j/hcr1-CTD*	*j/hcr1-NTD*	*j/hcr1-NTA1*
18±2 **1x**	144±13 **8x**	137±13 **7.5x**	N.D.	N.D.
24±2 **1x**	148±12 **6x**	155±28 **6.4x**	36±5 **1.5x**	99±3 **4x**

j/HCR1 + EV	*j/HCR1* + hc eIF1A	*j/hcr1Δ* + EV	*j/hcr1Δ* + hc eIF1A
27±1 **1x**	33±1 **1.2x**	135±3 **5x**	69±5 **2.5x**

Units of β-Galactosidase Activity
Activity relative to WT

Fig. 3. Genetic evidence that the deletion of j/hcr1-NTD (or the *NTA1* mutation) prevents derepression of GCN4 translation during starvation as a result of leaky scanning that is partially suppressible by high-copy eIF1A. (a) *j/hcr1*Δ imparts a Gcn$^-$ phenotype implicating j/HCR1 in *GCN4* translational control. H418 (*gcn2*Δ *j/HCR1*; row 1) and H428 (*GCN2 j/hcr1*Δ) transformants bearing YEp-j/HCR1 (row 2), YEplac181 (row 3), YEp-j/hcr1-NTD (row 4), YEp-j/hcr1-CTD (row 5), YEp-j/hcr1-NTA1 (row 6), and YEp-j/hcr1-NTD-NTA1 (row 7), respectively, were spotted in four serial 10-fold dilutions on SD (left) or SD containing 30 mM 3-AT (right) and then incubated at 30 °C for 2 and 3 days, respectively. (b) *j/hcr1*Δ prevents full derepression of *GCN4-lacZ* expression upon starvation. Isogenic H416 (*GCN2 j/HCR1*) and H428 were transformed with p180, grown in minimal media for 6 h, and β-galactosidase activities were measured in WCEs and expressed in nanomoles of *o*-nitrophenyl-*b*-D-galactopyranoside hydrolyzed per minute per milligram of protein. To induce *GCN4-lacZ* expression, we treated transformants grown in minimal media for 2 h with 10 mM 3-AT for 6 h. The table gives means and standard deviations obtained from at least six independent measurements with three independent transformants, and activity in *j/hcr1*Δ relative to wt, respectively. (c and d) Deletion of *j/hcr1*Δ or its NTD only dramatically increases leaky scanning. H428 transformants bearing YEp-j/HCR1, YEplac181, YEp-j/hcr1-CTD, YEp-j/hcr1-NTD, and YEp-j/hcr1-NTA1, respectively, were transformed with pM226 (c) and plig102-3 (d), respectively, and analyzed as in (b), except that they were not treated with 3-AT. (e) Overexpression of eIF1A partially suppresses the leaky scanning defect of *j/hcr1*Δ. Strains H416 and H428 transformed with the empty vector and YEpTIF11 (eIF1A), respectively, were transformed with plig102-3 and analyzed as in (d). (f) Overexpression of eIF1A partially suppresses the Slg$^-$ and Gcn$^-$ phenotypes of *j/hcr1*Δ. Strains H428 and H416 transformed with the empty vector and YEpTIF11, respectively, were spotted in four serial 10-fold dilutions on SD or SD + 30 mM 3-AT and incubated at 30 °C for 2 or 4 days.

$RRM_{170–274}$ in complex with $heIF3j_{35–69}$ by high-resolution NMR spectroscopy. Stereo views of the 10 lowest-energy structures (Supplementary Fig. 1) and structural statistics (Table 1) demonstrate a well-defined complex structure with low pairwise rmsd values of 1.19±0.4 Å for heavy atoms corresponding to residues 180–266 and 45–55 of heIF3b-RRM and heIF3j, respectively. The structure of

Table 1. Structural statistics of the heIF3b-RRM$_{170–275}$–heIF3j$_{35–69}$ complex

Restraints used for structure calculations	
Total NOE distance restraints	1853
Short range (intraresidue)	966
Medium range ($1<\|i-j\|<5$)	289
Long range ($\|i-j\|>=5$)	566
Intermolecular	32
Dihedral-angle restraints (ϕ and ψ)	113
Structural statistics	
Ramachandran plot[a] (%)	
Residues in the most favored regions	71.4
Residues in additionally allowed regions	27.0
Residues in generously allowed regions	1.3
Residues in disallowed regions	0.4
rmsd of atomic coordinates (Å)	
heIF3b-RRM$_{184–268}$–heIF3j$_{45–55}$ complex	
Backbone atoms	0.726
All heavy atoms	1.192

The 10 conformers with the lowest energies were selected for statistical analysis. Because of the absence of medium-range, long-range, and intermolecular NOEs involving residues 35–44 and 58–69 of heIF3j$_{35–69}$, these residues were not included in the calculations.

[a] Based on PROCHECK-NMR analysis.

heIF3b-RRM in the complex presents a typical RRM fold consisting of two perpendicular α helices packed against a four-stranded anti-parallel β-sheet (Fig. 4a and b).[33,34] The heIF3j N-terminal peptide is unstructured in free form (data not shown) and binds heIF3b-RRM in an extended conformation on the surface opposite to the β-sheet area of heIF3b-RRM (Fig. 4b). The heIF3j binding surface on heIF3b-RRM comprises helix α1 and L5. Eleven of 35 residues (Asp45-Asp55) of the negatively charged heIF3j$_{35–69}$ peptide, which are part of its NTA, directly contact heIF3b-RRM (Fig. 4c). The total buried surface area of the protein–protein interface is 1128.4 Å^2 (501.6 Å^2 on the heIF3b-RRM peptide and 626.8 Å^2 on the heIF3j peptide). The heIF3b-RRM interaction surface is characterized by positively charged residues from helix α1 (Arg199, Lys202, Lys209, and Lys213) and L5 (Lys254) that complement and position the negatively charged heIF3j$_{35–69}$ peptide (Fig. 4c). These interactions are illustrated by intermolecular nuclear Overhauser enhancements (NOEs) that bring Lys254-Hε into close contact with Asp54-H$^{\alpha}$, Lys254-H$^{\gamma}$ into close contact with Asp54-H$^{\beta}$, Lys202-Hε into close contact with Val48-H$^{\gamma}$, and Lys209-H$^{\beta}$ into close contact with Asp45-H$^{\alpha}$, respectively (Supplementary Fig. 2b). At the center of the NTA resides the highly conserved Trp52, which establishes a series of close contacts with heIF3b-RRM (Fig. 4c). The indole ring of Trp52 fills a hydrophobic pocket formed by residues from helix α1 (Leu203, Val206, and Ile210) and L5 (Tyr253, Leu255, and Phe261) (Fig. 4d). Intermolecular NOEs involving Trp52 ring atoms, such as H$^{\delta1}$ and H$^{\zeta2}$, with Ile210 and Ile207, as well as with Tyr253 and Leu255, represent key contacts for defining the hydrophobic pocket around Trp52 (Supplementary Fig. 2b). Binding of heIF3j unfolds the β-hairpin in L5 and induces a rearrangement of helix α1 and L5, as compared to the unbound heIF3b-RRM (Fig. 4e). This creates a more compact heIF3b-RRM conformation illustrated by a closer contact between Ile210 and Tyr253, which deepens the binding pocket filled by Trp52 of heIF3j.

Mutational analysis of the heIF3b-RRM–heIF3j-NTA interaction

To assess the relative contribution of key residues to heIF3b-RRM–heIF3j complex formation, we mutated several important interface residues. Binding of four heIF3j mutants (heIF3j-N51A, heIF3j-N51A-W52A, heIF3j-W52A, and heIF3j-D50K-D53K-D57K) to heIF3b-RRM was examined using isothermal titration calorimetry (ITC). The heIF3j mutants displayed significantly lower affinities than wt heIF3j (K_d = 20.3±0.4 μM). In this assay, we were unable to detect any heIF3b-RRM binding to heIF3j-W52A, heIF3j-N51A-W52A, and heIF3j-D50K-D53K-D57K, indicating K_d values larger than 10 mM, whereas heIF3j-N51A bound with a lower K_d of 55±0.3 μM (Fig. 5a). These results agree with our complex structure showing that heIF3j-Trp52 makes crucial hydrophobic contributions to heIF3b-RRM binding and that surrounding negatively charged heIF3j-NTA residues further stabilize complex formation (Fig. 4c).

We also performed histidine pull-down assays using three heIF3b-RRM mutants (heIF3b-RRM-F261A, heIF3b-RRM-I210A, and heIF3b-RRM-Y253A) to assess the contributions of hydrophobic heIF3b-RRM residues to heIF3j binding. All three heIF3b-RRM mutants displayed significantly reduced binding compared to wt heIF3b-RRM, validating the role of the heIF3b-RRM hydrophobic pocket in heIF3j recognition (Fig. 5b and c). Interestingly, hydrophobic amino acid residues in positions Leu203, Val206, Ile210, Tyr253, and Phe261 are highly conserved among eIF3b-RRMs from other species, indicating that the heIF3b-RRM–heIF3j recognition mode is preserved in other organisms (Supplementary Fig. 3).

Molecular determinants of eIF3j–eIF3b-RRM interaction are conserved throughout evolution

To investigate whether the critical determinants of the eIF3b–eIF3j interaction in yeast are similar in nature to those in humans, we first fused both halves of j/HCR1 in j/hcr1-NTD (residues 1–135) and j/hcr1-CTD (residues 136–265) (Fig. 6b) with the GST moiety and showed that the NTD, but not the CTD, of j/HCR1 specifically interacts with the ^{35}S-labeled fragment comprising b/PRT1-RRM (Fig. 6c, lane 4 *versus* lane 5). We then substituted the Trp37 residue corresponding to the key Trp52 of heIF3j and several surrounding acidic residues from its NTA with alanines or amino acids with the opposite charge (Fig. 6b). The resulting *j/hcr1-NTA1* mutation completely abolished binding to radiolabeled b/PRT1-RRM (Fig. 6c, lane 6). Similarly, alanine and

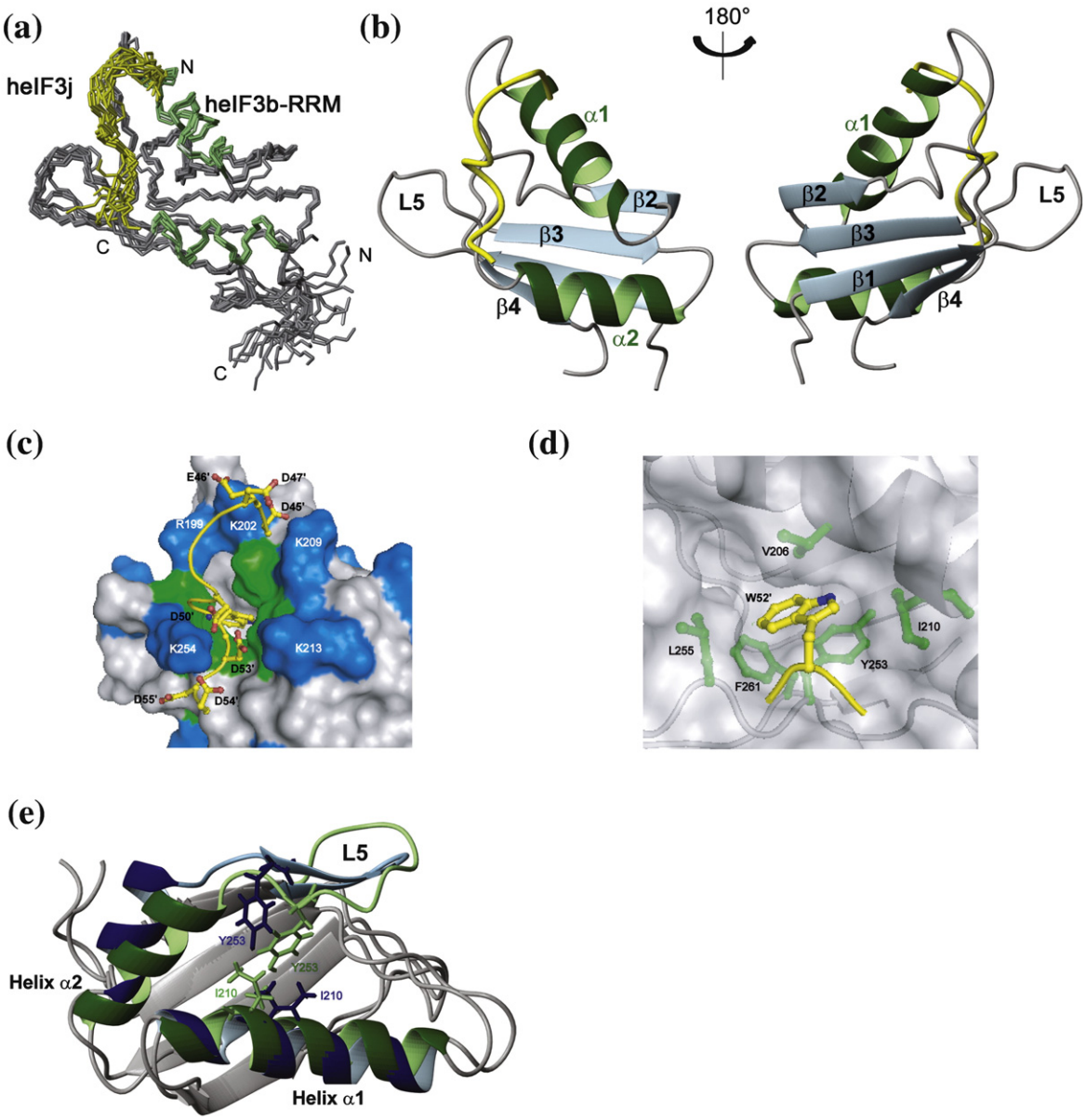

Fig. 4. Structure of the heIF3b-RRM–heIF3j complex. (a) NMR ensemble of the heIF3b-RRM–heIF3j peptide complex. The 10 lowest-energy structures between heIF3b-RRM$_{179–274}$ (gray and green) and heIF3j$_{45–55}$ (yellow) are shown. The structures were fitted using the backbone atoms C′, C$^{\alpha}$, and N of residues 184–264 of heIF3b-RRM and residues 45–55 of heIF3j. (b) Ribbon model for the lowest-energy conformer of the heIF3b-RRM (gray and green)–heIF3j (yellow) complex. Secondary structure elements of heIF3b-RRM are labeled. (c) Surface representation of contacts between the heIF3j peptide and heIF3b-RRM. Green and blue surfaces indicate hydrophobic and basic (labeled) heIF3b-RRM residues, respectively. heIF3j peptide is shown as a ribbon ball-and-stick representation, and most of its residues are numbered with primed numbers. The lowest-energy structure of heIF3b-RRM bound to the heIF3j peptide is shown. (d) Close-up view of the hydrophobic pocket binding the heIF3j peptide. heIF3b-RRM is displayed as a grayish semitransparent solvent-accessible surface with labeled hydrophobic side chains (green) shown below the surface. These residues form the walls of the hydrophobic pocket in which the aromatic ring of W52′ of the heIF3j peptide (yellow) is inserted (residues 51–53 only). (e) Comparison of the NMR structures of free heIF3b-RRM and heIF3j-bound heIF3b-RRM. The two structures are represented as ribbon models, with helices α1 and α2 and L5 shown in green for heIF3j-bound heIF3b-RRM and in blue for free heIF3b-RRM. The side chains of Y253 and I210 are shown in stick representation using the same coloring scheme to highlight closer contacts participating in a more compact conformation of heIF3b-RRM when bound to heIF3j.

opposite charge substitutions of the b/PRT1-RRM residues corresponding to critical residues in helix α1 and L5 of heIF3b in *b/prt1-α1+L5* (Fig. 6a) eliminated the interaction with GST-j/hcr1 (Fig. 6c, row 3).

To further determine whether disrupting this contact will prevent j/HCR1 association with eIF3 *in vivo*, we analyzed the formation of the entire eIF3-containing MFC in yeast cells by Ni^{2+} chelation chromatography using His_8-tagged *b/PRT1* as bait. As reported previously,[27] a fraction of a/TIF32, j/HCR1, eIF2, eIF5, and eIF1 copurified specifically with wt b/PRT1-His, but not with its untagged

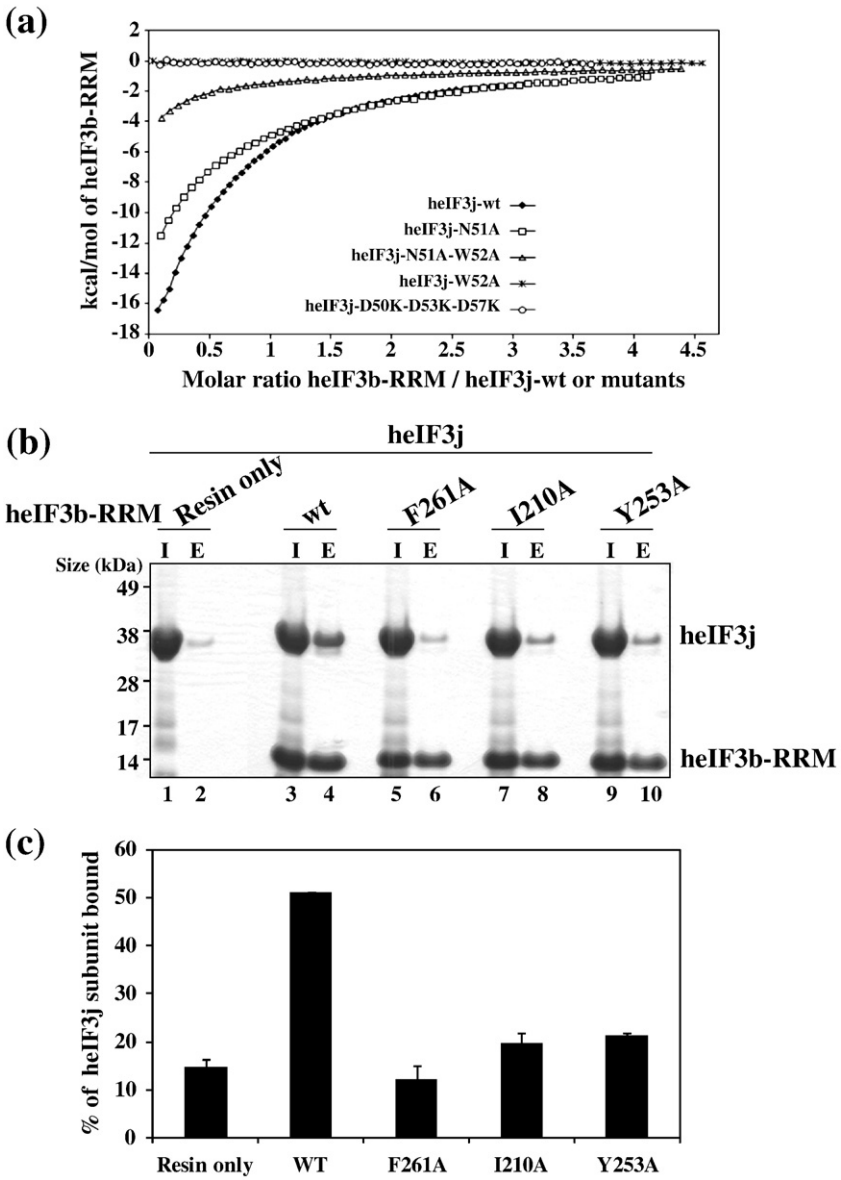

Fig. 5. Mutational analysis of the heIF3b-RRM–heIF3j-NTA interaction. (a) ITC of wt and mutant heIF3j with heIF3b-RRM. The panel shows fitted binding isotherms. Data points were obtained by integration of heat signals plotted against the molar ratio of heIF3b-RRM to wt or mutant heIF3j in the reaction cell. The continuous line represents a calculated curve using the best-fit parameters obtained by a nonlinear least-squares fit. The heIF3j construct used for each experiment is indicated in the panel. (b) Histidine pull-down assays using His_6-tagged wt or mutant heIF3b-RRM and untagged heIF3j. SDS-PAGE analysis of input (I) and eluted (E) fractions from the pull-down experiments, where the untagged heIF3j subunit was used with wt or mutant (F261A, I210A, and Y253A) heIF3b-RRM, as well as resin only as a control. (c) Quantification of the heIF3j fraction bound to heIF3b-RRM by analyzing the band intensity of the eluted fraction compared to the same band in the input fraction. Error bars represent the standard deviation between two individual experiments.

version (Fig. 7a, lanes 5–8 *versus* lanes 1–4). In sharp contrast, the *b/prt1-α1+L5* mutation (LFSK63-66AAAE_HRLF114-117AALA; Fig. 6a) specifically eliminated the association of only j/HCR1 (Fig. 7a, lanes 9–12). Similarly, the *j/hcr1-NTA1* mutation (V33A_Q35A_W37A_D38R_EEEE40-43RRRR; Fig. 6b) diminished the binding of j/HCR1 to the purified b/PRT1-His complex (Fig. 7b, lanes 9–12 *versus* lanes 5–8).

Finally, disrupting j/HCR1-NTA–b/PRT1-RRM interaction by *j/hcr1-NTA1* and *b/prt1-α1+L5* mutations, respectively, in living cells resulted in the Slg^- phenotype (Fig. 1e, row 5; Fig. 7c, row 2). No growth phenotype was observed with less extensive mutations in the *HCR1-NTA1* motif or when helix α1 and L5 of *PRT1* were mutated separately, arguing against the general refolding problems of these two motifs (data not shown).

b/prt1-α1+L5 mutation strongly affects the 40S association of eIF3

As mentioned above, the *b/prt1-rnp1* mutation substituting for the conserved residues of the RNP1

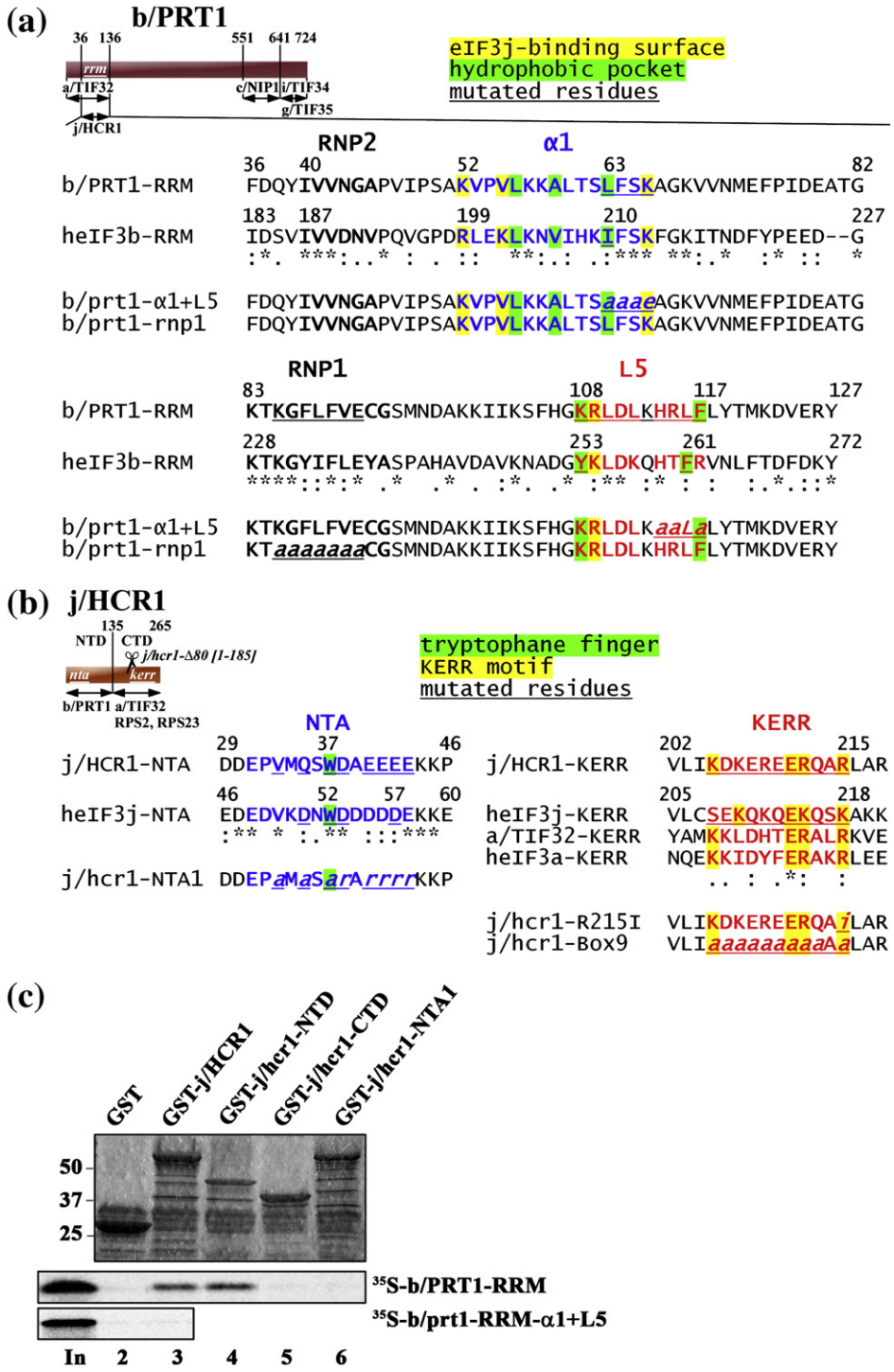

Fig. 6. Molecular determinants of the eIF3j–eIF3b-RRM interaction are evolutionary conserved. (a) Schematic of b/PRT1 showing the position of RRM (*rrm*). Arrows delimit minimal binding domains for the indicated proteins. The positions of RNPs (black), helix α1 (blue), and L5 (red) are indicated above the sequences aligned using the GCG Analysis Program. Residues corresponding to the heIF3j binding surface are highlighted in yellow; residues forming the hydrophobic pocket are highlighted in green. Underlined are b/PRT1 residues that were subjected to site-directed mutagenesis in this study or in previous studies.[12] (b) Same as in (a), except that the schematic of j/HCR1 is shown with locations of the NTA (*nta*), the C-terminal KERR motif (*kerr*), and the C-terminal truncation (*Δ80*). Sequences surrounding the NTA and KERR motifs of yeast and heIF3j or human eIF3a, respectively, are indicated. Underlined are j/HCR1 residues that were subjected to site-directed mutagenesis in this study or in previous studies.[25] The human Trp52 and the corresponding yeast Trp37 are highlighted in green; the key residues of the KERR motif are highlighted in yellow. (c) Full-length j/HCR1 (lane 3), its N-terminal domain (lane 4) or C-terminal domain (lane 5), the *NTA1* mutant (lane 6) fused to GST, and GST alone (lane 2) were tested for binding to ^{35}S-labeled wt b/PRT1-RRM [1–136] and b/PRT1-RRM-α1+L5; 10% of input amounts added to each reaction are shown in lane 1 (In).

motif forming the β3 strand of the four-stranded anti-parallel β-sheet with a stretch of alanines (Fig. 6a) eliminated j/HCR1 from the MFC[12] and severely affected the binding of the mutant form of eIF3 with the 40S subunit.[12] While this mutation occurs on the side opposite to that directly engaged in interacting with j/HCR1, based on our NMR structure,[20] it changes two amino acids in heIF3b-RRM (I233 and L235) and presumably also in b/PRT1-RRM at equivalent positions (L88 and V90), contributing to the hydrophobic core of the RRM fold. It is therefore conceivable that these substitutions interfere with proper folding; thus, the effects of *b/prt1-rnp1* cannot be directly related to the specific loss of contacts that the RRM of b/PRT1 makes. This assumption gains support from our observation that the Slg$^-$ phenotype of *b/prt1-rnp1*, but not of *b/prt1-α1+L5*, can be partially suppressed by high-copy j/HCR1 through mass action (Fig. 2f; data not shown). It is understandable that the elevated protein mass can drive the establishment of only that interaction, whose key determinants

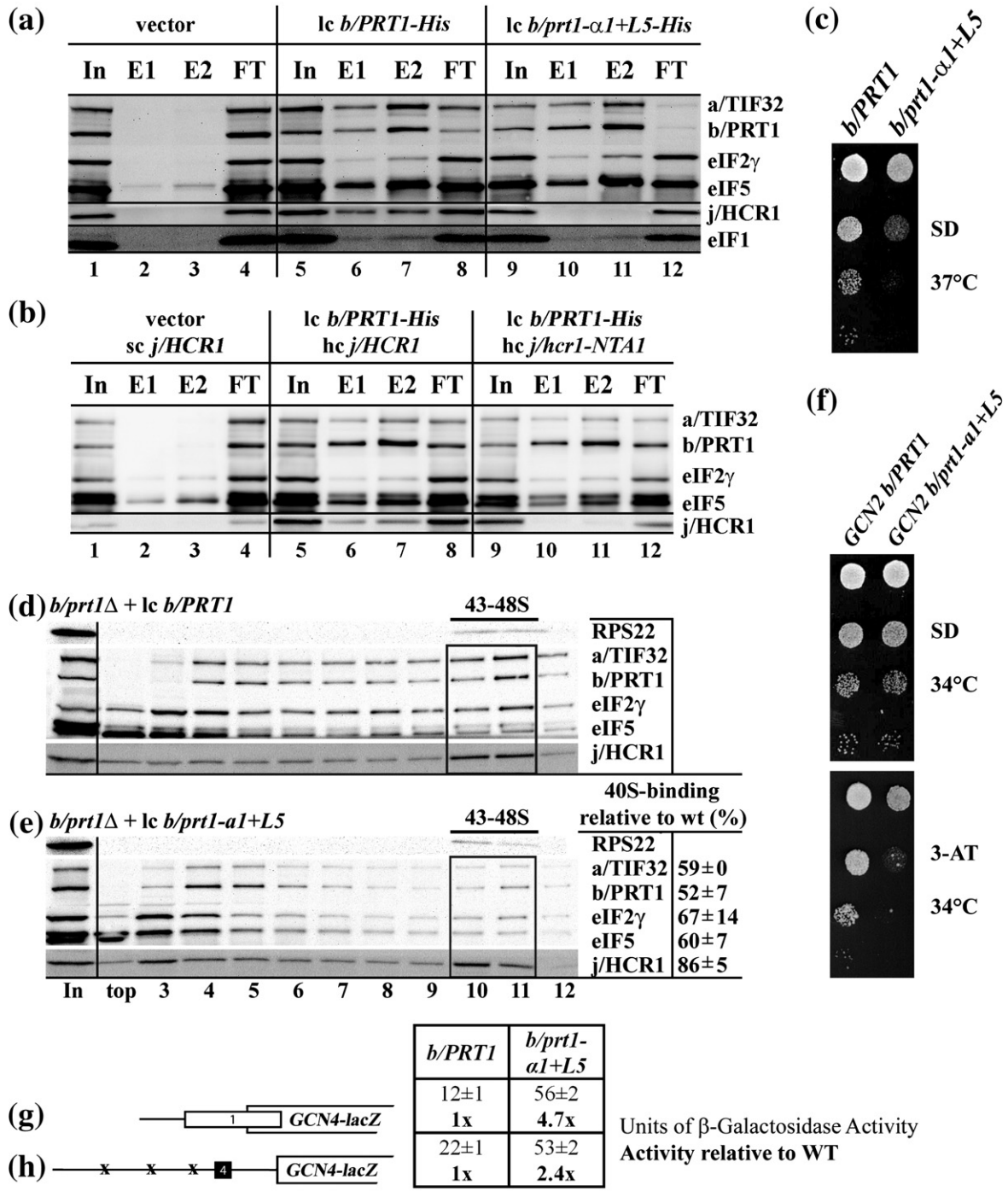

b/PRT1	*b/prt1-α1+L5*
12±1	56±2
1x	**4.7x**
22±1	53±2
1x	**2.4x**

Units of β-Galactosidase Activity
Activity relative to WT

Fig. 7 *(legend on next page)*

remain preserved in spite of potential destabilization of the protein fold.

To examine whether the *b/prt1-α1+L5* mutation specifically disrupting direct j/HCR1–b/PRT1-RRM contact also affects the 40S association of mutant eIF3, we measured the binding of selected eIF3 subunits and other MFC components to 40S subunits by formaldehyde cross-linking. We observed a relative ~45% decrease in the amounts of selected eIF3 subunits associated with 40S subunits in whole-cell extracts (WCEs) obtained from *b/prt1-α1+L5* cells compared to wt control (Fig. 7d and e, fractions 10 and 11). Similar reductions were also observed for eIF5 (~40%) and eIF2 (~35%). In keeping with our previous finding with *b/prt1-rnp1*,[12] amounts of the 40S-associated j/HCR1 were reduced only marginally (~15%). Since, under the conditions of our experiments, the data suggest that j/HCR1 does not play a key role in eIF3 association with the 40S subunit, this dramatic defect cannot be fully attributable to the loss of the j/HCR1–b/PRT1-RRM interaction, implying that helix α1 and L5 residues are most probably directly involved in bridging the 40S–eIF3 contact in yeast. Nevertheless, our observations that the *NTA1* mutation, which did not affect the 40S–eIF3 interaction (data not shown), failed to suppress the Slg^- phenotype of *b/prt1-rnp1* (Fig. 2f, last row) and that its own Slg^- phenotype was found to be partially suppressible by a plasmid overexpressing all three eIF2 subunits and $tRNA_i^{Met}$ (hc TC) (Fig. 2e, last two rows) seem to indicate that it does compromise the mild stimulatory effect of j/HCR1 on 40S binding by eIF3.

j/HCR1–b/PRT1-RRM interaction prevents leaky scanning over the AUG start codon

Our finding that the deletion of the NTD of j/HCR1 produced severe leaky scanning (Fig. 3c and d) and the fact that a modest leaky scanning defect was also observed with *b/prt1-rnp1*[12] provoked us to test whether disrupting the specific contact between j/HCR1 and b/PRT1-RRM will affect the level of leaky scanning in mutant cells. Indeed, *j/hcr1-NTA1* and *j/hcr1-NTD-NTA1* mutants displayed 3-AT sensitivity (Fig. 3a, last two rows) and greatly increased leaky scanning over uORF4 by ~4-fold (Fig. 3d, column 5). Similarly, the *b/prt1-α1+L5* mutant showed a reduced growth rate in the presence of 3-AT even at 34 °C (Fig. 7f) and also significantly increased leaky scanning over elongated uORF1 by ~4.7-fold (Fig. 7g) and over uORF4 by ~2.4-fold (Fig. 7h). Hence, these data strongly suggest that the evolutionary conserved j/HCR1-NTA–b/PRT1-RRM interaction ensures tight control over the stringent selection of the proper AUG start codon.

Discussion

NMR solution structure of the heIF3b-RRM–heIF3j-NTA interaction

eIF3 plays critical roles in virtually all stages of translation initiation, during reinitiation, in posttermination ribosomal recycling, and in the nonsense-mediated decay pathway.[8,9,35,36] In understanding how the numerous functions of eIF3 are encoded in its conserved subunits and their interactions, high-resolution structural studies of protein–protein interactions of eIF3 subunits are imminent. Using NMR spectroscopy, we revealed the first structure of an interaction among eIF3 subunits (between heIF3b-RRM and heIF3j-NTA) (Fig. 4) and showed that its disruption in yeast eliminated j/HCR1 association with MFC *in vivo* (Fig. 7). This interaction is driven by a conserved charge

Fig. 7. Destroying the hydrophobic pocket of the RRM of b/PRT1 prevents j/HCR1 association with eIF3 *in vivo*, reduces eIF3 binding to 40S subunits, and increases leaky scanning. (a and b) The NTA of j/HCR1 and helix α1 and L5 of b/PRT1-RRM are critically required for j/HCR1 association with MFC *in vivo*. (a) WCEs were prepared from H425 (*b/prt1*Δ) bearing untagged b/PRT1 (lanes 1–4), and H425 transformants with pRS-b/PRT1-His (lanes 5–8) and pRS-b/prt1-L5+α1-His (lanes 9–12) from which the untagged b/PRT1 was evicted on SD plates containing 5-fluoroorotic acid, respectively, were incubated with Ni^{2+} silica resin, and the bound proteins were eluted and subjected to Western blot analysis, with antibodies indicated on the right-hand side of individual strips. Lanes 1, 5, and 9 contained 5% of input WCEs (In); lanes 2, 6, and 10 contained 30% of fractions eluted from the resin (E1); lanes 3, 7, and 11 contained 60% of the same fractions (E2); and lanes 4, 8, and 12 contained 5% of flow-through (FT). (b) WCEs prepared from double transformants of H428 (*j/hcr1*Δ) bearing pRS315 and YCp-j/HCR1-DS-U (lanes 1–4), pRS-b/PRT1-His and YEp-j/HCR1-DS-U (lanes 5–8), or pRS-b/PRT1-His and YEp-j/hcr1-NTA1-U (lanes 9–12), respectively, were analyzed as in (a). (c–e) Mutating the hydrophobic pocket of the RRM of b/PRT1 results in the Slg^- phenotype and strongly affects the 40S association of eIF3. (c) H425 transformants as in (a) were spotted in four serial 10-fold dilutions on SD medium and incubated at 37 °C for 2 days. (d and e) H425 transformants as in (a) were grown in SD medium at 37 °C to an OD_{600} of ~1.5 and analyzed as in Fig. 3a–d, except that the resedimentation protocol was not applied. Mean proportions of the total proteins found in fractions 10 and 11 were calculated using NIH ImageJ from two independent experiments. The resulting values obtained with the indicated eIFs with the wt strain were set to 100%, and those obtained with the mutant strain were expressed as percentages of wt (SD given). (f–h) The *b/prt1*-α1+L5 mutation impairs derepression of GCN4 translation during starvation as a result of leaky scanning. (f) *b/prt1-α1+L5* imparts the Gcn^- phenotype. YAH06 (*GCN2 b/prt1*Δ) transformants carrying pRS-b/PRT1-His and pRS-b/prt1-L5+α1-His, respectively, were spotted in four serial 10-fold dilutions on SD (top) or SD containing 30 mM 3-AT (bottom) and then incubated at 34 °C for 2 and 3 days, respectively. (g and h) *b/prt1*-α1+L5 strongly increases leaky scanning. YAH06 transformants as in (f) were transformed with pM226 (g) and plig102-3 (h), respectively, and analyzed as in Fig. 5c and d.

complementarity between the subunits and an evolutionary conserved hydrophobic pocket on the backside of heIF3b-RRM, which accommodates the strictly conserved Trp residue in heIF3j-NTD (Supplementary Fig. 3). This recognition mode is also employed by the UHM family (U2AF homology motif) of noncanonical RRMs, which mediate protein–protein interactions through a conserved Arg-X-Phe motif in L5 and a negatively charged extended helix α1. UHM–ligand complexes share the crucial role of a conserved Trp residue from the ligand buried in a hydrophobic RRM pocket at the center of the protein interface, as in the case of the heIF3b-RRM–heIF3j complex,[37–39] suggesting a general mode of protein recognition by these noncanonical RRMs (Fig. 4).

eIF3j contributes to the delicate process of setting the reading frame for decoding, in cooperation with its conserved binding partner eIF3b-RRM and with eIF1A

In this study, we presented two unexpected findings on the role(s) of the j/HCR1 subunit of eIF3 in translation: (i) its NTD is sufficient to fulfill all functions of j/HCR1 needed to support the wt growth of yeast cells (Fig. 1e); and (ii) j/HCR1 is required for maintaining proper control over the AUG start codon selection, in cooperation with its binding partner b/PRT1 and with eIF1A (Fig. 3), implying that it most likely stays ribosome bound beyond mRNA recruitment, at least to the point of AUG recognition.

Consistent with the placement of heIF3j-CTD in the mRNA entry channel and ribosomal A site,[15] our *in vitro* binding assays revealed specific interactions between the CTD of j/HCR1 and RPS2 and RPS23, depending on its KERR motif (Fig. 1b and c). RPS23 is situated on the interface side under the A site, whereas RPS2 lies on the solvent side at the entry pore of the mRNA channel (Fig. 1d).[16] Placing the CTD of j/HCR1 into the mRNA entry channel suggests that the NTD of j/HCR1 most probably resides at the entry pore on the 40S solvent side, where the main body of eIF3 is thought to reside and thus where it could interact with the RRM of b/PRT1 (Fig. 1a).[14,18] (The RRM of b/PRT1 interacts with the C-terminal part of the a/TIF32 subunit,[10] which is also believed to occur near the entry pore of the mRNA binding track based on its previously reported interactions with helices h16–h18 and RPS0A.[8,14])

Given its specific location and its observed negative cooperativity with mRNA in 40S binding,[15] heIF3j was predicted to regulate access of the mRNA-binding cleft and to influence mRNA–40S subunit association during scanning and AUG recognition.[15] Our results showing that deletion of *j/HCR1* or of its NTD produces a severe leaky scanning defect (Fig. 3c and d) are in prefect agreement with this prediction and suggest that eIF3j may contribute to the stabilization of the properly formed preinitiation complexes at the start codon. A similar role in pausing scanning upon establishment of a correct initiation codon–anticodon base-pairing was proposed for eIF1A.[30] Interestingly, heIF3j showed negative cooperativity in 40S binding also with eIF1A,[15] and we indeed observed that the leaky scanning phenotype was partially (by ~50%) suppressed by overexpressing eIF1A (Fig. 3e). Furthermore, we found that destroying the specific contact between j/HCR1-NTA and b/eIF3b-RRM by *NTA1* and *α1+L5* mutations, respectively, also greatly increased leaky scanning phenotype, although not to the same extent as the deletion of the entire NTD (Figs. 3 and 7). Hence, it is conceivable that other regions of the NTD of j/HCR1 are further required for wt function. Given the fact that the b/PRT1 RRM but not j/HCR1 plays a critical role in stable eIF3 association with the 40S subunit (see the text below), these results strongly suggest that the major role of the evolutionary conserved interaction between eIF3j and eIF3b is to prevent skipping over the proper AUG start codon during scanning. Based on these observations, we propose the following model (Fig. 8).

Both terminal domains of yeast j/HCR1 make independent but synergistic interactions with the region on the 40S subunit, including the 40S mRNA entry channel, to at least partially block mRNA recruitment (Fig. 8a). It was shown that negative cooperativity between heIF3j and mRNA is neutralized upon TC recruitment to the P site, even though heIF3j remains in the mRNA-binding cleft.[15] Hence, we further propose that the recruitment of TC with other eIFs, including eIF3, may act together to clear the entry pore for mRNA recruitment, perhaps partially via establishment of j/HCR1-NTA–b/PRT1-RRM interaction (Fig. 8b). Upon commencement of scanning, eIF3j/HCR1, in cooperation with eIF3b/PRT1-RRM, most probably makes an indirect functional contact with eIF1A that could influence the conformation and activity of eIF1A in helping to decode the initiation codon in a way that would prevent leaky scanning, possibly by prompt switching to the scanning-arrested conformation when the start codon has entered the P site (Fig. 8c).

j/HCR1 was previously shown to stimulate 40S binding by eIF3 *in vivo*[12] and by its human orthologue *in vitro*.[7,22,28] Our *in vivo* formaldehyde cross-linking experiments (Fig. 2), combined with unpublished *in vitro* 40S–eIF3±j binding data from J. Lorsch's laboratory (J. Lorsch, personal communication, 2009), however suggest that this stimulatory activity of j/HCR1 might not be as strong as initially thought. With respect to this, the strong requirement of heIF3j for bringing purified eIF3 to the 40S subunit seems to indicate that yeast and human j subunits differ in the extent of this stimulation. Nevertheless, given the fact that the heIF3j requirement for 40S binding by eIF3 was suppressed by the TC, eIF1, eIF1A, or single-stranded RNA or DNA cofactors,[7,28] the physiological significance of these *in vitro* observations with heIF3j will require careful examination in living mammalian cells.

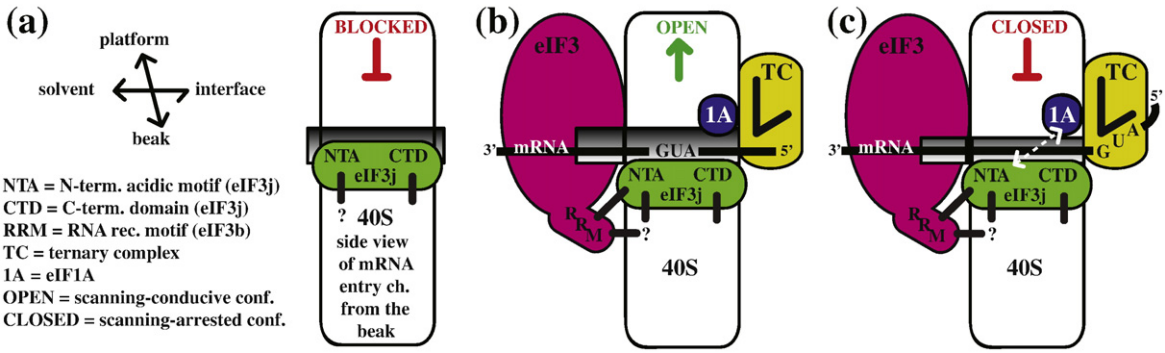

Fig. 8. eIF3j/HCR1 cooperates with eIF3b/PRT1 and eIF1A to ensure stringent selection of the AUG start codon. (a) In the absence of eIFs, eIF3j/HCR1 occupies the mRNA entry channel to at least partially block mRNA recruitment. (b) Recruitment of TC and eIF3 that interacts with the NTA of eIF3j/HCR1 via the RRM of eIF3b/PRT1 clears the mRNA entry channel, so that the ribosome can adopt the open/scanning-conducive conformation for mRNA recruitment. (c) Upon AUG recognition, eIF3j/HCR1, in cooperation with eIF3b/PRT1-RRM, functionally interacts with eIF1A to stimulate prompt switching to the closed/scanning-arrested conformation. Black thick lines represent direct interactions; the dotted line with arrowheads indicates functional interaction between eIF3j/HCR1 and eIF1A.

Unlike the *j/hcr1-NTA1* mutation, mutation of the conserved hydrophobic pocket residues in *b/prt1-α1+L5* dramatically reduced 40S occupancy by eIF3 and its associated eIFs *in vivo* (Fig. 7e). These findings strongly indicate that this activity of the b/PRT1-RRM region comprising the hydrophobic pocket is independent of its contact with the NTA of j/HCR1. Hence, we propose that the RRM features helix α1 and L5, in addition to preventing leaky scanning by interacting with j/HCR1, most likely also form an important intermolecular bridge between eIF3 and the 40S subunit (Fig. 8b) such as that created by the NTD of a/TIF32 and RPS0a.[8,14]

Finally, it is noteworthy that the expression of j/hcr1-NTD or CTD alone suppressed the 40S biogenesis defect of *j/hcr1*Δ cells[27] only partially (S.W. and L.V., unpublished observations), implying that the full-length j/HCR1 is needed for optimal function. Since j/hcr1-NTD fully supports wt growth, we find it highly unlikely for the 40S biogenesis defect to significantly contribute to *j/hcr1*Δ growth defects.

Materials and Methods

Construction of yeast strains and plasmids

To create SY73, we introduced H428 with YEp-j/hcr1-NTA1, and we selected the resulting transformants on media lacking leucine.

YAH06 was generated by a genetic cross of H426 (Table 2; same as H425 only MAT'alpha') and H428 (Table 2).[12] After tetrad dissection, spores with the slow-growth phenotype suppressible by *j/HCR1*, resistant to 3-AT, unable to grow on media containing 5-fluoroorotic acid, and autotrophic for tryptophan were selected.

A list of all PCR primers named below can be found in Supplementary Table 1:

pGEX-j/hcr1-NTD was made by inserting the BamHI-SalI-digested PCR product obtained with primers AD GST-HCR1 and AH-GST-HCR1-NTD-R, using the template pGEX-j/HCR1, into BamHI-SalI-digested pGEX-5X-3.

pGEX-j/hcr1-CTD was made by inserting the BamHI-SalI-digested PCR product obtained with primers AH-GST-HCR1-CTD and AD GST-HCR1-R, using the template pGEX-j/HCR1, into BamHI-SalI-digested pGEX-5X-3.

pGEX-j/hcr1-NTA1 was made by inserting the BamHI-SalI-digested PCR product obtained with primers AD GST-HCR1 and AD GST-HCR1-R, using the template YEp-j/hcr1-NTA1 (see the text below), into BamHI-SalI-digested pGEX-5X-3.

pT7-b/prt1-rrm-α1+L5 was made by inserting the NdeI-HindIII-digested PCR product obtained with primers LVPNDEI-724 and LVPC136-724, using the template pRS-b/prt1-L5+α1-His (see the text below), into NdeI-HindIII-digested pT7-7.[40]

pGEX-j/hcr1-BOX9 was made by inserting the BamHI-SalI-digested PCR product obtained with primers AD GST-HCR1 and AD GST-HCR1-R, using the template YEp-j/hcr1-BOX9 (see the text below), into BamHI-SalI-digested pGEX-5X-3.

pGEX-j/hcr1-Δ80 was made by inserting the BamHI-NcoI-digested PCR product obtained with primers AD GST-HCR1 and HCR1-80-NcoI-R, using the template YEp-j/HCR1-DS, into BamHI-NcoI-digested pGEX-5X-3.

pGEX-RPS2 was made by inserting the BamHI-SalI-digested PCR product obtained with primers RPS2-f

Table 2. Yeast strains used in this study

Strain	Genotype	Source or reference
H416[a]	*MATa leu2-3,112 ura3-52*	Nielsen *et al.*[12]
H417[a]	*MATa leu2-3,112 ura3-52 trp1*Δ	Nielsen *et al.*[11]
H425[a]	*MATa leu2-3,112 ura3-52 trp1*Δ *b/prt1*: :*hisG gcn2*: :*hisG (lc b/PRT1 URA3)*	Nielsen *et al.*[12]
H428[a]	*MATa leu2-3, 112 ura3-52 j/hcr1*Δ	Nielsen *et al.*[12]
SY73[a]	*MATa leu2-3, 112 ura3-52 j/hcr1*Δ *(hc j/hcr1-NTA1 LEU2)*	This study
YAH06	*MATa leu2-3,112 ura3-52 trp1*Δ *b/prt1*: :*hisG GCN2 (lc b/PRT1 URA3)*	This study
H3674[a]	*MATa leu2-3, 112 ura3-52 b/prt1-rnp1*	Nielsen *et al.*[12]

[a] Isogenic strains.

and RPS2-r, using the template pGBKT7-RPS2,[14] into BamHI-SalI-digested pGEX-5x-3.
pGBK-T7-RPS23 was made by inserting the BamHI-PstI digested PCR product obtained with primers RPS23-f and RPS23-r, using the template pGBKRPS23,[14] into BamHI-PstI cleaved pGBKT7 (Novagen).

To construct pRS-b/PRT1-HisXS, we used a pair of primers (AH-PRT1-BamHI and AH-PRT1-NotI-R), with pRSPRT1-His-LEU[12] as template. The PCR product thus obtained was digested with BamHI-NotI and inserted into BamHI-NotI-cleaved pRSPRT1-His-LEU. This subcloning step was performed to remove the second XbaI and SpeI sites immediately following the stop codon of b/PRT1 to facilitate subcloning of the RRM mutants.

pRS-b/prt1-L5+α1-His was constructed in two steps. First, two pairs of primers (AH-PRT1-ApaI and LV-RRM-AALA-R, and LV-RRM-AALA-R and AH-PRT1-XbaI-R) were used, with pRS-b/PRT1-HisXS as template. The PCR products thus obtained were used in a 1:1 ratio as templates for a third PCR amplification with primers AH-PRT1-ApaI and AH-PRT1-XbaI-R. The resulting PCR product was digested with ApaI-XbaI and inserted into ApaI-XbaI-cleaved pRS-b/PRT1-HisXS, producing pRS-b/prt1-AALA-His. In the second step, pRS-b/prt1-AALA-His was used as template for PCR with two pairs of primers: AH-PRT1-ApaI and AH-PRT1-A1B-R, and AH-PRT1-A1B and AH-PRT1-XbaI-R. The PCR products thus obtained were used in a 1:1 ratio as templates for a third PCR amplification with primers AH-PRT1-ApaI and AH-PRT1-XbaI-R. The resulting PCR product was digested with ApaI-XbaI and inserted into ApaI-XbaI-cleaved pRS-b/PRT1-HisXS.

YEp-j/HCR1-DS was constructed using the QuikChange® Multi Site-Directed Mutagenesis Kit (Stratagene) in accordance with the vendor's instructions. In step 1, PCR was performed with the kit-provided enzyme blend using primers DS HCR1-BHI and DS HCR1-NcoI, and YEpHCR1[26] as template. This subcloning step was performed to introduce the BamHI site immediately preceding the AUG start codon and the NcoI sites immediately following the stop codon of *j/HCR1* to facilitate subcloning of the j/HCR1 mutants.

YCp-j/HCR1-DS-U was constructed by inserting the 1289-bp HindIII-SacI fragment from YEp-j/HCR1-DS into YCpLVHCR1-U,[26] digested with HindIII-SacI.

YEp-j/HCR1-DS-U was constructed by inserting the 1289-bp HindIII-SacI fragment from YEp-j/HCR1-DS into YEplac195,[41] digested with HindIII-SacI.

YEp-j/hcr1-BOX9 was generated by fusion PCR. The following pairs of primers were used for separate PCR amplifications, using YEp-j/HCR1-DS as template: (1) DS HCR1-BHI and AH-HCR1-BOX+9-R; and (2) AH-HCR1-BOX+9 and AH-HCR1-NcoI-R. The PCR products thus obtained were used in a 1:1 ratio as templates for a third PCR amplification using primers DS HCR1-BHI and AH-HCR1-NcoI-R. The resulting PCR product was digested with BamHI and NcoI and ligated with BamHI-NcoI-cleaved YEp-j/HCR1-DS (replacing wt j/HCR1 with j/hcr1-BOX9).

YEp-j/hcr1-NTA1 was generated by fusion PCR. The following pairs of primers were used for separate PCR amplifications, using YEp-j/HCR1-DS as template: (1) DS HCR1-BHI and HCR1-NTA4-R; and (2) SW-HCR1-NTA2+4 and AH-HCR1-NcoI-R. The PCR products thus obtained were used in a 1:1 ratio as templates for a third PCR amplification using primers DS HCR1-BHI and AH-HCR1-NcoI-R. The resulting PCR product was digested with BamHI and NcoI and ligated with BamHI-NcoI-cleaved YEp-j/HCR1-DS (replacing wt *j/HCR1* with *j/hcr1-NTA1*).

YEp-j/hcr1-NTA1-U was constructed by inserting the 1289-bp HindIII-SacI fragment from YEp-j/hcr1-NTA1 into YEplac195,[41] digested with HindIII-SacI.

YEp-j/hcr1-NTD was constructed in two steps. First, the 817-bp insert obtained by digestion of pGEX-j/hcr1-NTD with BamHI and NotI was ligated into BamHI-NotI-cleaved pRS303.[42] The resulting plasmid was then cut with BamHI-SacI, and the insert containing *j/hcr1-NTD* was used to replace the full-length *j/HCR1* in the BamHI-SacI-cut YEp-j/HCR1-DS.

YEp-j/hcr1-CTD was made by inserting the BamHI-NcoI-digested PCR product obtained with primers AH-GST-HCR1-CTD and AH-HCR1-NcoI-R, using YEp-j/HCR1-DS as template, into BamHI-NcoI-cut YEp-j/HCR1-DS (replacing wt *j/HCR1* with *j/hcr1-CTD*).

YEp-j/hcr1-NTD-NTA1 was made by inserting the BamHI-NcoI-digested PCR product obtained with primers DS HCR1-BHI and SW HCR1-NTD-NcoI-R, using YEp-j/hcr1-NTA1 as template, into BamHI-NcoI-cut YEp-j/HCR1-DS (replacing wt *j/HCR1* with *j/hcr1-NTD-NTA1*).

Yeast biochemical methods

GST pull-down experiments with GST fusions and *in-vitro*-synthesized ^{35}S-labeled RPS2, RPS23a, j/hcr1-NTD, j/hcr1-CTD, and b/PRT1-RRM polypeptides (see Table 3 for vector descriptions) were conducted as follows. Individual GST fusion proteins were expressed in *Escherichia coli*, immobilized on glutathione-Sepharose beads, and incubated with 10 μl of ^{35}S-labeled potential binding partners at 4 °C for 2 h. The beads were washed three times with 1 ml of phosphate-buffered saline, and bound proteins were separated by SDS-PAGE. Gels were first stained with Gelcode Blue Stain Reagent (Pierce) and then subjected to autoradiography. (GST-RPS23 could not be tested due its insolubility in bacterial lysates.) Ni^{2+} chelation chromatography of eIF3 complexes containing His-tagged b/PRT1 from yeast WCEs and Western blot analysis were conducted as described in detail previously.[48] In short, WCEs were incubated with 4 μl of 50% Ni^{2+}-NTA-silica resin (Qiagen) suspended in 200 μl of buffer A for 2 h at 4 °C, followed by washing and elution. Fractionation of native preinitiation complexes in WCEs from HCHO cross-linked cells through sucrose gradients, including resedimentation analysis, were carried out in accordance with Valášek *et al.*[29]

NMR spectroscopy

NMR experiments were performed on Bruker AMX500 or AVANCE800 spectrometers equipped with cryoprobes and on a Bruker DMX600 spectrometer. ^{1}H, ^{13}C, and ^{15}N chemical shifts assignment was achieved by means of through-bond heteronuclear scalar correlations, with standard pulse sequences recorded on either ^{13}C/^{15}N-labeled heIF3b-RRM complexed with the heIF3j peptide or ^{13}C/^{15}N-labeled heIF3j peptide complexed with heIF3b-RRM in NMR buffer [20 mM deuterated–Tris (pH 7.5) and 100 mM NaCl] containing 10% $^{2}H_2O$. Acquisition of NOEs was accomplished using a series of standard three-dimensional (3D) heteronuclear experiments. Intermolecular NOEs between the heIF3b-RRM domain and the heIF3j peptides (long = residues 1–69 of heIF3j, with a deletion of six of seven nonconserved N-terminal alanine residues in accordance with ElAntak *et al.*,[20] or short = residues 35–69 of heIF3j) were obtained

Table 3. Plasmids used in this study

Plasmid	Description	Source or reference
pGEX-5X-3	Cloning vector for GST fusions	Smith and Johnson[43]
pGEX-j/HCR1	GST-j/hcr1 fusion plasmid from pGEX-5X-3	Valášek *et al.*[25]
pGEX-j/hcr1-NTD	GST-j/hcr1-NTD [1–135] fusion plasmid from pGEX-5X-3	This study
pGEX-j/hcr1-CTD	GST-j/hcr1-CTD [136–265] fusion plasmid from pGEX-5X-3	This study
pGEX-j/hcr1-NTA1	GST-j/hcr1-NTA1 fusion plasmid from pGEX-5X-3	This study
pT7-b/PRT1-RRM (ΔA)	*b/PRT1* [1–136] ORF cloned under T7 promoter	Valášek *et al.*[25]
pT7-b/prt1-rrm-α1 + L5	*b/PRT1* [1–136] ORF containing the *α1 + L5* mutation cloned under T7 promoter	This study
pGEX-j/hcr1-BOX9	GST-j/hcr1-BOX9 fusion plasmid from pGEX-5X-3	This study
pGEX-j/hcr1-Δ80	GST-j/hcr1-Δ80 [1–185] fusion plasmid from pGEX-5X-3	This study
pGBK-T7-RPS2	*RPS2* ORF cloned into pGBKT7, *TRP1* (Clontech)	Valášek *et al.*[14]
pGBK-T7-RPS23	*RPS23* ORF (without intron) cloned into pGBKT7, *TRP1* (Clontech)	This study
pGEX-RPS2	GST-RPS2 fusion plasmid from pGEX-5X-3	This study
pRS-b/PRT1-HisXS	Low-copy wt *b/PRT1* in *LEU2* plasmid from pRS315	This study
pRS-b/prt1-L5 + α1-His	Low-copy *b/PRT1* containing the *α1 + L5* mutation in *LEU2* plasmid from pRS315	This study
YEplac181	High-copy cloning vector, *LEU2*	Gietz and Sugino[41]
YEplac195	High-copy cloning vector, *URA3*	Gietz and Sugino[41]
YEp-j/HCR1-DS	High-copy wt *j/HCR1* coding region flanked by BamHI and NcoI sites, respectively, in *LEU2* plasmid from YEplac181	This study
YCp-j/HCR1-DS-U	Low-copy wt *j/HCR1* in *URA3* plasmid from YCplac33	This study
YEp-j/HCR1-DS-U	High-copy wt *j/HCR1* coding region flanked by BamHI and NcoI sites, respectively, in *URA3* plasmid from YEplac195	This study
YEp-j/hcr1-NTA1	High-copy *j/HCR1* containing the *NTA1* mutation in *LEU2* plasmid from YEplac181	This study
YEp-j/hcr1-NTA1-U	High-copy *j/HCR1* containing the *NTA1* mutation in *URA3* plasmid from YEplac195	This study
YEp-j/hcr1-NTD	High-copy *j/hcr1-NTD* [1–135] in *LEU2* plasmid from YEplac181	This study
YEp-j/hcr1-CTD	High-copy *j/hcr1-CTD* [136–265] in *LEU2* plasmid from YEplac181	This study
YEp-j/hcr1-NTD-NTA1	High-copy *j/hcr1-NTD* [1–135] containing the *NTA1* mutation in *LEU2* plasmid from YEplac181	This study
YEplac24	High-copy cloning vector, URA3	Botstein *et al.*[44]
p1780-IMT	High-copy *SUI2*, *SUI3*, *GCD11*, *IMT4*, and *URA3* plasmid from YEp24	Asano *et al.*[45]
p180 (YCp50-GCN4-lacZ)	Low-copy *URA3* vector containing wt *GCN4* leader	Mueller and Hinnebusch[46]
pM226	Derivative of pM199; ORF of uORF1 extends into the *GCN4-lacZ* coding region	Grant *et al.*[32]
plig102-3	Low-copy *URA3* vector with *GCN4* leader point mutations containing uORF4 only at its original position in front of the *GCN4-lacZ* coding region	Grant *et al.*[32]
pDSO22	High-copy *TIF11* (eIF1A), *URA3* plasmid from YEplac195	Olsen *et al.*[47]

from two-dimensional (2D) and 3D ^{13}C-filtered NOE spectroscopy (NOESY) experiments recorded on ^{13}C/^{15}N-labeled heIF3b-RRM complexed with the long or short heIF3j peptide and on the long or short ^{13}C/^{15}N-labeled heIF3j peptide complexed with heIF3b-RRM in a 100% $^{2}H_2O$ solution. Comparison of the intermolecular NOE pattern for the short and long heIF3j peptides revealed no significant differences; more importantly, no additional NOEs could be observed with the longer peptide. Therefore, the heIF3b-RRM complex with the shorter heIF3j peptide was chosen for high-resolution structure determination. All NMR samples were prepared in 20 mM deuterated Tris (pH 7.5) and 100 mM NaCl. The concentrations were 0.7 mM for the heIF3b-RRM domain, with the heIF3j peptides added at a concentration of 0.7–1.0 mM in order to saturate the heIF3b-RRM domain with the long or short heIF3j peptide. All spectra were recorded at 25 °C.

Structure calculation

The structure of the heIF3b-RRM–heIF3j$_{35–69}$ peptide complex was calculated using the program CYANA.[49] One thousand eight hundred fifty-three NOE-based distances derived from 3D heteronuclear NOESY experiments, as well as 113 dihedral-angle restraints (ϕ and ψ) obtained by an analysis of N, H^{α}, C^{α}, and C^{β} chemical shift values using the TALOS program,[50,51] were used in structure calculations. Seven iterations for structural calculations and distance restraint assignment were run with CYANA. One hundred structures were calculated, and the 10 structures having the lowest energies were adopted. These structures were then water refined in a minimization run using the SANDER module of AMBER 9.0.[52] The quality of each structure was assessed using the program PROCHECK-NMR.[53] A list of all restraints and structural statistics is presented in Table 1. Figures were prepared using the programs PyMOL‡ and MOLMOL.[54]

NMR structure determination of the heIF3b-RRM$_{170–274}$–heIF3j$_{35–69}$ complex

The N-terminal heIF3j$_{35–69}$ fragment of heIF3j displays the same binding mode as both full-length heIF3j and the larger N-terminal heIF3j$_{1–69}$ peptide, displaying very similar chemical shift perturbations in heIF3b-RRM[20] (Supplementary Fig. 2a). More importantly, the same binding mode of both N-terminal heIF3j fragments was

‡ http://pymol.sourceforge.net/

evidenced by virtually identical intermolecular NOEs of 11 residues surrounding Trp52 (Supplementary Fig. 2b). The structure of the complex was solved using 1916 experimental restraints that consist of 1853 distance restraints derived from NOE data, including 32 intermolecular NOEs extracted from isotope-filtered 2D and 3D experiments. In addition, 113 dihedral-angle restraints (ϕ and ψ angle restraints) were included from the analysis of $^{13}C^{\alpha/\beta}$ chemical shifts using the program TALOS.[51] Out of 100 calculated structures, the 10 lowest-energy structures having the best agreement with experimental restraints were subsequently refined in explicit solvent to improve the local geometry, electrostatics, and packing quality of the complex. Stereo views of the 10 lowest-energy structures (Supplementary Fig. 1) and structural statistics (Table 1) demonstrate a well-defined complex structure with low pairwise rmsd values of 1.19±0.4 Å for heavy atoms, corresponding to residues 180–266 and 45–55 of heIF3b-RRM and heIF3j, respectively.

Preparation of human proteins

His-tagged heIF3b-RRM domain and heIF3j subunit were constructed as described previously[20] and transformed in *E. coli* BL21(DE3) cells. Cultures for heIF3b-RRM, heIF3j, and their mutants were grown at 37 °C, and protein overexpression was induced by addition of 1 mM IPTG at an A_{600} of 0.8. Cells were harvested 3 h after induction. For isotope labeling, minimal media containing $^{15}NH_4Cl$ and [^{13}C]glucose were used. All protein samples were purified over a nickel-chelating column (HiTrap; Amersham Biosciences), and this was followed by TEV protease cleavage for His-tag removal. The reaction mixture was then reloaded on a HiTrap chelating column charged with nickel sulfate to remove all of the TEV protease, the His tag, and minor contaminating proteins. After purification, the proteins were exchanged with appropriate buffer for subsequent experiments and further concentrated.

Preparation of heIF3j peptide

A DNA fragment encoding the heIF3j peptide sequence (residues 35–69) was prepared by PCR from full-length heIF3j plasmid DNA, digested with NdeI and EcoRI, and ligated into a modified pET28a vector (containing an N-terminal His_6 tag fused to a lipoyl domain,[55] followed by a TEV cleavage site and the standard pET28a multiple cloning site; Novagen) digested with the same enzymes. *E. coli* BL21(DE3) cells were transformed with the heIF3j peptide construct and grown at 37 °C in rich LB medium or minimal media containing $^{15}NH_4Cl$ and [^{13}C]glucose for production of unlabeled or labeled peptide, respectively. Protein overexpression was induced by addition of 1 mM IPTG at an A_{600} of 0.8. The heIF3j peptide fused to lipoyl domain was purified over a nickel-chelating column. TEV protease was then used to separate the heIF3j peptide from the lipoyl domain. Isolation of the heIF3j peptide required loading on a nickel-chelating column. This was followed by ion exchange (HiTrap DEAE; Amersham Biosciences) for further purification of the peptide.

ITC experiments

All calorimetric titrations were performed on a VP-ITC microcalorimeter (MicroCal). Protein samples were extensively dialyzed against the ITC buffer containing 20 mM Hepes (pH 7.5) and 200 mM NaCl. All solutions were filtered using membrane filters (pore size, 0.2 μm) and thoroughly degassed for 20 min by gentle stirring under argon. The sample cell was filled with a 50 μM solution of full-length heIF3j wt or mutants and an injection syringe with 1 mM titrating heIF3b-RRM. Each titration typically consisted of a preliminary 2.5-μl injection, followed by 58 subsequent 5-μl injections every 210 s. All experiments were performed at 25 °C. Data for the preliminary injection, which are affected by diffusion of the solution from and into the injection syringe during the initial equilibration period, were discarded. Binding isotherms were generated by plotting heats of reaction normalized by moles of injectant *versus* the ratio of total injectant to total protein per injection. The data were fitted using Origin 7.0 (MicroCal).

Pull-down experiments

His_6-tagged heIF3b-RRM (wt and mutants) and untagged full-length heIF3j subunit were prepared as described above and buffer exchanged in equilibration buffer [50 mM sodium phosphate (pH 8) and 100 mM NaCl]. Each His_6-heIF3b-RRM construct was incubated with unlabeled heIF3j (final concentration of each protein, 30 μM) for 15 min at room temperature and loaded on His-select spin columns (Sigma) equilibrated with equilibration buffer. After two washing steps with equilibration buffer containing 5 mM imidazole, proteins were eluted with elution buffer [50 mM sodium phosphate (pH 8), 100 mM NaCl, and 250 mM imidazole]. The eluted proteins were resolved by denaturating gel electrophoresis and visualized by staining with InstantBlue (Novexin). The percentage of heIF3j-bound fraction was evaluated by measuring band intensities with the NIH ImageJ program.

Accession number

The coordinates of the complex have been deposited into the Protein Data Bank under accession code 2KRB.

Acknowledgements

We are thankful to Alan G. Hinnebusch for critical reading of the manuscript; Jon R. Lorsch for communicating the results prior to publication; the members of the Valášek, Lukavsky, and Krásný laboratories for helpful comments; Ji-Chun Yang for assistance with NMR data collection; Andreas G. Tzakos for help with the structure calculation and expression of mutant proteins; and Olga Krydová and Ilona Krupičková for technical and administrative assistance. This research was supported by The Wellcome Trusts grant 076456/Z/05/Z, National Institutes of Health research grant R01 TW007271 funded by Fogarty International Center, Fellowship of Jan E. Purkyne from the Academy of Sciences of the Czech Republic, Institutional Research Concept AV0Z50200510 (to L.V.), and the Medical Research Council (to P.J.L.).

Supplementary Data

Supplementary data associated with this article can be found, in the online version, at doi:10.1016/j.jmb.2009.12.047

References

1. Hinnebusch, A. G., Dever, T. E. & Asano, K. A. (2007). Mechanism of translation initiation in the yeast *Saccharomyces cerevisiae*. In (Sonenberg, N., Mathews, M. & Hershey, J. W. B., eds), pp. 225–268, Cold Spring Harbor Laboratory Press, Cold Spring Harbor, NY.
2. Pestova, T. V., Lorsch, J. R. & Hellen, C. U. T. (2007). The mechanism of translation initiation in eukaryotes. In (Sonenberg, N., Mathews, M. & Hershey, J. W. B., eds), pp. 87–128, Cold Spring Harbor Laboratory Press, Cold Spring Harbor, NY.
3. Passmore, L. A., Schmeing, T. M., Maag, D., Applefield, D. J., Acker, M. G., Algire, M. A. *et al.* (2007). The eukaryotic translation initiation factors eIF1 and eIF1A induce an open conformation of the 40S ribosome. *Mol. Cell*, **26**, 41–50.
4. Jivotovskaya, A., Valášek, L., Hinnebusch, A. G. & Nielsen, K. H. (2006). Eukaryotic translation initiation factor 3 (eIF3) and eIF2 can promote mRNA binding to 40S subunits independently of eIF4G in yeast. *Mol. Cell. Biol.* **26**, 1355–1372.
5. Mitchell, S. F. & Lorsch, J. R. (2008). Should I stay or should i go? Eukaryotic translation initiation factors 1 and 1a control start codon recognition. *J. Biol. Chem.* **283**, 27345–27349.
6. Valášek, L., Nielsen, K. H., Zhang, F., Fekete, C. A. & Hinnebusch, A. G. (2004). Interactions of eukaryotic translation initiation factor 3 (eIF3) subunit NIP1/c with eIF1 and eIF5 promote preinitiation complex assembly and regulate start codon selection. *Mol. Cell. Biol.* **24**, 9437–9455.
7. Unbehaun, A., Borukhov, S. I., Hellen, C. U. & Pestova, T. V. (2004). Release of initiation factors from 48S complexes during ribosomal subunit joining and the link between establishment of codon–anticodon base-pairing and hydrolysis of eIF2-bound GTP. *Genes Dev.* **18**, 3078–3093.
8. Szamecz, B., Rutkai, E., Cuchalova, L., Munzarova, V., Herrmannova, A., Nielsen, K. H. *et al.* (2008). eIF3a cooperates with sequences 5′ of uORF1 to promote resumption of scanning by post-termination ribosomes for reinitiation on GCN4 mRNA. *Genes Dev.* **22**, 2414–2425.
9. Hinnebusch, A. G. (2006). eIF3: a versatile scaffold for translation initiation complexes. *Trends Biochem. Sci.* **31**, 553–562.
10. Valášek, L., Nielsen, K. H. & Hinnebusch, A. G. (2002). Direct eIF2–eIF3 contact in the multifactor complex is important for translation initiation *in vivo*. *EMBO J.* **21**, 5886–5898.
11. Nielsen, K. H., Szamecz, B., Valasek, L., Jivotovskaya, A., Shin, B. S. & Hinnebusch, A. G. (2004). Functions of eIF3 downstream of 48S assembly impact AUG recognition and GCN4 translational control. *EMBO J.* **23**, 1166–1177.
12. Nielsen, K. H., Valášek, L., Sykes, C., Jivotovskaya, A. & Hinnebusch, A. G. (2006). Interaction of the RNP1 motif in PRT1 with HCR1 promotes 40S binding of eukaryotic initiation factor 3 in yeast. *Mol. Cell. Biol.* **26**, 2984–2998.
13. Yamamoto, Y., Singh, C. R., Marintchev, A., Hall, N. S., Hannig, E. M., Wagner, G. & Asano, K. (2005). The eukaryotic initiation factor (eIF) 5 HEAT domain mediates multifactor assembly and scanning with distinct interfaces to eIF1, eIF2, eIF3, and eIF4G. *Proc. Natl Acad. Sci. USA*, **102**, 16164–16169.
14. Valášek, L., Mathew, A., Shin, B. S., Nielsen, K. H., Szamecz, B. & Hinnebusch, A. G. (2003). The yeast eIF3 subunits TIF32/a and NIP1/c and eIF5 Make critical connections with the 40S ribosome *in vivo*. *Genes Dev.* **17**, 786–799.
15. Fraser, C. S., Berry, K. E., Hershey, J. W. & Doudna, J. A. (2007). 3j is located in the decoding center of the human 40S ribosomal subunit. *Mol. Cell*, **26**, 811–819.
16. Spahn, C. M., Beckmann, R., Eswar, N., Penczek, P. A., Sali, A., Blobel, G. & Frank, J. (2001). Structure of the 80S ribosome from *Saccharomyces cerevisiae*—tRNA ribosome and subunit–subunit interactions. *Cell*, **107**, 373–386.
17. Srivastava, S., Verschoor, A. & Frank, J. (1992). Eukaryotic initiation factor 3 does not prevent association through physical blockage of the ribosomal subunit–subunit interface. *J. Mol. Biol.* **220**, 301–304.
18. Siridechadilok, B., Fraser, C. S., Hall, R. J., Doudna, J. A. & Nogales, E. (2005). Structural roles for human translation factor eIF3 in initiation of protein synthesis. *Science*, **310**, 1513–1515.
19. Zhou, M., Sandercock, A. M., Fraser, C. S., Ridlova, G., Stephens, E., Schenauer, M. R. *et al.* (2008). Mass spectrometry reveals modularity and a complete subunit interaction map of the eukaryotic translation factor eIF3. *Proc. Natl Acad. Sci. USA*, **105**, 18139–18144.
20. ElAntak, L., Tzakos, A. G., Locker, N. & Lukavsky, P. J. (2007). Structure of eIF3b RNA recognition motif and its interaction with eIF3j: structural insights into the recruitment of eIF3b to the 40S ribosomal subunit. *J. Biol. Chem.* **282**, 8165–8174.
21. Methot, N., Rom, E., Olsen, H. & Sonenberg, N. (1997). The human homologue of the yeast Prt1 protein is an integral part of the eukaryotic initiation factor 3 complex and interacts with p170. *J. Biol. Chem.* **272**, 1110–1116.
22. Fraser, C. S., Lee, J. Y., Mayeur, G. L., Bushell, M., Doudna, J. A. & Hershey, J. W. (2004). The j-subunit of human translation initiation factor eIF3 is required for the stable binding of eIF3 and its subcomplexes to 40S ribosomal subunits *in vitro*. *J. Biol. Chem.* **279**, 8946–8956.
23. Asano, K., Phan, L., Anderson, J. & Hinnebusch, A. G. (1998). Complex formation by all five homologues of mammalian translation initiation factor 3 subunits from yeast *Saccharomyces cerevisiae*. *J. Biol. Chem.* **273**, 18573–18585.
24. Phan, L., Zhang, X., Asano, K., Anderson, J., Vornlocher, H. P., Greenberg, J. R. *et al.* (1998). Identification of a translation initiation factor 3 (eIF3) core complex, conserved in yeast and mammals, that interacts with eIF5. *Mol. Cell. Biol.* **18**, 4935–4946.
25. Valášek, L., Phan, L., Schoenfeld, L. W., Valášková, V. & Hinnebusch, A. G. (2001). Related eIF3 subunits TIF32 and HCR1 interact with an RNA recognition motif in PRT1 required for eIF3 integrity and ribosome binding. *EMBO J.* **20**, 891–904.
26. Valášek, L., Hašek, J., Trachsel, H., Imre, E. M. & Ruis, H. (1999). The *Saccharomyces cerevisiae HCR1* gene encoding a homologue of the p35 subunit of human translation eukaryotic initiation factor 3 (eIF3) is a high copy suppressor of a temperature-sensitive

mutation in the Rpg1p subunit of yeast eIF3. *J. Biol. Chem.* **274**, 27567–27572.
27. Valášek, L., Hašek, J., Nielsen, K. H. & Hinnebusch, A. G. (2001). Dual function of eIF3j/Hcr1p in processing 20S pre-rRNA and translation initiation. *J. Biol. Chem.* **276**, 43351–43360.
28. Kolupaeva, V. G., Unbehaun, A., Lomakin, I. B., Hellen, C. U. & Pestova, T. V. (2005). Binding of eukaryotic initiation factor 3 to ribosomal 40S subunits and its role in ribosomal dissociation and anti-association. *RNA*, **11**, 470–486.
29. Valášek, L., Szamecz, B., Hinnebusch, A. G. & Nielsen, K. H. (2007). *In vivo* stabilization of preinitiation complexes by formaldehyde cross-linking. *Methods Enzymol.* **429**, 163–183.
30. Fekete, C. A., Mitchell, S. F., Cherkasova, V. A., Applefield, D., Algire, M. A., Maag, D. *et al.* (2007). N- and C-terminal residues of eIF1A have opposing effects on the fidelity of start codon selection. *EMBO J.* **26**, 1602–1614.
31. Hinnebusch, A. G. (2005). Translational regulation of GCN4 and the general amino acid control of yeast. *Annu. Rev. Microbiol.* **59**, 407–450.
32. Grant, C. M., Miller, P. F. & Hinnebusch, A. G. (1994). Requirements for intercistronic distance and level of eIF-2 activity in reinitiation on GCN4 mRNA varies with the downstream cistron. *Mol. Cell. Biol.* **14**, 2616–2628.
33. Clery, A., Blatter, M. & Allain, F. H. T. (2008). RNA recognition motifs: boring? Not quite.. *Curr. Opin. Struct. Biol.* **18**, 290–298.
34. Nagai, K., Oubridge, C., Ito, N., Avis, J. & Evans, P. (1995). The RNP domain—a sequence-specific RNA-binding domain involved in processing and transport of RNA. *Trends Biochem. Sci.* **20**, 235–240.
35. Pisarev, A. V., Hellen, C. U. T. & Pestova, T. V. (2007). Recycling of eukaryotic posttermination ribosomal complexes. *Cell*, **131**, 286–299.
36. Isken, O., Kim, Y. K., Hosoda, N., Mayeur, G. L., Hershey, J. W. B. & Maquat, L. E. (2008). Upf1 phosphorylation triggers translational repression during nonsense-mediated mRNA decay. *Cell*, **133**, 314–327.
37. Kielkopf, C. L., Lucke, S. & Green, M. R. (2004). U2AF homology motifs: protein recognition in the RRM world. *Genes Dev.* **18**, 1513–1526.
38. Corsini, L., Bonnal, S., Basquin, J., Hothorn, M., Scheffzek, K., Valcarcel, J. & Sattler, M. (2007). U2AF-homology motif interactions are required for alternative splicing regulation by SPF45. *Nat. Struct. Mol. Biol.* **14**, 620–629.
39. Selenko, P., Gregorovic, G., Sprangers, R., Stier, G., Rhani, Z., Kramer, A. & Sattler, M. (2003). Structural basis for the molecular recognition between human splicing factors U2AF(65) and SF1/mBBP. *Mol. Cell*, **11**, 965–976.
40. Tabor, S. & Richardson, C. C. (1987). DNA sequence analysis with a modified bacteriophage T7 DNA polymerase. *Proc. Natl Acad. Sci. USA*, **84**, 4767–4771.
41. Gietz, R. D. & Sugino, A. (1988). New yeast–*Escherichia coli* shuttle vectors constructed with *in vitro* mutagenized yeast genes lacking six-base pair restriction sites. *Gene*, **74**, 527–534.
42. Sikorski, R. S. & Hieter, P. (1989). A system of shuttle vectors and yeast host strains designed for efficient manipulation of DNA in *Saccharomyces cerevisiae*. *Genetics*, **122**, 19–27.
43. Smith, D. B. & Johnson, K. S. (1988). Single-step purification of polypeptides expressed in *Escherichia coli* as fusions with glutathione *S*-transferase. *Gene*, **67**, 31–40.
44. Botstein, D., Falco, S. C., Stewart, S. E., Brennan, M., Scherer, S., Stinchcomb, D. T. *et al.* (1979). Sterile host yeasts (SHY): a eukaryotic system of biological containment for recombinant DNA experiments. *Gene*, **8**, 17–24.
45. Asano, K., Clayton, J., Shalev, A. & Hinnebusch, A. G. (2000). A multifactor complex of eukaryotic initiation factors eIF1, eIF2, eIF3, eIF5, and initiator $tRNA^{Met}$ is an important translation initiation intermediate *in vivo*. *Genes Dev.* **14**, 2534–2546.
46. Mueller, P. P. & Hinnebusch, A. G. (1986). Multiple upstream AUG codons mediate translational control of *GCN4*. *Cell*, **45**, 201–207.
47. Olsen, D. S., Savner, E. M., Mathew, A., Zhang, F., Krishnamoorthy, T., Phan, L. & Hinnebusch, A. G. (2003). Domains of eIF1A that mediate binding to eIF2, eIF3 and eIF5B and promote ternary complex recruitment *in vivo*. *EMBO J.* **22**, 193–204.
48. Nielsen, K. H. & Valášek, L. (2007). *In vivo* deletion analysis of the architecture of a multi-protein complex of translation initiation factors. *Methods Enzymol.* **431**, 15–32.
49. Guntert, P. (2004). Automated NMR structure calculation with CYANA. *Methods Mol. Biol.* **278**, 353–378.
50. Cornilescu, G., Delaglio, F. & Bax, A. (1999). Protein backbone angle restraints from searching a database for chemical shift and sequence homology. *J. Biomol. NMR*, **13**, 289–302.
51. Delaglio, F., Grzesiek, S., Vuister, G. W., Zhu, G., Pfeifer, J. & Bax, A. (1995). NMRPipe—a multidimensional spectral processing system based on Unix pipes. *J. Biomol. NMR*, **6**, 277–293.
52. Case, D. A., Darden, T. A., Cheatham, T. E., Simmerling, C. L., Wang, J., Duke, R. E. *et al.* (2006). University of California, San Francisco, San Francisco, CA.
53. Laskowski, R. A., Rullmannn, J. A., MacArthur, M. W., Kaptein, R. & Thornton, J. M. (1996). AQUA and PROCHECK-NMR: programs for checking the quality of protein structures solved by NMR. *J. Biomol. NMR*, **8**, 477–486.
54. Koradi, R., Billeter, M. & Wuthrich, K. (1996). MOLMOL: a program for display and analysis of macromolecular structures.*J. Mol. Graphics*, **14**, 51–55; 29–32.
55. Dodd, R. B., Allen, M. D., Brown, S. E., Sanderson, C. M., Duncan, L. M., Lehner, P. J. *et al.* (2004). Solution structure of the Kaposi's sarcoma-associated herpesvirus K3 N-terminal domain reveals a novel E2-binding C_4HC_3-type RING domain. *J. Biol. Chem.* **279**, 53840–53847.

The C-terminal region of eukaryotic translation initiation factor 3a (eIF3a) promotes mRNA recruitment, scanning, and, together with eIF3j and the eIF3b RNA recognition motif, selection of AUG start codons.

Chiu W.L., Wagner S., Herrmannová A., Burela L., Zhang F., Saini A.K., Valášek L., Hinnebusch A.G.

Mol Cell Biol. 2010 Sep;30(18):4415-34.
PMID: 20584985

In this study we functionally characterized the C-terminal region of a/TIF32 and its interactions with j/HCR1 and the b/PRT1 RNA recognition motif (RRM). The a/TIF32-CTD contains the HCR1-like domain (HLD) with a conserved "KERR" motif and a BOX6 element.

KERR and Box6 mutations in the a/TIF32-HLD impaired general translation initiation and mRNA recruitment by 43S preinitiation complexes. In addition, they also produced phenotypes indicating reduced efficiency of scanning and AUG recognition, and impaired translational induction of *GCN4*. As the interaction with j/HCR1 was weakened in the a/TIF32-HLD mutants, the growth phenotypes could be partially suppressed by overexpression of j/HCR1. Interestingly, deletion of either the j/HCR1-NTD or normally dispensable j/HCR1-CTD led to exacerbation of growth phenotypes, suggesting that both domains are critically required when the a/TIF32-HLD function(s) is compromised. Furthermore, mutations in both the a/TIF32-HLD and j/HCR1 destabilized the integrity of the b/PRT1-RRM-j/HCR1-a/TIF32-HLD eIF3 module that is required to prevent leaky scanning over the AUG start codons.

Finally, we also revealed that the extreme CTD of a/TIF32 binds to small ribosomal proteins RPS2 and RPS3 suggesting that the b/PRT1-RRM-j/HCR1-a/TIF32-CTD module occurs near the mRNA entry channel.

MOLECULAR AND CELLULAR BIOLOGY, Sept. 2010, p. 4415–4434 Vol. 30, No. 18
0270-7306/10/$12.00 doi:10.1128/MCB.00280-10

The C-Terminal Region of Eukaryotic Translation Initiation Factor 3a (eIF3a) Promotes mRNA Recruitment, Scanning, and, Together with eIF3j and the eIF3b RNA Recognition Motif, Selection of AUG Start Codons▽

Wen-Ling Chiu,[1] Susan Wagner,[2] Anna Herrmannová,[2] Laxminarayana Burela,[1]† Fan Zhang,[1] Adesh K. Saini,[1] Leoš Valášek,[2]* and Alan G. Hinnebusch[1]*

Laboratory of Gene Regulation and Development, Eunice Kennedy Shriver National Institute of Child Health and Human Development, NIH, Bethesda, Maryland 20892,[1] and Laboratory of Regulation of Gene Expression, Institute of Microbiology AVCR, Videnska 1083, Prague 142 20, Czech Republic[2]

Received 12 March 2010/Returned for modification 26 April 2010/Accepted 14 June 2010

The C-terminal domain (CTD) of the a/Tif32 subunit of budding yeast eukaryotic translation initiation factor 3 (eIF3) interacts with eIF3 subunits j/Hcr1 and b/Prt1 and can bind helices 16 to 18 of 18S rRNA, suggesting proximity to the mRNA entry channel of the 40S subunit. We have identified substitutions in the conserved Lys-Glu-Arg-Arg (KERR) motif and in residues of the nearby box6 element of the a/Tif32 CTD that impair mRNA recruitment by 43S preinitiation complexes (PICs) and confer phenotypes indicating defects in scanning and start codon recognition. The normally dispensable CTD of j/Hcr1 is required for its binding to a/Tif32 and to mitigate the growth defects of these a/Tif32 mutants, indicating physical and functional interactions between these two domains. The a/Tif32 CTD and the j/Hcr1 N-terminal domain (NTD) also interact with the RNA recognition motif (RRM) in b/Prt1, and mutations in both subunits that disrupt their interactions with the RRM increase leaky scanning of an AUG codon. These results, and our demonstration that the extreme CTD of a/Tif32 binds to Rps2 and Rps3, lead us to propose that the a/Tif32 CTD directly stabilizes 43S subunit-mRNA interaction and that the b/Prt1-RRM–j/Hcr1–a/Tif32-CTD module binds near the mRNA entry channel and regulates the transition between scanning-conducive and initiation-competent conformations of the PIC.

Eukaryotic translation initiation factor 3 (eIF3) is a multisubunit protein complex that has been implicated in several steps of the translation initiation pathway (reviewed in reference 19). These steps include recruitment of the eIF2–GTP–Met-tRNA$_i^{Met}$ ternary complex (TC) and other eIFs to the small (40S) ribosomal subunit to form the 43S preinitiation complex (PIC), mRNA recruitment by the 43S PIC, and subsequent scanning of the 5′ untranslated region (UTR) for an AUG start codon. The eIF3 in the budding yeast *Saccharomyces cerevisiae* is composed of only 6 subunits (a/Tif32, b/Prt1, c/Nip1, i/Tif34, g/Tif35, and j/Hcr1), which have homologs in the larger, 13-subunit eIF3 complex in mammals. Yeast eIF3 can be purified with the TC, eIF1, and eIF5 in a ribosome-free assembly called the multifactor complex (MFC) (2), whose formation appears to promote assembly or stability of the 43S PIC and to stimulate scanning and AUG selection (10, 23, 32, 42, 48, 49, 51).

In mammals, there is evidence that eIF3 enhances recruitment of mRNA by interacting directly with eIF4G, the "scaffold" subunit of mRNA cap-binding complex eIF4F, and forming a protein bridge between mRNA and the 43S PIC (24, 25, 35). In budding yeast, direct eIF3-eIF4G interaction has not been detected, and the eIF3-binding domain (25) is not evident in yeast eIF4G. Moreover, depletion of eIF3, but not eIF4G, from yeast cells provokes a strong decrease in the amount of an mRNA (*RPL41A*) associated with native PICs (23). However, since depletion of eIF3 also reduced the amounts of other MFC components associated with PICs, it remained unclear whether eIF3 acts directly in mRNA recruitment.

In favor of a direct role for eIF3, cross-linking analysis of reconstituted mammalian 48S PICs identified contacts of subunits eIF3a and eIF3d with mRNA residues 8 to 17 nucleotides (nt) upstream of the AUG codon, suggesting that these subunits form an extension of the mRNA exit channel (37). Consistent with this, we found that the N-terminal domain (NTD) of yeast a/Tif32 binds Rps0A, located near the mRNA exit pore, and functionally interacts with sequences 5′ to the regulatory upstream open reading frame 1 (uORF1) in *GCN4* mRNA (42). Despite these advances, *in vivo* evidence supporting a direct role of eIF3 in mRNA recruitment by 43S PICs is lacking.

Recently, there has been progress in elucidating the molecular mechanisms involved in ribosomal scanning and AUG selection. Reconstituted mammalian 43S PICs containing only eIF1, -1A, and -3 and the TC can scan the leader of an unstructured message and form a stable 48S PIC at the 5′-proximal AUG codon (35). eIF1 and -1A are thought to promote

* Corresponding author. Mailing address for Alan G. Hinnebusch: Laboratory of Gene Regulation and Development, Eunice Kennedy Shriver National Institute of Child Health and Human Development, NIH, Bethesda, MD 20892. Phone: (301) 496-4480. Fax: (301) 496-6828. E-mail: ahinnebusch@nih.gov. Mailing address for Leoš Valášek: Laboratory of Regulation of Gene Expression, Institute of Microbiology AVCR, Videnska 1083, Prague 142 20, Czech Republic. Phone: 420-241-062-288. Fax: 420-241-062-665. E-mail: valasekl@biomed.cas.cz.

† Present address: Department of Biotechnology, Sreenidhi Institute of Science and Technology, Hyderabad, A.P., India.

▽ Published ahead of print on 28 June 2010.

scanning by stabilizing an open conformation of the 40S subunit (6, 13, 26, 27), which appears to involve opening the "latch" on the mRNA entry channel formed by helices 18 and 34 of 18S rRNA (33). eIF1A also promotes a mode of TC binding conducive to scanning (39) and seems to prevent full accommodation of Met-tRNA$_i^{Met}$ in the P site at non-AUG codons (53). The GTP bound to eIF2 is hydrolyzed, in a manner stimulated by eIF5, but release of phosphate (P_i) from eIF2-GDP-P_i is blocked by eIF1 (1). Entry of AUG into the P site triggers relocation of eIF1 from its binding site on the 40S subunit (27), allowing P_i release (1) and stabilizing the closed, scanning-arrested conformation of the 40S subunit (33).

Mutations in eIF1 and eIF1A that reduce the stringency of start codon recognition have been isolated by their ability to increase initiation at a UUG codon in *his4* alleles lacking the AUG start codon (the Sui$^-$ phenotype) (6, 12, 13, 29, 38, 39, 52). eIF1A mutations with the opposite effect of lowering UUG initiation in the presence of a different Sui$^-$ mutation (the Ssu$^-$ phenotype) were also obtained (13, 39). Previously, we identified Sui$^-$ and Ssu$^-$ mutations in the N-terminal domain of eIF3 subunit c/Nip1, which alter its contacts with eIF1, -2, and -5, suggesting that integrity of the MFC is important for the accuracy of AUG selection (49).

Several genetic findings also implicate eIF3 in the efficiency of scanning and AUG recognition. The *prt1-1* point mutation in b/Prt1 (S518F) (11) impairs translational control of *GCN4* mRNA in a manner suggesting a reduced rate of scanning between the short uORFs involved in this control mechanism (30). Disrupting an interaction between a hydrophobic pocket of the noncanonical RNA recognition motif (RRM) in the N terminus of b/Prt1 (henceforth referred to as b/RRM) and a Trp residue in the N-terminal acidic motif of j/Hcr1 (Trp-37) severely reduces the efficiency of initiation at the AUG of uORF1 in *GCN4* mRNA, the phenomenon of leaky scanning, implicating the connection between the b/RRM and j/Hcr1 NTD (henceforth referred to as j/NTD) in efficient AUG recognition (10). Similarly, a multiple Ala substitution in RNP1 of the b/RRM evoked leaky scanning of the AUG codon of *GCN4* uORF1 (uAUG-1) (32).

Interestingly, besides the b/RRM-j/NTD contact, the b/RRM can simultaneously bind to the j/Hcr1-like domain (HLD) in a/Tif32, and j/Hcr1 also independently binds a/Tif32 (50). This network of interactions involving the b/RRM, a/Tif32-HLD, and j/Hcr1 segments was shown to stabilize an eIF3 subassembly (50), referred to below as the b/RRM–j/Hcr1–a/Tif32-CTD module; however, it was not known whether the a/Tif32 HLD component of this module also participates in AUG recognition or other specific steps of initiation.

In this report, we provide evidence that the evolutionarily conserved KERR motif in the a/Tif32 HLD (hereafter referred to as a/HLD) functions to enhance mRNA recruitment by 43S PICs, processivity of scanning, and the efficiency of AUG recognition. The identification of Ssu$^-$ phenotypes for both KERR mutations and replacement of a nearby element (box6) further implicates the a/HLD in promoting the closed, scanning-arrested conformation of the PIC at start codons. Combining these results with our finding that the a/Tif32 CTD binds the 40S proteins Rps3 and Rps2 and the recent evidence that j/Hcr1 promotes AUG recognition and binds Rps2 leads us to propose that the a/HLD is positioned near the 40S mRNA entry channel, where it promotes mRNA binding and, together with j/Hcr1 and the b/RRM, modulates the transition between the open and closed conformations of the PIC during scanning and AUG recognition.

MATERIALS AND METHODS

Construction of yeast strains and plasmids. The yeast strains and plasmids used in all experiments are listed in Tables 1 and 2, respectively. Yeast strain YAH04 was generated by a genetic cross of H428 and del′32a9A (Table 1) as a haploid ascospore resistant to 3-amino-1,2,4-triazole (3-AT) and geneticin but unable to grow on 5-fluoroorotic acid (5-FOA) and autotrophic for tryptophan. YAH05 was generated by a cross of H428 and H2923 (Table 1) as an ascospore resistant to 3-AT and geneticin, unable to grow on 5-FOA, and autotrophic for tryptophan. To generate strains AY51 and AY52, YAH04 was transformed with pRS-a/TIF32-DS-His and pRS-a/tif32-R731I-His-L, respectively, and the resident *TIF32 URA3* plasmid was evicted on 5-FOA. To create strains YSW731 and YSW725, del′32a9A was transformed with pRS-a/tif32-R731I-His-L and pWLCB01, respectively, and the resident *TIF32 URA3* plasmid was evicted on 5-FOA. To create strain H3708, H2994 was transformed with YCpTIF32-His-U and then with a PCR fragment containing the *tif32*Δ::*KanMX4* allele amplified from the appropriate deletion mutant from the *Saccharomyces* Genome Deletion Project (15), purchased from Research Genetics, selecting for resistance to G418. To generate yeast strains H3711, H3714, H3715, and WLCY01 to WLCY03, H3708 was transformed with low-copy-number (lc) *LEU2* plasmids harboring the appropriate *TIF32-His* alleles, and the resident *TIF32 URA3* plasmid was evicted on 5-FOA. To create strain WLCY22, primers YLR192C-A and YLR192C-D were used to amplify a PCR product containing the *hcr1*Δ::*KanMX4* allele from strain 6704. H2994 was transformed with the purified DNA fragment by selecting for G418 resistance. Strains WLCY06 to WLCY09, were generated by (i) deleting *RPL11B* from H3708 by transformation with the HindIII-BamHI fragment containing *rpl11b*Δ::*LEU2* from plasmid pL16b-ΔLeu, selecting for Leu$^+$ clones, and (ii) replacing the resident *TIF32 URA3* plasmid with the appropriate single-copy (sc) *TRP1* plasmids harboring *TIF32-His* alleles by counterselection on 5-FOA medium. To generate strain H3774, 1D2-2D was transformed with pRB53, and the resident *DED1 URA3* plasmid was evicted on 5-FOA.

Yeast biochemical methods. Glutathione *S*-transferase (GST) pulldown experiments with GST fusions and *in vitro*-synthesized ^{35}S-labeled polypeptides (Table 2 lists vector descriptions) were conducted as follows. Individual GST fusion proteins were expressed in *Escherichia coli*, immobilized on glutathione-Sepharose beads, and incubated with 10 μl of ^{35}S-labeled potential binding partners at 4°C for 2 h. The beads were washed 3 times with 1 ml of phosphate-buffered saline, and bound proteins were separated by SDS-PAGE. Gels were first stained with Gelcode Blue Stain Reagent (Pierce) and then subjected to autoradiography. Nickel chelation chromatography of eIF3 complexes containing His_8-tagged a/Tif32 or b/Prt1 from yeast whole-cell extracts (WCEs) and Western blot analysis were conducted as described in detail previously (31). In short, WCEs were incubated with 4 μl of 50% Ni-nitrilotriacetic acid (NTA)-silica resin (Qiagen) suspended in 200 μl of buffer A for 2 h at 4°C, followed by washing and elution. For assaying expression of *GCN4-lacZ* reporters, β-galactosidase activities in WCEs were measured as described previously (18). For assaying luciferase reporters, cells were disrupted with glass beads in 50 mM Tris-HCl (pH 7.5), 1 mM 4-(2-aminoethyl)-benzenesulfonyl fluoride hydrochloride (AEBSF), and WCEs were assayed for luciferase activities using the luminescence reader Monolight 3010 (BD Biosciences) according to the supplier's protocol (Promega).

Analysis of polysome profiles and native 43S/48S PICs. For polysome analysis, strains were grown in yeast extract-peptone-dextrose (YPD) at 30°C, shifted to 36°C, and cultured for 6 h (A_{600}, ~1). Cycloheximide was added (50 μg/ml) 5 min prior to harvesting, and WCEs were prepared in breaking buffer (20 mM Tris-HCl, pH 7.5, 50 mM KCl, 10 mM $MgCl_2$, 1 mM dithiothreitol [DTT], 5 mM NaF, 1 mM phenylmethylsulfonyl fluoride [PMSF], 1× Complete Protease Inhibitor Mix tablets without EDTA [Roche]). Five A_{260} units of WCEs was separated by velocity sedimentation on a 4.5 to 45% sucrose gradient by centrifugation at 39,000 rpm for 2.5 h in an SW41Ti rotor (Beckman). Gradient fractions were collected and scanned at 254 nm to visualize ribosomal species.

For analysis of native 43S PICs, cells were cultured as described above and cross-linked with 1% formaldehyde prior to being harvested. WCEs were prepared in breaking buffer, and 25 A_{260} units was separated by velocity sedimentation on a 7.5 to 30% sucrose gradient by centrifugation at 41,000 rpm for 5 h in an SW41Ti rotor. Fractions (0.7 ml) were collected, precipitated by adding 1.7 volumes of 100% ethanol, resuspended in SDS loading buffer, and resolved by

TABLE 1. Yeast strains used in this study

Strain	Genotype	Source or reference
H428[a]	*MAT***a** *leu2-3,112 ura3-52 hcr1*::*KanMX3*	32
H2923	*MAT*α *leu2-3,112 ura3-52 trp1*Δ *prt1*::*hisG gcn2*::*hisG* pRS316-*PRT1* (*PRT1 URA3*)	30
del′32a9A[a]	*MAT*α *leu2-3,112 ura3-52 trp1*Δ *tif32*::*hisG gcn2*::*hisG* YCp-a/TIF32-His-U (*TIF32 URA3*)	42
YAH04[a]	*MAT***a** *leu2-3,112 ura3-52 trp1*Δ *GCN2 hcr1*::*KanMX3 tif32*::*hisG* YCp-a/TIF32-His-U (*TIF32-His URA3*)	This study
YAH05[a]	*MAT***a** *leu2-3,112 ura3-52 GCN2 hcr1*::*KanMX3 prt1*::*hisG* pRS316-*PRT1* (*PRT1 URA3*)	This study
AY51[a]	*MAT***a** *leu2-3,112 ura3-52 trp1*Δ *GCN2 hcr1*::*KanMX3 tif32*::*hisG* pRS-a/TIF32 DS-His (*TIF32-His LEU2*)	This study
AY52[a]	*MAT***a** *leu2-3,112 ura3-52 trp1*Δ *GCN2 hcr1*::*KanMX3 tif32*::*hisG* pRS-a/tif32-R731I-His (*tif32-His-R731I LEU2*)	This study
YSW731[a]	*MAT*α *leu2-3,112 ura3-52 trp1*Δ *tif32*::*hisG gcn2*::*hisG* pRS-a/tif32-R731I-His-L (*tif32-His-R731I LEU2*)	This study
YSW725[a]	*MAT*α *leu2-3,112 ura3-52 trp1*Δ *tif32*::*hisG gcn2*::*hisG* pRS-a/tif32-H725P-His-L (*tif32-His-H725P LEU2*)	This study
H2994[b]	*MAT***a** *ura3-52 trp1-63 leu2-3,112 his4-301*(*AUU*)	49
H3708[b]	*MAT***a** *ura3-52 trp1-63 leu2-3,112 his4-301*(*AUU*) *tif32*Δ::*KanMX4* YCp-a/TIF32-His-U (*TIF32-His URA3*)	This study
H3711[b]	*MAT***a** *ura3-52 trp1-63 leu2-3,112 his4-301*(*AUU*) *tif32*Δ::*KanMX4* pRS-a/tif32-box2-His-L (*tif32-His-box2 LEU2*)	This study
H3714[b]	*MAT***a** *ura3-52 trp1-63 leu2-3,112 his4-301*(*AUU*) *tif32*Δ::*KanMX4* pRS-a/tif32-box5-His-L (*tif32-His-box5 LEU2*)	This study
H3715[b]	*MAT***a** *ura3-52 trp1-63 leu2-3,112 his4-301*(*AUU*) *tif32*Δ::*KanMX4* pRS-a/tif32-box6-His-L (*tif32-His-box6 LEU2*)	This study
WLCY01[b]	*MAT***a** *ura3-52 trp1-63 leu2-3,112 his4-301*(*AUU*) *tif32*Δ*::KanMX4* pRS-a/TIF32-His-L (*TIF32-His LEU2*)	This study
WLCY02[b]	*MAT***a** *ura3-52 trp1-63 leu2-3,112 his4-301*(*AUU*) *tif32*Δ::*KanMX4* pWLCB01 (*tif32-His-H725P LEU2*)	This study
WLCY03[b]	*MAT***a** *ura3-52 trp1-63 leu2-3,112 his4-301*(*AUU*) *tif32*Δ::*KanMX4* pRS-a/tif32-R731I-His-L (*tif32-His-R731I LEU2*)	This study
WLCY06[b]	*MAT***a** *ura3-52 trp1-63 leu2-3,112 his4-301*(*AUU*) *tif32*Δ::*KanMX4 rpl11b*Δ::*LEU2* pWLCB02 (*TIF32-His TRP1*)	This study
WLCY07[b]	*MAT***a** *ura3-52 trp1-63 leu2-3,112 his4-301*(*AUU*) *tif32*Δ::*KanMX4 rpl11b*Δ::*LEU2* pWLCB03 (*tif32-His-H725P TRP1*)	This study
WLCY08[b]	*MAT***a** *ura3-52 trp1-63 leu2-3,112 his4-301*(*AUU*) *tif32*Δ::*KanMX4 rpl11b*Δ::*LEU2* pWLCB04 (*tif32-His-R731I TRP1*)	This study
WLCY09[b]	*MAT***a** *ura3-52 trp1-63 leu2-3,112 his4-301*(*AUU*) *tif32*Δ::*KanMX4 rpl11b*Δ::*LEU2* pWLCB05 (*tif32-His-box6 TRP1*)	This study
1D2-2D	*MAT ura3-1 trp1-1 his3-11,15 leu2-3,112 can1-100 ade2-1 ded1*::*HISMX6* (*DED1 URA3*)	22
H3774	*MAT ura3-1 trp1-1 his3-11,15 leu2-3,112 can1-100 ade2-1 ded1*::*HISMX6* pRB53(*ded1-57 LEU2*)	This study
6704	*MAT***a** *hcr1*::*KanMX4 his3-*Δ*1 leu2-*Δ*0 ura3-*Δ*0 met15-*Δ*0*	Research Genetics
WLCY22[b]	*MAT***a** *ura3-52 trp1-63 leu2-3,112 his4-301*(*AUU*) *hcr1*Δ::*KanMX4*	This study
H2879[c]	*MAT***a** *leu2-3,112 ura3-52*	30
H3675[c]	*MAT***a** *leu2-3,112 ura3-52 hcr1*Δ	32

[a] Isogenic strains.
[b] Isogenic strains.
[c] Isogenic strains.

SDS-PAGE, followed by Western blotting with antibodies against the relevant eIFs. For analysis of 48S PICs, total RNA was isolated from 0.3 ml of gradient fractions, prepared as described above by hot-phenol extraction, and resuspended in 50 μl of diethyl pyrocarbonate (DEPC)-treated H_2O. Two microliters of RNA was subjected to reverse transcription with SuperScript III reverse transcriptase (Invitrogen). Aliquots of cDNA were diluted 10-fold, and PCR amplifications were performed on 2 μl of diluted cDNA in 20-μl reaction mixtures prepared with the Brilliant II SYBR green qPCR Master Mix (Stratagene) and primers for *RPL41A* (0.3 μM) or 18S rRNA (0.4 μM) using the Mx3000P system (Stratagene).

RESULTS

Substitutions in the a/HLD impair general translation initiation. To identify functionally important residues in the C-terminal portion of the a/HLD, we introduced Ala substitutions in consecutive blocks of 10 (or in one instance 11) residues between amino acids (aa) 642 and 791 (dubbed boxes 1 to 15 [Fig. 1A]). The mutations were generated in plasmid-borne *TIF32-His*, encoding His_8-tagged a/Tif32, and introduced into a *tif32*Δ strain by plasmid shuffling (5). Except for *box9*, none of these mutations was lethal, allowing eviction of the resident *TIF32*$^+$ *URA3* plasmid on medium containing 5-FOA, and only three of the mutations produced detectable slow-growth (Slg^-) phenotypes: *box2*, *-5*, and *-6* (summarized in Fig. 1A). The *tif32-box9* allele was lethal whether present on an lc or high-copy-number (hc) plasmid (data not shown). We also subjected the *TIF32* CTD to random mutagenesis and identified three mutant alleles with temperature-sensitive (Ts^-) phenotypes, only one of which produced a single-amino-acid substitution (H725P). The other two Ts^- mutants contained C-terminal truncations of the Tif32 CTD and were not studied further.

Interestingly, the histidine residue replaced by the *H725P* mutation is located in the region altered by the lethal Ala replacement of box9 and is only 6 residues N-terminal to the R731I substitution produced by the *rpg1-1* allele described previously (44) (Fig. 1A). These mutations all replace a region of sequence conservation among a/Tif32 homologs, designated the KERR motif after its conserved residues (K^{721}-X_5-E^{727}-R^{728}-X_2-R^{731}) (10), which is also conserved in the C-terminal region of j/Hcr1 (Fig. 1A and B). Based on the identification of multiple substitutions in the KERR motif, and of box6 only 20 residues upstream, which impaired the essential function of a/Tif32, we selected these mutations for further analysis.

The two KERR mutations, *H725P* and *R731I*, impair growth

TABLE 2. Plasmids used in this study

Plasmid	Description	Source or reference
pRS-b/PRT1-HisXS	*PRT1-His* in lc *LEU2* plasmid, from pRS315	10
YEplac195	hc *URA3* vector	16
YEp-j/HCR1-DS	*HCR1* coding region flanked by BamHI and NcoI sites, respectively, in hc *LEU2* plasmid, from YEplac181	10
YEp-j/HCR1-DS-U	*HCR1* coding region flanked by BamHI and NcoI sites, respectively, in hc *URA3* plasmid, from YEplac195	10
YEp-j/hcr1-NTD	*hcr1-NTD* [1-135] in hc *LEU2* plasmid, from YEplac181	10
YEp-j/hcr1-NTD-U	*hcr1-NTD* [1-135] in hc *URA3* plasmid, from YEplac195	This study
YEp-j/hcr1-CTD	*hcr1-CTD* [136-265] in hc *LEU2* plasmid, from YEplac181	10
YEp-j/hcr1-CTD-U	*hcr1-CTD* [136-265] in hc *URA3* plasmid, from YEplac195	This study
YEp-j/hcr1-R215I-DS	*hcr1-R215I* in hc *LEU2* plasmid, from YEplac181	This study
YEp-j/hcr1-R215I-U	*hcr1-R215I* in hc *URA3* plasmid, from YEplac195	This study
YEp-j/hcr1-box6	*hcr1-box6* in hc *LEU2* plasmid, from YEplac181	This study
YEp-j/hcr1-box6-U	*hcr1-box6* in hc *URA3* plasmid, from YEplac195	This study
YEp-j/hcr1-box6-R215I	*hcr1-box6-R215I* in hc *LEU2* plasmid, from YEplac181	This study
YEp-j/hcr1-box6-R215I-U	*hcr1-box6-R215I* in hc *URA3* plasmid, from YEplac195	This study
YCp-j/HCR1-DS-U	*HCR1* in lc *URA3* plasmid, from YCplac33	10
YCp-j/HCR1-DS-L	*HCR1* in lc *LEU2* plasmid, from YCplac111	This study
YCp-j/hcr1-R215I-U	*hcr1-R215I* in lc *URA3* plasmid, from YCplac33	This study
pRS-a/TIF32-His-L	*TIF32-His* in lc *LEU2* plasmid, from pRS315	48
pRS-a/tif32-Box9-His-L	*tif32-box9-His*, encoding 11 Ala substitutions in box9 (aa 721 to 732) in lc *LEU2* plasmid, from pRS315	This study
pRS-a/tif32-R731I-His-L	*tif32-R731I-His* in lc *LEU2* plasmid, from pRS315	This study
pWLCB01	*tif32-H725P-His* in lc *LEU2* plasmid, from pRS315	This study
pGEX-5X-3	Cloning vector for GST fusions	40
pGEX-b/PRT1-RRM	Encodes GST-b/prt1-RRM [1-136] fusion, from pGEX-5X-3	50
pT7-a/TIF32	*TIF32* ORF under T7 promoter	3
pT7-HLD	Encodes *TIF32*[483-786] under T7 promoter	This study
pT7-HLD-box6	Encodes *tif32-box6*[483-786] under T7 promoter	This study
pT7-HLD-box9	Encodes *tif32-box9*[483-786] under T7 promoter	This study
pT7-HLD-R731I	Encodes *tif32-R731I*[483-786] under T7 promoter	This study
pGEX-j/HCR1	Encodes GST-j/HCR1 fusion, from pGEX-5X-3	50
pGEX-j/hcr1-NTD	Encodes GST-j/hcr1-NTD [1-135] fusion, from pGEX-5X-3	10
pGEX-j/hcr1-CTD	Encodes GST-j/hcr1-CTD [136-265] fusion, from pGEX-5X-3	10
pGEX-j/hcr1-BOX6	Encodes GST-j/hcr1-box6 fusion, from pGEX-5X-3	This study
pGEX-j/hcr1-BOX9	Encodes GST-j/hcr1-box9 fusion, from pGEX-5X-3	10
pGEX-j/hcr1-R215I	Encodes GST-j/hcr1-R215I fusion, from pGEX-5X-3	This study
YEp-j/HCR1-W	*HCR1* in hc *TRP1* plasmid, from YEplac112	46
YEp-j/hcr1-R215I-DS-W	*hcr1-R215I* in hc *TRP1* plasmid, from YEplac112	This study
pGBK-T7-RPS2	*RPS2* ORF in pGBKT7, *TRP1* (Clontech)	47
pGAD-T7-RPS3	*RPS3* ORF in pGADT7, *LEU2* (Clontech)	47
pGBK-T7-RPS0e	*RPS0A* ORF (lacking intron) in GBKT7, *TRP1* (Clontech)	This study
pGEX-RPS2	Encodes GST-RPS2 fusion, from pGEX-5X-3	10
pGEX-a/TIF32-Δ4	Encodes GST-a/TIF32-Δ4[790-964] fusion, from pGEX-5X-3	48
pRS-a/tif32-box6-His-L	*tif32-box6-His* in lc *LEU2* plasmid, from pRS315	This study
YEp tif32-box + 9-His-L	*tif32-box9-His* in hc *LEU2* plasmid, from YEplac181	This study
YCplac22	Single-copy *TRP1* vector	16
p4280/YCpSUI3-S264Y-W	*SUI3-S264Y* in single-copy *TRP1* plasmid, from YCplac22	49
p4281/YCpSUI5-G31R-W	*SUI5-G31R*/*TIF5-G31R* in single-copy *TRP1* plasmid, from YCplac22	49
pAS57	*tif11Δ125-153* in hc *TRP1* plasmid, from YEplac112	This study
pM226	Derivative of pM199; elongated uORF1 extends into the *GCN4-lacZ* coding region	18
p180	*GCN4-lacZ* with WT leader in single-copy *URA3* plasmid, from YCp50	20
p227	*GCN4-lacZ* with point mutations in all 4 uAUGs in single-copy *URA3* plasmid, from YCp50	28
p209	*GCN4-lacZ* with point mutations in uAUGs 2 to 4 in single-copy *URA3* plasmid, from YCp50	17
p367	*HIS4-lacZ* in single-copy *URA3* plasmid	9
p391	*HIS4-UUG-lacZ*, with TTG replacing ATG start codon, in single-copy *URA3* plasmid	9
p4642/pJM753	*L0LUC* reporter in single-copy *URA3* plasmid	4
p4645/pJM261	*L2LUC* reporter in single-copy *URA3* plasmid	4
pWLCB06	*GCN4-lacZ* lacking all uORFs, with hairpin insertion between nt +481 and +482 in single-copy *URA3* plasmid, from YCp50	This study
pWLCB07	*GCN4-lacZ* lacking all uORFs, with hairpin insertion between nt +481 and +482 in single-copy *URA3* plasmid, from YCp50	This study

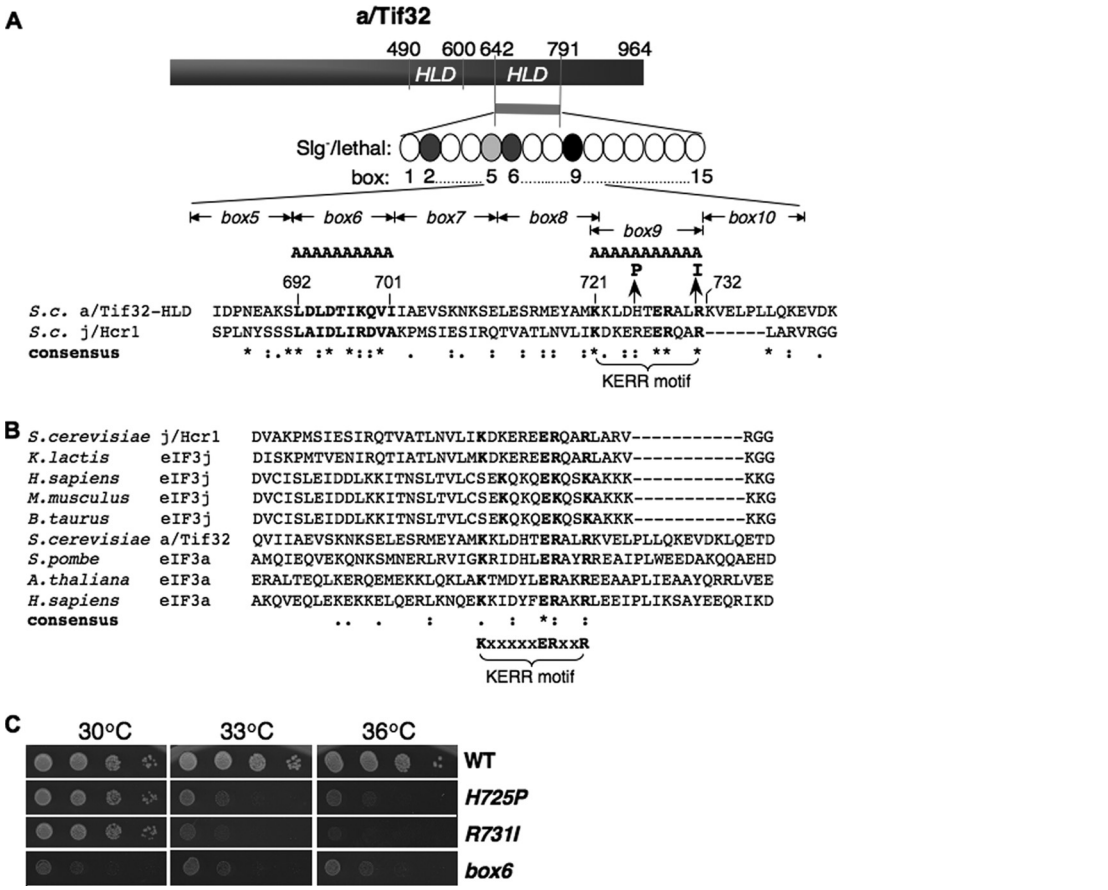

FIG. 1. a/HLD substitutions impair cell growth. (A) Schematic representation of a/Tif32, indicating N- and C-terminal halves of the j/Hcr1-like domain (*HLD*). The CTD of a/Tif32 subjected to mutagenesis is indicated as a bar and string of ovals (boxes 1 to 15) representing 10 consecutive residues replaced by alanines. Shades of gray indicate the degree of Slg$^-$ phenotype, and black indicates lethality. A sequence alignment of the C-terminal portion of the a/HLD with j/Hcr1 (residues 168 to 222) is shown, indicating the nature of *tif32* mutations *box6*, *box9*, *H725P*, and *R731I* above and the KERR motif below. *S.c.*, *S. cerevisiae*. Asterisks, amino acids conserved in all sequences; colons, homologous substitutions; periods, nonhomologous substitutions; boldface, box6 region and KERR motif conserved residues. (B) ClustalW2 was used to align regions of j/Hcr1 and the a/HLD using sequences from the indicated species (*K.lactis*, *Kluyveromyces lactis*; *H.sapiens*, *Homo sapiens*; *M.musculus*, *Mus musculus*; *B.taurus*, *Bos taurus*; *S.pombe*, *Schizosaccharomyces pombe*; *A.thaliana*, *Arabidopsis thaliana*) with the following accession numbers (in the order shown, from the top): NP_013293, Q6CMJ8, O75822, Q66JS6, Q0VCU8, NP_009635, CAA21076, Q9LD55, and Q14152. (C) Phenotypes of *tif32* a/HLD mutants. Serial dilutions of *GCN2 his4-301 tif32*Δ strains harboring lc plasmids with *TIF32*$^+$*-His* (WLCY01), *tif32-H725P-His* (WLCY02), *tif32-R731I-His* (WLCY03), or *tif32-box6-His* (H3715) were spotted on synthetic dextrose minimal medium supplemented with histidine, tryptophan, and uracil (SD+HWU) and incubated at the indicated temperatures for 3 days.

only at elevated temperatures (33°C and 36°C), whereas the *box6* mutation confers Slg$^-$ at all temperatures (Fig. 1C). All three mutations provoke substantial (>3-fold) reductions in the polysome/monosome (P/M) ratio after incubation at 36°C (Fig. 2A), indicating marked reductions in rates of translation initiation *in vivo*. Importantly, none of the mutations, including lethal *box9*, reduced the steady-state level of a/Tif32 protein (Fig. 2B, right and left).

a/HLD substitutions impair 48S PIC assembly. To determine whether the *tif32* mutations affect association of eIF3 or other components of the MFC with native 40S subunits, we employed formaldehyde cross-linking of living cells to stabilize native 43S/48S PICs. WCEs were separated by sedimentation through sucrose gradients, and the gradient fractions were subjected to Western analysis with antibodies against MFC components and the 40S subunit protein Rps22. The Western signals in the 40S fractions were quantified and normalized to Rps22 levels, and the mean eIF/40S ratio for each MFC component was determined from replicate experiments. After growth at 36°C, neither *H725P* nor *R731I* produced a reduction in the eIF/40S ratios compared to the wild type (WT) (Fig. 3A and B), suggesting that the rate-limiting defects conferred by these mutations occur at a step following 43S PIC assembly. The *box6* mutation leads to reductions of from 25 to 50% in the eIF/40S ratios for MFC constituents, including subunits of eIF3, eIF2γ, eIF5, and possibly eIF1, but does not reduce the level of 40S-bound eIF1A, which is not an MFC component (Fig. 3C). These findings suggest that a portion of the initiation defect in this mutant involves a reduced rate of formation, or decreased stability, of 43S PICs.

To examine the effects of the KERR and box6 substitutions on 48S PIC assembly, we measured the amounts of *RPL41A* mRNA associated with native 48S complexes in extracts of cross-linked cells. These experiments were conducted using

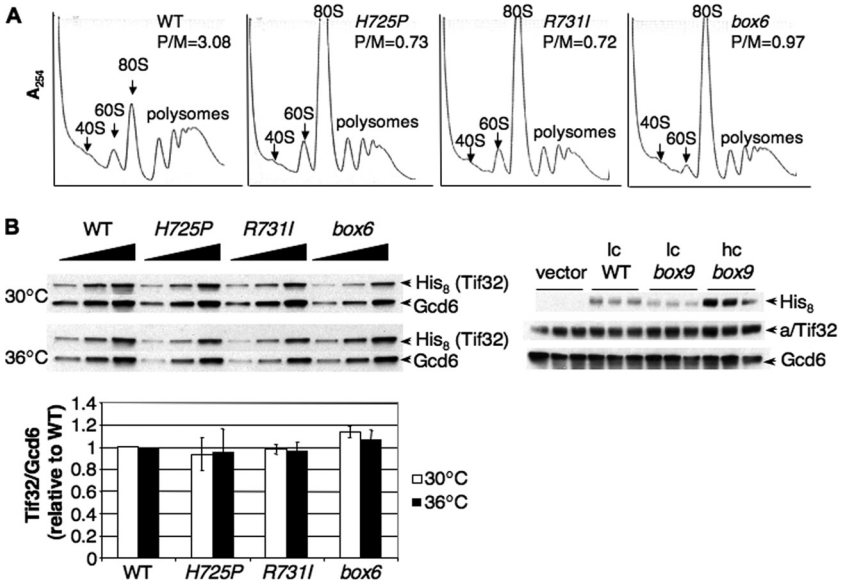

FIG. 2. a/HLD substitutions impair translation initiation. (A) Polysome profiles of the strains shown in Fig. 1C cultured in YPD medium at 30°C and shifted to 36°C for 6 h, with cycloheximide added just prior to harvesting. WCEs were separated by velocity sedimentation through 4.5 to 45% sucrose gradient centrifugation, and fractions were collected while scanning at 254 nm to visualize ribosomal species and determine P/M ratios. (B) Western analysis of a/Tif32 proteins. (Left) WCEs were prepared from the strains in panel A after being cultured in YPD at 30°C or after being shifted to 36°C for 6 h. Aliquots (2.5, 5, and 10 μl in successive lanes) were separated by SDS-PAGE and subjected to Western analysis with monoclonal antibodies against His_8 epitope or polyclonal antibodies against Gcd6. The amounts of His_8-a/Tif32 were normalized to the Gcd6 amounts measured in the same lanes, and the resulting ratios were normalized to those measured in WT cells (set to 1.0). The mean and standard errors calculated from replicate determinations are plotted in the histogram below. (Right) Western analysis of WCEs from transformants of *TIF32*$^+$ strain H2994 harboring lc WT *TIF32-His* or lc or hc *tif32-box9-His* and cultured in synthetic complete medium lacking uracil at 30°C. (Because of its lethality, expression of His_8-a/Tif32-box9 was examined in cells containing *TIF32*$^+$).

isogenic strains lacking one of the genes encoding the 60S protein Rpl11 (*RPL11B*), as the reduced level of 60S subunits, and attendant reduced rate of 60S subunit joining, produced by *rpl11BΔ* increases the concentration of 48S PICs (23). This accentuates the peak of 48S-associated *RPL41A* mRNA relative to the free *RPL41A* mRNP and facilitates quantification of the 48S species. Using real-time quantitative reverse transcription (RT)-PCR to assay *RPL41A* mRNA and 18S rRNA in each fraction, we found that all three mutations significantly reduced the mean *RPL41A* mRNA/18S rRNA ratio by 40 to 50% in three replicate experiments (Fig. 3D). Although the total amount of *RPL41A* mRNA was lower in the mutants, there was an obvious shift in the distribution of *RPL41A* mRNA toward free mRNP, indicating a substantial underutilized pool of free mRNP. It seems possible that the reduced amounts of total *RPL41A* mRNA in the mutants results from increased degradation due to its decreased recruitment by 43S PICs, leading to an underestimate of the actual defect in 48S assembly. Marked reductions in the *RPL41A* mRNA/18S rRNA ratio, coupled with a relative accumulation of free *RPL41A* mRNPs, were also observed for all three *tif32* mutations in the *RPL11* background (data not shown). Hence, we conclude that the *tif32* mutations impair the assembly or stability of 48S PICs. The decrease in 48S abundance provoked by *box6* could arise partly from its effect on 43S assembly (Fig. 3C), while the KERR mutations seem to impair a function specifically required for mRNA recruitment.

a/HLD mutations impair *GCN4* translational induction and increase leaky scanning of uAUG-1. We next examined the *tif32* mutations for defects in the efficiency of scanning and AUG recognition, using *GCN4* translational control as a sensitive genetic reporter of this process (21). *GCN4* encodes a transcriptional activator of amino acid biosynthetic genes whose translation is derepressed by amino acid starvation when formation of TC is reduced by phosphorylation of eIF2α by kinase Gcn2. This regulation is mediated by the four uORFs in the *GCN4* mRNA leader. Under nonstarvation conditions, ribosomes scan from the cap and translate uORF1, and the fraction that resumes scanning will rebind the TC; reinitiate at uORF2, -3, or -4; and subsequently dissociate from the mRNA, failing to translate *GCN4*. When the TC level drops under starvation conditions, a portion the subunits rescanning from uORF1 do not rebind the TC until after bypassing uORF2 to -4, and reinitiate at *GCN4* instead. Thus, translation of uORF1, and the ability of ribosomes to reinitiate downstream following termination at uORF1, is crucial for induction of *GCN4* translation in starved cells.

Mutations that impair derepression of *GCN4* translation confer sensitivity to inhibitors of amino acid biosynthesis, including sulfometuron (SM), indicating a Gcn$^-$ phenotype (21). Interestingly, all three *tif32* mutations confer sensitivity to SM at permissive (30°C) and semipermissive (33°C) temperatures (Fig. 4A) and produce dramatic reductions in derepression of a *GCN4-lacZ* reporter containing all four uORFs in cells treated with SM at 33°C (Fig. 4B, construct i). Only *box6* reduced expression of the construct lacking all four uORFs (Fig. 4B, ii), but the magnitude of the effect, 10 to 20%, was far less than that observed for the uORF-containing construct.

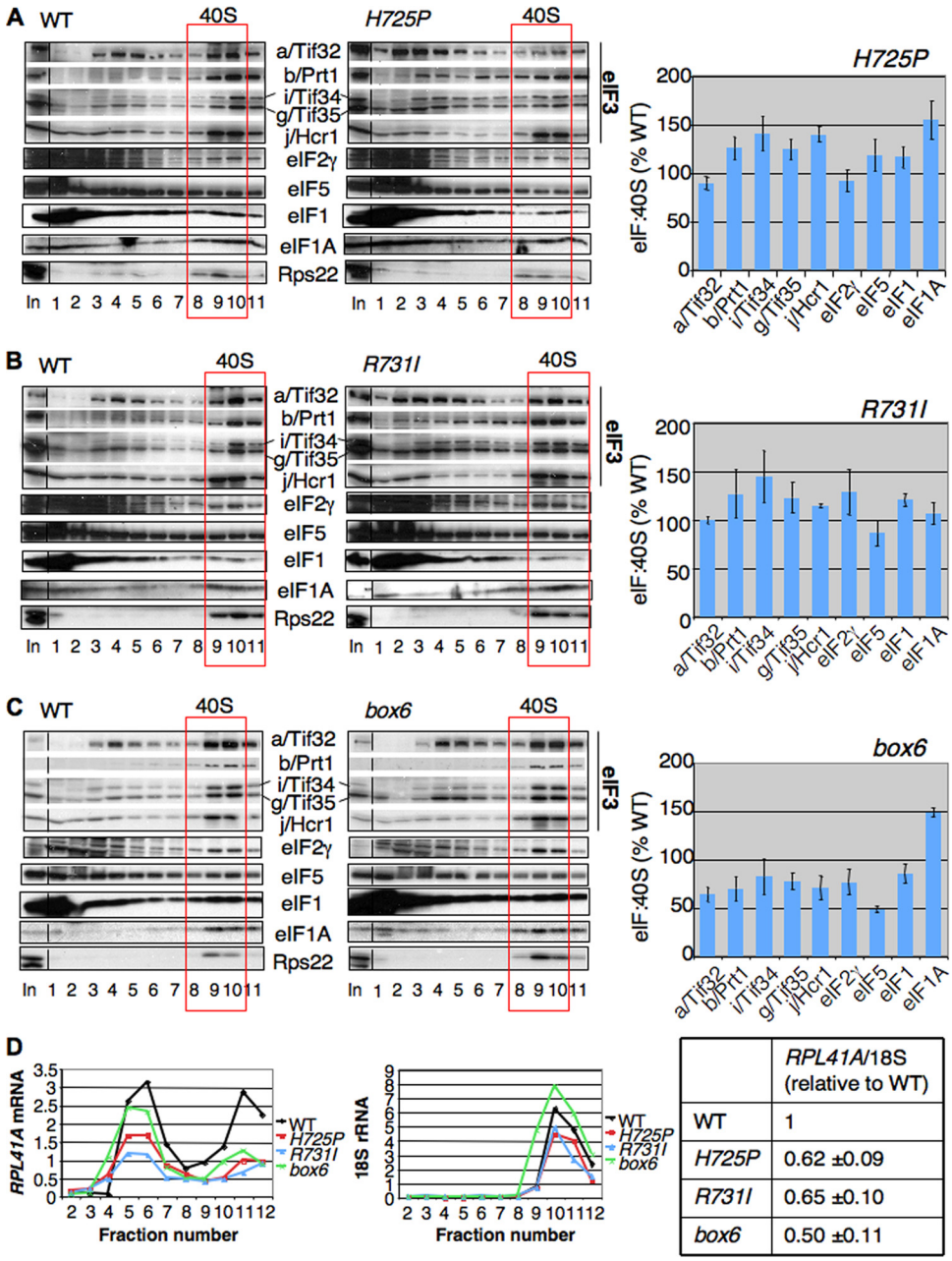

	RPL41A/18S (relative to WT)
WT	1
H725P	0.62 ±0.09
R731I	0.65 ±0.10
box6	0.50 ±0.11

FIG. 3. a/Tif32 KERR substitutions diminish native 48S PICs containing *RPL41A* mRNA. (A to C) Strains shown in Fig. 1C were grown in YPD at 30°C and shifted to 36°C for 6 h, and the cells were cross-linked with HCHO for 1 h prior to being harvested. WCEs were sedimented through 7.5 to 30% sucrose gradients, and fractions were subjected to Western analysis with antibodies against the indicated proteins. The amounts of each factor in the 40S fractions (boxed) were normalized for the Rps22 level, and the ratios of the eIF/40S levels in the mutant to those in the WT were plotted in the adjoining histograms (means ± standard errors [SE]; $n = 3$). (D) (Left) *rpl11b*Δ strains isogenic to those in panels A to C were cultured and cross-linked as described above. Total RNA was extracted from each fraction, and the amounts of 18S rRNA and *RPL41A* mRNA were measured by real-time quantitative PCR (qPCR). The amounts of mRNA were calculated as $2^{-CT} \times 10^{-7}$ for *RPL41A* mRNA and $2^{-CT} \times 10^{-4}$ for 18S rRNA. (Right) The ratio of *RPL41A* mRNA in fractions 10 to 12 to 18S rRNA in fractions 9 to 11 was calculated for each mutant and normalized to the corresponding value for WT (means ± SE; $n = 4$). Student's *t* test indicated that the value for each mutant differed significantly from that for the WT ($P < 0.01$).

Hence, the *tif32* mutations impair derepression of *GCN4* translation.

Western analysis of WCEs from cells induced with SM revealed no significant reduction in eIF2α phosphorylation in any of the mutants (data not shown). This suggested that the mutations impair one or more steps in the *GCN4* reinitiation mechanism, which could include decreased recognition of uORF1 by "leaky scanning" of its start codon (uAUG-1), loss of posttermination 40S subunits at the uORF1 stop codon, or a reduced rate of scanning by reinitiating ribosomes between

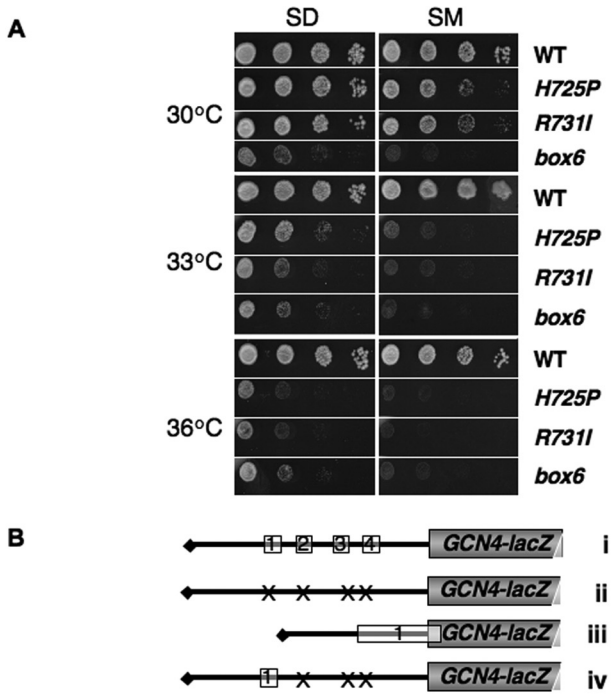

		GCN4-lacZ activity (U) at 33°C/ Relative to WT				
	SM	WT	*H725P*	*R731I*	*box6*	*box6 norm.*
i	-	17 ±3.3 100%	17 ±1.8 100%	12 ±1.7 71%	12 ±1.0 71%	16 94%
	+	245 ±53 100%	33 ±5 13%	15 ±3 6%	27 ±5 11%	36 15%
ii	-	2000 ±280 100%	2000 ±170 100%	2000 ±80 100%	1500 ±95 75%	2000 100%
	+	2100 ±250 100%	2300 ±290 110%	2100 ±120 100%	1800 ±75 85%	2400 115%
iii	-	10 ±1 100%	25 ±2.4 250%	27 ±4 270%	14 ±1.4 140%	19 190%
iv	-	390 ±60 100%	460 ±29 120%	660 ±32 170%	330 ±16 85%	440 110%

FIG. 4. a/HLD mutations impair derepression of *GCN4* translation and increase leaky scanning of uAUG-1. (A) a/HLD mutants have Gcn$^-$ phenotypes. Serial dilutions of the strains in Fig. 1C were spotted on SD+HWU and SD+HWU containing 0.5 μg/ml SM and incubated at 30°C, 33°C, or 36°C for 3 days. (B) a/HLD mutations alter expression of *GCN4-lacZ* reporters. Shown are the strains in Fig. 1C harboring *GCN4-lacZ* reporter plasmid p180 (i), p227 (ii), pM226 (iii), or p209 (iv), containing the 5′ UTR configurations shown schematically, with Xs indicating AUG mutations in uORFs. Transformants were grown in SD+HWU (−) or SD+HWU containing 0.5 μg/ml SM (+), as indicated in the left-hand column, at 33°C for 6 h, and β-galactosidase activity (in nmol of *o*-nitrophenyl-β-D-galactopyranoside cleaved per min per mg) was assayed in WCEs. The means and SE from four independent transformants are reported, along with the means expressed as a percentage of the corresponding WT value. The values in the column "*box6 norm.*" are the results from column "*box6*" normalized to correct for the different expression of construct ii (without SM) in *box6* versus WT cells.

uORF1 and uORF4. Analysis of a construct containing a single elongated version of uORF1, which permits *GCN4-lacZ* expression only by leaky scanning of uAUG-1, revealed an ~2.6-fold increase in *GCN4-lacZ* expression in the *H725P* and *R731I* mutants (Fig. 4B, iii). A smaller but significant increase of 1.9-fold was observed for *box6* after normalizing for its effect on the expression of *GCN4-lacZ* lacking a uORF (Fig. 4B, iii, *box6 norm.*). Thus, all three *tif32* mutations moderately increased leaky scanning of uAUG-1.

Analysis of a construct containing only WT uORF1 at its normal location, which allows a high level of reinitiation at *GCN4*, revealed increases in expression of 1.1- to 1.7-fold (Fig. 4B, iv). These results eliminate the possibility that the mutations reduce the number of posttermination 40S subunits that

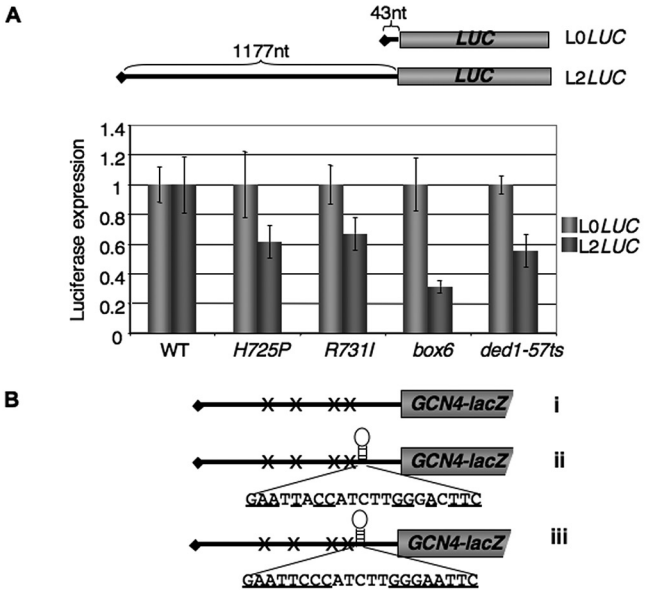

		GCN4-lacZ activity (U) at 33°C/ Relative to WT						
		WT	***H725P***	***R731I***	***box6***	***box6 norm.***	***ded1-57***	***ded1 norm.***
i		1700 ±280 100%	1700 ±105 100%	1800 ±70 106%	1400 ±130 82%	1700 100%	4200 ±510 247%	1700 100%
ii	ΔH= 0.3 kcal	1500 ±140 100%	1100 ±25 73%	1300 ±130 87%	750 ±5 50%	910 61%	3200 ±180 213%	1300 87%
iii	ΔH= -8.7 kcal	210 ±8 100%	195±0.2 93%	240 ±8 110%	42 ±3 20%	51 24%	110 ±5 52%	45 21%

FIG. 5. Evidence that a/HLD substitutions confer scanning defects *in vivo*. (A) Effects of a/HLD mutations on expression of *LUC* reporters with 5′ UTRs of different lengths. The yeast strains in Fig. 1C and H3774 (*ded1-57*), harboring the plasmid-borne L0*LUC* or L2*LUC* reporters under the control of the *GAL1* promoter with the indicated 5′ UTR lengths, were grown in SD supplemented with adenine, histidine, and tryptophan at 30°C to an A_{600} of ~0.6, shifted to the same medium containing galactose instead of glucose, and incubated at 36°C for 6 h. Luciferase activities were assayed in WCEs, and the means and SE from 6 independent transformants for L2*LUC* were normalized to the corresponding values for L0*LUC*. (B) The yeast strains from panel A were transformed with *GCN4-lacZ* reporter plasmid p227 (i), pWCB07 (ii), or pWCB06 (iii), indicated schematically as in Fig. 4B, except that constructs ii and iii contained the indicated sequences inserted 21 nt 5′ of the *GCN4* AUG codon, with complementary bases underlined. The cells were cultured in SD+HW at 33°C for 6 h, and β-galactosidase activities were assayed in WCEs of four independent transformants. Means ± SE ($n = 4$) and activities as percentages of WT values are indicated. The values in the columns "*box6 norm.*" and "*ded1 norm.*" are the results from columns "*box6*" and "*ded1-57*" normalized to correct for the different expression levels of construct i in *box6* or *ded1-57* versus WT cells.

resume scanning following termination at uORF1, a defect observed previously for truncation of the a/Tif32 NTD (42), as this defect would decrease expression of the solitary-uORF1 construct. In fact, *R731I* confers a significant increase in expression of this solitary-uORF1 construct ($P < 0.01$) that is too large to be explained solely by the amount of leaky scanning of uAUG-1 that occurs in this strain (Fig. 4B, 660 − 390 = 270 units, from row 6, versus 27 − 10 = 17 units, from row 5). Hence, *R731I* might also reduce the rate of scanning by reinitiating 40S subunits, as this would increase the number of subunits that rebind the TC before reaching *GCN4* and thereby increase *GCN4-lacZ* expression from the solitary-uORF1 construct (row 6).

Evidence for scanning defects in *tif32* box6 and KERR mutants. We also examined the effects of *tif32* mutations on the expression of two luciferase constructs designed to reveal defects in the processivity of ribosomal scanning, as they differ greatly in 5′ UTR lengths at 43 nt (*L0-LUC*) and 1,177 nt (*L2-LUC*) (4). Consistent with previous findings (4), the *ded1-57* mutation, affecting DEAD box RNA helicase (Ded1) (8), has a greater effect on expression of the reporter with the long 5′ UTR, lowering the ratio of *L2-LUC* to *L0-LUC* expression by 45% after cells were shifted to 36°C. Interestingly, all three *tif32* mutations have effects similar to those of the *ded1-57* mutation. While it is conceivable that a longer 5′ UTR would reduce the efficiency of 43S PIC attachment, we think it is more likely that the *tif32* mutations disproportionately reduce expression of the *L2-LUC* reporter because they diminish the processivity of ribosomal scanning (Fig. 5A).

We also examined the effects of the *tif32* mutations on the inhibitory effect of a stem-loop structure inserted in the 5′ UTR of the *GCN4-lacZ* construct lacking a uORF, which diminished translation in WT cells by a factor of ~8 (Fig. 5B,

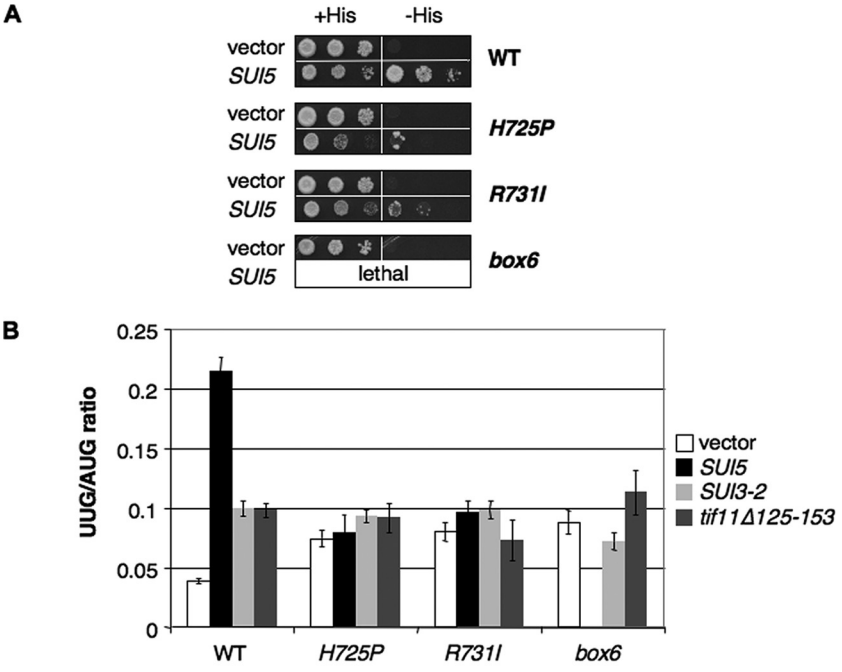

C

	UUG/AUG ratio			
	Relative to WT	Relative to vector		
	vector	*SUI5*	*SUI3-2*	*tif11Δ125-153*
WT	0.04±0.001 1X	0.21 ±0.011 5.3X	0.10 ±0.006 2.5X	0.10 ±0.006 2.5X
H725P	0.07 ±0.007 1.9X	0.08 ±0.015 1.1X	0.09 ±0.005 1.3X	0.09 ±0.012 1.3X
R731I	0.08 ±0.008 2.0X	0.10 ±0.009 1.3X	0.10 ±0.007 1.3X	0.07 ±0.017 0.9X
box6	0.09 ±0.01 2.3X	lethal	0.07 ±0.007 0.8X	0.11 ±0.019 1.2X

FIG. 6. a/HLD mutations suppress UUG initiation in Sui$^-$ mutants. (A) Suppression of His$^+$/Sui$^-$ phenotypes of *SUI5*. Serial dilutions of *his4-301* strains in Fig. 1C harboring empty vector or a *SUI5* plasmid were grown at 30°C on SD+H for 3 days or SD for 7 days. (B and C) Suppression of increased UUG/AUG initiation ratio. Strains from Fig. 1C carrying empty vector or the *SUI5*, *SUI3-2*, or *tif11Δ125-153* plasmid and harboring *HIS4-lacZ* reporter plasmids with an AUG or UUG start codon were grown in SD+H medium and assayed for β-galactosidase activity in WCEs. The mean ratios and SE of UUG versus AUG reporter expression from six independent transformants are shown, with the fold increases relative to the WT for the vector transformants of each strain in the column "vector" and the fold increases relative to vector for each plasmid-borne Sui$^-$ allele in each strain in the remaining three columns.

WT, iii versus i). Whereas the *H725P* and *R731I* mutations did not affect sensitivity to the stem-loop, *box6* increased the inhibitory effect 4-fold (Fig. 5B, iii, WT versus *box6 norm*.). Importantly, *box6* had a substantially smaller effect (~40% reduction) on a construct harboring an insertion with alterations eliminating 2 of the 7 predicted base pairs of the stem-loop (Fig. 5B, ii, WT versus *box6 norm*.), which dramatically reduced the predicted minimum free energy of the inserted hairpin structure (ΔH) and inhibitory effect of the insertion in WT cells (Fig. 5B, WT, ii versus iii). Interestingly, the *ded1-57* mutation also greatly increased sensitivity to the more stable stem-loop, by a factor of ~5, after normalizing for its effect on expression of the parental construct lacking uORF. Thus, in the several different assays shown in Fig. 4 and 5, the *H725P*, *R731I*, and *box6* mutations exhibited defects in scanning and efficient AUG selection, with *H725P* and *R731I* showing similar effects and differing in some respects from *box6*.

a/HLD substitutions suppress the enhanced UUG initiation conferred by dominant Sui$^-$ mutations. Previously, we showed that eIF1A mutations that exhibit Gcn$^-$ phenotypes and increase leaky scanning of *GCN4* uORF1, like the *tif32* a/HLD mutants, also exhibit Ssu$^-$ phenotypes, suppressing initiation at UUG start codons in Sui$^-$ mutants (13). The Sui$^-$ phenotype is manifested in strains containing the *his4-301* allele, which lacks the ATG start codon and confers histidine auxotrophy (His$^-$ phenotype). By increasing initiation at the third (UUG) codon in *his4-301* mRNA, Sui$^-$ mutations allow growth on medium lacking histidine (−His). As shown previ-

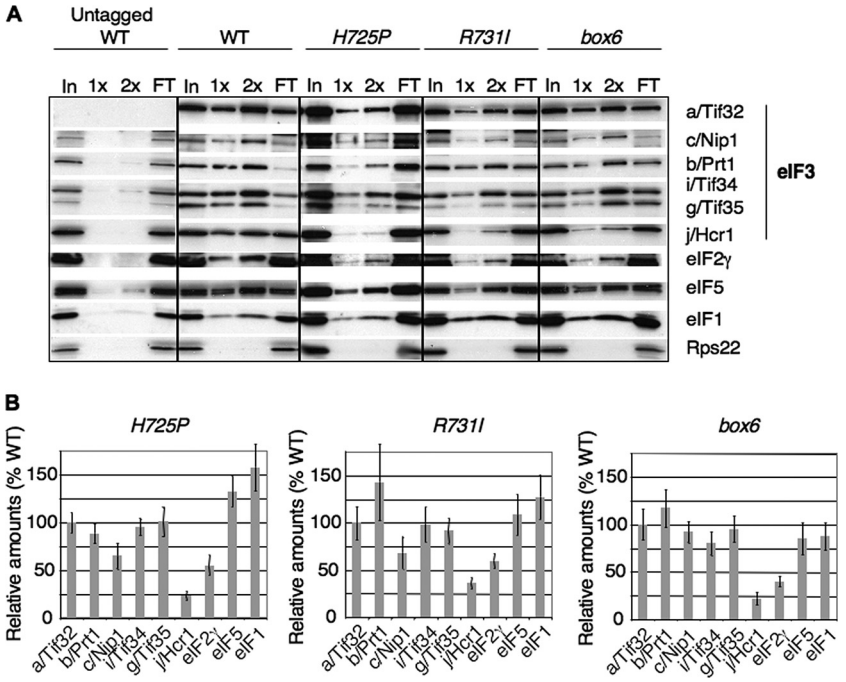

FIG. 7. a/HLD substitutions weaken interactions of eIF3 with j/Hcr1 and eIF2. (A) Strains described in Fig. 1C were cultured in YPD medium at 30°C and shifted to 36°C for 6 h. WCEs were incubated with Ni-NTA-silica resin, and bound proteins were eluted and subjected to Western blot analysis with antibodies against the His_8 epitope (for a/Tif32) or against the factors listed on the right. Three percent of input WCE (In), 15% and 30% of the eluate (1× and 2×), and 3% of flowthrough (FT) were analyzed in successive lanes. (B) Western signals for each factor in the eluates from panel A were normalized to that of His_8-a/Tif32, and the ratio of each *tif32* mutant to WT was plotted (means ± SE; $n = 3$).

ously, the dominant Sui^- allele *SUI5* (encoding the eIF5-G31R mutant) allowed *TIF32*$^+$ *his4-301* cells to grow in −His medium (Fig. 6A, rows 1 and 2). Interestingly, the His^+ phenotype of *SUI5* was diminished by the *H725P* and *R731I* mutations at 30°C (Fig. 6A, rows 4 and 6 versus 2), suggesting that these *tif32* mutations have Ssu^- phenotypes at the permissive growth temperature. The *box6* mutation is synthetically lethal with *SUI5*, and *H725P* and *R731I* cells are barely viable at 33°C in the presence of *SUI5* (data not shown). Given that *SUI5* reduces the efficiency of AUG initiation, as well as increasing the frequency of UUG initiation (26), these observations might be explained by proposing that the combined deleterious effects of *SUI5* and the *tif32* mutations on AUG recognition greatly reduce cell viability.

To confirm the Ssu^- phenotypes of *H725P* and *R731I* mutants, we measured the expression of matched *HIS4-lacZ* reporters containing AUG or UUG start codons. Indeed, all three *tif32* mutations completely eliminated the ability of *SUI5* and two other dominant Sui^- mutations affecting eIF2β (*SUI3-2*) or eIF1A (*tif11Δ125-153*) to increase the efficiency of UUG initiation. Thus, in the *TIF32*$^+$ strain, the dominant Sui^- mutations increased the UUG/AUG initiation ratio by factors of 2.5 to 5 but had little effect on the UUG/AUG ratio in the *tif32* mutants (Fig. 6B and C). Interestingly, the *tif32* mutations by themselves produced an ~2-fold increase in the UUG/AUG ratio in cells bearing an empty vector, suggesting that, besides being Ssu^-, they also confer a moderate Sui^- phenotype in otherwise WT cells (Fig. 6B and C, vector). Examination of the absolute expression levels of the UUG and AUG reporters (data not shown) revealed that the *H725P* and *R731I* mutations lowered the expression of both reporters but had a greater effect on AUG than on UUG initiation (increasing the UUG/AUG ratio) in otherwise WT cells and had a greater effect on UUG than AUG (reducing the UUG/AUG ratio) in the *SUI5* background. Together, these findings indicate that the *tif32* mutations impair one or more mechanisms that ensure accurate selection of AUG start codons, increasing the relative frequency of UUG initiation on their own but completely masking the effects of Sui^- alterations in eIF2, eIF5, and eIF1A on the UUG/AUG ratio.

***tif32* KERR mutations reduce j/Hcr1 association with eIF3 in a manner contributing to their growth phenotypes.** In view of our findings that the a/Tif32 KERR substitutions do not affect MFC binding to native 40S subunits (Fig. 3A and B), we wondered whether they might alter intersubunit interactions within eIF3 as a way of impairing its functions in mRNA recruitment, scanning, or AUG recognition in the 48S PIC. Accordingly, we measured the copurification of MFC components with His_8-tagged a/Tif32 in nickel chelation chromatography of WCEs. Following growth at 36°C, the *H725P*, *R731I*, and *box6* mutants all displayed significant reductions in copurifying j/Hcr1 (relative to the yield of His_8-a/Tif32), with little additional effect on other MFC components, except for an ~50% reduction in the amount of eIF2 associated with the complex (Fig. 7A and B).

It was shown previously that overexpressing j/Hcr1 from an hc plasmid partially suppressed the Ts^- phenotype of *tif32-R731I* (46). As all three substitutions in the a/HLD reduce j/Hcr1 association with eIF3, we asked whether the growth defects conferred by *H725P* and *box6* are also suppressible by

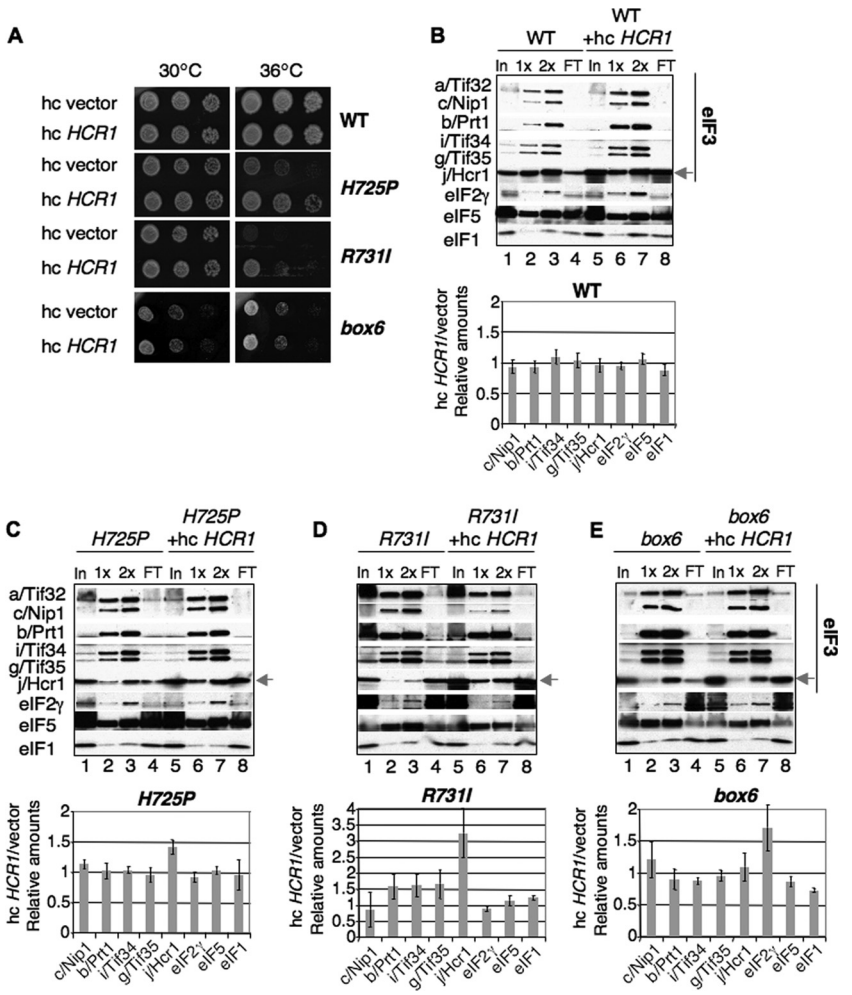

FIG. 8. Overexpression of j/Hcr1 partially suppresses the Ts$^-$ phenotypes of *tif32* KERR mutants and restores j/Hcr1 association with eIF3. (A) Serial dilutions of the strains from Fig. 1C harboring an hc empty vector or hc *HCR1* plasmid were spotted on SD+HWU and incubated at 30°C or 36°C for 3 days. (B to E) Nickel chelation chromatography of WCEs from strains in panel A was conducted as for Fig. 7A. Western signals were quantified, and the ratios of normalized values for hc *HCR1* versus empty vector are plotted in the histograms (means ± SE; $n = 3$).

hc *HCR1*. Interestingly, hc *HCR1* partially suppressed the Ts$^-$ phenotype of *H725P*, as well as *R731I*, but not the Slg$^-$ phenotype of the *box6* mutant (Fig. 8A). Consistent with this, hc *HCR1* increased the yield of j/Hcr1 copurifying with His_8-tagged a/Tif32 from *H725P* and *R731I* cells, but not from *box6* or WT cells (Fig. 8B to E, cf. lanes 2 to 3 versus 6 to 7 in the blots and adjoining histograms). These findings suggest that the initiation defects conferred by *H725P* and *R731I* can be partially corrected by restoring j/Hcr1 association with eIF3 in the PIC.

The fact that the *H725P* and *R731I* mutations reduce the amounts of j/Hcr1 and eIF2γ that copurify with His_8-a/Tif32 (Fig. 7A and B), but not the amounts bound to 40S subunits *in vivo*, can be explained by proposing that the mutations impair only a subset of the interactions that stabilize j/Hcr1 and eIF2 association with eIF3, eIF5, and eIF1 in the MFC. Loss of these interactions is sufficient to allow j/Hcr1 and eIF2 to dissociate from eIF3 when the factors are free of the ribosome during affinity purification *in vitro*, but not to provoke j/Hcr1 and eIF2 dissociation from native PICs *in vivo*, owing to their independent interactions with the 40S subunit and the ability of the ribosome to bridge association among MFC components (47, 48).

Given that the *tif32* mutations alter the j/Hcr1-like region of a/Tif32, we explored what regions in overexpressed j/Hcr1 are required to suppress the growth defects of the KERR mutants. The N-terminal 135 residues of j/Hcr1 are necessary and sufficient to complement the Slg$^-$ phenotype in *hcr1*Δ *TIF32*$^+$ cells (10), and consistent with this, eliminating the j/Hcr1 NTD (j/NTD) in the *hcr1-CTD* allele eliminates the ability of hc *HCR1* to suppress the *tif32* KERR mutants containing chromosomal *HCR1*$^+$ (Table 3, column 5). Interestingly, although eliminating the j/Hcr1 CTD (j/CTD) in the *hcr1-NTD* allele has no effect on complementation of *hcr1*Δ (10), it destroys the suppressor activity of hc *HCR1* (Table 3, column 3). As noted above, the j/CTD contains sequences similar to box6 and the box9/KERR motif of a/Tif32 (Fig. 1A; see Fig. 10A). Introducing the 10-Ala substitution of box6 into j/Hcr1 by the *hcr1-box6* allele also abolished the ability of hc *HCR1* to suppress the *tif32* KERR mutants without affecting complementation of

TABLE 3. Effects of *HCR1* mutations on suppression of the Ts$^-$ phenotypes of *tif32-R731I* and *tif32-H725P* mutants[a]

Strain	Growth				
	Empty vector	hc *HCR1*	hc *hcr1-NTD*	hc *hcr1-box6*	hc *hcr1-CTD*
tif32-R731I HCR1	−	+	−	−	−
tif32-H725P HCR1	−	+	−	−	−
*TIF32 hcr1*Δ	−	+	+	+	−

[a] *tif32*Δ *HCR1*$^+$ strains YSW731 and YSW725 harboring pRS-a/tif32-R731I-His-L (*tif32-R731I HCR1*) and pWLCB01 (*tif32-H725P HCR1*), respectively, or *hcr1*Δ strain H428 (*TIF32 hcr1*Δ), were transformed with YEplac195 (Empty vector), YEp-j/HCR1-DS-U (Hc *HCR1*), YEp-j/hcr1-NTD-U (Hc *hcr1-NTD*), YEp-j/hcr1-box6-U (Hc *hcr1-box6*), and YEp-j/hcr1-CTD-U (Hc *hcr1-CTD*) and examined for growth at 36°C as described in the legend to Fig. 8A, and the results are summarized qualitatively (+, growth; −, no growth).

the *hcr1*Δ mutant (Table 3, column 4). Thus, both the critical NTD and the dispensable CTD of j/Hcr1, including the box6 element, are required for the ability of overexpressed j/Hcr1 to boost translation initiation in the *tif32* KERR mutants.

Having found that suppression of the *tif32* KERR mutations by hc WT *HCR1* is associated with increased interaction of j/Hcr1 with eIF3, we examined whether the loss of dosage suppression by hc *HCR1* conferred by different *hcr1* mutations is associated with diminished interaction of the cognate mutant j/Hcr1 proteins with eIF3. In fact, we showed recently that destroying the specific contact between the b/Prt1 RRM and j/Hcr1 by site-specific mutations abolished association of j/Hcr1 with His_8-tagged b/Prt1 and other MFC components in WCEs (10). Hence, as expected, removing the entire NTD (in construct *hcr1-CTD*) also completely eliminated j/HCR1 from the MFC (Fig. 9A, lanes 14 and 15 versus 6 and 7 and adjoining histogram). Likewise, eliminating j/CTD in *j/hcr1-NTD*, substituting box6, or altering the KERR motif with a substitution (R215I) equivalent to R731I in a/Tif32 all had similar effects of impairing association of the mutant j/Hcr1 proteins with His_8-b/Prt1 (Fig. 9A, lanes 10 and 11 versus 6 and 7). The results in Table 3 and Fig. 9 together indicate that both the NTD and CTD of j/Hcr1 are required for its tight binding to eIF3 and the

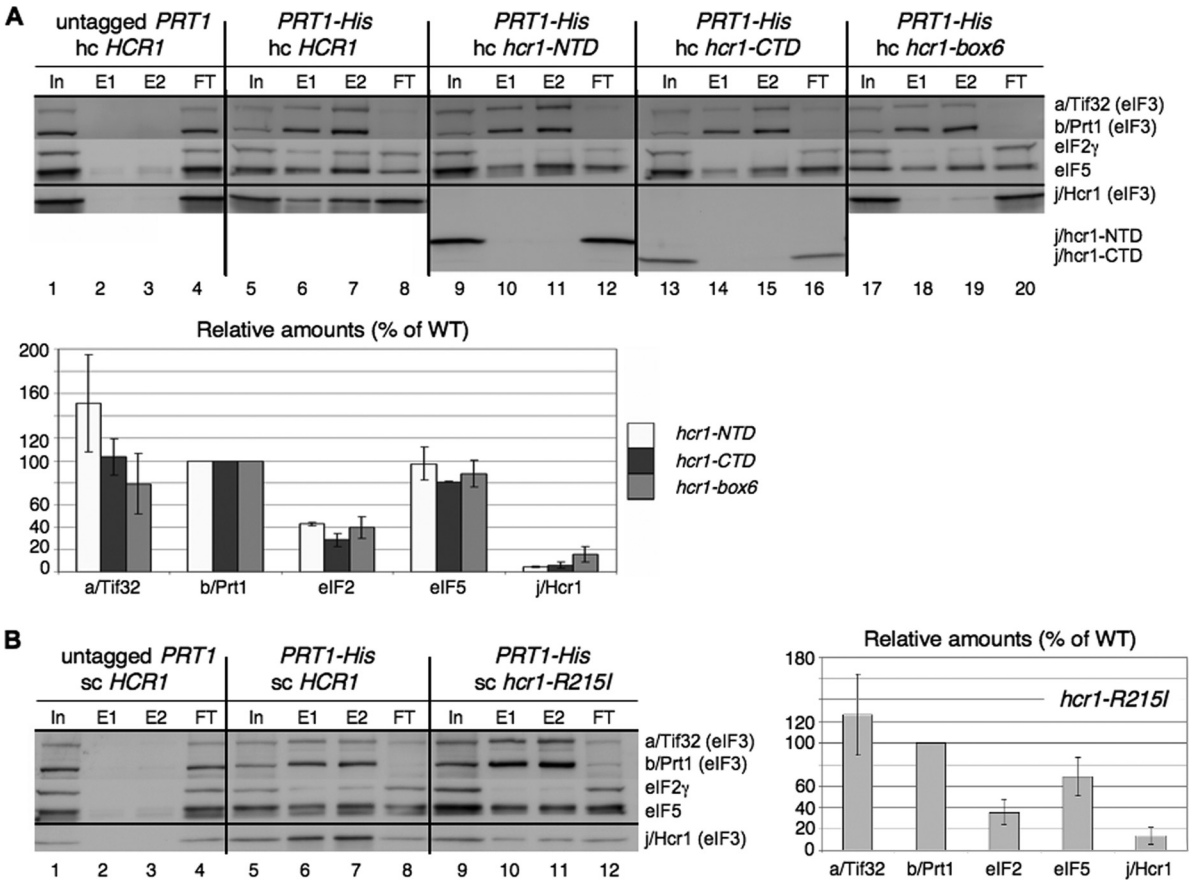

FIG. 9. The NTD, box6, and KERR motif in the CTD of j/Hcr1 are required for its association with eIF3. (A) WCEs were prepared from a transformant of YAH05 (*prt1*Δ *hcr1*Δ pRS316-*PRT1* [*PRT1 URA3*]) containing plasmid YEp-j/HCR1-DS (lanes 1 to 4) or from YAH05 derivatives lacking pRS316-*PRT1* and containing pRS-b/PRT1-His and YEp-j/HCR1-DS-U (lanes 5 to 8), pRS-b/PRT1-His and YEp-j/hcr1-NTD-U (lanes 9 to 12), pRS-b/PRT1-His and YEp-j/hcr1-CTD-U (lanes 13 to 16), or pRS-b/PRT1-His and YEp-j/hcr1-box6-U (lanes 17 to 20), cultured in SD at 30°C. Nickel chelation chromatography and Western blot analysis were conducted as for Fig. 7A, except that 5% of input WCEs (In), 30% (E1) or 60% (E2) of the eluates, and 5% of flowthrough (FT) was loaded. Mean Western signals were normalized to those of b/Prt1-His_8 and plotted as percentages of the corresponding values calculated for the *HCR1*$^+$ strain. (B) Same as panel A, except that WCEs were prepared from a YAH05 transformant harboring YCp-j/HCR1-DS-L (lanes 1 to 4) or YAH05 derivatives lacking pRS316-*PRT1* and containing pRS-b/PRT1-His and YCp-j/HCR1-DS-U (lanes 5 to 8) or pRS-b/PRT1-His and YCp-j/hcr1-R215I-U (lanes 9 to 12).

TABLE 4. Synthetic sick phenotypes of *tif32 hcr1* double mutants[a]

Transformant	Growth[b]						
	WT	None (vector)	*hcr1-CTD*	*hcr1-R215I*	*hcr1-box6*	*hcr1-NTD*	*hcr1-box6-R215I*
TIF32	8+	5+	6+	8+	8+	8+	8+
tif32-R731I	4+	1+	1+	4+	3+	2+	1+
tif32-box6	5+	2+	2+	5+	2+	3+	2+
tif32-H725P	5+	1+	ND	5+	3+	ND	1+

[a] Transformants of *tif32*Δ *hcr1*Δ strain YAH04 harboring combinations of pRS-a/TIF32-His-L (*TIF32*), pRS-a/tif32-R731I-His-L (*tif32-R731I*), pRS-a/tif32-box6-His-L (*tif32-box6*), and pWLCB01 (*tif32-H725P*) with YEp-j/HCR1-DS-U (WT), YEplac195 (None), YEp-j/hcr1-CTD-U (*hcr1-CTD*), YEp-j/hcr1-R215I-U (*hcr1-R215I*), YEp-j/hcr1-box6-U (*hcr1-box6*), YEp-j/hcr1-NTD-U (*hcr1-NTD*), and YEp-j/hcr1-box6-R215I-U (*hcr1-box6-R215I*), from which the original covering plasmid carrying *TIF32 URA3* was evicted on 5-FOA, were examined for growth at 30°C (for *tif32-R731I* and *tif32-H725P*) or 37°C (for *tif32-box6*), and the results are summarized qualitatively. Note that the *tif32* mutant alleles confer a Slg$^-$ phenotype at 30°C in this strain background that is not evident in the strains shown in Fig. 1.

[b] 8+, WT growth; 1+, the lowest growth rate observed; 2+ to 7+, different degrees of growth discernible between these two extremes.

ability to suppress a/Tif32 KERR substitutions when overexpressed.

Interestingly, all of the j/Hcr1 mutations we examined reduced the amount of eIF2γ copurifying with His_8-b/Prt1 (Fig. 9), similar to our findings above that KERR and box6 substitutions in a/Tif32 reduce copurification of both j/Hcr1 and eIF2γ with His_8-a/Tif32. We showed previously that the extreme CTD of a/Tif32 is critical for eIF2 and j/Hcr1 association with eIF3 in the MFC *in vivo* (48). Perhaps binding of j/Hcr1 to the extreme CTD of a/Tif32 is required to "prime" the conformation of this domain for stable interaction with eIF2. In this view, loss of eIF2 from the MFC caused by mutations in j/Hcr1 or the a/HLD is an indirect consequence of impaired j/Hcr1 association with the a/Tif32 CTD.

We showed recently that overexpressing the three subunits of eIF2 and $tRNA_i^{Met}$, the macromolecular components of the TC, partially suppresses the growth defect of *hcr1*Δ cells (10), consistent with the contribution of j/Hcr1 to proper association of the TC with the MFC. In contrast, we found that overexpressing the components of the TC does not suppress the growth defects of the a/HLD substitutions (data not shown), suggesting that weakened interaction of the TC with the MFC is not the rate-limiting defect in these *tif32* mutants. As discussed below, this is consistent with the fact that the a/HLD substitutions impair certain aspects of initiation that are unaffected by elimination of j/Hcr1.

Mutations in both the NTD and CTD of j/Hcr1 exacerbate the growth defects of a/HLD substitutions. In addition to the fact that overexpressing j/Hcr1 partially suppresses the Ts$^-$ phenotype of the *tif32-R731I HCR1*$^+$ mutant, it was shown previously that deleting *HCR1* exacerbates the effect of this *tif32* mutation on cell growth (46), producing a stronger Slg$^-$ phenotype at 30°C than was displayed by either single mutant (Table 4, rows 1 and 2 and columns 1 and 2). We observed the same synthetic sick interaction on combining *hcr1*Δ with the *tif32-box6* or *tif32-H725P* mutation (Table 4, rows 3 and 4 and columns 1 and 2). As might be expected, absence of the critical NTD in the *hcr1-CTD* allele also produced synthetic sick interactions with *tif32-R731I* and *tif32-box6* (Table 4, rows 1 to 3 and column 3 versus 1). Importantly, both the absence of the normally dispensable CTD in *hcr1-NTD* and the *hcr1-box6* mutation likewise exacerbated the Slg$^-$ phenotypes of the *tif32* mutations (Table 4, columns 5 and 6 versus column 1). Moreover, the KERR mutation *hcr1-R215I* further exacerbated the effect of *hcr1-box6*, as revealed in the *hcr1-box6-R215I tif32* triple mutants (Table 4, columns 4 and 7 versus column 1).

The foregoing results indicate that, even though the j/CTD is dispensable for growth in WT cells, it is critically required, together with the j/NTD, when the a/HLD is compromised and that both the box6 and KERR elements in j/Hcr1 contribute to its ability to complement *tif32* mutations. As shown in Table 3, both the j/CTD and j/NTD are also required for the ability of overexpressed j/Hcr1 to suppress *tif32* KERR mutations. These findings imply that the NTD and CTD of j/Hcr1 either functionally substitute for an activity of the a/HLD or enhance the ability of the a/HLD to carry out its function when impaired by KERR or box6 substitutions.

Substitutions in the KERR and box6 elements in both a/Tif32 and j/Hcr1 destabilize the b/RRM–j/Hcr1–a/Tif32-CTD module. Previously, we showed that both j/Hcr1 and a/Tif32 can interact directly with the RRM domain in b/Prt1, so that the b/RRM can bridge a/Tif32-j/Hcr1 interaction (50), and we showed recently that the NTD of j/Hcr1 mediates its direct interaction with the b/RRM (10). a/Tif32 and j/Hcr1 can also interact directly, but the domains involved were not determined, except that regions both N terminal and C terminal to the a/HLD contribute to the interaction (50) (summarized in Fig. 10B). To gain further insights into the consequences of a/HLD and j/Hcr1 mutations for eIF3 integrity, we examined their effects on interactions between different components of the b/RRM–j/Hcr1–a/Tif32-CTD module.

As observed previously (50), *in vitro*-translated ^{35}S-labeled a/Tif32 interacts specifically with GST-j/Hcr1 in a pulldown assay (Fig. 10C, lanes 1 to 3). Absence of the CTD in the GST-j/Hcr1-NTD, or absence of the NTD in GST-j/Hcr1-CTD, essentially eliminates the interaction with a/Tif32 (Fig. 10C, lanes 3 to 5). Consistent with this, substitutions in box6, box9, or R215I in the j/CTD strongly impair GST-j/Hcr1 binding to a/Tif32 (Fig. 10D). Thus, whereas the j/NTD is critical for binding the b/RRM (10), the j/CTD, including its box6 and KERR elements, is more crucial for j/Hcr1-a/Tif32 interaction.

Consistent with previous findings that the a/HLD is not required for j/Hcr1-a/Tif32 interaction (50), we observed no effect of box6 or KERR substitutions in a/TIF32 on its binding to j/Hcr1 *in vitro* (data not shown). Interestingly, however, these substitutions impair binding of the a/HLD to a GST-b/Prt1-RRM fusion (Fig. 10E), indicating that the box6 and

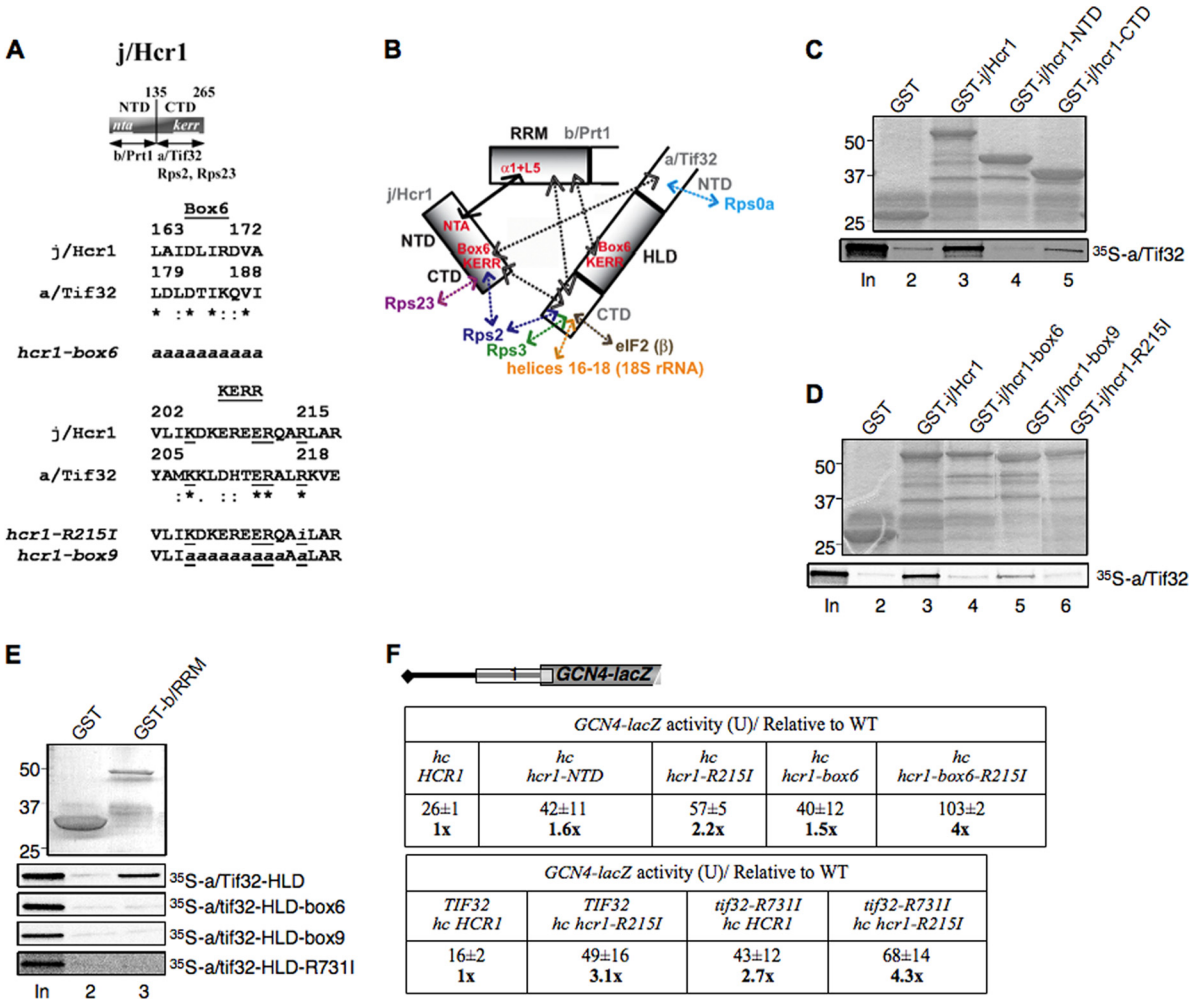

GCN4-lacZ activity (U)/ Relative to WT				
hc HCR1	*hc hcr1-NTD*	*hc hcr1-R215I*	*hc hcr1-box6*	*hc hcr1-box6-R215I*
26±1 **1x**	42±11 **1.6x**	57±5 **2.2x**	40±12 **1.5x**	103±2 **4x**

GCN4-lacZ activity (U)/ Relative to WT			
TIF32 hc HCR1	*TIF32 hc hcr1-R215I*	*tif32-R731I hc HCR1*	*tif32-R731I hc hcr1-R215I*
16±2 **1x**	49±16 **3.1x**	43±12 **2.7x**	68±14 **4.3x**

FIG. 10. Effects of box6 and KERR substitutions in j/CTD and a/HLD on binary interactions in the b/RRM–j/Hcr1–a/Tif32-CTD module and leaky scanning of *GCN4* uAUG-1. (A) Schematic of j/Hcr1 showing the positions of the N-terminal acidic (*nta*) and KERR (*kerr*) motifs, with arrows delimiting minimal binding domains for the indicated proteins. Shown below are sequence alignments of the box6 and KERR segments of j/Hcr1 and a/Tif32, indicating identical (*) or conserved (:) positions, the KERR residues (underlined), and substitutions present in the indicated *hcr1* mutants. Lowercase letters indicate j/Hcr1 residues that were subjected to site-directed mutagenesis. (B) Summary of molecular interactions of components of the b/RRM–j/Hcr1–a/Tif32-CTD module. The shaded rectangles represent the b/RRM, a/HLD, and full-length j/Hcr1. The solid arrow indicates interaction between the NTA motif of j/Hcr1 and helix α1 and loop L5 of the b/RRM, whose structural determinants are known. The dashed arrows depict other interactions that were mapped previously or determined in this study. The results presented here establish the roles of box6 and KERR residues in the a/HLD in binding to the b/RRM and of the equivalent residues in j/CTD in binding a/Tif32 regions flanking the a/HLD. (C) Both the NTD and CTD of j/Hcr1 are required for binding to a/Tif32 *in vitro*. GST fusions to full-length j/Hcr1 (lane 3), the j/NTD (lane 4) or j/CTD (lane 5), or GST alone (lane 2), were tested for binding to full-length ^{35}S-a/TIF32 in pulldown assays. The GST fusions visualized by Coomassie blue staining (top) and the ^{35}S-a/TIF32 visualized by autoradiography (bottom) in the bound fractions are shown in lanes 2 to 5. Lane 1 contains 10% of the input ^{35}S-a/TIF32. (D) The KERR motif and box6 of j/Hcr1 are critical for its binding to a/Tif32. Same as panel C, except that GST fusions to full-length j/Hcr1 (lane 3) or its box6 (lane 4), box9 (lane 5), or R215I (lane 6) mutant derivatives were examined. (E) Substitutions in the KERR motif and box6 in the a/HLD strongly reduce its binding to the b/RRM. A GST fusion to the b/RRM (aa 1 to 136) or GST alone was tested for binding to the indicated WT and mutant derivatives of ^{35}S-a/HLD (aa 490 to 790). (F) Leaky-scanning phenotypes of substitutions in box6 or KERR residues of j/Hcr1 or a/Tif32. (Top) Transformants of *hcr1*Δ strain H428 bearing plasmid YEp-j/HCR1, YEp-j/hcr1-NTD, YEp-j/hcr1-R215I, YEp-j/hcr1-Box6, or YEp-j/hcr1-Box6-R215I and containing *GCN4-lacZ* reporter plasmid pM226 were analyzed for β-galactosidase activities as for Fig. 4B (iii). Mean values and standard errors from 6 or more measurements of three transformants containing pM226 are shown, along with activities in the *hcr1* strains normalized to that in the *HCR1* strain. All values were normalized to correct for any differences among the strains in expression of the reporter lacking uORF on p227. (Bottom) Same as above, but using AY51 (*TIF32-His*) or AY52 (*tif32-R731I-His*) transformants bearing YEp-j/HCR1-W or YEp-j/hcr1-R215I-DS-W, respectively.

KERR elements in the a/HLD are crucial for its direct binding to the b/RRM. Together, the binding data in Fig. 10 indicate that substitutions in the a/HLD and j/CTD impair distinct interactions in the b/RRM–j/Hcr1–a/Tif32-CTD module. These destabilizing effects could be a contributing factor in the synthetic sick interactions produced by combining *tif32* box6 or KERR mutations with mutations affecting the NTD or CTD of j/Hcr1.

It is intriguing that the a/HLD substitutions impair j/Hcr1 association with eIF3 (Fig. 7A), even though, as described above, they do not affect direct j/Hcr1-a/Tif32 interaction but

disrupt binding of the a/HLD to the b/RRM instead. To explain this finding, it could be proposed that the a/HLD-b/RRM interaction stabilizes the conformation of the b/RRM competent for binding the j/NTD and that the *tif32* KERR mutations disrupt this indirect contribution of the a/HLD to j/Hcr1-b/RRM interaction. The fact that the c/Nip1 subunit of eIF3 stabilizes interaction between a/Tif32 and b/Prt1 by binding to both of these subunits (48) could explain why association of b/Prt1 with eIF3 is not reduced by the a/Tif32 KERR substitutions (Fig. 7A and B), despite the fact that they weaken the a/HLD-b/RRM contact.

Integrity of the b/RRM–j/Hcr1–a/Tif32-CTD module is required to prevent leaky scanning. It was of interest to determine whether destabilizing the b/RRM–j/Hcr1–a/Tif32-CTD module in different ways would impair the same steps in translation initiation. This possibility is supported by our previous finding that impairing the j/NTD-b/RRM interaction leads to increased leaky scanning of the elongated version of *GCN4* uORF1, the same phenotype described here for the box6 and KERR substitutions in the a/HLD. Thus, 4- to 5-fold increases in leaky scanning were observed for substitutions in the b/RRM, including the RNP1 motif (32) and the j/NTD interaction surface in alpha helix 1 and loop 5 of the b/RRM, and an ~8-fold increase occurred with elimination of the j/NTD by the *hcr1-CTD* mutation (10). Hence, we investigated whether mutations in the j/CTD affecting its direct interaction with a/Tif32 would likewise increase leaky scanning.

Eliminating the j/CTD (in *hcr1-NTD*) or replacing its box6 or KERR elements produced only small increases of 1.5- to 2-fold in leaky scanning, much less than the ~8-fold increase observed on eliminating the j/NTD (in *hcr1-CTD*) (10). Interestingly, combining the box6 and R215I substitutions in the *hcr1-box6 R215* double mutant increased leaky scanning by a factor of ~4 (Fig. 10F). Given that the j/CTD is largely dispensable for WT recognition of *GCN4* uAUG-1, it is possible that the j/hcr1-box6 R215I mutant protein interferes with the function of the a/HLD in a way that reduces recognition of uAUG-1. Combining *hcr1-R215I* with *tif32-R731I* in a double mutant did not produce a statistically significant increase in leaky scanning compared to that seen for each single mutant (Fig. 10F), consistent with the possibility that *hcr1-R215I* increases leaky scanning by interfering with the function of the a/HLD. In any event, it seems clear that the j/CTD and its interaction with a/Tif32 is less important than the j/NTD-b/RRM interaction for efficient AUG recognition.

Given that the a/HLD substitutions reduce mRNA recruitment by native 43S complexes (Fig. 3D), we wondered if disrupting the b/RRM-j/Hcr1 interaction would also impair this step of PIC assembly. At odds with this possibility, there is no defect in *RPL41A* mRNA binding to native 43S complexes in *hcr1*Δ cells (data not shown). Consistent with this, we found previously that replacing RNP1 of the b/RRM had no effect on 40S binding of *RPL41A* mRNA (32). Thus, the function of the a/HLD in mRNA recruitment does not require an intact b/RRM-j/NTD interaction. A similar conclusion holds for the role of the a/HLD in suppressing UUG initiation (Ssu^- phenotype), as we found that *hcr1*Δ does not significantly reduce the elevated UUG/AUG initiation ratio conferred by the dominant Sui^- alleles *SUI5*, *SUI3-2*, and *tif11*Δ*-125-153* (data not shown). Together, these findings indicate that disrupting different components of the b/RRM–j/Hcr1–a/Tif32-CTD module can have differential effects on individual steps of the initiation pathway.

The extreme CTD of a/Tif32 interacts with the 40S proteins Rps2 and Rps3. We showed previously that the extreme CTD of a/Tif32 (residues 791 to 964) can bind directly to helices 16 to 18 of 18S rRNA (47). This interaction could implicate a/Tif32 in regulating the connection between h16 and Rps3 on the solvent side of the 40S subunit that stabilizes the open conformation of the latch of the mRNA channel (33). Consistent with this possibility, we found that the a/Tif32 CTD also interacts specifically with Rps3. Thus, a GST fusion to the a/Tif32 CTD (aa 791 to 964) binds to ^{35}S-Rps3, but not to ^{35}S-Rps0 (Fig. 11A). (Rps0 was previously shown to interact with a/Tif32 NTD [47].) Remarkably, the GST-a/Tif32-CTD fusion also binds to Rps2 (Fig. 11A), which is situated near the mRNA entry channel adjacent to Rps3 on the solvent side of the 40S subunit (Fig. 11C, top). The a/Tif32 CTD does not bind to Rps23 (Fig. 11A), which resides on the interface side of the mRNA entry channel (41). Interaction of a/Tif32 with Rps2 was confirmed in pulldown assays using GST-Rps2 and *in vitro*-translated a/Tif32 (Fig. 11B). Interestingly, we found recently that the CTD of j/Hcr1 also binds to Rps2 *in vitro*, in a manner impaired by mutations in its KERR motif (10). Thus, it seems very likely that the entire b/RRM–j/Hcr1–a/Tif32-CTD module is situated near the mRNA entry channel pore.

DISCUSSION

In this study, we showed that substitutions in the KERR motif (H725P and R731I) and Ala substitution for nearby residues 692 to 701 (box6) in the a/HLD impair its essential function in translation initiation, at least partly by reducing the recruitment of *RPL41A* mRNA to native 40S subunits *in vivo*. We reported previously that depletion of the entire eIF3 complex from cells impaired *RPL41A* mRNA recruitment *in vivo*; however, TC binding to native 40S subunits also was reduced (23). Because base pairing of $tRNA_i^{Met}$ with AUG stabilizes 48S PICs (27, 36), a large portion of the defect in mRNA recruitment in cells depleted of eIF3 could be secondary to reduced TC recruitment. As the *tif32* KERR substitutions reduce 40S binding of *RPL41A* mRNA without diminishing 43S complexes, our results provide the strongest evidence yet that eIF3, and a/Tif32 in particular, has a direct role in mRNA recruitment by 43S complexes *in vivo*.

In addition to impairing mRNA recruitment, replacing the KERR motif or box6 in a/Tif32 produces phenotypes indicating reduced efficiency of scanning or AUG recognition. First, these mutations preferentially decrease translation of a luciferase reporter with a long 5′ UTR, resembling a substitution in DEAD box helicase Ded1 (4), suggesting that the a/HLD enhances scanning processivity. The *box6* mutation also resembles the *ded1-57* mutation in reducing the ability to scan through a stem-loop structure inserted in the *GCN4* mRNA leader ~400 nt from the 5′ end.

Second, the KERR and box substitutions strongly impair the derepression of *GCN4* translation (Gcn^- phenotype) without affecting eIF2α phosphorylation, indicating that they prevent reinitiating ribosomes from bypassing the inhibitory uORF2 to -4 in cells with reduced TC levels. We ruled out the possibility

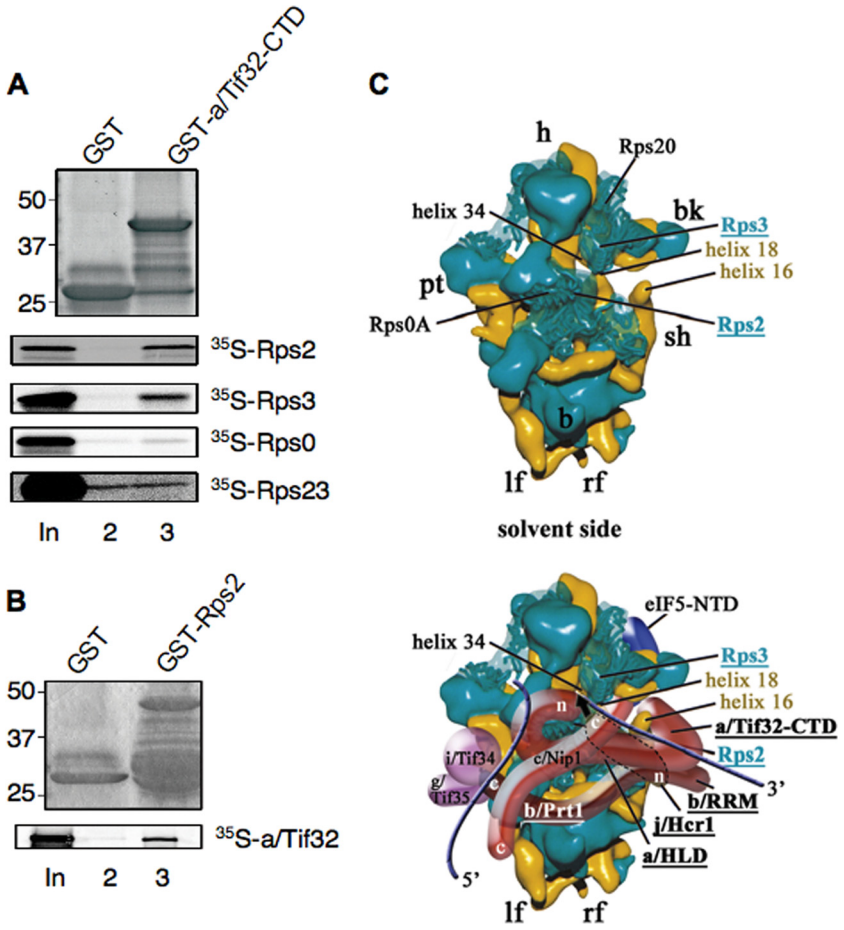

FIG. 11. a/Tif32 CTD interacts with Rps2 and Rps3 *in vitro*: a hypothetical model for binding of a/Tif32 CTD near the mRNA entry channel pore of the 40S subunit. (A and B) The extreme CTD of a/Tif32 interacts with Rps2 and Rps3 *in vitro*. (A) A GST fusion to the a/Tif32-CTD (aa 791 to 964) or GST alone was tested for binding to ^{35}S-labeled full-length Rps2, Rps3, Rps0, or Rps23, as shown in Fig. 10C. (B) Same as panel A, except that Rps2 fused to GST was examined for binding to ^{35}S-a/Tif32. (C) Hypothetical location of eIF3 on the solvent side of the *S. cerevisiae* 40S subunit based on cryo-EM reconstruction (adapted from reference 47). The 40S subunit is shown from the solvent side, with RNA segments in yellow and proteins in green. The positions of Rps2, Rps3, helices 16 and 18 of 18S rRNA, the a/HLD and CTD of a/Tif32, the b/RRM, and j/Hcr1 are highlighted in color and/or boldface. The mRNA exit channel is indicated by an arrow. The blue lines represent mRNA. The positions of Rps2 and Rps3 were modified according to reference 43.

that posttermination 40S subunits cannot resume scanning following translation of uORF1 but observed a moderate increase in leaky scanning of uAUG-1 in the KERR and box6 mutants. The *R731I* KERR mutation also seems to reduce the rate of scanning by posttermination 40S subunits between uORF1 and -4. It seems unlikely, however, that the magnitude of these two defects can account for the nearly complete block to induction of *GCN4* translation observed in these mutants. Hence, we presume that the KERR and box6 substitutions produce additional defects that depend on the presence of 48S PICs at uAUG-2 to -4 in order to be expressed and thus cannot be detected with *GCN4-lacZ* reporters containing uORF1 alone.

The box6 and KERR substitutions in a/Tif32 also affect the accuracy of start codon recognition, as they completely suppress the ability of dominant Sui$^-$ mutations in eIF5, eIF2β, and eIF1A to increase the UUG/AUG ratio—a pronounced Ssu$^-$ phenotype. Previously, we described eIF1A mutations that resemble the a/HLD substitutions in conferring both increased leaky scanning of *GCN4* uAUG-1 and Ssu$^-$ phenotypes (13) and proposed that such mutations destabilize the closed, scanning-incompatible conformation of the 48S PIC with AUG or UUG in the P site. The decreased ratio of UUG to AUG initiation conferred by Ssu$^-$ mutations implies that the defect in accessing the closed conformation is more pronounced at UUG than at AUG. Thus, the a/HLD substitutions could likewise destabilize the closed PIC conformation as a means of reducing recognition of uAUG-1 in otherwise WT cells and of UUG start codons in Sui$^-$ mutants, such as *SUI5.* Examining the matched *HIS4-lacZ* reporters revealed that, in otherwise WT cells, the a/HLD KERR substitutions reduce initiation at both AUG and UUG but have a greater effect at AUG, producing a weak Sui$^-$ phenotype. This trend is reversed in *SUI5* and other Sui$^-$ mutants, where the a/HLD mutations have a greater effect on UUG than on AUG initiation, conferring the Ssu$^-$ phenotype. Thus, it appears that the a/HLD substitutions impede the transition from the open to the closed conformation in a complex way, diminishing the greater probability of the transition at AUG in otherwise wild-

type cells and overriding the effect of *SUI5* and other Sui$^-$ mutations in boosting the transition at UUG codons.

The proposal that the a/HLD mutations destabilize the closed PIC conformation as the means of reducing start codon recognition is consistent with the fact that a/Tif32 interacts with components of the 40S subunit located near the mRNA entry channel pore on the solvent side of the 40S subunit. Thus, the extreme CTD of a/Tif32 can bind an rRNA segment containing h16-h18 (47), and we found here that it also binds Rps2 and Rps3 *in vitro*. Hydroxyl radical cleavage mapping of mammalian eIF3 in the 48S PIC is also consistent with the idea that a segment of eIF3 interacts with h16 (37). Interestingly, cryo-electron microscopy (EM) analysis suggests that Rps3 plays a key role in opening and closing the mRNA entry channel latch, stabilizing the closed position by interacting with h34 but interacting with h16 on the solvent side of the 40S subunit to promote the open-latch conformation (33). It is tempting to consider that the a/Tif32 CTD, by interacting with Rps3, h16, or h18, can modulate the mRNA entry channel latch as a way of influencing the transition from open to closed PIC conformations. If so, then *tif32* a/HLD mutations could reduce the efficiency of uAUG-1 selection and of UUG selection in Sui$^-$ mutants by destabilizing the interaction of Rps3 with h34, or the h18-h34 connection, to impede latch closing on start codon recognition. The proximity of the a/Tif32-CTD to Rps2 and Rps3 at the mRNA entry channel pore might also underlie the ability of the a/HLD to promote mRNA recruitment, serving as an extension of the mRNA binding channel in the manner suggested for mammalian eIF3a and eIF3d (37) and yeast a/Tif32-NTD (42).

Interestingly, the *tif32* a/HLD mutations also produce phenotypes suggesting the opposite effect of destabilizing the open, scanning-compatible conformation of the PIC, as they appear to reduce the processivity of scanning. To account for the seemingly opposite effects of the *tif32* a/HLD mutations on scanning and start codon selection, it could be proposed that they reduce the rate or extent of switching in both directions between the fully open and fully closed conformations of the PIC.

The a/Tif32 KERR and box6 substitutions weaken interactions of j/Hcr1 with the eIF3 complex in WCEs. Both the growth defects and reduced j/Hcr1 association with eIF3 are partially rescued by overexpressing j/Hcr1, suggesting that the a/HLD mutations disrupt a critical function of a/Tif32 in a manner that can be mitigated by restoring j/Hcr1 association with eIF3. This conclusion is consistent with our finding that the *hcr1-box6* mutation, or eliminating the entire CTD or NTD of j/Hcr1, impairs j/Hcr1 association with eIF3 and also destroys suppression of the a/Tif32 KERR mutants by overexpressed j/Hcr1. Given that the a/Tif32 KERR substitutions impair its direct binding to the b/RRM, one possibility is that partial suppression of these *tif32* mutations by hc *HCR1* involves the ability of j/Hcr1 to bridge interaction between a/Tif32 and the b/Prt1 RRM and to stabilize the b/RRM–j/Hcr1–a/Tif32-CTD module in mutant eIF3. This mechanism could also account for our finding that the growth defects conferred by the a/Tif32 KERR mutations are exacerbated by mutations affecting either the NTD or CTD of j/Hcr1 in cells lacking WT j/Hcr1.

An alternative explanation for the genetic interactions could be that j/Hcr1 and the a/HLD have overlapping functions in one or more steps of initiation. In this view, overexpressing WT j/Hcr1 increases its ability to functionally compensate for a/HLD defects in a manner dependent on both the NTD and CTD of j/Hcr1. Likewise, mutating either domain of j/Hcr1 would prevent it from complementing a/HLD defects in cells lacking WT j/Hcr1. According to this model, the j/CTD is required for robust growth only in the presence of a/HLD mutations, because their shared function can be fully executed by the wild-type a/HLD.

One line of evidence consistent with the model of overlapping functions is that increased leaky scanning is a phenotype conferred by mutations affecting either the a/HLD or j/Hcr1. Because we did not observe a significant additive effect on leaky scanning on combining equivalent KERR substitutions in the a/HLD and the j/CTD, it is possible that these related segments act coordinately and that each single KERR substitution disrupts most of the activity they provide as a unit. Considering that the strongest effects on leaky scanning have been observed by eliminating the j/NTD-b/RRM interaction (10), and given our finding that a/HLD substitutions weaken j/Hcr1 association with eIF3, it could be argued that the leaky-scanning phenotype of the a/HLD mutations is an indirect consequence of reduced interaction of j/Hcr1 with the b/RRM. This might be unlikely, however, as we found that overexpressing WT j/Hcr1 did not mitigate the leaky-scanning defect in *tif32-R731I* cells (data not shown). Hence, we favor the idea that both the j/NTD-b/RRM interaction and the box6/KERR elements of the a/HLD and j/CTD make independent contributions to efficient AUG recognition and to blocking of leaky scanning. As the CTD of j/Hcr1 also interacts with Rps2 (10), it is highly likely that the entire b/Prt1-RRM–j/Hcr1–a/Tif32-CTD module is positioned near the mRNA entry channel by the multiple interactions of the j/CTD and a/Tif32 CTD with Rps2, Rps3, and h16-h18 (Fig. 11C). Accordingly, the leaky-scanning phenotypes of mutations in the b/RRM, j/Hcr1, or a/HLD might all involve destabilizing the closed conformation of the PIC at AUG codons.

Other findings indicate that the a/HLD and j/Hcr1 have distinct functions in translation initiation. Although related in sequence, the results presented here and elsewhere indicate clearly that they make different interactions within the b/Prt1-RRM–j/Hcr1–a/Tif32-CTD module. In addition, whereas a/HLD substitutions impair mRNA recruitment by 43S complexes and confer Ssu$^-$ phenotypes, neither defect was observed in *hcr1*Δ cells. The fact that *hcr1*Δ reduces recognition of uAUG-1 (10) but does not suppress UUG initiation in Sui$^-$ mutants seems to indicate that eliminating j/Hcr1 destabilizes the closed conformation equally with UUG or AUG in the P site so as not to alter the UUG/AUG initiation ratio in Sui$^-$ mutants. The fact that the *tif32* mutations exert this effect preferentially at UUG start codons suggests a difference between j/Hcr1 and the a/HLD in how they regulate access to the closed PIC conformation. The fact that overexpressing TC partially suppresses the growth defect in *hcr1*Δ, but not in the *tif32* mutant cells, suggests that the defects in mRNA recruitment and/or start codon selection conferred by the a/HLD substitutions (but lacking in *hcr1*Δ cells) contribute more than the impaired eIF2 association with the MFC to the overall reduction in translation rates in the *tif32* mutants.

Another function that distinguishes the a/HLD from j/Hcr1 is the role of j/Hcr1 in the final stage of 40S ribosome biogenesis occurring in the cytoplasm (45). It could be proposed that the strong leaky-scanning phenotype conferred by *hcr1*Δ (10) results indirectly from the decreased levels of 40S subunits present in this mutant. To evaluate this possibility, we measured leaky scanning of *GCN4* uAUG-1 (in the manner described in the legend to Fig. 4B) in three mutants harboring deletions of one of two duplicate genes encoding a 40S subunit protein, *RPS14A*, *RPS18A*, or *RPS23A*, all of which confer reductions in 40S subunit levels at least as great as those found in *hcr1*Δ cells (7, 34, 45). We found that all three *rps* mutants displayed moderate (20 to 40%) reductions, rather than an increase, in leaky scanning (data not shown). Hence, the leaky-scanning phenotype of *hcr1*Δ most likely reflects a direct role for j/Hcr1 in promoting start codon recognition.

Hydroxyl radical mapping data position the CTD of mammalian eIF3j in the 40S mRNA entry channel and A site on the interface side of the 40S subunit, and it was shown that eIF3j antagonizes 40S subunit binding by mRNA in a manner overcome by the bound TC. It was proposed that by interacting with the decoding center, the eIF3j CTD would coordinate binding of mRNA with initiation factors and modulate 40S subunit-mRNA interactions during scanning and AUG selection (14). Consistent with this, the j/Hcr1 CTD can bind *in vitro* to Rps23 (10), which is located near the A site and mRNA entry channel on the interface side of the 40S subunit (41). Given that interactions of the j/CTD with both Rps2 and Rps23 require its KERR motif (10), it seems plausible that the j/CTD "toggles" between 40S binding sites on Rps23 (on the interface side) and Rps2 (on the solvent side) in performing its proposed roles in regulating PIC assembly and scanning. In contrast, the a/Tif32 CTD binds to Rps2 and Rps3, but not Rps23, suggesting that the function(s) of a/Tif32 shared with, or modulated by, j/Hcr1 is executed from the solvent side of the 40S subunit.

ACKNOWLEDGMENTS

We are grateful to the members of the Hinnebusch, Valášek, Dever, and Krásný laboratories for helpful comments. We thank Jean Fringer and Tom Dever for the *rps* mutants.

This work was supported in part by the Intramural Research Program of the NIH (A.G.H.) and by The Wellcome Trusts grant 076456/Z/05/Z, NIH research grant R01 TW007271 funded by Fogarty International Center, Czech Science Foundation 305/10/0335, and Inst. Research Concept AV0Z50200510 to L.V.

REFERENCES

1. **Algire, M. A., D. Maag, and J. R. Lorsch.** 2005. Pi release from eIF2, not GTP hydrolysis, is the step controlled by start-site selection during eukaryotic translation initiation. Mol. Cell **20:**251–262.
2. **Asano, K., J. Clayton, A. Shalev, and A. G. Hinnebusch.** 2000. A multifactor complex of eukaryotic initiation factors eIF1, eIF2, eIF3, eIF5, and initiator $tRNA^{Met}$ is an important translation initiation intermediate in vivo. Genes Dev. **14:**2534–2546.
3. **Asano, K., L. Phan, J. Anderson, and A. G. Hinnebusch.** 1998. Complex formation by all five homologues of mammalian translation initiation factor 3 subunits from yeast *Saccharomyces cerevisiae*. J. Biol. Chem. **273:**18573–18585.
4. **Berthelot, K., M. Muldoon, L. Rajkowitsch, J. Hughes, and J. E. McCarthy.** 2004. Dynamics and processivity of 40S ribosome scanning on mRNA in yeast. Mol. Microbiol. **51:**987–1001.
5. **Boeke, J. D., J. Trueheart, G. Natsoulis, and G. R. Fink.** 1987. 5-Fluoroorotic acid as a selective agent in yeast molecular genetics. Methods Enzymol. **154:**164–175.
6. **Cheung, Y. N., D. Maag, S. F. Mitchell, C. A. Fekete, M. A. Algire, J. E. Takacs, N. Shirokikh, T. Pestova, J. R. Lorsch, and A. G. Hinnebusch.** 2007. Dissociation of eIF1 from the 40S ribosomal subunit is a key step in start codon selection in vivo. Genes Dev. **21:**1217–1230.
7. **Chiocchetti, A., J. Zhou, H. Zhu, T. Karl, O. Haubenreisser, M. Rinnerthaler, G. Heeren, K. Oender, J. Bauer, H. Hintner, M. Breitenbach, and L. Breitenbach-Koller.** 2007. Ribosomal proteins Rpl10 and Rps6 are potent regulators of yeast replicative life span. Exp. Gerontol. **42:**275–286.
8. **Chuang, R. Y., P. L. Weaver, Z. Liu, and T. H. Chang.** 1997. Requirement of the DEAD-Box protein ded1p for messenger RNA translation. Science **275:**1468–1471.
9. **Donahue, T. F., and A. M. Cigan.** 1988. Genetic selection for mutations that reduce or abolish ribosomal recognition of the *HIS4* translational initiator region. Mol. Cell. Biol. **8:**2955–2963.
10. **Elantak, L., S. Wagner, A. Herrmannova, M. Karaskova, E. Rutkai, P. Lukavsky, and L. Valasek.** 2010. The indispensable N-terminal half of eIF3j/HCR1 cooperates with its structurally conserved binding partner eIF3b/PRT1-RRM and with eIF1A in stringent AUG selection. J. Mol. Biol. **396:**1097–1116.
11. **Evans, D. R. H., C. Rasmussen, P. J. Hanic-Joyce, G. C. Johnston, R. A. Singer, and C. A. Barnes.** 1995. Mutational analysis of the Prt1 protein subunit of yeast translation initiation factor 3. Mol. Cell. Biol. **15:**4525–4535.
12. **Fekete, C. A., D. J. Applefield, S. A. Blakely, N. Shirokikh, T. Pestova, J. R. Lorsch, and A. G. Hinnebusch.** 2005. The eIF1A C-terminal domain promotes initiation complex assembly, scanning and AUG selection in vivo. EMBO J. **24:**3588–3601.
13. **Fekete, C. A., S. F. Mitchell, V. A. Cherkasova, D. Applefield, M. A. Algire, D. Maag, A. Saini, J. R. Lorsch, and A. G. Hinnebusch.** 2007. N- and C-terminal residues of eIF1A have opposing effects on the fidelity of start codon selection. EMBO **26:**1602–1614.
14. **Fraser, C. S., K. E. Berry, J. W. Hershey, and J. A. Doudna.** 2007. eIF3j is located in the decoding center of the human 40S ribosomal subunit. Mol. Cell. **26:**811–819.
15. **Giaever, G., A. M. Chu, L. Ni, C. Connelly, L. Riles, S. Veronneau, S. Dow, A. Lucau-Danila, K. Anderson, B. Andre, A. P. Arkin, A. Astromoff, M. El-Bakkoury, R. Bangham, R. Benito, S. Brachat, S. Campanaro, M. Curtiss, K. Davis, A. Deutschbauer, K. D. Entian, P. Flaherty, F. Foury, D. J. Garfinkel, M. Gerstein, D. Gotte, U. Guldener, J. H. Hegemann, S. Hempel, Z. Herman, D. F. Jaramillo, D. E. Kelly, S. L. Kelly, P. Kotter, D. LaBonte, D. C. Lamb, N. Lan, H. Liang, H. Liao, L. Liu, C. Luo, M. Lussier, R. Mao, P. Menard, S. L. Ooi, J. L. Revuelta, C. J. Roberts, M. Rose, P. Ross-Macdonald, B. Scherens, G. Schimmack, B. Shafer, D. D. Shoemaker, S. Sookhai-Mahadeo, R. K. Storms, J. N. Strathern, G. Valle, M. Voet, G. Volckaert, C. Y. Wang, T. R. Ward, J. Wilhelmy, E. A. Winzeler, Y. Yang, G. Yen, E. Youngman, K. Yu, H. Bussey, J. D. Boeke, M. Snyder, P. Philippsen, R. W. Davis, and M. Johnston.** 2002. Functional profiling of the Saccharomyces cerevisiae genome. Nature **418:**387–391.
16. **Gietz, R. D., and A. Sugino.** 1988. New yeast-Escherichia coli shuttle vectors constructed with in vitro mutagenized yeast genes lacking six-base pair restriction sites. Gene **74:**527–534.
17. **Grant, C. M., and A. G. Hinnebusch.** 1994. Effect of sequence context at stop codons on efficiency of reinitiation in *GCN4* translational control. Mol. Cell. Biol. **14:**606–618.
18. **Grant, C. M., P. F. Miller, and A. G. Hinnebusch.** 1994. Requirements for intercistronic distance and level of eIF-2 activity in reinitiation on GCN4 mRNA varies with the downstream cistron. Mol. Cell. Biol. **14:**2616–2628.
19. **Hinnebusch, A. G.** 2006. eIF3: a versatile scaffold for translation initiation complexes. Trends Biochem. Sci. **31:**553–562.
20. **Hinnebusch, A. G.** 1985. A hierarchy of *trans*-acting factors modulate translation of an activator of amino acid biosynthetic genes in *Saccharomyces cerevisiae*. Mol. Cell. Biol. **5:**2349–2360.
21. **Hinnebusch, A. G.** 2005. Translational regulation of GCN4 and the general amino acid control of yeast. Annu. Rev. Microbiol. **59:**407–450.
22. **Iost, I., M. Dreyfus, and P. Linder.** 1999. Ded1p, a DEAD-box protein required for translation initiation in Saccharomyces cerevisiae, is an RNA helicase. J. Biol. Chem. **274:**17677–17683.
23. **Jivotovskaya, A. V., L. Valasek, A. G. Hinnebusch, and K. H. Nielsen.** 2006. Eukaryotic translation initiation factor 3 (eIF3) and eIF2 can promote mRNA binding to 40S subunits independently of eIF4G in yeast. Mol. Cell. Biol. **26:**1355–1372.
24. **Koromilas, A. E., A. Lazaris-Karatzas, and N. Sonenberg.** 1992. mRNAs containing extensive secondary structure in their 5′ non-coding region translate efficiently in cells overexpressing initiation factor eIF-4E. EMBO J. **11:**4153–4158.
25. **LeFebvre, A. K., N. L. Korneeva, M. Trutschl, U. Cvek, R. D. Duzan, C. A. Bradley, J. W. Hershey, and R. E. Rhoads.** 2006. Translation initiation factor eIF4G-1 binds to eIF3 through the eIF3e subunit. J. Biol. Chem. **281:**22917–22932.
26. **Maag, D., M. A. Algire, and J. R. Lorsch.** 2006. Communication between eukaryotic translation initiation factors 5 and 1A within the ribosomal pre-initiation complex plays a role in start site selection. J. Mol. Biol. **356:**724–737.
27. **Maag, D., C. A. Fekete, Z. Gryczynski, and J. R. Lorsch.** 2005. A conforma-

tional change in the eukaryotic translation preinitiation complex and release of eIF1 signal recognition of the start codon. Mol. Cell. **17:**265–275.
28. **Mueller, P. P., and A. G. Hinnebusch.** 1986. Multiple upstream AUG codons mediate translational control of *GCN4*. Cell **45:**201–207.
29. **Nanda, J. S., Y. N. Cheung, J. E. Takacs, P. Martin-Marcos, A. K. Saini, A. G. Hinnebusch, and J. R. Lorsch.** 2009. eIF1 controls multiple steps in start codon recognition during eukaryotic translation initiation. J. Mol. Biol. **394:**268–285.
30. **Nielsen, K. H., B. Szamecz, L. Valasek, A. Jivotovskaya, B. S. Shin, and A. G. Hinnebusch.** 2004. Functions of eIF3 downstream of 48S assembly impact AUG recognition and GCN4 translational control. EMBO J. **23:**1166–1177.
31. **Nielsen, K. H., and L. Valasek.** 2007. In vivo deletion analysis of the architecture of a multiprotein complex of translation initiation factors. Methods Enzymol. **431:**15–32.
32. **Nielsen, K. H., L. Valasek, C. Sykes, A. Jivotovskaya, and A. G. Hinnebusch.** 2006. Interaction of the RNP1 motif in PRT1 with HCR1 promotes 40S binding of eukaryotic initiation factor 3 in yeast. Mol. Cell. Biol. **26:**2984–2998.
33. **Passmore, L. A., T. M. Schmeing, D. Maag, D. J. Applefield, M. G. Acker, M. A. Algire, J. R. Lorsch, and V. Ramakrishnan.** 2007. The eukaryotic translation initiation factors eIF1 and eIF1A induce an open conformation of the 40S ribosome. Mol. Cell **26:**41–50.
34. **Paulovich, A. G., J. R. Thompson, J. C. Larkin, Z. Li, and J. L. Woolford, Jr.** 1993. Molecular genetics of cryptopleurine resistance in Saccharomyces cerevisiae: expression of a ribosomal protein gene family. Genetics **135:**719–730.
35. **Pestova, T. V., and V. G. Kolupaeva.** 2002. The roles of individual eukaryotic translation initiation factors in ribosomal scanning and initiation codon selection. Genes Dev. **16:**2906–2922.
36. **Peterson, D. T., W. C. Merrick, and B. Safer.** 1979. Binding and release of radiolabeled eukaryotic initiation factors 2 and 3 during 80 S initiation complex formation. J. Biol. Chem. **254:**2509–2519.
37. **Pisarev, A. V., V. G. Kolupaeva, M. M. Yusupov, C. U. Hellen, and T. V. Pestova.** 2008. Ribosomal position and contacts of mRNA in eukaryotic translation initiation complexes. EMBO J. **27:**1609–1621.
38. **Reibarkh, M., Y. Yamamoto, C. R. Singh, F. del Rio, A. Fahmy, B. Lee, R. E. Luna, M. Ii, G. Wagner, and K. Asano.** 2008. Eukaryotic initiation factor (eIF) 1 carries two distinct eIF5-binding faces important for multifactor assembly and AUG selection. J. Biol. Chem. **283:**1094–1103.
39. **Saini, A. K., J. S. Nanda, J. R. Lorsch, and A. G. Hinnebusch.** 2010. Regulatory elements in eIF1A control the fidelity of start codon selection by modulating tRNA (i) (Met) binding to the ribosome. Genes Dev. **24:**97–110.
40. **Smith, D. B., and K. S. Johnson.** 1988. Single-step purification of polypeptides expressed in Escherichia coli as fusions with glutathione S-transferase. Gene **67:**31–40.
41. **Spahn, C. M., R. Beckmann, N. Eswar, P. A. Penczek, A. Sali, G. Blobel, and J. Frank.** 2001. Structure of the 80S ribosome from Saccharomyces cerevisiae—tRNA ribosome and subunit-subunit interactions. Cell **107:**373–386.
42. **Szamecz, B., E. Rutkai, L. Cuchalova, V. Munzarova, A. Herrmannova, K. H. Nielsen, L. Burela, A. G. Hinnebusch, and L. Valasek.** 2008. eIF3a cooperates with sequences 5′ of uORF1 to promote resumption of scanning by post-termination ribosomes for reinitiation on GCN4 mRNA. Genes Dev. **22:**2414–2425.
43. **Taylor, D. J., B. Devkota, A. D. Huang, M. Topf, E. Narayanan, A. Sali, S. C. Harvey, and J. Frank.** 2009. Comprehensive molecular structure of the eukaryotic ribosome. Structure **17:**1591–1604.
44. **Valášek, L.** 1998. Characterization of RPG1, the large subunit of the yeast *S. cerevisiae* initiation translation factor 3 (eIF3). Ph.D. thesis. University of Vienna, Vienna, Austria.
45. **Valášek, L., J. Hašek, K. H. Nielsen, and A. G. Hinnebusch.** 2001. Dual function of eIF3j/Hcr1p in processing 20 S pre-rRNA and translation initiation. J. Biol. Chem. **276:**43351–43360.
46. **Valášek, L., J. Hašek, H. Trachsel, E. M. Imre, and H. Ruis.** 1999. The *Saccharomyces cerevisiae HCRI* gene encoding a homologue of the p35 subunit of human translation eukaryotic initiation factor 3 (eIF3) is a high copy suppressor of a temperature-sensitive mutation in the Rpg1p subunit of yeast eIF3. J. Biol. Chem. **274:**27567–27572.
47. **Valášek, L., A. Mathew, B. S. Shin, K. H. Nielsen, B. Szamecz, and A. G. Hinnebusch.** 2003. The Yeast eIF3 subunits TIF32/a and NIP1/c and eIF5 make critical connections with the 40S ribosome in vivo. Genes Dev. **17:**786–799.
48. **Valášek, L., K. H. Nielsen, and A. G. Hinnebusch.** 2002. Direct eIF2-eIF3 contact in the multifactor complex is important for translation initiation in vivo. EMBO J. **21:**5886–5898.
49. **Valasek, L., K. H. Nielsen, F. Zhang, C. A. Fekete, and A. G. Hinnebusch.** 2004. Interactions of eukaryotic translation initiation factor 3 (eIF3) subunit NIP1/c with eIF1 and eIF5 promote preinitiation complex assembly and regulate start codon selection. Mol. Cell. Biol. **24:**9437–9455.
50. **Valášek, L., L. Phan, L. W. Schoenfeld, V. Valásková, and A. G. Hinnebusch.** 2001. Related eIF3 subunits TIF32 and HCR1 interact with an RNA recognition motif in PRT1 required for eIF3 integrity and ribosome binding. EMBO J. **20:**891–904.
51. **Yamamoto, Y., C. R. Singh, A. Marintchev, N. S. Hall, E. M. Hannig, G. Wagner, and K. Asano.** 2005. The eukaryotic initiation factor (eIF) 5 HEAT domain mediates multifactor assembly and scanning with distinct interfaces to eIF1, eIF2, eIF3, and eIF4G. Proc. Natl. Acad. Sci. U. S. A. **102:**16164–16169.
52. **Yoon, H. J., and T. F. Donahue.** 1992. The *sui1* suppressor locus in *Saccharomyces cerevisiae* encodes a translation factor that functions during $tRNA_i^{Met}$ recognition of the start codon. Mol. Cell. Biol. **12:**248–260.
53. **Yu, Y., A. Marintchev, V. G. Kolupaeva, A. Unbehaun, T. Veryasova, S. C. Lai, P. Hong, G. Wagner, C. U. Hellen, and T. V. Pestova.** 2009. Position of eukaryotic translation initiation factor eIF1A on the 40S ribosomal subunit mapped by directed hydroxyl radical probing. Nucleic Acids Res. **37:**5167–5182.

The RNA recognition motif of eukaryotic translation initiation factor 3g (eIF3g) is required for resumption of scanning of posttermination ribosomes for reinitiation on GCN4 and together with eIF3i stimulates linear scanning.

Cuchalová L., Kouba T., Herrmannová A., Dányi I., Chiu W.L., Valášek L.

Mol Cell Biol. 2010 Oct;30(19):4671-86.
PMID: 20679478

Here we provide the first functional analysis of two so far uncharacterized essential eIF3 subunits, i/TIF34 and g/TIF35, and show that both subunits stimulate linear scanning. Specific mutations in i/TIF34 and g/TIF35 produced severe growth defects and decreased the rate of translation initiation *in vivo* without affecting the eIF3 integrity or 48S PIC formation.

Both mutations also interfered with the *GCN4* translational control mechanism, which relies on four short upstream open reading frames (uORFs) found in its mRNA leader. The first, uORF1, allows efficient reinitiation while the other three uORFs do not. The expression of *GCN4* is tightly regulated in nutrient-dependent manner; the *GCN4* expression is repressed during non-starvation conditions and becomes activated only upon amino acid starvation. The i/TIF34 mutant prevented full derepression of *GCN4* during starvation by impairing the rate of scanning, whereas g/TIF35 mutant impeded resumption of scanning after translation of uORF1. Furthermore, g/TIF35 mutant also reduced processivity of scanning through stable secondary structures.

We also identified specific interactions between g/TIF35 and small ribosomal proteins RPS3 and RPS20 that placed the i/TIF34-g/TIF35 mini-module in the vicinity of the mRNA entry channel.

MOLECULAR AND CELLULAR BIOLOGY, Oct. 2010, p. 4671–4686 Vol. 30, No. 19
0270-7306/10/$12.00 doi:10.1128/MCB.00430-10

The RNA Recognition Motif of Eukaryotic Translation Initiation Factor 3g (eIF3g) Is Required for Resumption of Scanning of Posttermination Ribosomes for Reinitiation on *GCN4* and Together with eIF3i Stimulates Linear Scanning▽

Lucie Cuchalová,[1] Tomáš Kouba,[1] Anna Herrmannová,[1] István Dányi,[1] Wen-ling Chiu,[2] and Leoš Valášek[1]*

Laboratory of Regulation of Gene Expression, Institute of Microbiology AVCR, v.v.i., Prague, Czech Republic,[1] and Laboratory of Gene Regulation and Development, Eunice Kennedy Shriver National Institute of Child Health and Human Development, NIH, Bethesda, Maryland 20892[2]

Received 13 April 2010/Returned for modification 25 May 2010/Accepted 26 July 2010

Recent reports have begun unraveling the details of various roles of individual eukaryotic translation initiation factor 3 (eIF3) subunits in translation initiation. Here we describe functional characterization of two essential *Saccharomyces cerevisiae* eIF3 subunits, g/Tif35 and i/Tif34, previously suggested to be dispensable for formation of the 48S preinitiation complexes (PICs) *in vitro*. A triple-Ala substitution of conserved residues in the RRM of g/Tif35 (*g/tif35-KLF*) or a single-point mutation in the WD40 repeat 6 of i/Tif34 (*i/tif34-Q258R*) produces severe growth defects and decreases the rate of translation initiation *in vivo* without affecting the integrity of eIF3 and formation of the 43S PICs *in vivo*. Both mutations also diminish induction of *GCN4* expression, which occurs upon starvation via reinitiation. Whereas *g/tif35-KLF* impedes resumption of scanning for downstream reinitiation by 40S ribosomes terminating at upstream open reading frame 1 (uORF1) in the *GCN4* mRNA leader, *i/tif34-Q258R* prevents full *GCN4* derepression by impairing the rate of scanning of posttermination 40S ribosomes moving downstream from uORF1. In addition, *g/tif35-KLF* reduces processivity of scanning through stable secondary structures, and g/Tif35 specifically interacts with Rps3 and Rps20 located near the ribosomal mRNA entry channel. Together these results implicate g/Tif35 and i/Tif34 in stimulation of linear scanning and, specifically in the case of g/Tif35, also in proper regulation of the *GCN4* reinitiation mechanism.

The initiation phase of protein synthesis is promoted by numerous proteins or protein complexes called eukaryotic initiation factors (eIFs). The multiprotein eIF3 complex, together with eIFs 1, 1A, and 5, promotes recruitment of the Met-tRNA$_i^{Met}$/eIF2/GTP ternary complex (TC) to the small ribosomal subunit (40S), producing the 43S preinitiation complex (PIC). At least in yeast, eIFs 1, 3, and 5 and the TC occur in a preformed unit called the multifactor complex (MFC), which enhances the efficiency of the 43S PIC assembly process (reviewed in reference 20). The eIF4F complex, containing the cap-binding eIF4E and the scaffold protein eIF4G, then mediates recruitment of an mRNA to the 43S PIC with the help of eIF3 and the poly(A)-binding protein. The resulting 48S PIC traverses the 5′ untranslated region (UTR) of mRNA, searching usually for the first AUG codon while unwinding secondary structures in an ATP-dependent reaction stimulated by helicases eIF4A and eIF4B (reviewed in reference 39). This intricate process is called scanning, and its precise molecular mechanism is still poorly understood. It is known that the presence of the TC and eIFs 1, 1A, and 3 in reconstituted mammalian 43S PICs is sufficient for scanning through the unstructured leaders of model mRNAs (38). eIFs 1 and 1A are thought to promote scanning by induction of a conformational change of the 40S head. This change, characterized by opening the latch formed by helices 18 (h18) and 34 (h34) of 18S rRNA and establishing a new interaction between RPS3 and h16, stabilizes the small subunit in an open/scanning-conducive state (36). When the start codon is recognized by the anticodon of Met-tRNA$_i^{Met}$, the concerted action of eIFs 1, 1A, 2, and 5 stimulates a reverse conformational change of the 40S subunit that reforms the h18-h34 latch and arrests scanning (reviewed in reference 27). Upon subunit joining mediated by eIF5B, the 80S couple commences elongation.

Over the last decade, functions of several subunits of the most complex initiation factor, eIF3, and its complete subunit composition have been investigated in yeasts, plants, and mammals (reviewed in reference 17). In *Saccharomyces cerevisiae*, eIF3 comprises five core essential subunits (a/Tif32, b/Prt1, c/Nip1, i/Tif34, and g/Tif35) and one noncore subunit (j/Hcr1). These all have corresponding orthologs in the more complex mammalian eIF3, which contains seven additional nonconserved subunits. Despite recent progress, the true composition of the core of mammalian eIF3 remains somewhat obscure. One study aimed at reconstitution of a human eIF3 *in vitro* suggested that the functional core contains three nonconserved subunits, e, f, and h, in place of eIF3i and -g (25), whereas other work based on tandem mass spectrometry and solution disruption assays identified three stable modules, one of which,

* Corresponding author. Mailing address: Laboratory of Regulation of Gene Expression, Institute of Microbiology AVCR, v.v.i., Videnska 1083, Prague, Czech Republic. Phone: 420 241 062 288. Fax: 420 241 062 665. E-mail: valasekl@biomed.cas.cz.

▽ Published ahead of print on 2 August 2010.

composed of a, b, i, and g subunits, closely resembled the yeast eIF3 core (62).

A systematic effort was devoted to mapping the binding site of eIF3 on the 40S subunit. We found that the extreme N-terminal domain (NTD) of a/Tif32 forms a crucial intermolecular bridge between eIF3 and the 40S subunit (49) and that the RNA recognition motif (RRM) of b/Prt1 and the extreme C-terminal domain (CTD) of c/Nip1 also play direct roles in anchoring eIF3 to the ribosome (9, 33, 51). In addition, we observed that deleting the CTD of a/Tif32 reduced 40S association with the MFC when the connection between eIF3 and eIF5/Tif5 in the MFC was impaired by the *tif5-7A* mutation (51). Importantly, our findings that the a/Tif32 CTD interacts with helices 16 to 18 of 18S rRNA (51) and Rps2 and Rps3 (6), that the a/Tif32 NTD binds to ribosomal proteins Rps0A and Rps10A (51), and that the j/Hcr1 CTD interacts with Rps2 (9) suggested that yeast eIF3 associates with the solvent-exposed side of the 40S subunit, as others have proposed for mammalian eIF3 (45, 48).

Functional studies revealed that j/Hcr1, the only nonessential subunit of yeast eIF3, forms together with the a/Tif32 CTD and the RRM of b/Prt1 an eIF3 subassembly that ensures stringency of the AUG start codon selection by blocking leaky scanning (6, 9, 33). Likewise, the c/Nip1 subunit was implicated in regulation of the AUG decoding mechanism owing to the fact that its NTD associates directly or indirectly with the key actors in this process, such as eIF1, eIF5, and the TC (53). On the other hand, the *prt1-1* point mutation in b/Prt1 and single point substitutions in the conserved KERR motif of a/TIF32-CTD were among other effects suggested to reduce the rate of ribosomal scanning (6, 31). Given the essentiality of all core subunits, a surprising result came from a biochemical study that suggested that the a/Tif32-b/Prt1-c/Nip1 subcomplex lacking g/Tif35 and i/Tif34 subunits is sufficient to stimulate the TC and mRNA recruitment to the 40S subunit and even to promote efficient translation *in vitro* (40). These findings were subsequently supported by pioneering work that used reconstituted mammalian eIF3 and suggested that eIF3i and -g are dispensable for active mammalian eIF3 formation *in vitro* (25).

Besides playing these canonical roles in general translation initiation, eIF3 was also implicated in the gene-specific translational control mechanism termed reinitiation (REI) in yeast, plant, and mammalian cells (35, 42, 49). REI is utilized to up- or downregulate translation of regulatory proteins, such as transcription factors and proto-oncogenes, in response to various environmental stimuli (22). In general, it relies on the ability of the small ribosomal subunit to remain attached to the mRNA following termination of translation on a short upstream ORF (uORF) in order to resume scanning on the same mRNA molecule. The next critical step of REI is *de novo* recruitment of the TC, which is required to recognize the next AUG codon; therefore, REI can be delicately regulated by manipulating the eIF2/GTP levels (8). The uORFs thus possess the exquisite potential to function as context-dependent *cis* regulators of translation.

The best-studied example of the REI mechanism is the translational control of yeast *GCN4*, a transcriptional activator of a large number of biosynthetic genes (reviewed in reference 18). The mRNA leader of *GCN4* contains four short uORFs that differ dramatically in their capacity to promote efficient REI. Whereas uORFs 2 to 4 are very inefficient, uORF1 allows the majority of 40S ribosomes terminating at its stop codon to remain mRNA bound and resume scanning. This ability requires two segments of uORF1: enhancer sequences upstream of its start codon, and the last codon plus ~12 nucleotides (nt) after the stop codon (12, 14). We have recently demonstrated that the 5′ enhancer of uORF1 functionally interacts with the extreme NTD of a/Tif32 at or near the mRNA exit channel of the posttermination 40S subunit. This interaction was proposed to be instrumental in stabilizing the 40S subunit on the mRNA to enable resumption of scanning for efficient REI on a downstream ORF (49). Under nutrient-replete conditions characterized by high levels of the TC, nearly all of the rescanning 40S ribosomes after uORF1 will rebind the TC before reaching uORFs 2 to 4, translate one of these uORFs, and dissociate from the mRNA. Amino acid starvation leads to phosphorylation of eIF2α by the kinase Gcn2, converting eIF2/GDP from a substrate to a competitive inhibitor of its GEF, eIF2B, thus reducing the concentration of TC. Low TC levels derepress *GCN4* translation by allowing ~50% of rescanning 40S ribosomes to rebind TC after bypassing the trap of uORFs 2 to 4 and to reinitiate at *GCN4* instead. Failure to induce expression of *GCN4* in response to a shortage of amino acids in various mutants confers increased sensitivity to inhibitors of amino acid biosynthetic enzymes, and this has been designated the Gcn$^-$ phenotype.

In this report, we performed functional analysis of two small essential eIF3 subunits, g/Tif35 and i/Tif34, whose contributions to general translation initiation were virtually unknown. Site-directed substitutions in the RRM of g/Tif35 in *g/tif35-KLF* produced no impact on its RNA-binding affinity, on the integrity of eIF3 in the MFC, or on formation of the 43S PICs. Nevertheless, the *g/tif35-KLF* mutation markedly reduced rates of translation initiation and decreased the processivity of scanning through a stable secondary structure inserted into the 5′-UTR of uORF-less *GCN4* mRNA. In addition, *g/tif35-KLF* provoked a strong Gcn$^-$ phenotype owing to the inability of posttermination 40S subunits at *GCN4*'s uORF1 to resume scanning for reinitiation downstream; this resembles the previously described phenotype of the *a/tif32-Δ8* mutant (49). Detailed genetic analysis revealed, however, that the g/Tif35 RRM and the a/Tif32 NTD ensure efficient resumption of scanning by different mechanisms. Like *g/tif35-KLF*, the Q258R mutation of the WD40 repeat 6 of i/Tif34 also produced a severe Gcn$^-$ phenotype. However, in contrast to *g/tif35-KLF*, *i/tif34-Q258R* allowed resumption of scanning after uORF1 but significantly reduced the rate of scanning. Consistently, the Gcn$^-$ phenotype of *i/tif34-Q258R* was partially suppressible by cooverexpressing scanning-promoting factors eIF1 and eIF1A. Together these results provide the first insights into the functional contributions of the essential i/Tif34 and g/Tif35 subunits of yeast eIF3 to general translation initiation as well as to translational control of *GCN4* expression.

MATERIALS AND METHODS

Construction of yeast strains and plasmids. To create H464, H421 (Table 1) was first transformed with YEpTIF35-T (Table 2), and YEp-TIF35-U was evicted by growth on 5-fluoroorotic acid (5-FOA) medium. The resulting strain was transformed to Ura$^+$ with the integrative *GCN2* plasmid pHQ835 (kindly provided by Hongfang Qiu) digested with SnaBI. Ura$^-$ segregants were obtained

TABLE 1. Yeast strains used in this study

Strain[a]	Genotype	Source or reference
H464§	*MAT***a** *leu2-3,112 ura3-52*::*GCN2 trp1*Δ *tif35*Δ (YEp-TIF35-U)	This study
H421§	*MAT***a** *leu2-3,112 ura3-52 trp1 gcn2*Δ *tif35*Δ (YEp-TIF35-U)	Klaus H. Nielsen
H111§	*MAT***a** *leu2-3,112 ura3-52*::*GCN2 trp1*Δ *tif35*Δ (YCp22-g/TIF35-screen)	This study
H112§	*MAT***a** *leu2-3,112 ura3-52*::*GCN2 trp1*Δ *tif35*Δ (YCp22-g/tif35-KLF)	This study
YBS47¶	*MAT***a** *leu2-3,112 ura3-52 trp1*Δ *gcn2*Δ *a/tif32*Δ *URA3*::*GCN2 ura3* (pRSeIF3a-HIS-L)	49
YBS53¶	*MAT***a** *leu2-3,112 ura3-52 trp1*Δ *gcn2*Δ *a/tif32*Δ *URA3*::*GCN2 ura3* (pRSeIF3a-Δ8-HIS-L)	49
H450‖	*MAT***a** *leu2-3,112 ura3-52*::*GCN2 trp1*Δ *tif34*Δ (YEp-TIF34 (*URA3*))	This study
H420‖	*MAT***a** *leu2-3,112 ura3-52 trp1 gcn2*Δ *tif34*Δ (YEp-TIF34 (*URA3*))	Klaus H. Nielsen
H120‖	*MAT***a** *leu2-3,112 ura3-52*::*GCN2 trp1*Δ *tif34*Δ (YCp111-i/TIF34)	This study
H121‖	*MAT***a** *leu2-3,112 ura3-52*::*GCN2 trp1*Δ *tif34*Δ (YCp111-i/tif34-Q258R)	This study

[a] Strains that share a footnote symbol (§, ¶, or ‖) are isogenic strains.

by selecting for growth on medium containing 5-FOA, and the resulting H464 was tested for the presence of integrated *GCN2* by growth on medium containing 3-aminotriazole (3-AT). YEp-TIF35-U was reintroduced into the verified strain, which was then grown on Trp^+ medium to enable spontaneous loss of the *TRP1* covering plasmid, YEpTIF35-T.

To produce H111 and H112, H461 was transformed with YCp22-g/TIF35-screen andYCp22-g/tif35-KLF, respectively, and the resident *g/TIF35 URA3* plasmid was evicted on 5-FOA-containing medium.

To create H450, H420 (Table 1) was first transformed with YEpTIF34-T (Table 2), and YEp-TIF34-U was evicted by growth on 5-FOA medium. The resulting strain was transformed to Ura^+ with the integrative *GCN2* plasmid pHQ835 digested with SnaBI. Ura^- segregants were obtained by selecting for growth on medium containing 5-FOA, and the resulting H450 was tested for the presence of integrated *GCN2* by growing on medium containing 3-AT. YEp-TIF34-U was reintroduced into the verified strain, which was then grown on Trp^+ medium to enable spontaneous loss of the *TRP1* covering plasmid, YEpTIF34-T.

To produce H120 and H121, H450 was transformed with YCp111-i/TIF34 and YCp111-i/tif34-Q258R, respectively, and the resident *i/TIF34 URA3* plasmid was evicted on medium containing 5-FOA.

YCp22-g/TIF35-screen was generated by fusion PCR. The following pairs of primers were used for separate PCR amplifications using Ycp22-g/TIF35-help (see below) as template: (i) 3gSalIr and 3gHistag and (ii) 3gNdeI and 3gHistagr. The PCR products thus obtained were used in a 1:1 ratio as templates for a third PCR amplification using primers 3gSalIr and 3gNdeI. The resulting PCR product was digested with SalI and NdeI and ligated with SalI-NdeI-cleaved Ycp22-g/TIF35-help (replacing wild-type [WT] g/*TIF35* with 8×His-tagged g/*TIF35-His*). Ycp22-g/TIF35-help was constructed by inserting the 1,394-bp KpnI-SalI fragment from YEpTIF35-T into YCplac22 digested with KpnI-SalI.

YCp22-g/tif35-KLF was generated by fusion PCR. The following pairs of primers were used for separate PCR amplifications using YCp22-g/tif35-LF (see below) as template: (i) 3gKLF and 3gXhoIr and (ii) 3gNdeI and 3gKLFr. The PCR products thus obtained were used in a 1:1 ratio as templates for a third PCR amplification using primers 3gXhoIr and 3gNdeI. The resulting PCR product was digested with XhoI and NdeI and ligated with XhoI-NdeI-cleaved YCp22-g/tif35-LF (replacing g/*tif35-LF* with g/*tif35-KLF-His*).

YCp22-g/tif35-LF was also generated by fusion PCR. The following pairs of primers were used for separate PCR amplifications using Ycp22-g/TIF35-screen as template: (i) 3gLF and 3gXhoIr and (ii) 3gNdeI and 3gLFr. The PCR products thus obtained were used in a 1:1 ratio as templates for a third PCR amplification using primers 3gXhoIr and 3gNdeI. The resulting PCR product was digested with XhoI and NdeI and ligated with XhoI-NdeI-cleaved Ycp22-g/TIF35-screen (replacing WT g/*TIF35-His* with g/*tif35-LF-His*).

pGEX-g/tif35-KLF was made by inserting the XhoI-BamHI-digested PCR product, obtained with primers pGEX35NTD and pGEX35RRMr using the template YCp22-g/tif35-KLF, into XhoI-BamHI-digested pGEX-5X-3.

YEp-SUI1+TIF11was constructed by inserting the 1,134-kb SalI-SacI fragment from pDSO22 into YEpSUI1-U digested with SalI-SacI.

YEpTIF2(4A)-L was constructed by inserting the 2,026-kb SphI-BHI fragment from YEpTIF2(4A)-U into YEplac181 digested with SphI-BHI.

A list of all PCR primers named above can be found in Table 3.

Yeast biochemical methods. Glutathione *S*-transferase (GST) pulldown experiments with GST fusions and *in vitro*-synthesized ^{35}S-labeled polypeptides (see Table 2 for vector descriptions) were conducted as follows. Individual GST-fusion proteins were expressed in *Escherichia coli*, immobilized on glutathione-Sepharose beads, and incubated with 10 μl of ^{35}S-labeled potential binding partners at 4°C for 2 h. The beads were washed three times with 1 ml of phosphate-buffered saline, and bound proteins were separated by SDS-PAGE. Gels were first stained with Gelcode Blue stain reagent (Pierce) and then subjected to autoradiography. Ni^{2+} chelation chromatography of eIF3 complexes containing 8×His-tagged g/Tif35 from yeast whole-cell extracts (WCEs) and Western blot analysis were conducted as described in detail previously (32). In short, WCEs were incubated at 4°C for 2 h with 4 μl of 50% Ni^{2+}-nitrilotriacetic acid–silica resin (Qiagen) suspended in 200 μl of buffer A, followed by washing and elution. β-Galactosidase assays and polysome profile analysis were conducted as described previously (12, 55).

mRNA binding assay. ^{32}P-labeled *Xenopus laevis* β-globin mRNA was prepared *in vitro* using the MAXIscript SP6 transcription kit (Ambion Inc.), [α-^{32}P]UTP (10 mCi/ml), and the pKA18 vector (4) linearized with BamHI, according to the vendor's instructions. The transcript of the first 354 nucleotides of *X. laevis* β-globin mRNA was purified using a size exclusion column (NucAway spin column; Ambion, Inc.).

WT and mutant g/Tif35 proteins fused to the GST moiety and immobilized on glutathione-Sepharose beads were incubated with 100 ng of ^{32}P-labeled *X. laevis* β-globin mRNA in 250 μl of the binding buffer (10 mM HEPES [pH 7.6], 3 mM $MgCl_2$, 40 mM KCl, 5% glycerol, 1 mM dithiothreitol, 1.5% 2-β-mercaptoethanol) for 30 min at 26°C. (To increase specificity of binding, 200 ng of yeast total tRNA [Sigma] was added to each reaction mixture as a competitor RNA.) The beads were then washed three times with 1 ml of binding buffer, and bound β-globin mRNA was separated by electrophoresis on 5.5% denaturing (8 M urea) polyacrylamide gel, followed by autoradiography. For control experiments, the same procedure was carried out using beads containing only the GST moiety or beads preincubated with bacterial extracts derived from plain *E. coli* BL21 cells.

RESULTS

Multiple substitutions of the conserved residues of the RRM of g/Tif35 reduce efficiency of translation initiation. The functionally important yet nonessential C-terminal domain of g/Tif35 is formed by the canonical RRM previously shown to possess nonspecific RNA-binding activity (15). A typical RRM contains two RNP sites in β-sheets 1 and 3, with four highly conserved positions always occupied by a set of either aromatic or basic residues that critically contribute to RNA binding, namely, RNP1 positions 1 (R or K), 3 (F/Y), and 5 (F/Y) and RNP2 position 2 (F/Y) (for a review, see reference 24). An unpublished nuclear magnetic resonance structure of the human heIF3g RRM (K. Tsuda, Y. Muto, M. Inoue, T. Kigawa, T. Terada, M. Shirouzu, and S. Yokoyama, unpublished data) (protein data bank accession code 2CQ0) (Fig. 1A) shows that RNP2 and RNP1 are typically aligned next to each other in a four-stranded anti-parallel β-sheet packed against two perpendicular α-helices. Interestingly, all of the eIF3g RRM homologs differ from the classical RRM at position 2 of RNP2, in

TABLE 2. Plasmids used in this study

Plasmid	Description	Source or reference
p180 (YCp50-*GCN4-lacZ*)	Low-copy-number *URA3* vector containing wild-type *GCN4* leader	29
P227	Low-copy-number *URA3* vector containing *GCN4* leader without uORFs	26
pM226	Derivative of pM199; ORF of uORF1 extends into the *GCN4-lacZ* coding region	13
pA80z	Low-copy-number *URA3* vector containing *GCN4* leader with solitary uORF4 at the position of uORF1	1
pG67	Low-copy-number *URA3* vector containing uORF1 only, placed 32 nt from *GCN4-lacZ*	13
pM199	Low-copy-number *URA3* vector containing uORF1 only, at the position of uORF4 (140 nt from *GCN4-lacZ*)	13
p209	Low-copy-number *URA3* vector containing uORF1 only, at its original position (350 nt from *GCN4-lacZ*)	13
P1014l	Low-copy-number *URA3* vector containing uORF1 only, placed 640 nt from *GCN4-lacZ*	13
pBS64	Derivative of pM128; low-copy-number *URA3* vector containing *GCN4* leader with uORF1 at its original position, with the CCCCGG substitution of the −21 AAAATT −16 region in its 5′-UTR	49
pBS62	Derivative of pM128; low-copy-number *URA3* vector containing *GCN4* leader with uORF1 at its original position with 40-nt deletion in its 5′-UTR (from −61 to −21)	49
pVM11	Derivative of pM128; low-copy-number *URA3* vector containing *GCN4* leader with uORF1 at its original position with 46-nt deletion in its 5′-UTR (from −61 to −15)	49
pBS63	Derivative of pM128; low-copy-number *URA3* vector containing *GCN4* leader with uORF1 at its original position with 160-nt deletion in its 5′-UTR (from −181 to −21)	49
pWCB07	*GCN4-lacZ* lacking all uORFs, with hairpin insertion between nt +481 and +482 in single-copy *URA3* plasmid, from YCp50	This study
pWCB06	*GCN4-lacZ* lacking all uORFs, with hairpin insertion between nt +481 and +482 in single-copy *URA3* plasmid, from YCp50	This study
YCplac22	Single-copy cloning vector, *TRP1*	11
YEp-TIF35	High-copy-number *g/TIF35 URA3* plasmid from YEplac195	3
YEp-TIF34	High-copy-number *i/TIF34 URA3* plasmid from YEplac195	3
YCp22-g/TIF35-screen	Single-copy *g/TIF35-His TRP1* plasmid from YCplac22	This study
YCp22-g/tif35-KLF	Single-copy *g/tif35-KLF-His TRP1* plasmid from YCplac22	This study
pGEX-5X-3	Cloning vector for GST fusions	46
pGEX-g/TIF35	GST-g/Tif35 fusion plasmid from pGEX-5X-3	3
pGEX-g/tif35-KLF	GST-g/tif35-KLF fusion plasmid from pGEX-5X-3	This study
pGBK-T7-RPS3	*RPS3* ORF cloned into pGBKT7, *TRP1* (Clontech)	51
pGBK-T7-RPS20	*RPS20* ORF cloned into pGBKT7, *TRP1* (Clontech)	51
pGBK-T7-RPS2	*RPS2* ORF cloned into pGBKT7, *TRP1* (Clontech)	51
pT7-Δ7-b/PRT1	*b/PRT1*[641–724] ORF cloned under T7 promoter	54
pT7-i/TIF34	*i/TIF34* ORF cloned under T7 promoter	3
YEplac195	High-copy-number cloning vector, *URA3*	11
YEplac181	High-copy-number cloning vector, *LEU2*	11
YEplac112	High-copy-number cloning vector, *TRP1*	11
YEpSUI1-U	High-copy-number *SUI1 URA3* plasmid from YEplac195	53
pDSO22	High-copy-number *TIF11 URA3* plasmid from YEplac195	34
YEp-SUI1+TIF11	High-copy-number *SUI1 TIF11 URA3* plasmid from YEplac195	This study
YEp-SUI1+TIF11-W	High-copy-number *SUI1 TIF11 TRP1* plasmid from YEplac112	10
YEpTIF2(4A)-U	High-copy-number *TIF2 URA3* plasmid from YEplac195	7
YEpTIF2(4A)-L	High-copy-number *TIF2 LEU2* plasmid from YEplac181	This study
YEpTIF4631(4G)-U	High-copy-number *TIF4631 URA3* plasmid from YEplac195	7
pCF82	High-copy-number *SUI1 TRP1* plasmid from YEplac112	10
YCpL-i/TIF34-HA	Single-copy *i/TIF34-HA LEU2* plasmid from YCplac111	3
YCpL-i/tif34-HA-3 (Q258R)	Single-copy *i/tif34-HA-Q258R LEU2* plasmid from YCplac111	3
YEpTIF35-T	High-copy-number *g/TIF35 TRP1* plasmid from YEplac112	54
YEpTIF34-T	High-copy-number *i/TIF34 TRP1* plasmid from YEplac112	54
pKA18	β-Globin under SP6 promoter	4

that eIF3g has a basic as opposed to aromatic residue at that position (Fig. 1B). It is thus conceivable that the stacking interaction that the aromatic residue in position 2 normally establishes with mRNA is replaced by ionic attraction with a phosphate group in the RNA backbone. Surprisingly, the yeast protein also differs in position 3 of RNP1 (L versus F) (Fig. 1B).

In an effort to elucidate the role of g/Tif35 in translation, we first mutated conserved residues in either one or both RNPs (shown schematically in Fig. 1A and B) and tested the resulting mutants for slow growth (Slg^-) and temperature-sensitive (Ts) phenotypes. Whereas neither individual RNP mutant showed any growth defects (data not shown), the combination of both RNP1 and RNP2 mutations in *g/tif35-K194A-L235A-F237A* (henceforth termed *g/tif35-KLF*) resulted in the Ts phenotype without having any effect on the steady-state levels of the g/Tif35 protein in cells (Fig. 1C). The *g/tif35-KLF* mutation was found to provoke substantial (~3-fold) reductions in the polysome:monosome (P/M) ratio at 34°C (Fig. 1D), indicating a marked decrease in the rate of translation initiation *in vivo*.

TABLE 3. Primers used in this study

Primer name	Primer sequence (5′–3′)
3gSalIr	CTGCAGGTCGACCTCTTCACGATCTGCAAAAGTCCCAA
3gNdeI	CGACCATATGACCATGAACTGTCCATT
3gHistagr	AAACAAGTGCAGAGCATATTCTGTGCATCTCGAGCTAATGATGATGATGATGAT GATGATGTTCCTTAACCTTAGGTTTGGACCA
3gHistag	ATGCACAGAATATGCTCTGCACTTGTT
3gLF	CAAAGAAACAGGTAAATCAAGAGGTGCAGCCGCTGTTACCTTTTCGAGCGAAG AAGTTGCCGAACA
3gLFr	TCTTGATTTACCTGTTTCTTTGTTTCT
3gXhoIr	GTGCATCTCGAGCTAATGATGATGATGATG
3gKLFr	AGTACACATATCATCACGTTCTCTAGA
3gKLF	TGATGATATGTGTACTTTGGCAATTATGCAAGTTAATGAAAATGCCGATGAAAA
pGEX35NTD	AATAAGGATCCCCATGAGTGAAGTTGCACCAGAG
pGEX35RRMr	AATAACTCGAGCTATTCCTTAACCTTAGGTTTGGA

g/Tif35 associates with eIF3 via two contacts with subunits i/Tif34 and b/Prt1; it was previously shown that its C-terminal RRM is not required for either of these interactions (3). Indeed, the *g/tif35-KLF* mutation did not affect binding of mutant g/Tif35 (fused to the GST moiety) to radiolabeled i/Tif34 and b/Prt1 in an *in vitro* pulldown experiment (Fig. 2A, second and third panels). It also had no impact on the integrity of the MFC as judged from affinity purification of the WT and mutant 8×His-tagged g/Tif35 proteins by nickel chelation chromatography followed by analysis of the yields of copurifying proteins by Western blot hybridization (Fig. 2B). Finally, no effect on the association of any of the MFC components with the 40S subunits *in vivo* was observed, as expected (data not shown).

To examine whether mutating the RNPs of g/Tif35 affected its RNA-binding affinity, WT and mutant g/Tif35 fused to a GST moiety were incubated with *in vitro*-synthesized ^{32}P-labeled β-globin mRNA, and the amount of bound mRNA species was quantified. As shown in Fig. 2A (fourth panel), the *g/tif35-KLF* mutation had no effect on the affinity of g/Tif35 for β-globin mRNA, indicating that none of the targeted residues critically contributes to g/Tif35's RNA-binding activity. Nevertheless, given the marked impact of the *KLF* mutation on the rate of translation initiation, we decided to explore the nature of its defect further.

The RRM of g/Tif35 is required for full derepression of *GCN4* expression under starvation conditions. According to previous reports, neither yeast nor mammalian eIF3g appears to be required for assembly of the 48S PIC, which includes sequential recruitment of the TC and mRNA to the 40S subunit (25, 40). Hence, we decided to examine whether g/Tif35 might contribute to processes following the assembly of the 48S PIC in living cells, such as scanning and AUG recognition. We tested the *g/tif35-KLF* mutant for specific phenotypes indicating impairment of translational control of *GCN4* expression (18). This mechanism has been extensively used in the past as a valuable genetic tool for dissecting the contributions of individual eIFs to initiation (9, 10, 19, 31, 33, 49, 53, 61). Mutants defective in TC formation and/or its recruitment to the 40S subunit constitutively derepress *GCN4* expression, imparting a so-called Gcd$^-$ phenotype, whereas mutants that fail to derepress *GCN4* under starvation conditions provoke a Gcn$^-$ phenotype, which signals defects in the steps following assembly of 48S PICs such as processivity of scanning, AUG recognition, or subunit joining (9, 16, 23, 31, 53, 60).

In agreement with reports arguing against the involvement of g/Tif35 in stimulation of TC loading onto the 40S subunits, *g/tif35-KLF* did not display the Gcd$^-$ phenotype (data not shown). On the other hand, the *g/tif35-KLF* cells imparted the severe Gcn$^-$ phenotype, as they failed to grow in the presence of 3-AT (an inhibitor of histidine biosynthetic genes) at 34°C (Fig. 3A). The effect of 3-AT can only be overcome by sufficient upregulation of *GCN4* expression, as illustrated by the fact that 30 mM 3-AT completely prevented growth of *g/TIF35*$^+$ *gcn2*Δ cells, in which eIF2α cannot be phosphorylated and thus the TC levels remain high and *GCN4* fully repressed (Fig. 3A). It should be noted that phosphorylation of eIF2α by Gcn2 upon starvation was not affected in *g/tif35-KLF GCN2* cells, ruling out this possible mechanism for the Gcn$^-$ phenotype (data not shown). Using the *GCN4-lacZ* reporter containing all four uORFs, we measured derepression in *g/tif35-KLF* cells in response to 3-AT at 34°C and showed that it was reduced by a factor of ~5 (Fig. 3B, construct i, row 2). The little to no reduction in expression from the uORF-less *GCN4-lacZ* construct clearly suggests that the observed derepression defect is not caused by changes in *GCN4-lacZ* mRNA levels (Fig. 3B, construct ii). (It should be noted that mRNAs produced from all *GCN4-lacZ* constructs used throughout the study are highly stable owing to the fact that they all contain an intact stabilizer element [STE] that prevents the natural *GCN4* mRNA from undergoing nonsense-mediated decay [44, 49].) Together, these results imply that the RRM of g/Tif35 is required for proper upregulation of *GCN4* expression upon starvation and indicate that its function in general translation initiation might be associated with the steps following formation of the 48S PIC.

The RRM of g/Tif35 promotes resumption of scanning of posttermination ribosomes on uORF1 of *GCN4*. To determine what postassembly step(s) might be perturbed by *g/tif35-KLF*, we analyzed a battery of *GCN4-lacZ* reporters that varied in their *GCN4* mRNA leader sequences. Defects in AUG start codon recognition or subunit joining may lead to the Gcn$^-$ phenotype if the 48S PIC scans over the AUG start codon of uORF1 (leaky scanning); this can be monitored with a construct in which uORF1 is elongated and overlaps the beginning of *GCN4*. This elongated version of uORF1 blocks ~99% of all scanning ribosomes from reaching the *GCN4* start site, indicating that only ~1% of ribosomes show leaky scanning of uORF1 in WT cells (13). As shown in Fig. 3B (construct iii), we

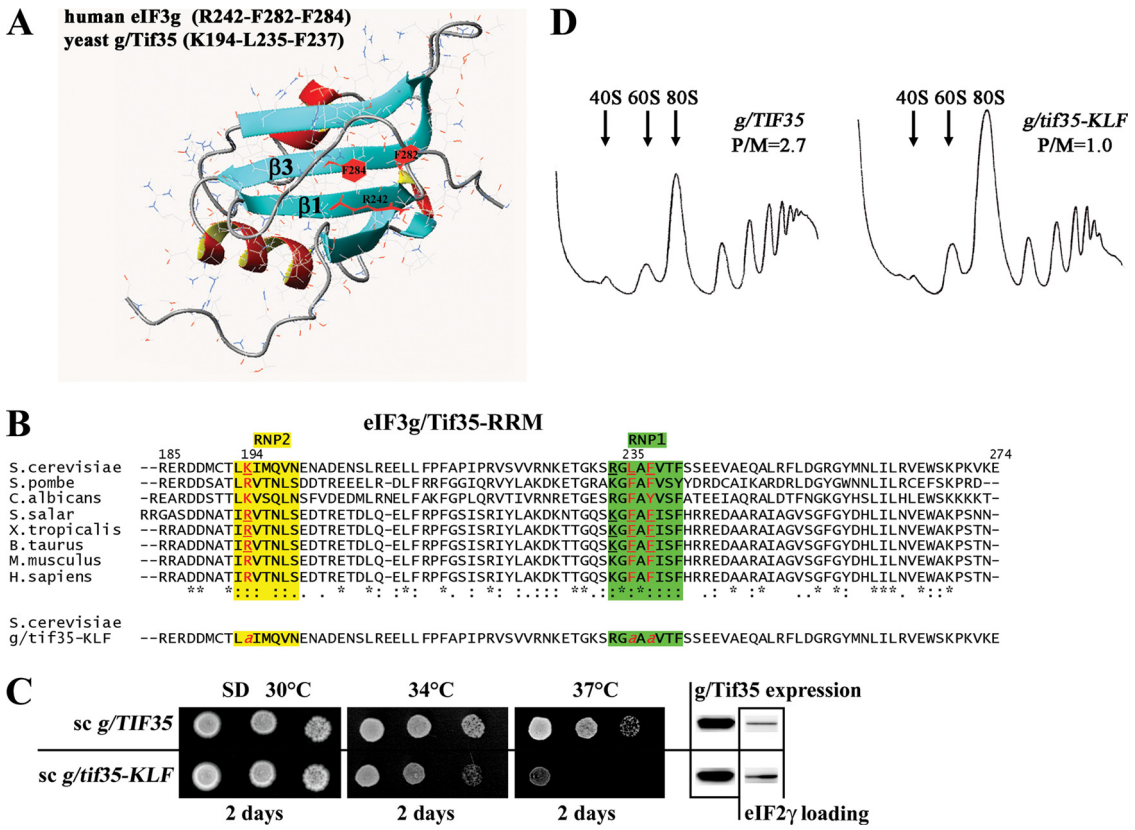

FIG. 1. The triple-Ala substitution of the highly conserved residues in RNPs of the g/Tif35 RRM in *g/tif35-KLF* impairs cell growth and the rate of general translation initiation. (A) The unpublished nuclear magnetic resonance solution structure of the human heIF3g RRM (K. Tsuda et al., unpublished; Protein Data Bank accession code 2CQ0) displays a canonical RRM fold with a four-stranded antiparallel β-sheet packed against two perpendicular α-helices. The highly conserved Arg242 in position 2 of RNP2 in β-sheet 1 and Phe282 and Phe284 in positions 3 and 5 of RNP1 in β-sheet 3 of human eIF3g RRM correspond to Lys194 and to Leu235 and Phe237, respectively, of yeast g/Tif35-RRM and are highlighted in red. (B) Amino acid sequence alignment of g/Tif35-RRM of *Saccharomyces cerevisiae* with that of other species. The amino acid sequence of *S. cerevisiae* g/Tif35 (accession number NP_010717) between residues 185 and 274 (the terminal residue) is aligned with its *Schizosaccharomyces pombe* (accession number CAA18400), *Candida albicans* (accession number Q59ZV5), *Salmo salar* (accession number ACI69727), *Xenopus tropicalis* (accession number Q28CY2), *Bos taurus* (accession number Q3ZC12), *Mus musculus* (accession number Q9Z1D1), and *Homo sapiens* (accession number O75821) homologs. The alignment was conducted with ClustalW (http://www.ch.embnet.org/software/ClustalW.html). Highly conserved sequences of RNP2 and RNP1 are shown in yellow and green, respectively, with the key residues that were subjected to site-directed mutagenesis highlighted in red. The sequence of *g/tif35-KLF* generated in this study is given at the bottom. (C) *g/tif35-KLF* severely impairs cell growth at elevated temperatures. The H464 (*g/tif35*Δ) strain was transformed with YCp22-g/Tif35-screen (top row) and YCp22-g/tif35-KLF (bottom row), and the resident YEp-TIF35-U (*URA3*) plasmid was evicted on medium containing 5-FOA. The resulting strains were then spotted in four serial 10-fold dilutions on SD medium and incubated at 30, 34, and 37°C for 2 days. The far right columns show results of Western analysis of WCEs from the very same strains grown at 34°C, using anti-g/Tif35 (g/Tif35 expression; lane 1) and anti-GCD11 (eIF2γ loading; lane 2) antibodies. (D) The *g/tif35-KLF* mutant reduces rates of translation initiation *in vivo*. Polysome profiles are shown for the strains in panel C cultured in YPD medium at 34°C and treated with cycloheximide just prior to harvesting. WCEs were separated by velocity sedimentation through a 5-to-45% sucrose gradient centrifugation at 39,000 rpm for 2.5 h. The gradients were collected and scanned at 254 nm to visualize the ribosomal species. Positions of 40S, 60S, and 80S species are indicated by arrows, and P/M ratios are given above the profiles.

observed a marginal ~1.5-fold increase in *GCN4-lacZ* expression from this construct in *g/tif35-KLF* cells, which would by no means account for a strong derepression defect (Fig. 3B, construct i). Also, little to no increase in β-galactosidase activity was detected with a construct containing only uORF4 (Fig. 3B, construct iv), which allows a negligible level of REI and thus very effectively blocks translation of downstream ORFs (13). Together these results indicate that the *KLF* mutation does not significantly affect stringency of the start codon selection. It is worth noting that results in Fig. 3B (constructs iii and iv) additionally eliminate the possibility that induction of *GCN4-lacZ* is reduced in *g/tif35-KLF* cells due to a decrease in the reporter mRNA level, as this effect should apply equally to the mutant constructs, yet expression of these constructs was higher than in the WT cells.

The derepression defect in *g/tif35-KLF* cells can be also explained by a reduction in the rate of scanning of ribosomes progressing from uORF1 to uORF4 (i.e., slow scanning) or in their decreased stability on the mRNA during scanning (i.e., abortive scanning). To test this, we analyzed constructs carrying only uORF1 at four different positions relative to *GCN4-lacZ* (Fig. 3B, constructs v to viii). If the 40S subunits were more prone to dissociating from the mRNA during scanning, then a decrease in the *GCN4-lacZ* activity would be expected. This was indeed observed; however, one would also predict that the probability of the 40S falling off would increase with

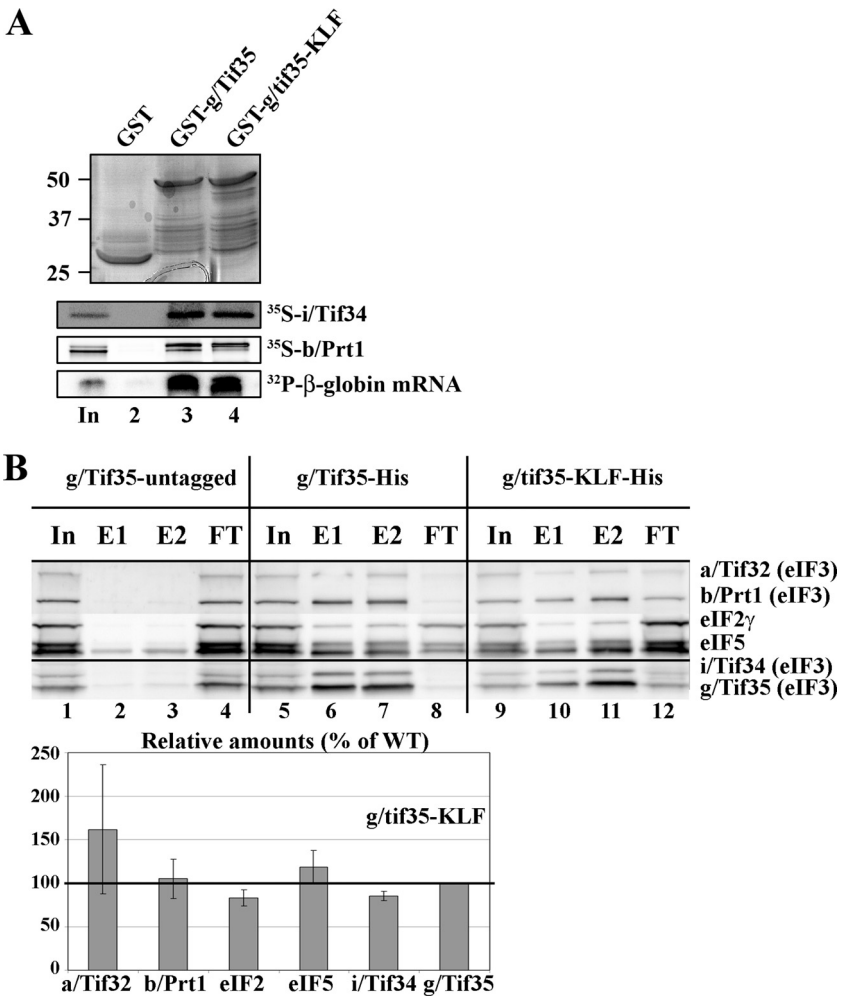

FIG. 2. The *g/tif35-KLF* mutant neither affects the integrity of eIF3 in the MFC nor impairs the RNA-binding activity of g/Tif35. (A) The *g/tif35-KLF* mutation does not reduce binding of g/TIF35 to b/Prt1, i/Tif34, or β-globin mRNA *in vitro*. Full-length WT g/Tif35 (lane 3) and mutant g/tif35-KLF (lane 4) fused to GST, and also GST alone (lane 2), were tested for binding to ^{35}S-labeled b/Prt1 and i/Tif34 and to ^{32}P-labeled β-globin mRNA. Lane 1 (In) contains 10% and 2.5% of input amounts of proteins and RNA, respectively, added to each reaction mixture. (B) The *g/tif35-KLF* mutation does not prevent g/Tif35 from associating with eIF3 in the MFC *in vivo*. WCEs were prepared from H421 (*g/tif35*Δ) bearing untagged g/Tif35 (lanes 1 to 4), H111 expressing 8×His-tagged g/Tif35 (lanes 5 to 8), and H112 expressing 8×His-tagged g/tif35-KLF (lanes 9 to 12). The WCEs were incubated with Ni^{2+}-silica resin, and the bound proteins were eluted and subjected to Western blot analysis. Lanes 1, 5, and 9 contained 5% of the input WCEs (In); lanes 2, 6, and 10 contained 30% fractions eluted from the resin (E1); lanes 3, 7, and 11 contained 60% of the same fractions (E2); lanes 4, 8, and 12 contained 5% of the flowthrough (FT). The Western signals for a/Tif32, b/Prt1, eIF2, eIF5, and i/Tif34 in the E1 and E2 fractions for the WT *g/TIF35* and mutant *g/tif35-KLF* strains were quantified, combined, normalized for the amounts of WT g/Tif35 in these fractions, and these data are plotted in the histogram on the right as percentages of the corresponding values calculated for the WT *g/TIF35*.

the increasing distance to scan through, thus producing a gradual decrease in activity, which is not the case (compare constructs v to viii). Therefore, it is highly unlikely that abortive scanning could explain the Gcn$^-$ phenotype. Slower scanning would, on the other hand, increase *GCN4-lacZ* expression from all four constructs (particularly those with shorter-than-normal spacers between uORF1 and *GCN4-lacZ* [constructs v and vi]) by providing the scanning 40S subunits more time to rebind TC before reaching the next AUG start codon. However, the fact that *g/tif35-KLF* decreased, rather than increased, expression from all four constructs to a similar extent (~57 to 77%) strongly argues against both of these explanations. In fact, the observed phenotype closely resembles that of the *a/tif32-Δ8* mutation only recently shown to interfere with the key first step of REI: resumption of scanning of postterminated ribosomes on the uORF1 stop codon (49).

As shown previously (13), *GCN4-lacZ* expression starts to plateau when the intercistronic distance between uORF1 and *GCN4-lacZ* exceeds the length of the natural 350-nt spacer, indicating saturated TC reacquisition (Fig. 3B, compare constructs viii and vii). The fact that *g/tif35-KLF* plateaus at an equal length but with expression of ~40% of the WT level, as expected, further supports our conclusion that the REI-competent PICs in the mutant cells are reduced to 40% of normal (Fig. 3C). These results hence strongly suggest that besides the NTD of a/Tif32, the RRM of g/Tif35 represents yet another eIF3 domain that is critically required for retention of the postterminated 40S subunits

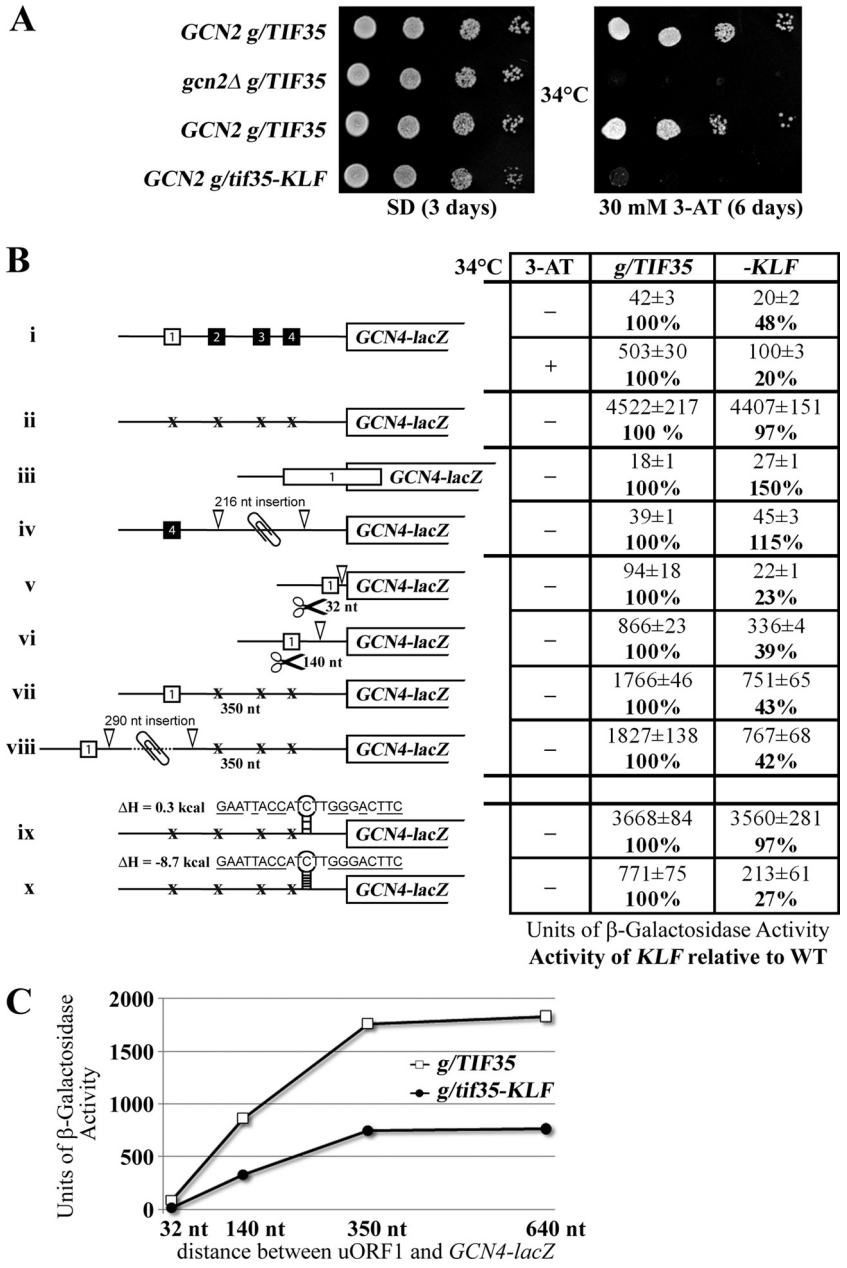

FIG. 3. *g/tif35-KLF* reduces processivity of scanning and interferes with the reinitiation process by preventing posttermination retention of the 40S ribosome on *GCN4* mRNA. (A) *g/tif35-KLF* imparts a strong Gcn$^-$ phenotype, implicating g/Tif35 in regulation of translational control of *GCN4* expression. Isogenic strain H464 (*GCN2 g/TIF35*; row 1) and H421 (*gcn2*Δ *g/TIF35*; row 2) transformed with an empty vector YCplac22 and strain H111 (*GCN2 g/tif35*Δ YCp22-g/TIF35-screen; row 3) and H112 (*GCN2 g/tif35*Δ YCp22-g/tif35-KLF; row 4) were spotted in four serial 10-fold dilutions on SD (left panel) or SD containing 30 mM 3-AT (right panel) and then incubated at 34°C for 3 or 6 days, respectively. (B, construct i) *g/tif35-KLF* reduces basal expression of *GCN4-lacZ* and prevents its full derepression upon starvation. H111 and H112 were transformed with p180 and grown in minimal medium for 6 h, and the β-galactosidase activities were measured in the WCEs and are expressed in units of nmol of *o*-nitrophenyl-β-D-galactopyranoside hydrolyzed per min per mg of protein. To induce *GCN4-lacZ* expression, strains grown in minimal medium for 2 h were treated with 10 mM 3-AT for 6 h. The mean values and standard deviations obtained from at least six independent measurements with three independent transformants, along with the activities the *g/tif35-KLF* mutant strain relative to the corresponding WT, are given in the table. White versus black squares indicate REI-permissive (uORF1) versus REI-nonpermissive (uORFs 2 to 4) uORFs. (Constructs ii to iv) The failure of *g/tif35-KLF* to derepress *GCN4-lacZ* is not caused by leaky scanning. H111 and H112 were transformed with p227 (ii), pM226 (iii), and pA80z (iv) and analyzed as for construct (i), except that they were not treated with 3-AT. Xs point to mutations eliminating the AUG start codons of uORFs 1 to 4. A paperclip symbol indicates an insertion of the nucleotide sequence. (Constructs v to viii) *g/tif35-KLF* blocks induction of *GCN4* expression by reducing the amount of posttermination 40S ribosomes on uORF1, which resume scanning for reinitiation downstream. H111 and H112 were transformed with pG67 (v), pM199 (vi), p209 (vii), or p1014l (viii) and analyzed as described for constructs ii to iv. Scissors indicate deletions of the nucleotide sequence. (Constructs ix and x) *g/tif35-KLF* increases the translation-inhibitory effect of a stable stem-loop structure inserted in the 5′-UTR of uORF-less *GCN4* mRNA. H111 and H112 were transformed with pWCB07 (ix) or pWCB06 (x) and analyzed as described for construct i. Both constructs contain the indicated sequences (with complementary bases underlined) inserted 21 nt 5′ of the *GCN4* AUG codon. (C) β-Galactosidase activities obtained for constructs v to viii in panel B, with WT and *g/tif35-KLF* cells were plotted as a function of the intercistronic distance between uORF1 and the AUG start codon of *GCN4-lacZ*.

on the mRNA, representing a crucial prerequisite for efficient REI.

The g/Tif35 RRM stimulates scanning through structured mRNA leaders. Our finding that the *g/tif35-KLF* mutation impairs resumption of scanning from uORF1 implies that the utility of the *GCN4* translational control as a tool to examine postassembly defects in general translation initiation is in this case limited. In particular, any effect of this mutation on the rate of scanning would be masked by its inability to start scanning downstream of uORF1.

To circumvent this obstacle, we compared WT and mutant *g/tif35-KLF* cells in terms of their abilites to scan through stem-loop structures inserted into the 5′-UTR of a *GCN4-lacZ* fusion lacking all four uORFs (Fig. 3B, constructs ix and x). Whereas a relatively weak stem-loop structure (Δ*H*, 0.3 kcal) reduced the *GCN4-lacZ* expression to the same degree in both WT and *g/tif35-KLF* cells (by ~20%) (Fig. 3B, compare construct ix with ii), a stable stem-loop (Δ*H*, −8.7 kcal) had ~4-fold stronger impact on translation in the mutant versus WT cells, where it diminished *GCN4-lacZ* expression by 85% (Fig. 3B, compare constructs x and ii). These results implicate g/Tif35 in stimulating processivity of scanning on mRNAs with structured 5′-UTRs—the first function in general translation initiation ever attributed to this small essential eIF3 subunit.

The a/Tif32 NTD and g/Tif35 RRM functional domains stimulate resumption of scanning by related but not identical mechanisms. It is believed that linear scanning is promoted by several initiation factors, including eIFs 1, 1A, 4G, 4A, and 4B and a helicase, Ded1, and its yeast homolog Dbp1 (reviewed in reference 39). In addition, eIF4G and eIF4A were shown to be required for resumption of scanning after translation of a short uORF in mammalian cells (43). Thus, we next wished to investigate whether some of these proteins could suppress defects of *g/tif35-KLF* and *a/tif32-Δ8* mutants in processivity of scanning and/or in resumption of scanning that produce the Gcn$^-$ phenotype. Toward this end, we overexpressed the proteins individually or in combinations in our mutant strains while scoring for growth effects on SD and 3-AT plates.

None of the factors suppressed the Gcn$^-$ phenotype of either of the mutants (Fig. 4A and C and data not shown); by contrast, an increased gene dosage of eIF1 (both alone and in combination with high-copy-number [hc] eIF1A) actually exacerbated the Gcn$^-$ phenotype of both of them (Fig. 4A and C, rows 5 and 6 versus 3). This effect of eIF1 was further verified in our reporter assay, which showed that *g/tif35-KLF* introduced with hc eIF1 conferred a severe derepression defect even at 30°C (Fig. 4B). In addition, the Gcn$^-$ phenotype of *a/tif32-Δ8* cells was exacerbated by overexpression of eIF4A or its cooverexpression with eIF4G; however, no such effect was observed in *g/tif35-KLF* cells (Fig. 4A and C). Hence, even though we did not observe any suppression effect and have at present no solid explanation for the exacerbation defects, the latter findings at least indicate that the *g/tif35-KLF* and *a/tif32-Δ8* mutations might differ in their effects on resumption of scanning.

The high propensity of *GCN4*'s uORF1 for REI depends on its short length (three codons) and enhancer sequences both 5′ and 3′ of uORF1 (reviewed in reference 18). The 5′ enhancer promotes retention of posttermination 40S subunits on the *GCN4* mRNA by interacting with the NTD of a/Tif32 (49). To explore whether or not g/Tif35-RRM acts in a similar manner, we transformed the *g/tif35-KLF* strain with *GCN4-lacZ* constructs containing solitary uORF1 with progressive deletions of its 5′ enhancer sequence and examined effects of combining the *KLF* with the 5′ enhancer deletions on REI. Previously, epistatic interactions were observed between the 5′ enhancer deletion mutants and *a/tif32-Δ8* (49). In agreement with this study, replacement of the nt −21-AAAATT-nt 16 stretch with CCCCGG or deletions of 40 (Δ*40*) or 46 (Δ*46*) nt from nt −21 upstream of the 5′ sequences of uORF1 progressively reduced the induction of *GCN4-lacZ* expression in WT cells (Fig. 5B, constructs i to iv). The *g/tif35-KLF* mutation reduced expression of *GCN4-lacZ* in the WT uORF1-only construct by ~50% (Fig. 3B, construct vii, and 5B, construct i), and none of the other deletion constructs further decreased this activity. Essentially the same effect was previously observed in *a/tif32-Δ8* cells. However, in striking contrast to *a/tif32-Δ8*, a complete deletion of the 5′ enhancer in Δ*160*, which diminishes *GCN4-lacZ* induction to ~17% in both WT cells (Fig. 5B, construct v) and *a/tif32-Δ8* cells (49), had a negligible additive effect in *g/tif35-KLF* cells (Fig. 5B, compare the ~45% reduction with construct v versus the ~51% reduction with construct iv). Together these findings further suggest that the g/Tif35 RRM and a/Tif32 NTD make synergistic yet independent contributions to the stabilization of posttermination 40S subunits on the *GCN4* mRNA. The fact that combining the *KLF* and Δ*8* mutations in the *tif35*Δ *tif32*Δ double deletion strain resulted in synthetic lethality corroborates this suggestion (data not shown). More importantly, however, our observations also indicate that even though the *g/tif35-KLF* mutation by itself substantially reduces the resumption-of-scanning capacity of 40S ribosomes after uORF1, it concurrently diminishes the requirement of the uORF1 5′ enhancer sequences for efficient REI (see Discussion).

g/Tif35 interacts with the 40S beak proteins Rps20 and Rps3. To gain more insight into the role of the g/Tif35 RRM in the REI mechanism, we wished to predict the g/Tif35 position on the 40S ribosome. Toward this end we tested GST-g/Tif35 for interactions against all 33 small ribosomal proteins (Rps), which were synthesized and ^{35}S-labeled in rabbit reticulocyte lysates. Among all small ribosomal proteins, only Rps3 and Rps20 strongly interacted with GST-g/Tif35; these interactions were independent of the *KLF* mutation (Fig. 6A and data not shown). (Rps2 is shown for specificity, as it lies near Rps3 and 20 [Fig. 6B].)

Based on homology modeling with *E. coli* ribosomal proteins, both Rps3 and -20 were suggested to form the beak on the solvent-exposed side of the 40S subunit (47) (Fig. 6B). The fact that g/Tif35 specifically interacted only with two Rpss occurring next to each other is significant and suggests that this eIF3 subunit most likely occurs somewhere between the head-lobe and the beak regions (Fig. 6C). Based on these and other interactions identified between the a/Tif32 CTD and Rpss 2 and 3 (6) and between the c/Nip1 and the 40S head proteins (T. Kouba and L. Valášek, unpublished observations), we modified our original model for the position of eIF3 on the 40S subunit (51) as follows. The c/Nip1 CTD and the b/Prt1 CTD interacting with i/Tif34 and g/Tif35 were moved upwards to the head region, with the b/Prt1-CTD/i/Tif34/g/Tif35 module stretching toward the beak in proximity of the mRNA entry

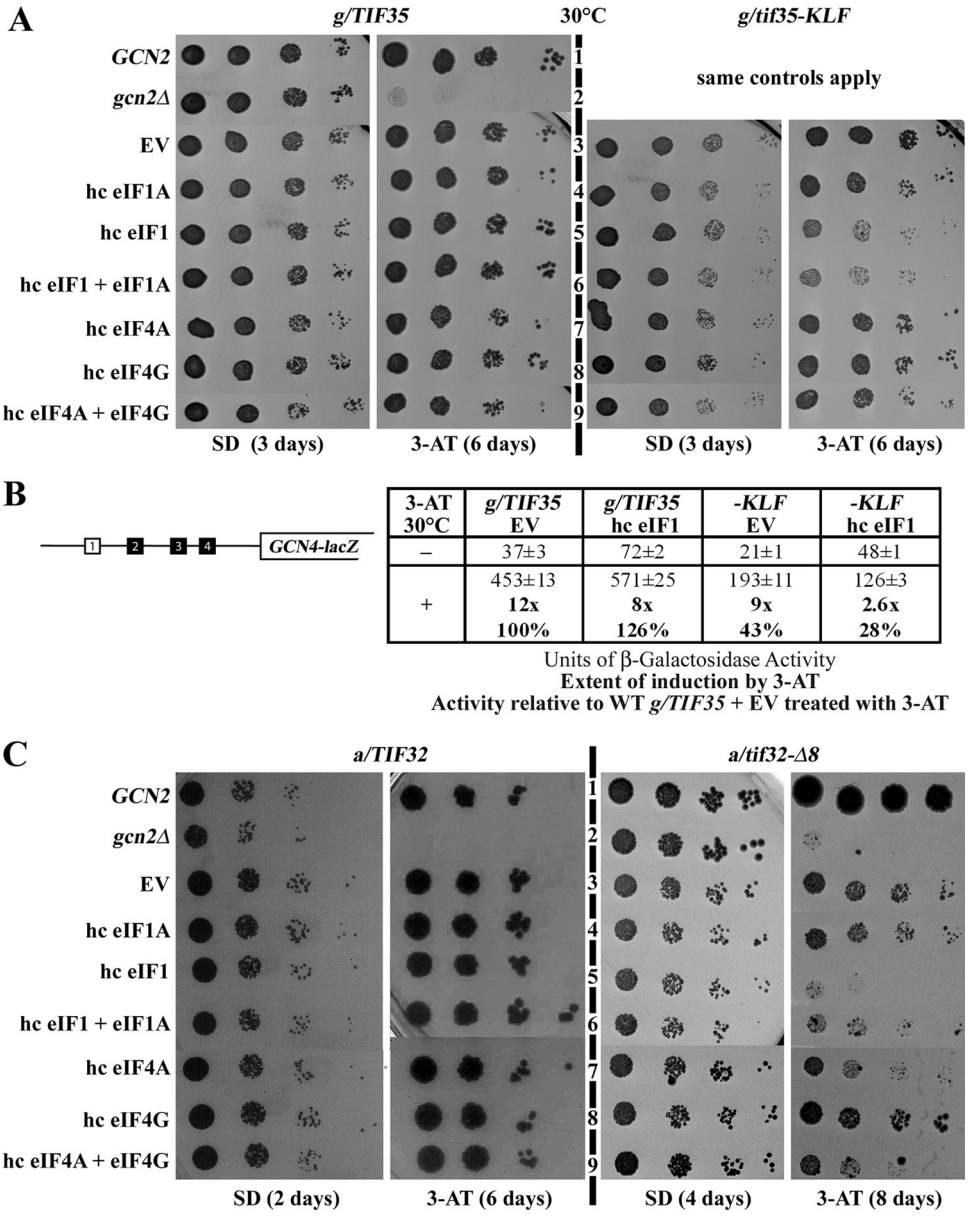

FIG. 4. Overexpression of eIF1 in *g/tif35-KLF* diminishes *GCN4* upregulation upon starvation even at 30°C. (A) Overexpression of eIF1 in *g/tif35-KLF* produces the Gcn$^-$ phenotype at 30°C. Isogenic strains H111(*g/TIF35*) and H112 (*g/tif35-KLF*) were transformed with the following combinations of two vectors: empty vectors YEplac195 and YEplac181 (EV; row 3), pDSO22 and YEplac181 (hc eIF1A; row 4), YEpSUI1-U and YEplac181 (eIF1; row 5), YEp-SUI1 + TIF11 and YEplac181 (eIF1 + eIF1A; row 6), YEpTIF2(4A)-U and YEplac181 (hc eIF4A; row 7), YEpTIF4631(4G)-U and YEplac181 (eIF4G; row 8), YEpTIF2(4A)-L and YEpTIF4631(4G)-U (hc eIF4A + eIF4G; row 9). These strains, together with control strains H464 (*GCN2*; row 1) and H421 (*gcn2*Δ; row 2) transformed with YEplac195 and YEplac181, were spotted in four serial 10-fold dilutions on SD or SD medium containing 30 mM 3-AT and incubated at 30°C for 3 or 6 days, respectively. (B) High-copy-number expression of eIF1 in *g/tif35-KLF* severely blocks induction of *GCN4-lacZ* expression. Isogenic strains H111 (*g/TIF35*) and H112 (*g/tif35-KLF*) transformed either with empty vector YEplac112 (EV) or pCF82 (hc eIF1) were further transformed with p180 and analyzed as described for construct i in Fig. 3B. (C) Overexpression of eIF1 or eIF4A exacerbates the Gcn$^-$ phenotype of *a/tif32-Δ8*. Isogenic strains YBS47 (*a/TIF32*) and YBS53 (*a/tif32-Δ8*) were transformed with the same combinations of two vectors as described for panel A, spotted together with the control strains (as for panel A) in four serial 10-fold dilutions on SD or SD containing 30 mM 3-AT, and incubated at 30°C for 2 to 8 days, as indicated.

channel (Fig. 6C). The a/Tif32 NTD interacts with Rps0 and is thus thought to occur in the vicinity of the mRNA exit channel, where it could interact with the 5′ feature of uORF1 (49). Hence, since both a/Tif32-NTD and g/Tif35-RRM seem to occupy different positions on the back of the 40S, it is indeed conceivable that the nature of their involvement in the initial REI phase is mechanistically different, at least to a certain extent.

i/Tif34 stimulates the rate of scanning. Since eIF3i was, alongside eIF3g, suggested to be dispensable for assembly of the functional 48S PIC in both yeast and mammals (25, 40), we next decided to examine the role of yeast i/Tif34 in scanning

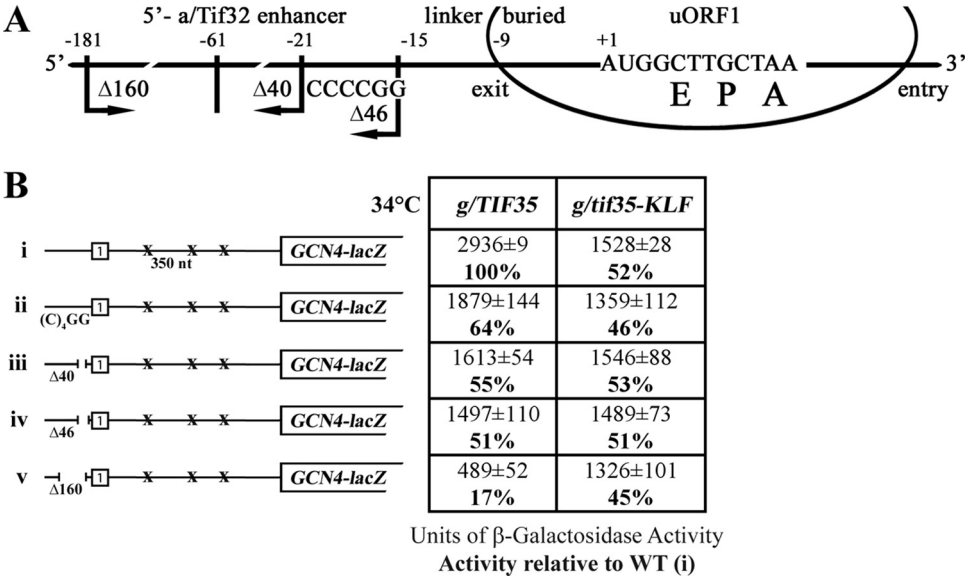

FIG. 5. The *g/tif35-KLF* mutation diminishes the requirement of uORF1 5′ enhancer sequences for efficient REI. (A) Schematic showing the predicted position of the 40S ribosome terminating at the stop codon of uORF1 from the *GCN4* mRNA leader (based on data from reference 49). E, P, and A sites of the 40S ribosomes are aligned with the last two coding triplets and the TAA stop codon. The locations of the 5′ enhancer (labeled 5′-a/Tif32 enhancer to denote the interaction with the NTD of a/Tif32), linker, and buried parts of the sequences upstream of uORF1 are indicated at the top; the 3′ boundaries of the Δ*40* deletion (identical to Δ*160*), Δ*46* deletion, and the $(C)_4GG$ multiple substitution are shown below the line depicting mRNA. (B, constructs i to v) The same experiment as described for construct i in Fig. 3B, except that H111 and H112 were transformed with p209, pBS64, pBS62, pVM11, and pBS63 (constructs i to v, respectively) and analyzed without 3-AT treatment. Activities relative to WT are given as percentages in boldface in the table to the right of the schematics.

and other postassembly processes, in a similar manner as described above for g/Tif35. Yeast i/Tif34 is composed of seven WD40 repeats assembled into a propeller ring and has been shown to interact with the NTD of g/Tif35 and the extreme CTD of b/Prt1 (3, 52). Previously, three growth-defective i/Tif34 mutants were generated and characterized for binding defects (3). Of these, only the *i/tif34-3-HA* (henceforth *i/tif34-Q258R*) mutation, mapping into the WD repeat 6, had no effect on i/Tif34 interactions with g/Tif35 and b/Prt1, yet it showed a >2-fold reduction in the translational rates *in vivo*. These findings indicate that the *Q258R* mutations might have a functional defect rather than a simple assembly problem. Therefore, we selected the *Q258R* mutant for further analysis.

As expected, *i/tif34-Q258R* did not produce the Gcd$^-$ phenotype, which would indicate a defect in TC recruitment *in vivo* (data not shown). However, it did provoke a strong Gcn$^-$ phenotype in the presence of 3-AT (Fig. 7A), resulting from an ~3-fold reduction in the *GCN4* derepression (Fig. 7B, construct i). (This defect was not caused by insufficient phosphorylation of eIF2α [data not shown].) Detailed examination revealed that *i/tif34-Q258R* modestly increases skipping of the AUG start codon of a short uORF preceding the *GCN4-lacZ* gene (by a factor of ~2) (Fig. 7B, constructs iii and iv). More importantly, however, *i/tif34-Q258R* confers strong (~3-fold and ~2.5-fold) increases in expression of the *GCN4-lacZ* constructs containing solitary uORF1 with the 32-nt and 140-nt spacers, respectively (Fig. 7B, constructs v and vi), that are too large to be explained merely by the amount of leaky scanning (compare, for example, construct vi in Fig. 7B, with 1991 − 817, or 1,174 units, with construct iii, with 62 − 28, or 34 units).) Furthermore, increasing the spacing between uORF1 and the *GCN4-lacZ* start site to the natural 350 nt progressively increased *GCN4-lacZ* expression in both strains, as expected; however, the β-galactosidase activity was still ~1.5-fold higher in *i/tif34-Q258R* versus WT cells (Fig. 7B, construct vii). These results are consistent with a defect in the rate of scanning, where the slower-scanning PICs are provided with more time to rebind TC before reaching the next start codon and the closer the solitary uORF1 is to *GCN4-lacZ*, the greater the increase in the frequency of REI. On the other hand, no effect on scanning through stem-loop structures inserted into the uORF-less leader of *GCN4-lacZ* was observed in *i/tif34-Q258R* cells (data not shown), in contrast to *g/tif35-KLF* (Fig. 3B, constructs ix and x). Together, these findings strongly suggest that *i/tif34-Q258R* provokes the Gcn$^-$ phenotype partially by modest leaky scanning over uORF1 but mainly by severe impairment of the rate of scanning between uORF1 and uORF4, which results in an increased number of 40S subunits that rebind TC before reaching inhibitory uORFs 2 to 4. Since *i/tif34-Q258R* has apparently no effect on resumption of scanning, we propose that both observed defects apply equally well to translation of any mRNA in the *Q258R* mutant cells. To our knowledge this is the strongest evidence obtained to date that implicates an eIF3 subunit in stimulating the rate of scanning *in vivo*.

Finally, we examined whether some of the aforementioned scanning-promoting factors could suppress the Gcn$^-$ phenotype of *i/tif34-Q258R*. Strikingly, whereas an increased gene dosage of eIF1 exacerbated the Gcn$^-$ phenotype of the *Q258R* mutant, combined overexpression of eIF1 and eIF1A (i.e., two factors implicated in promotion of scanning [37, 38]) partially suppressed it (Fig. 8A, rows 6 versus 4). This suppression effect

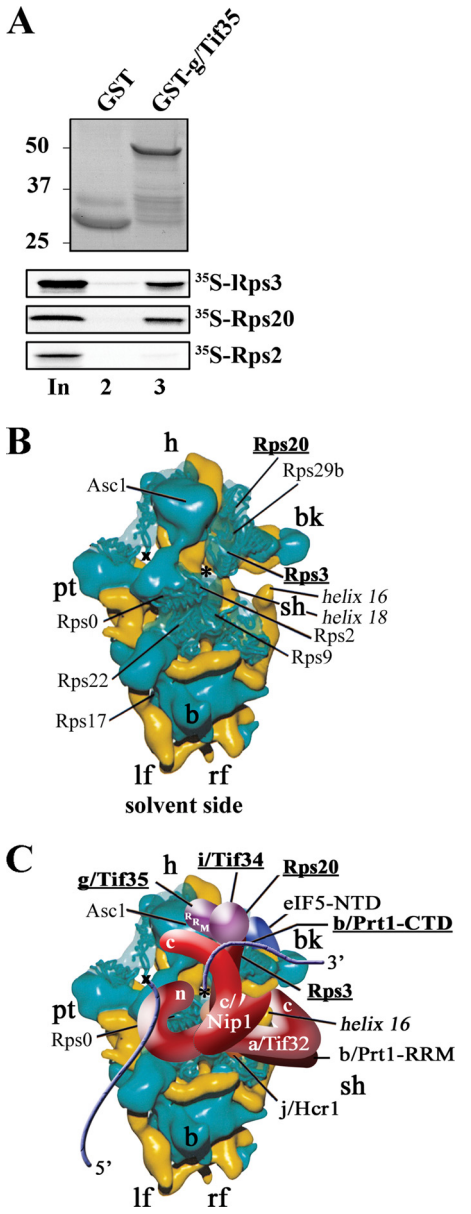

FIG. 6. g/Tif35 specifically interacts with Rps3 and Rps20 situated on the beak of the solvent-exposed side of the 40S subunit. Also shown in a revised model of the hypothetical location of eIF3 on the *S. cerevisiae* small ribosomal subunit. (A) g/Tif35 fused to GST (lane 3) or GST alone (lane 2) was tested for binding to ^{35}S-labeled Rps3, -20, and -2 essentially as described for Fig. 2A. (B and C) Revised hypothetical location of the *S. cerevisiae* eIF3 on the back side of the 40S subunit, based on the data presented in this study and data from reference 51. The cryo-electron microscopy reconstruction of the 40S subunit is shown from the solvent side, with RNA segments in yellow and proteins in green. Positions of Rps3 and Rps20, i/Tif34, the RRM of g/Tif35, and the extreme CTD of b/Prt1 are highlighted in bold. The mRNA entry and exit channels are designated by an asterisk and an X, respectively. The blue lines represent mRNA. Positions of Rps2, -3, and -9 were modified according to findings described in reference 50.

of eIF1 and eIF1A was further verified with the results of our reporter assay, where we showed that simultaneous overexpression of eIF1 and eIF1A increased the *GCN4-lacZ* activity in the *i/tif34-Q258R* cells treated with 3-AT by ~3.5-fold but had no such an effect in the WT cells (Fig. 8B). Finally, we also observed that overexpression of the RNA helicase eIF4A, alone or in combination with eIF4G, greatly exacerbated the Slg$^-$ phenotype of *i/tif34-Q258R*, whereas overexpression of eIF4G alone partially suppressed it (Fig. 8A, rows 7 to 9). Although the molecular basis of these synthetic phenotypes remains to be elucidated, the observed genetic interactions of *i/tif34-Q258R* with the key scanning-promoting factors lend further support to our conclusion that i/Tif34 enhances the rate of the ribosomal scanning.

DISCUSSION

In this paper we have focused on functional characterization of two small subunits of eIF3, g/Tif35 and i/Tif34, the cellular roles of which have remained highly elusive even though these subunits are essential for the viability of yeast cells (15, 21, 30). We found that substitutions of conserved residues of the RRM of g/Tif35 in *g/tif35-KLF* significantly reduced processivity of scanning through a stable stem-loop structure inserted into the uORF-less *GCN4* mRNA leader; this prevented a large proportion of scanning PICs from reaching the coding region (Fig. 3). We also demonstrated that the single point mutation Q258R, mapping to the WD40 repeat 6 of i/Tif34, markedly impairs the rate of scanning of the 40S ribosomes that translate uORF1 and resume scanning downstream (Fig. 7B). The latter severe scanning defect, under starvation conditions with a limited supply of the TC, provides sufficient time for 40S ribosomes en route from uORF1 to *GCN4* to rebind TC before reaching inhibitory uORFs 2 to 4 and thus blocks induction of *GCN4* expression and produces the Gcn$^-$ phenotype (Fig. 7A).

It can be argued that the *GCN4* model system used to explore the scanning properties of posttermination 40S subunits is not suitable for general studies of linear scanning by 48S PICs initiating *de novo* at the mRNA's 5′ end. However, as McCarthy and colleagues elegantly demonstrated, ribosomes scan with the same efficiency after termination on short uORFs as they do when starting from the 5′ cap; therefore, scanning in general is highly processive, with an extremely low off-rate (5). These observations thus validate the employed assay and make our findings applicable to the mechanism of canonical linear scanning. Hence, given that both i/Tif34 and g/Tif35 are dispensable for formation of the 48S PIC at the mRNA's 5′ end in both yeast and mammals (25, 40), and that neither the *i/tif34-Q258R* nor *g/tif35-KLF* mutation affects the integrity of the eIF3 complex (Fig. 2B and reference 3), our results provide the first evidence to date that directly implicates two eIF3 subunits in promoting the rate and processivity of scanning in living cells.

Ostensibly at odds with these conclusions, i/Tif34 and g/Tif35 were found to be dispensable for translation in *in vitro* cell-free systems. Specifically, using the ribosome-binding–toeprinting assay, the mammalian study measured formation of 48S PICs at the AUG codon of β-globin mRNA after a 5-min incubation of all components in a reaction buffer followed by a 10-min incubation with a reverse transcriptase mixture (25). The yeast study monitored the extent of a functional rescue of luciferase mRNA translation in a heat-inactivated *b/prt1-1* extract 70 min after addition of various eIF3 subcomplexes pu-

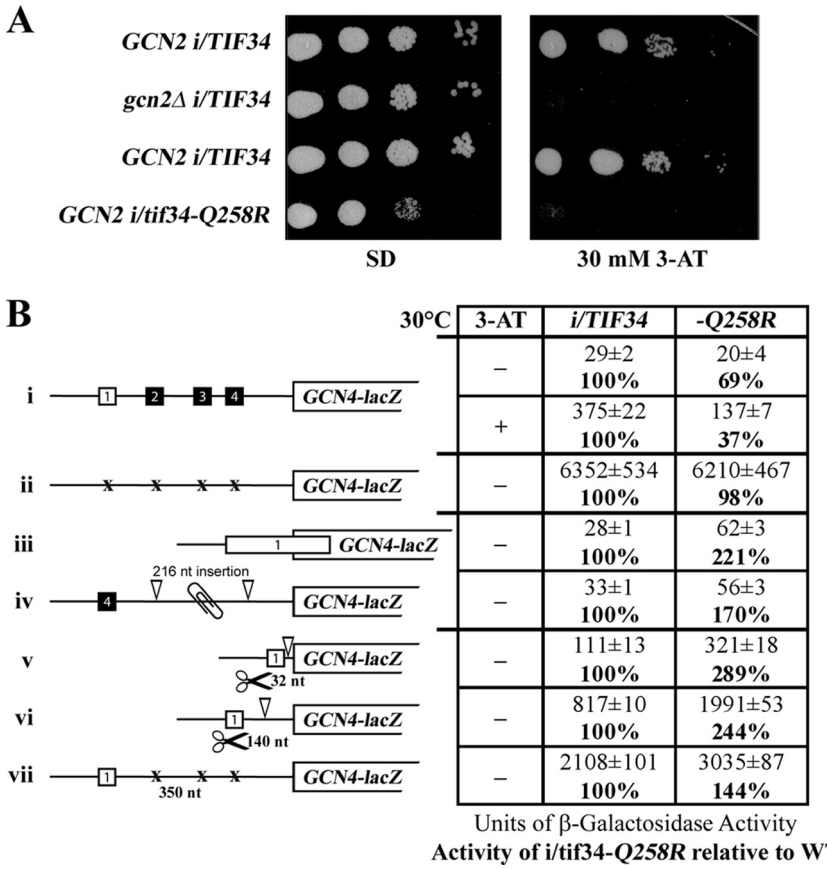

FIG. 7. Genetic evidence that *i/tif34-Q258R* prevents induction of *GCN4* expression by a combination of modestly increased leaky scanning of uORF1 and a severe reduction in the rate of scanning from uORF1. (A) *i/tif34-Q258R* imparts a strong Gcn$^-$ phenotype, implicating i/Tif34 in regulation of translational control of *GCN4*. Isogenic strains H450 (*GCN2 i/TIF34*; row 1) and H420 (*gcn2*Δ *i/TIF34*; row 2) transformed with empty vector YCplac111 and strains H120 (*GCN2 i/tif34*Δ YCp111-i/TIF34; row 3) and H121 (*GCN2 i/tif34*Δ YCp111-i/tif34-Q258R; row 4) were spotted in four serial 10-fold dilutions on SD (left panel) or SD containing 30 mM 3-AT (right panel) and then incubated at 30°C for 6 or 8 days, respectively. (B, construct i) *i/tif34-Q258R* prevents full derepression of *GCN4-lacZ* expression upon starvation. Isogenic strains H120 (*i/TIF34*) and H121 (*i/tif34-Q258R*) were transformed with p180 and analyzed as described for construct i in Fig. 3B. (Constructs ii to iv) The *i/tif34-Q258R* mutation increases leaky scanning over the AUG start codon. H120 and H121 were transformed with p227 (ii), pM226 (iii), and pA80z (iv) and analyzed as described for constructs ii to iv in Fig. 3B. (Constructs v to vii) The *i/tif34-Q258R* mutation reduces the rate of scanning of posttermination 40S ribosomes from uORF1. H120 and H121 were transformed with pG67 (v), pM199 (vi), or p209 (vii) and analyzed as described for constructs ii to iv in Fig. 3B.

rified by Ni chelation chromatography (40). In this way the a/Tif32-b/Prt1-c/Nip1 subcomplex was found to be nearly as active as the five-subunit complex, whereas the b/Prt1-i/Tif34-g/Tif35 subcomplex was practically inactive. It must be noted, however, that both approaches focused on the end points of the reactions that were monitored and did not follow the kinetics. As such, neither of them would likely be sensitive enough to detect qualitative defects in the rate and processivity of scanning.

At the same time, it is fair to note that the simple assumption that i/Tif34 and g/Tif35 are merely required to augment activities of other eIFs in scanning would not explain their essentiality for cellular viability in yeasts. To account for this fact, we propose the following. It has been established by numerous labs that the "strength" of a particular mRNA is determined by the presence of stable secondary structures in its 5′-UTR; in general, the closer these structures are to the 5′ cap, the more inhibitory they become (reviewed in reference 22). It is conceivable that a suboptimal rate of scanning might have dramatically diverse effects on translatability of mRNAs differing in both the length and the complexity of their 5′-UTRs. The essential character of both small eIF3 subunits might explained by suggesting that the loss of their stimulatory effects on scanning predominantly compromises translation of a subset of critical mRNAs encoding tightly regulated genes, such as those involved in cell cycle regulation, signal transduction, etc.—mRNAs which often have long 5′-UTRs rich in secondary structures (22, 56). This proposal is consistent with earlier observations showing that (i) specific mutations in i/Tif34 or overexpression of its fission yeast homolog Sum1 deregulates progression through the cell cycle and affects mating and the osmotic stress response (21, 57) and (ii) overexpression of human eIF3i, often observed in carcinomas, resulted in cell size increase, proliferation enhancement, cell cycle progression, and anchorage-independent growth (2). Indeed, we cannot rule out that there might be other essential functions for these two proteins in translation or even func-

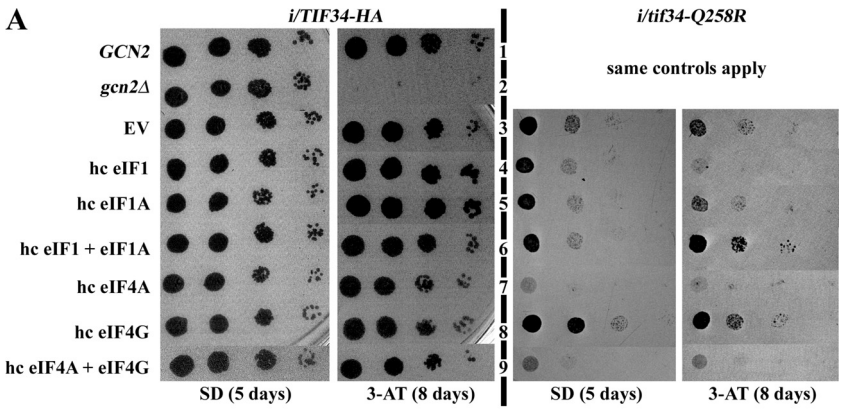

B

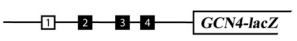

3-AT 34°C	*i/TIF34* EV	*i/TIF34* hc eIFs 1+1A	*-Q258R* EV	*-Q258R* hc eIFs 1+1A
-	23±1	26±1	31±1	40±1
+	379±2 **16x** **100%**	255±4 **10x** **67%**	47±2 **1.5x** **12%**	172±20 **4.3x** **45%**

Units of β-Galactosidase Activity
Extent of induction by 3-AT
Activity relative to WT *i/TIF34* + EV treated with 3-AT

FIG. 8. Simultaneous overexpression of eIFs 1 and 1A partially suppresses the Gcn$^-$ phenotype of *i/tif34-Q258R*. (A) Isogenic strains H120 (*i/TIF34*) and H121 (*i/tif34-Q258R*) were transformed with the same combinations of two vectors as for Fig. 4A, spotted together with H450 (*GCN2*; row 1) and H420 (*gcn2*Δ; row 2) transformed with YEplac195 and YEplac181 in four serial 10-fold dilutions on SD or SD containing 10 mM 3-AT, and incubated at 30°C for 5 or 8 days. (B) High-copy-number expression of eIFs 1 and 1A increases the *GCN4-lacZ* activity in the *i/tif34-Q258R* cells treated with 3-AT. Isogenic strains H120 (*i/TIF34*) and H121 (*i/tif34-Q258R*) transformed either with empty vector YEplac112 (EV) or YEp-SUI1+TIF11-W (hc eIF1 + eIF1A) were further transformed with p180 and analyzed as described for construct i in Fig. 3B.

tions that are independent of eIF3. It will be important to subject those regions of both subunits that were not studied here to systematic mutagenesis and investigate their potential roles in translation and beyond.

In support of the *i/TIF34* role in scanning, the Gcn$^-$ phenotype of its Q258R mutant was partially suppressed by simultaneous overexpression of eIFs 1 and 1A (Fig. 8), i.e., the two master regulators of scanning (38). Interestingly, overexpression of only eIF1 conversely worsened the effect of *i/tif34-Q258R* on derepression of *GCN4*, as did overexpression of eIF1 alone or in combination with eIF1A in *g/tif35-KLF* cells (Fig. 4). In addition, sole overexpression of the eIF4A helicase exacerbated the Slg$^-$ phenotype of *i/tif34-Q258R* but not that of *g/tif35-KLF* cells (Fig. 4 and 8). In both mutants, no effects were associated with other helicases implicated in translation initiation, such as Ded1, Dbp1, and eIF4B. Scanning consists of two linked processes: unwinding of secondary structures in the 5′-UTR and ribosomal movement along it. The 43S PICs can scan unstructured 5′-UTRs without factors associated with RNA unwinding and are thus intrinsically capable of movement along mRNA (38). Omission of eIF1A substantially reduces this ability and lack of eIF1 almost abrogates it, indicating that movement of the 43S complexes requires the open/scanning-conducive conformation induced by the synergistic actions of eIF1 and eIF1A (36). Furthermore, scanning along 5′-UTRs containing even weak secondary structures requires ATP and eIF4A, eIF4G, and eIF4B (38). However, the mechanism by which these factors assist scanning remains unknown. That said, our suppression and synthetic exacerbation genetic data might indicate that *i/tif34-Q258R* impedes full opening of the mRNA entry channel (i.e., the adoption of the scanning-conducive conformation), perhaps in a manner that could be corrected by the mass action of eIF1 and eIF1A. Alternatively, or in addition, both the *Q258R* and *KLF* mutations could predominantly interfere with the action of at least one of the initiation-specific helicases. Given the fact that g/Tif35 specifically interacts with Rps20 and mainly with Rps3 (Fig. 6), which is directly involved in transition between the closed/scanning-incompetent and open/scanning-conducive conformations of the 40S ribosome (36), it could be further proposed that this g/Tif35-Rps3 contact places i/Tif34 in a favorable position to influence the latter conformational transitions. (It should be noted that we did not detect any specific interactions between i/Tif34 and any of the 33 ribosomal proteins.) At the same time, the predicted position of g/Tif35 above the mRNA entry channel may enable its RRM to stimulate scanning by presenting mRNAs to the decoding center and/or by promoting the action of helicases. These options resonate with recent findings suggesting that mammalian eIF3 forms an extension of the mRNA-binding channel that might contribute to scanning (41). g/Tif35 could, for example, act in cooperation with eIF4B, a cofactor for the RNA helicase activity of eIF4F, since yeast g/Tif35 and eIF4B were found to interact (58). At odds with this scenario, however, we did not observe any binding between these two proteins in our GST pulldown assays (data not shown).

It is intriguing that the *g/tif35-KLF* mutation dramatically reduced induction of *GCN4* expression under amino acid starvation by impairing resumption of scanning of posttermination ribosomes from uORF1. The strongest evidence supporting

the nature of this defect was provided by demonstrating that irrespective of the intercistronic distance between uORF1 and the start codon of *GCN4-lacZ*, the efficiency of REI on *GCN4* in the *g/tif35-KLF* cells remained at ~30 to 40% of the WT (Fig. 3). These and other results thus implicate the RRM of g/Tif35, along with the a/Tif32 NTD, in stabilizing uORF1 posttermination 40S ribosomes on *GCN4* mRNA and/or in promoting resumption of scanning for REI downstream. Intriguingly, eIF3g has also been shown to play a critical role in the REI mechanism in plants, where it interacted with the cauliflower mosaic virus transactivator, TAV, and promoted translation reinitiation of viral polycistronic mRNAs (35).

The key feature of *GCN4*'s uORF1 is its ability to allow a high frequency of resumption of scanning after its translation; this ability depends on its short length (three codons) and its 5′ and 3′ enhancer sequences (18). Importantly, we have recently demonstrated that the postinitiation retention of eIF3 on 80S ribosomes translating uORF1 is likewise critical for uORF1's full REI capacity, owing to the fact that the 5′ enhancer sequences interact with the NTD of a/Tif32 and thus stabilize the posttermination 40S subunit on *GCN4* mRNA (49).

Several lines of evidence suggest that even though both the a/Tif32 NTD and the g/Tif35 RRM are critical for this initial REI phase, their individual roles differ. First, combining *g/tif35-KLF* with the N-terminal deletion of a/Tif32 in *a/tif32-Δ8* resulted in a synthetic lethal phenotype. Also, our suppression/exacerbation analysis with scanning-promoting eIFs at high copy numbers revealed different effects on the Gcn$^-$ phenotypes of *g/tif35-KLF* versus *a/tif32-Δ8* mutants (Fig. 4). Third, the a/Tif32 NTD and the g/Tif35 RRM domains seem to occur on opposing pores of the mRNA-binding channel. Furthermore, our detailed genetic analysis strongly suggests that the g/Tif35 RRM does not promote resumption of scanning in cooperation with the 5′ enhancer of uORF1 (Fig. 5). Finally, the indisputable functional importance of uORF1's 5′ enhancer is practically eliminated in the background of the *KLF* mutation (Fig. 5B, construct v). Interestingly, somewhat similar results were observed when the *GCN4* leader lacking the 5′ enhancer sequences of uORF1 was placed in front of the recombinant *GAL1-lacZ* gene (28). The resulting construct was unexpectedly fully capable of conferring the *GCN4*-like mode of translational control upon the *GAL1-lacZ* transcript. Besides the coding sequence, the only other region in which the *GCN4-lacZ* and *GAL1-lacZ* constructs differed were their 3′-UTRs, which corresponded to the genuine chromosomal sequence of each gene. These findings might imply that the *GCN4* 3′-UTR plays an inhibitory role in the *GCN4* translational control mechanism, perhaps as a part of the 5′-cap/eIF4E/eIF4G/PAB1/3′-UTR closed-loop structure (59). It will be intriguing to examine how exactly the g/Tif35 RRM and the *GCN4* 3′-UTR contribute to reinitiation and whether there is any functional connection between them.

ACKNOWLEDGMENTS

We are thankful to the members of the Valášek and Krásný laboratories for helpful comments and to Olga Krydová for technical and administrative assistance. We are also indebted to Monica Liu for critical reading of the manuscript and Olga Janoušková and Edit Rutkai for their help with site-directed mutagenesis of the g/Tif35-RRM and GST pulldown experiments with the small ribosomal proteins, respectively.

This research was supported by the Howard Hughes Medical Institute, The Wellcome Trust grant 076456/Z/05/Z, a Fellowship of Jan E. Purkyne from the Academy of Sciences of the Czech Republic, and Institutional Research Concept AV0Z50200510.

REFERENCES

1. **Abastado, J. P., P. F. Miller, B. M. Jackson, and A. G. Hinnebusch.** 1991. Suppression of ribosomal reinitiation at upstream open reading frames in amino acid-starved cells forms the basis for *GCN4* translational control. Mol. Cell. Biol. **11:**486–496.
2. **Ahlemann, M., R. Zeidler, S. Lang, B. Mack, M. Münz, and O. Gires.** 2006. Carcinoma-associated eIF3i overexpression facilitates mTOR-dependent growth transformation. Mol. Carcinog. **45:**957–967.
3. **Asano, K., L. Phan, J. Anderson, and A. G. Hinnebusch.** 1998. Complex formation by all five homologues of mammalian translation initiation factor 3 subunits from yeast *Saccharomyces cerevisiae*. J. Biol. Chem. **273:**18573–18585.
4. **Asano, K., H.-P. Vornlocher, N. J. Richter-Cook, W. C. Merrick, A. G. Hinnebusch, and J. W. B. Hershey.** 1997. Structure of cDNAs encoding human eukaryotic initiation factor 3 subunits: possible roles in RNA binding and macromolecular assembly. J. Biol. Chem. **272:**27042–27052.
5. **Berthelot, K., M. Muldoon, L. Rajkowitsch, J. Hughes, and J. E. G. McCarthy.** 2004. Dynamics and processivity of 40S ribosome scanning on mRNA in yeast. Mol. Microbiol. **51:**987–1001.
6. **Chiu, W. L., S. Wagner, A. Herrmannova, L. Burela, F. Zhang, A. K. Saini, L. Valasek, and A. G. Hinnebusch.** 28 June 2010. The C-terminal region of eIF3a promotes mRNA recruitment, scanning and, together with eIF3j and the eIF3b RRM, selection of AUG start codons. Mol. Cell Biol. doi:10.1128/MCB.00280-10.
7. **de la Cruz, J., I. Iost, D. Kressler, and P. Linder.** 1997. The p20 and Ded1 proteins have antagonistic roles in eIF4E-dependent translation in Saccharomyces cerevisiae. Proc. Natl. Acad. Sci. U. S. A. **94:**5201–5206.
8. **Dever, T. E., L. Feng, R. C. Wek, A. M. Cigan, T. D. Donahue, and A. G. Hinnebusch.** 1992. Phosphorylation of initiation factor 2α by protein kinase GCN2 mediates gene-specific translational control of *GCN4* in yeast. Cell **68:**585–596.
9. **ElAntak, L., S. Wagner, A. Herrmannova, M. Karáskova, E. Rutkai, P. J. Lukavsky, and L. Valášek.** 2010. The indispensable N-terminal half of eIF3j co-operates with its structurally conserved binding partner eIF3b-RRM and eIF1A in stringent AUG selection. J. Mol. Biol. **396:**1097–1116.
10. **Fekete, C. A., S. F. Mitchell, V. A. Cherkasova, D. Applefield, M. A. Algire, D. Maag, A. K. Saini, J. R. Lorsch, and A. G. Hinnebusch.** 2007. N- and C-terminal residues of eIF1A have opposing effects on the fidelity of start codon selection. EMBO J. **26:**1602–1614.
11. **Gietz, R. D., and A. Sugino.** 1988. New yeast-Escherichia coli shuttle vectors constructed with in vitro mutagenized yeast genes lacking six-base pair restriction sites. Gene **74:**527–534.
12. **Grant, C. M., and A. G. Hinnebusch.** 1994. Effect of sequence context at stop codons on efficiency of reinitiation in *GCN4* translational control. Mol. Cell. Biol. **14:**606–618.
13. **Grant, C. M., P. F. Miller, and A. G. Hinnebusch.** 1994. Requirements for intercistronic distance and level of eIF-2 activity in reinitiation on GCN4 mRNA varies with the downstream cistron. Mol. Cell. Biol. **14:**2616–2628.
14. **Grant, C. M., P. F. Miller, and A. G. Hinnebusch.** 1995. Sequences 5′ of the first upstream open reading frame in *GCN4* mRNA are required for efficient translational reinitiation. Nucleic Acids Res. **23:**3980–3988.
15. **Hanachi, P., J. W. B. Hershey, and H. P. Vornlocher.** 1999. Characterization of the p33 subunit of eukaryotic translation initiation factor-3 from *Saccharomyces cerevisiae*. J. Biol. Chem. **274:**8546–8553.
16. **Hannig, E. M., A. M. Cigan, B. A. Freeman, and T. G. Kinzy.** 1992. *GCD11*, a negative regulator of *GCN4* expression, encodes the γ subunit of eIF-2 in *Saccharomyces cerevisiae*. Mol. Cell. Biol. **13:**506–520.
17. **Hinnebusch, A. G.** 2006. eIF3: a versatile scaffold for translation initiation complexes. Trends Biochem. Sci. **31:**553–562.
18. **Hinnebusch, A. G.** 2005. Translational regulation of GCN4 and the general amino acid control of yeast. Annu. Rev. Microbiol. **59:**407–450.
19. **Hinnebusch, A. G., K. Asano, D. S. Olsen, L. O. N. Phan, K. H. Nielsen, and L. Valasek.** 2004. Study of translational control of eukaryotic gene expression using yeast. Ann. N. Y. Acad. Sci. **1038:**60–74.
20. **Hinnebusch, A. G., T. E. Dever, and K. A. Asano.** 2007. Mechanism of translation initiation in the yeast Saccharomyces cerevisiae, p. 225–268. *In* N. Sonenberg, M. Mathews, and J. W. B. Hershey (ed.), Translational control in biology and medicine. Cold Spring Harbor Laboratory Press, Cold Spring Harbor, NY.
21. **Humphrey, T., and T. Enoch.** 1998. Sum1, a highly conserved WD-repeat protein, suppresses S-M checkpoint mutants and inhibits the osmotic stress cell cycle response in fission yeast. Genetics **148:**1731–1742.
22. **Kozak, M.** 2005. Regulation of translation via mRNA structure in prokaryotes and eukaryotes. Gene **361:**13–37.
23. **Lee, J. H., T. V. Pestova, B. S. Shin, C. Cao, S. K. Choi, and T. E. Dever.** 2002. Initiation factor eIF5B catalyzes second GTP-dependent step in eu-

karyotic translation initiation. Proc. Natl. Acad. Sci. U. S. A. **99:**16689–16694.
24. **Maris, C., C. Dominguez, and F. H.-T. Allain.** 2005. The RNA recognition motif, a plastic RNA-binding platform to regulate post-transcriptional gene expression. FEBS J. **272:**2118–2131.
25. **Masutani, M., N. Sonenberg, S. Yokoyama, and I. H.** 2007. Reconstitution reveals the functional core of mammalian eIF3. EMBO J. **26:**3373–3383.
26. **Miller, P. F., and A. G. Hinnebusch.** 1989. Sequences that surround the stop codons of upstream open reading frames in *GCN4* mRNA determine their distinct functions in translational control. Genes Dev. **3:**1217–1225.
27. **Mitchell, S. F., and J. R. Lorsch.** 2008. Should I stay or should I go? Eukaryotic translation initiation factors 1 and 1a control start codon recognition. J. Biol. Chem. **283:**27345–27349.
28. **Mueller, P. P., S. Harashima, and A. G. Hinnebusch.** 1987. A segment of *GCN4* mRNA containing the upstream AUG codons confers translational control upon a heterologous yeast transcript. Proc. Natl. Acad. Sci. U. S. A. **84:**2863–2867.
29. **Mueller, P. P., and A. G. Hinnebusch.** 1986. Multiple upstream AUG codons mediate translational control of *GCN4*. Cell **45:**201–207.
30. **Naranda, T., M. Kainuma, S. E. McMillan, and J. W. B. Hershey.** 1997. The 39-kilodalton subunit of eukaryotic translation initiation factor 3 is essential for the complex's integrity and for cell viability in *Saccharomyces cerevisiae*. Mol. Cell. Biol. **17:**145–153.
31. **Nielsen, K. H., B. Szamecz, L. J. Valasek, A., B. S. Shin, and A. G. Hinnebusch.** 2004. Functions of eIF3 downstream of 48S assembly impact AUG recognition and GCN4 translational control. EMBO J. **23:**1166–1177.
32. **Nielsen, K. H., and L. Valášek.** 2007. In vivo deletion analysis of the architecture of a multi-protein complex of translation initiation factors. Methods Enzymol. **431:**15–32.
33. **Nielsen, K. H., L. Valášek, C. Sykes, A. Jivotovskaya, and A. G. Hinnebusch.** 2006. Interaction of the RNP1 motif in PRT1 with HCR1 promotes 40S binding of eukaryotic initiation factor 3 in yeast. Mol. Cell. Biol. **26:**2984–2998.
34. **Olsen, D. S., E. M. Savner, A. Mathew, F. Zhang, T. Krishnamoorthy, L. Phan, and A. G. Hinnebusch.** 2003. Domains of eIF1A that mediate binding to eIF2, eIF3 and eIF5B and promote ternary complex recruitment *in vivo*. EMBO J. **22:**193–204.
35. **Park, H. S., A. Himmelbach, K. S. Browning, T. Hohn, and L. A. Ryabova.** 2001. A plant viral "reinitiation" factor interacts with the host translational machinery. Cell **106:**723–733.
36. **Passmore, L. A., T. M. Schmeing, D. Maag, D. J. Applefield, M. G. Acker, M. A. Algire, J. R. Lorsch, and V. Ramakrishnan.** 2007. The eukaryotic translation initiation factors eIF1 and eIF1A induce an open conformation of the 40S ribosome. Mol. Cell **26:**41–50.
37. **Pestova, T. V., S. I. Borukhov, and C. U. T. Hellen.** 1998. Eukaryotic ribosomes require initiation factors 1 and 1A to locate initiation codons. Nature **394:**854–859.
38. **Pestova, T. V., and V. G. Kolupaeva.** 2002. The roles of individual eukaryotic translation initiation factors in ribosomal scanning and initiation codon selection. Genes Dev. **16:**2906–2922.
39. **Pestova, T. V., J. R. Lorsch, and C. U. T. Hellen.** 2007. The mechanism of translation initiation in eukaryotes, p. 87–128. *In* N. Sonenberg, M. Mathews, and J. W. B. Hershey (ed.), Translational control in biology and medicine. Cold Spring Harbor Laboratory Press, Cold Spring Harbor, NY.
40. **Phan, L., L. W. Schoenfeld, L. Valášek, K. H. Nielsen, and A. G. Hinnebusch.** 2001. A subcomplex of three eIF3 subunits binds eIF1 and eIF5 and stimulates ribosome binding of mRNA and $tRNA_i^{Met}$. EMBO J. **20:**2954–2965.
41. **Pisarev, A. V., C. U. T. Hellen, and T. V. Pestova.** 2007. Recycling of eukaryotic posttermination ribosomal complexes. Cell **131:**286–299.
42. **Pöyry, T. A., A. Kaminski, E. J. Connell, C. S. Fraser, and R. J. Jackson.** 2007. The mechanism of an exceptional case of reinitiation after translation of a long ORF reveals why such events do not generally occur in mammalian mRNA translation. Genes Dev. **21:**3149–3162.
43. **Pöyry, T. A., A. Kaminski, and R. J. Jackson.** 2004. What determines whether mammalian ribosomes resume scanning after translation of a short upstream open reading frame? Genes Dev. **18:**62–75.
44. **Ruiz-Echevarria, M. J., and S. W. Peltz.** 2000. The RNA binding protein Pub1 modulates the stability of transcripts containing upstream open reading frames. Cell **101:**741–751.
45. **Siridechadilok, B., C. S. Fraser, R. J. Hall, J. A. Doudna, and E. Nogales.** 2005. Structural roles for human translation factor eIF3 in initiation of protein synthesis. Science **310:**1513–1515.
46. **Smith, D. B., and K. S. Johnson.** 1988. Single-step purification of polypeptides expressed in Escherichia coli as fusions with glutathione S-transferase. Gene **67:**31–40.
47. **Spahn, C. M., R. Beckmann, N. Eswar, P. A. Penczek, A. Sali, G. Blobel, and J. Frank.** 2001. Structure of the 80S ribosome from Saccharomyces cerevisiae-tRNA ribosome and subunit-subunit interactions. Cell **107:**373–386.
48. **Srivastava, S., A. Verschoor, and J. Frank.** 1992. Eukaryotic initiation factor 3 does not prevent association through physical blockage of the ribosomal subunit-subunit interface. J. Mol. Biol. **220:**301–304.
49. **Szamecz, B., E. Rutkai, L. Cuchalova, V. Munzarova, A. Herrmannova, K. H. Nielsen, L. Burela, A. G. Hinnebusch, and L. Valášek.** 2008. eIF3a cooperates with sequences 5′ of uORF1 to promote resumption of scanning by post-termination ribosomes for reinitiation on GCN4 mRNA. Genes Dev. **22:**2414–2425.
50. **Taylor, D. J., B. Devkota, A. D. Huang, M. Topf, E. Narayanan, A. Sali, S. C. Harvey, and J. Frank.** 2009. Comprehensive molecular structure of the eukaryotic ribosome. Structure **17:**1591–1604.
51. **Valášek, L., A. Mathew, B. S. Shin, K. H. Nielsen, B. Szamecz, and A. G. Hinnebusch.** 2003. The yeast eIF3 subunits TIF32/a and NIP1/c and eIF5 make critical connections with the 40S ribosome in vivo. Genes Dev. **17:**786–799.
52. **Valášek, L., K. H. Nielsen, and A. G. Hinnebusch.** 2002. Direct eIF2-eIF3 contact in the multifactor complex is important for translation initiation in vivo. EMBO J. **21:**5886–5898.
53. **Valášek, L., K. H. Nielsen, F. Zhang, C. A. Fekete, and A. G. Hinnebusch.** 2004. Interactions of eukaryotic translation initiation factor 3 (eIF3) subunit NIP1/c with eIF1 and eIF5 promote preinitiation complex assembly and regulate start codon selection. Mol. Cell. Biol. **24:**9437–9455.
54. **Valášek, L., L. Phan, L. W. Schoenfeld, V. Valášková, and A. G. Hinnebusch.** 2001. Related eIF3 subunits TIF32 and HCR1 interact with an RNA recognition motif in PRT1 required for eIF3 integrity and ribosome binding. EMBO J. **20:**891–904.
55. **Valášek, L., B. Szamecz, A. G. Hinnebusch, and K. H. Nielsen.** 2007. In vivo stabilization of preinitiation complexes by formaldehyde cross-linking. Methods Enzymol. **429:**163–183.
56. **van der Velden, A. W., and A. A. M. Thomas.** 1999. The role of the 5′ untranslated region of an mRNA in translation regulation during development. Int. J. Biochem. Cell Biol. **31:**87–106.
57. **Verlhac, M.-H., R.-H. Chen, P. Hanachi, J. W. B. Hershey, and R. Derynck.** 1997. Identification of partners of TIF34, a component of the yeast eIF3 complex, required for cell proliferation and translation initiation. EMBO J. **16:**6812–6822.
58. **Vornlocher, H. P., P. Hanachi, S. Ribeiro, and J. W. B. Hershey.** 1999. A 110-kilodalton subunit of translation initiation factor eIF3 and an associated 135-kilodalton protein are encoded by the *Saccharomyces cerevisiae TIF32* and *TIF31* genes. J. Biol. Chem. **274:**16802–16812.
59. **Wells, S. E., P. E. Hillner, R. D. Vale, and A. B. Sachs.** 1998. Circularization of mRNA by eukaryotic translation initiation factors. Mol. Cell **2:**135–140.
60. **Williams, N. P., A. G. Hinnebusch, and T. F. Donahue.** 1989. Mutations in the structural genes for eukaryotic initiation factors 2α and 2β of *Saccharomyces cerevisiae* disrupt translational control of *GCN4* mRNA. Proc. Natl. Acad. Sci. U. S. A. **86:**7515–7519.
61. **Yamamoto, Y., C. R. Singh, A. Marintchev, N. S. Hall, E. M. Hannig, G. Wagner, and K. Asano.** 2005. The eukaryotic initiation factor (eIF) 5 HEAT domain mediates multifactor assembly and scanning with distinct interfaces to eIF1, eIF2, eIF3, and eIF4G. Proc. Natl. Acad. Sci. U. S. A. **102:**16164–16169.
62. **Zhou, M., A. M. Sandercock, C. S. Fraser, G. Ridlova, E. Stephens, M. R. Schenauer, T. Yokoi-Fong, D. Barsky, J. A. Leary, J. W. Hershey, J. A. Doudna, and C. V. Robinson.** 2008. Mass spectrometry reveals modularity and a complete subunit interaction map of the eukaryotic translation factor eIF3. Proc. Natl. Acad. Sci. U. S. A. **105:**18139–18144.

Structural analysis of an eIF3 subcomplex reveals conserved interactions required for a stable and proper translation pre-initiation complex assembly.

Herrmannová A.*, Daujotyte D.*, Yang J.C., Cuchalová L., Gorrec F., Wagner S., Dányi I., Lukavsky P.J., Valášek L.

Nucleic Acids Res. 2012 Mar;40(5):2294-311.

PMID: 22090426

*These authors contributed equally to this work

In this study we reported the first atomic-resolution structure of the interaction between two essential yeast eIF3 subunits. We showed that residues 654-700 of b/PRT1 are sufficient for binding of i/TIF34. We identified two major contacts mediated by conserved residues in blades 5 and 6 of the i/TIF34 beta-propeller. Mutating the residues on both sides of these contacts resulted in severe growth phenotypes. These mutations specifically impaired binding of b/PRT1 and i/TIF34 *in vitro* and eliminated i/TIF34, and surprisingly also g/TIF35, association with eIF3 and 40S subunits *in vivo*. Unexpectedly, 40S-association of other eIF3 subunits and eIF5 was also destabilized, which led to formation of aberrant PIC containing only eIF1 and eIF2. These aberrant PICs could not initiate properly and dramatically increased leaky scanning over the AUG start codon, suggesting that the contacts between mRNA and ribosomal decoding site are impaired. Interestingly, the overexpression of g/TIF35 suppressed leaky scanning and growth defects, most probably by preventing formation of these aberrant PICs. Overexpression of eIF1 also partially suppresses leaky scanning but by a different mechanism.

Nucleic Acids Research, 2011, 1–18
doi:10.1093/nar/gkr765

Structural analysis of an eIF3 subcomplex reveals conserved interactions required for a stable and proper translation pre-initiation complex assembly

Anna Herrmannová[1], Dalia Daujotytė[2], Ji-Chun Yang[2], Lucie Cuchalová[1], Fabrice Gorrec[2], Susan Wagner[1], István Dányi[1], Peter J. Lukavsky[2,*] and Leoš Shivaya Valášek[1,*]

[1]Laboratory of Regulation of Gene Expression, Institute of Microbiology ASCR, v.v.i., Videnska 1083, Prague, 142 20, the Czech Republic and [2]MRC-Laboratory of Molecular Biology, Structural Studies Division, Hills Road, Cambridge, CB2 0QH, UK

Received May 24, 2011; Revised August 31, 2011; Accepted September 1, 2011

ABSTRACT

Translation initiation factor eIF3 acts as the key orchestrator of the canonical initiation pathway in eukaryotes, yet its structure is greatly unexplored. We report the 2.2 Å resolution crystal structure of the complex between the yeast seven-bladed β-propeller eIF3i/TIF34 and a C-terminal α-helix of eIF3b/PRT1, which reveals universally conserved interactions. Mutating these interactions displays severe growth defects and eliminates association of eIF3i/TIF34 and strikingly also eIF3g/TIF35 with eIF3 and 40S subunits *in vivo*. Unexpectedly, 40S-association of the remaining eIF3 subcomplex and eIF5 is likewise destabilized resulting in formation of aberrant pre-initiation complexes (PICs) containing eIF2 and eIF1, which critically compromises scanning arrest on mRNA at its AUG start codon suggesting that the contacts between mRNA and ribosomal decoding site are impaired. Remarkably, overexpression of eIF3g/TIF35 suppresses the leaky scanning and growth defects most probably by preventing these aberrant PICs to form. Leaky scanning is also partially suppressed by eIF1, one of the key regulators of AUG recognition, and its mutant *sui1*^{G107R} but the mechanism differs. We conclude that the C-terminus of eIF3b/PRT1 orchestrates co-operative recruitment of eIF3i/TIF34 and eIF3g/TIF35 to the 40S subunit for a stable and proper assembly of 48S pre-initiation complexes necessary for stringent AUG recognition on mRNAs.

INTRODUCTION

Canonical translation initiation ensures timely and spatially coordinated formation of the trimeric complex between the 40S small ribosomal subunit (40S subunit), initiator Met-tRNA$_i^{Met}$ and an mRNA at its extreme 5′ end, and concludes with the assembly of an elongation-competent 80S ribosome at the authentic AUG start codon. The entire process is orchestrated by numerous eukaryotic initiation factors (eIFs) with eIF3 representing the most intricate factor (1). The multiple essential roles of eIF3 during initiation include stabilization of eIF2/GTP/Met-tRNA$_i^{Met}$ ternary complex (TC) binding to 40S subunits, recruitment of 5′-^{7m}G capped mRNAs to 40S subunits, assistance in scanning of the 5′ untranslated region (5′ UTR) of the mRNA, and finally in aiding AUG initiation codon recognition (2).

This crucial involvement of eIF3 in nearly every step of translation initiation is also reflected in its structural complexity. Mammalian eIF3 consists of at least 13 subunits (eIF3a-m) assembled into a 750 kDa particle. In budding yeast, eIF3 comprises five essential core subunits (a/TIF32, b/PRT1, c/NIP1, i/TIF34, g/TIF35) and one loosely associated, non-essential subunit j/HCR1, all of which have corresponding orthologs in mammals (1).

*To whom correspondence should be addressed. Tel: +42 (0) 241 062 288; Fax: +42 (0) 241 062 665; Email: valasekl@biomed.cas.cz
Correspondence may also be addressed to Peter J. Lukavsky. Tel: +41 (0)44 633 39 40; Fax: +41 (0)44 633 12 94; Email: lpeter@mol.biol.ethz.ch
Present addresses:
Peter J. Lukavsky, Institute of Molecular Biology and Biophysics, ETH Hönggerberg, Schafmattstrasse 20, Zürich, Switzerland.
Dalia Daujotyte, Lexogen GmbH, Campus Vienna Biocenter 5, 1030 Vienna, Austria.

The authors wish it to be known that, in their opinion, the first two authors should be regarded as joint First Authors.

At least in yeast, this core eIF3 complex associates with eIFs 1, 5 and the TC *in vivo* to form the so-called multifactor complex (MFC). Surprisingly, detailed biochemical analysis carried out with purified eIF3 subcomplexes identified that the trimeric complex of a/TIF32, b/PRT1 and c/NIP1 promoted TC and mRNA recruitment to the 40S subunit and even stimulated translation *in vitro* on a model mRNA as efficiently as the wild-type (wt) five subunit complex (3). Hence given the fact that i/TIF34 and g/TIF35 subunits are otherwise essential for cell proliferation and their individual depletions result in a typical polysome run-off (4), these results perhaps indicate that their contributions to general translation initiation have a more stimulatory character. Indeed, we have recently shown that both small eIF3 subunits augment various aspects of linear scanning and, as such, may have differential effects on efficiency of translation of coding mRNAs containing short, less structured versus long, highly structured 5′ UTRs (5). Interestingly, *in vitro* reconstitution of human eIF3 also supported the dispensability of highly conserved eIF3g and eIF3i in stimulation of canonical eIF3 functions. Instead, non-conserved eIF3e, eIF3f and eIF3h in complex with eIF3a, eIF3b, and eIF3c were proposed to be the functionally indispensable subunits of mammalian eIF3 (6). In contrast, however, two other groups reported purification of a human eIF3 subcomplex closely resembling the yeast core eIF3 complex (7,8). Hence more experiments are required to clarify these discrepancies.

The structural complexity of eIF3 is well illustrated by its elaborate subunit–subunit interaction web, which has been mapped in great detail for yeast eIF3 and its associated eIFs (9). The b/PRT1 subunit serves as the major scaffolding subunit of eIF3 and associates with the other core subunits in both yeast and mammals (7–10). The b/PRT1 N-terminal domain (NTD) contains a conserved RNA recognition motif (RRM) (11,12), which provides an interaction surface for the C-terminal half of a/TIF32 and the NTD of j/HCR1 (12,13), followed by a middle domain predicted to fold into two β-propeller structures (14), the second of which contains a binding site for c/NIP1. Finally, the extreme C-terminal domain (CTD) of the b/PRT1 scaffold is required for association of i/TIF34 and g/TIF35 subunits (10). Whereas i/TIF34 is predicted to adopt a seven-bladed β-propeller structure made up of seven WD-40 repeats with unknown binding sites for b/PRT1 and g/TIF35, the latter subunit interacts with i/TIF34 and b/PRT1 through its NTD containing a predicted Zn-finger domain (10). The g/TIF35-CTD then adopts an RRM fold that is not involved in any subunit–subunit interactions (9,10). Better understanding of all functions of individual interactions among eIF3 subunits clearly requires more detailed information at the molecular level; however, no atomic structures of any yeast eIF3 subunits have been determined to date.

Here we report the 2.2 Å resolution crystal structure of the i/TIF34 subunit in complex with the minimal CTD of b/PRT1 (654–700), the boundaries of which we defined by solution NMR spectroscopy. Mutating the conserved residues mediating the b/PRT1—i/TIF34 contact results in lethality or severe growth phenotypes owing to the loss of the i/TIF34-g/TIF35 mini-module from the rest of eIF3 and from pre-initiation complexes (PICs). Since binding of the remaining a/TIF32-b/PRT1-c/NIP1 subcomplex and eIF5 is also unexpectedly destabilized, aberrant PICs containing eIFs 2 and 1 accumulate and dramatically increase leaky scanning over the AUG start codon in the manner suppressible by overexpression of g/TIF35 and eIF1. Hence we propose that stable association of the i/TIF34–g/TIF35 mini-module with the rest of eIF3 *via* b/PRT1 significantly stabilizes binding of eIF3 and eIF5 to the nascent pre-initiation complexes *in vivo*. This way these critical interactions serve to prevent accumulation of mis-assembled PICs on mRNAs and thus ensure stringent selection of the AUG start codon.

MATERIALS AND METHODS

Protein expression and purification

DNA fragments encoding yeast i/TIF34 and b/PRT1(630–724) were prepared by PCR from pGEX–TIF34 or pGEX–PRT1, respectively (10), using appropriate primers and subcloned into pET28a vector (Novagen) with a Tobacco Etch Virus (TEV) protease cleavage site instead of the original thrombin cleavage site. A DNA fragment encoding b/PRT1(654–700) was prepared by PCR from b/PRT1(630–724) plasmid DNA and subcloned into a modified pET28a vector (Novagen, containing an N-terminal His_6-tag fused to a lipoyl domain (12,15) followed by a TEV cleavage site and the standard pET28a multiple cloning site). Point mutations in b/PRT1(630–724) were introduced following the QuickChange protocol (Stratagene). Proteins were expressed in *Escherichia coli* Rosetta(DE3) cells (Novagen) in LB rich or M9 minimal media supplemented with $^{15}NH_4Cl$ or $^{15}NH_4Cl$ and ^{13}C-glucose. Protein expression was induced by addition of 1 mM IPTG at OD_{600} of ~0.8 and further incubation for 14 h at 16° C. All proteins were purified using two 5 mL HiTrap chelating columns (HiTrap, GE Healthcare) in series and charged with nickel sulfate under standard conditions (lysis and loading buffer A: 20 mM HEPES pH 7.5, 500 mM NaCl, 30 mM imidazole, 10% glycerol (w/v), 5 mM 2-mercaptoethanol; elution buffer B: same as buffer A with 300 mM imidazole). For b/PRT1 peptides this was followed by TEV protease cleavage for His_6-tag or His_6-tag lipoyl fusion removal (dialysis buffer for TEV cleavage at room temperature: 20 mM HEPES pH 7.5, 150 mM NaCl, 10% glycerol, 5 mM 2-mercaptoethanol), while i/TIF34 was left uncleaved. TEV cleavage reaction mixtures were then reloaded onto HiTrap chelating columns to remove the His_6-TEV protease, the His_6-tag or His_6-tag lipoyl fusion as well as minor contaminating proteins using buffers A and B (see above). After purification, the proteins were dialyzed 3 times against 2 L storage/NMR buffer (50 mM sodium phosphate buffer pH 7.5, 150 mM NaCl, 5 mM 2-mercaptoethanol).

Purified His_6–i/TIF34 and b/PRT1 proteins were assembled into complexes at a 1:1.2 molar ratio, concentrated using Vivaspin 20 mL centrifugal devices

with 10 000 MWCO (Sartorius) and passed over a Sephacryl S-200 gel filtration column (GE Healthcare) using storage/NMR buffer as running buffer. Fractions corresponding to the 1:1 complex were pooled, concentrated to 7–10 mg/ml and either used directly for NMR experiments or dialyzed against 2 times 2 L crystallization buffer (20 mM HEPES pH 7.5, 150 mM NaCl, 5 mM 2-mercaptoethanol) using Slide-A-Lyzer 0.5 mL dialysis cassettes with 10 000 MWCO (Thermo Scientific).

NMR spectroscopy

NMR experiments were performed on Bruker DMX600 or AVANCE800 spectrometers equipped with cryoprobes. Partial protein backbone assignments of $^{13}C/^{15}N$-labeled b/PRT1(630–724) in complex with unlabeled His_6–i/TIF34 were achieved by means of through-bond heteronuclear scalar correlations with standard pulse sequences from the Bruker pulse sequence library. Chemical shift patterns upon binding of ^{15}N-labeled b/PRT1(630–724) or b/PRT1(654–700) to His_6–i/TIF34 were compared using standard ^{15}N-HSQC and ^{15}N-TROSY pulse sequences. All NMR samples were prepared in NMR buffer (see above) with addition of 10% D_2O (v/v) at protein concentrations of 100–200 μM. All spectra were recorded at 20° C.

Defining the minimal i/TIF34-binding domain of b/PRT1 by NMR spectroscopy

Residues 641–724 of b/PRT1 were previously shown to be required for i/TIF34-binding *in vitro* (9,10). Crystallization of proteins and their complexes is often hindered by flexible, unstructured tails and this prompted us to further define the precise boundaries of the interaction site by NMR spectroscopy (16,17). To achieve this, we expressed unlabeled i/TIF34 and a $^{13}C,^{15}N$-labeled C-terminal fragment of b/PRT1 spanning residues 630–724 and recorded ^{15}N-HSQC spectra of the peptide both in the free and i/TIF34-bound form. The spectrum of the free 10 kDa peptide displays severe resonance overlap in the amide region and mainly random coil chemical shifts indicative of no intrinsic secondary structure as also confirmed by CD spectroscopy (data not shown and Supplementary Figure S1A). Upon binding of i/TIF34 to the b/PRT1 peptide, a 50 kDa complex is formed with much slower tumbling times of the bound peptide in solution resulting in shorter transverse relaxation times and concomitant broadening of amide signals from b/PRT1 residues participating in the interaction with i/TIF34. On the other hand, a significant portion of the sharper random coil crosspeaks of b/PRT1 remains unchanged indicating that they are not part of the i/TIF34 binding interface. For several of these random coil resonances much longer transverse relaxation times allowed us to obtain backbone assignments using standard triple resonance experiments. We unambiguously assigned a four amino acid stretch spanning residues Q651-M654 from the N-terminus as well as the entire extreme C-terminus starting at residue A701 of b/PRT1, while the middle segment spanning residues 655–700 could not be assigned due to short transverse relaxation times from an interaction with i/TIF34. We therefore designed and expressed a ^{15}N-labeled peptide comprising residues 654–700 of the C-terminus of b/PRT1. This shorter peptide displays the same broad, shifted resonances when bound to i/TIF34 as the longer ^{15}N-labeled peptide comprising residues 630–724, including a downfield shifted Trp-NεH crosspeak of W674, but lacks the sharp random coil Trp-NεH crosspeak (W644) from the N-terminal half of the longer peptide (Supplementary Figure S1B). This unambiguously defines that the minimum i/TIF34 binding site of b/PRT1 comprises residues 654–700. This conclusion is also confirmed by isothermal titration calorimetry (ITC), which displays very similar affinities for the long b/PRT1(630–724) and the minimal C-terminal peptide of b/PRT1(654–700) with K_D-values of 81 nM and 160 nM, respectively (Supplementary Figure S1C). Thus optimized complex of yeast full-length i/TIF34 and the 654–700 fragment of b/PRT1, lacking b/PRT1 random coil segments, was subjected to crystallization and after optimization yielded well diffracting crystals suitable for structure determination of the complex.

Crystallization

Crystallization screening by sitting drop vapor diffusion was performed with 200 nl drops (1:1 ratio of protein solution to mother liquor) against 1600 commercial conditions at room temperature. Crystals were obtained in 0.1 M Tris–HCl pH 8.8, 0.1 M Li_2SO_4, 28% PEG 4000, 2–8% 1,5-diAminoPentane dihydrochloride. Heavy atom derivatives were obtained by soaking crystals in saturated solutions of K_2PtCl_4 (potassium tetrachloroplatinate (II) and $C_2H_5HgSC_6H_4CO_2Na$ (sodium ethyl-mercurithiosalicylate, thiomersal) for 2–5 min.

Diffraction data collection and structure determination

Native diffraction dataset was collected from a single crystal at 100K at the Diamond synchrotron facility (UK) on beamline I03. Data of heavy atom derivatives were collected using a MAR-DTB image-plate detector and rotating anode X-ray generator. The data were indexed with MOSFLM (18) and further processed using SCALA (19) and TRUNCATE (20) from CCP4 package (21). Experimental phases were obtained by MIR, combining Pt and Hg derivatives, scaling them to the native dataset and further processing with SHARP (22). Although the phase information from the Pt derivative was weak beyond (and at) 3.8 Å resolution, adding it significantly improved the experimental map. PHYRE server (23) homology modeling solution of i/TIF34 was used as a search model in Phaser (24) to find second molecule in the asymmetric unit. Map was improved with solvent flattening in Parrot (25). Major part of the model was built with Buccaneer (26), with remaining parts hand-built using Coot (27). Iterative rounds of model building in Coot, refinement with Refmac (28) and validation using MolProbity server (29) were ultimately performed without non-crystallographic symmetry (NCS). Initially, NCS was applied during the first rounds of

refinement but no significant improvement was observed. Therefore we decided not to use NCS in the refinement, especially since one part of the protein (the flexible loop) was different between the two molecules. The final structure consists of four protein chains: B and D—i/TIF34, E and F—b/PRT1(654–700). Chains B and D have TEV protease cleavage site, and therefore start at the residue Glu-9 leaving methionine as the first amino acid. Chain B contains residues −9 to 259 and 273 to 342, chain D −9 to 342, chains E and F 661 to 699. Data collection and refinement statistics are summarized in Supplementary Table S1.

Yeast strains, plasmids, and biochemical methods

Lists of strains and plasmids used in this study (Supplementary Tables S3–S5), details of their construction, as well as description of all well-established biochemical assays used throughout the study can be found in the Supplementary Data.

RESULTS

The overall crystal structure of i/TIF34–b/PRT1(654–700) complex

Using solution NMR spectroscopy, we defined the minimal C-terminal i/TIF34-binding site of b/PRT1(654–700) lacking any b/PRT1 random coil segments, which could hinder crystallization (16,17) (Figure 1A, Supplementary Figures S1 and S2A, 'Material and Methods' section). The crystallographic structure of thus optimized yeast i/TIF34–b/PRT1(654–700) complex was determined at 2.2 Å resolution by MIR heavy atom phasing (data statistics in Supplementary Table S1). Two complexes were found in the asymmetric unit and both of them displayed excellent electron density (Supplementary Figures S3 and S4) except for a few terminal residues of both the b/PRT1 and i/TIF34 molecules and a specific loop region spanning well-conserved residues 260–272 in one of the two i/TIF34 molecules (discussed in more detail later).

The i/TIF34 subunit adopts a seven-bladed β-propeller fold with a short, bent α-helix at the C-terminus (Figure 1B). As commonly seen in β-propeller structures (30), one β-sheet of the last blade 7 is formed by N-terminal residues 1–7, while the subsequent amino acid residues consecutively form blades 1–7 (Figure 1C). Phylogenetic analysis shows that the most conserved residues comprise blades 1, 2, 6 and 7 (Figure 1D and Supplementary Figure S2A) and that several loops between the blades also include highly conserved residues. The β-propeller structure usually serves as a platform for protein–protein interactions (31). Interacting protein partners often bind to the top or bottom of the β-propeller structure, but binding along the groove between blades has also been observed (32–34). The b/PRT1(654–700) fragment binds to the bottom side of the β-propeller along the loops of blades 5 and 6 of i/TIF34 (Figure 1B). The b/PRT1 residues 663 to 689 form a long α-helix while the extended C-terminus (residues 690–699) advances towards the central cavity of the i/TIF34 β-propeller and is held mostly by contacts *via* main chain atoms (Figure 1B). These interactions are independent of the contacts between the two complexes within the asymmetric unit (Supplementary Figures S3 and S4).

The b/PRT1-binding interface of i/TIF34 comprises residues from β-sheets and loops in blades 5 and 6 (Figure 1B). The total buried surface area of the b/PRT1–i/TIF34 interface is 1028.7 $Å^2$ and 1054.6 $Å^2$ (complex I and complex II, respectively, in Supplementary Figure S4) as calculated using PISA (35). The b/PRT1-interacting surface of i/TIF34 bears a few important charged regions (Figure 2A; left). The remaining surface of this side of the β-propeller shows dominantly negative charge, while patches of positive charge dominate around the central cavity on the top side of the β-propeller (formed by blades 2–5, Figure 2A; right). This charge distribution is conserved suggesting distinct interfaces for the interactions with other components of the translational machinery (Figures 1D, 2A and Supplementary Figure S2A).

Seven residues of the b/PRT1(654–700) fragment are in close proximity (<3.5 Å apart) for direct contact with eight residues of i/TIF34. In both proteins, the interacting residues involve highly conserved amino acids (Figure 1D and Supplementary Figure S2A; and also listed in Supplementary Table S2). At the b/PRT1–i/TIF34 interface hydrogen bonds are formed between the most conserved residues Y677-D224 and R678-D207/T209 (Figure 2B and Supplementary Figure S2B), implying that these residues are crucial for b/PRT1–i/TIF34 complex formation. The second important feature of the complex interface is the insertion of the aromatic ring of b/PRT1 W674 into a pocket of i/TIF34 formed by hydrophobic amino acids (L231 and I281 as well as the conserved L222) and the side chains of polar amino acids (Y210 and K280 as well as the conserved K232 and E250) (Figure 2C, D and Supplementary Figure S2B). The nearest i/TIF34 residues are within 3.8–4.8 Å of W674. W674 probably makes a π–cation interaction with K280 (36) and additional hydrophobic interactions with the other 'pocket' residues (Figure 2D). Phylogenetic investigation shows that in other organisms including human, frog and *Drosophila*, Phe or Tyr is found instead of Trp and K280 replaced by either Leu or Val, implying conservation of the hydrophobic nature of this interaction (Supplementary Figure S2A). In addition to the specific side chain contacts along the α-helix of b/PRT1, there is a series of interactions between main chain atoms of the extended C-terminal part of b/PRT1 starting with N690 and i/TIF34 residues in blades 5 and 6 (Supplementary Table S2). Interestingly, none of the i/TIF34 residues directly interacting with b/PRT1 appeared in previous mutational studies by Asano and co-workers (10). For direct comparison see Supplementary Figure S5 and the corresponding text.

The major difference between the two i/TIF34–b/PRT1(654–700) complexes in the asymmetric unit lies within the loop made of residues 260–272 in blade 6 of i/TIF34 on the opposite side of the b/PRT1 binding interface. One of the complexes has well-defined electron

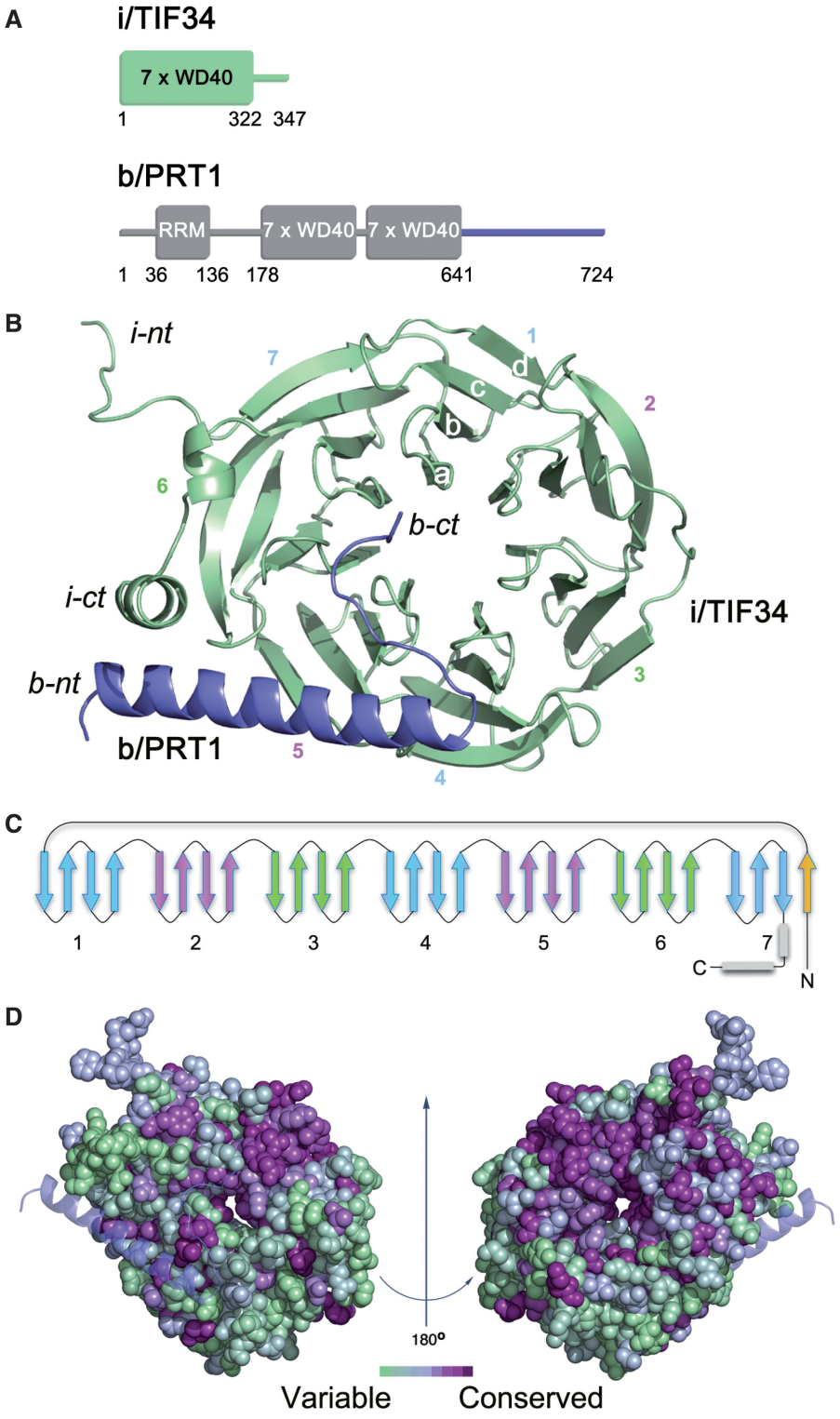

Figure 1. Structure of i/TIF34–b/PRT1 complex. (**A**) Schematic drawing of the predicted protein domains of yeast i/TIF34 (top) and b/PRT1 subunits of eIF3 (bottom). The folded domains and their boundaries are indicated. Predicted unstructured regions are shown as lines. (**B**) Overview of the structure: cartoon representation of i/TIF34 (green) and b/PRT1(654–700) (blue). WD-40 blades 1–7, β-strands a–d of blade 1 and N-terminus (nt) and C-terminus (ct) are labeled. The complex is shown from the bottom side of the β-propeller, where loops occur between strands a–b and c–d. (**C**) Topology diagram of the i/TIF34 fold. (**D**) Space-filling view of the i/TIF34 in complex with b/PRT1 (bottom view, left and top view, right), colored according to sequence conservation. A gradient of green to purple indicates the degree of phylogenetic conservation, with variable shown as green and most conserved as dark purple. The conservation heat plot of the i/TIF34 surface was generated by ConSurf using multiple alignment of Human, *Drosophila*, *Arabidopsis* and *Saccharomyces cerevisiae* i/TIF34 protein homologues. All structural figures were generated using PyMOL (http://www.pymol.org).

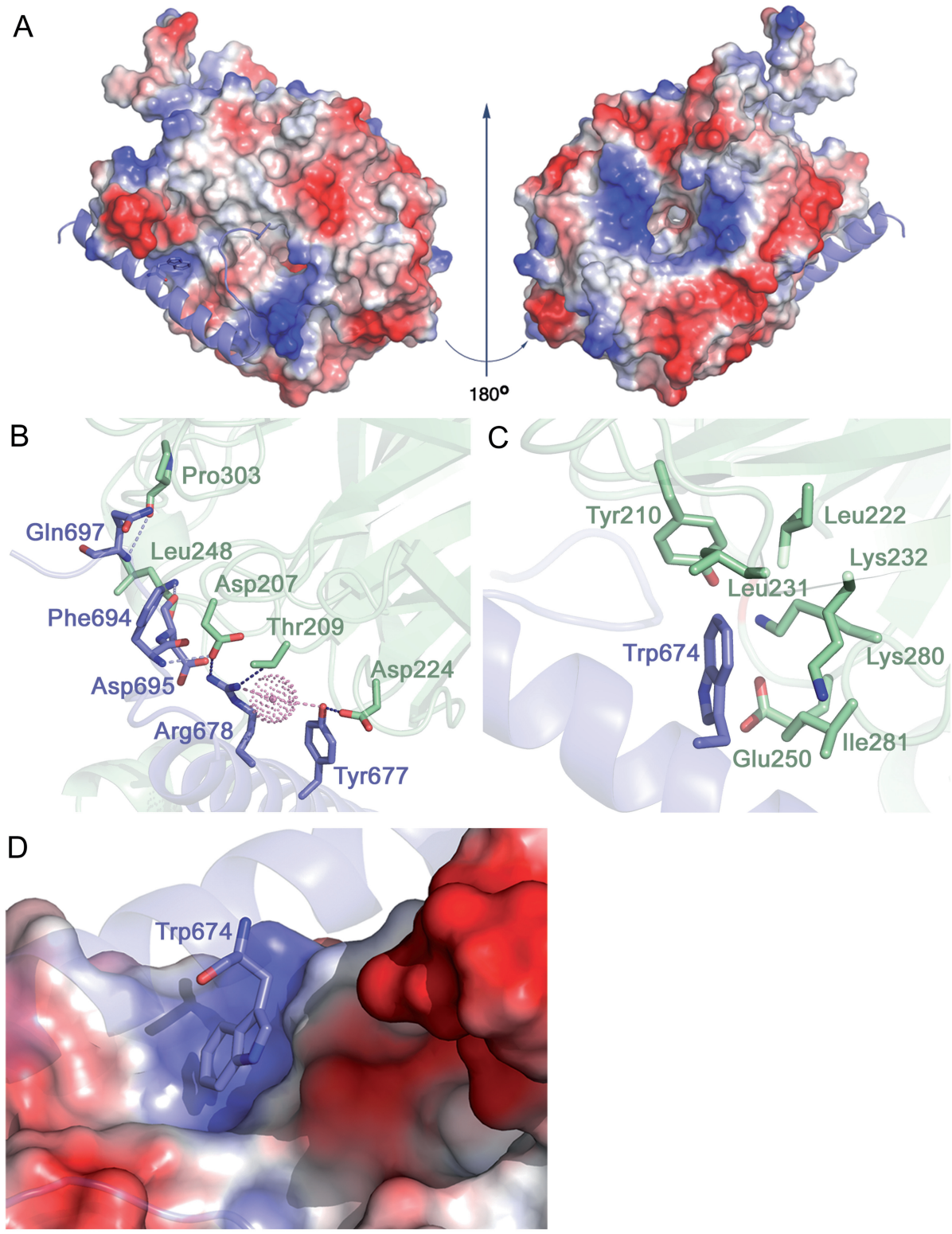

Figure 2. Molecular details of i/TIF34 and b/PRT1 interactions. (**A**) Electrostatic potential (±5kT/e) of the solvent-accessible surface of i/TIF34 in complex with b/PRT1(654–700) rendered on the molecular surface of the complex. A gradient of blue to red shows positive to negative charge, respectively, as calculated using PyMOL built-in APBS tools (55). PQR file for analysis of Poisson–Boltzmann electrostatics calculations was generated using PDB2PQR tool (56) and further used for APBS. b/PRT1(654–700) is shown as a cartoon in blue. View from the b/PRT1 binding site is shown on the left; the 'reverse' side of i/TIF34 shown on the right has negative charge clustering at the highly conserved blade 1 (upper part), blades 4 and 5 (the bottom part) and positive charge around the central cavity. (**B–C**) The i/TIF34-b/PRT1 binding interface involves highly conserved amino acids from both proteins. i/TIF34 is shown in green, b/PRT1 in blue. (**B**) Y677 and R678 from b/PRT1 form H-bonds (blue) with D207, T209 and D224 from i/TIF34 (only interacting side chains are shown). Other residues making contacts (light blue) via main chain atoms are also shown in sticks. One water molecule (shown in dots) is in close proximity (light pink) to R678 NH1 (2.6 Å) and Y677 OH (3.3 Å). (**C**) b/PRT1 W674 is surrounded by hydrophobic and charged amino acids (only side chains are shown), which form a shallow pocket. (**D**) Surface representation of the i/TIF34 hydrophobic pocket, which accommodates b/PRT1 W674. This interaction serves as a 'lock' for the i/TIF34 and b/PRT1 interaction interface.

density surrounding these residues (complex II in Supplementary Figure S6A), whereas the other molecule lacks defined electron density around this area (position of the residues omitted from the PDB file are indicated by the red arrow in Supplementary Figure S6A). The well-defined loop in complex II contacts another symmetry-related i/TIF34 molecule (residues 80–87 and 130–139; not shown) and forms a salt bridge between E270 and K91 in the same chain of the symmetry-related complex fixing the loop in a detectable state. The flexible loop residues are predominantly negatively charged (Supplementary Figure S6B) and residues 260–279 display high sequence conservation from yeast to human (Supplementary Figure S2A) suggesting an important interaction module with either the 40S subunits or other partners within the eIF3 complex.

Disrupting the conserved b/PRT1–i/TIF34 interaction results in lethality or severe growth phenotypes

To confirm the critical aspects of the b/PRT1–i/TIF34 contacts revealed by the structure analysis and to investigate the functional consequences of their loss in living cells, we first substituted Y677 and R678 (alone or in combination), or W674 of b/PRT1 with Ala, Asp or Phe residues, respectively, and tested them for growth phenotypes. The corresponding mutations were generated in a plasmid copy of *PRT1-His*, encoding His_8-tagged b/PRT1, and introduced into a *prt1Δ* strain harboring wt *PRT1* on a *URA3* plasmid, which was subsequently evicted by counter-selection on medium containing 5-fluoroorotic acid (5-FOA). Whereas the double *Y677A R678D* mutation is lethal and the *Y677A R678A* (dubbed *YR/AA* herein) double mutant imparts a very severe slow growth (Slg–) phenotype, individual *Y677A* and *R678A* substitutions show little to no effect on growth rates (Figure 3A). Severe Slg^- and temperature sensitive (Ts^-) phenotypes are also found associated with the *W674A* mutation. Strikingly, the 'phylogenetic correction' substitution in *W674F* (see above) displays wt-like behavior under all tested conditions (Figure 3A; summarized in 3C). Importantly, *in vitro* electrophoretic mobility shift assays performed with recombinant purified i/TIF34 and b/PRT1-CTD(630–724) variants confirm these *in vivo* results: b/prt1-W674F mutant protein competes well with wt b/PRT1-CTD for i/TIF34 binding, whereas b/prt1-W674A and the YR/AA double mutant are not able to compete for i/TIF34 binding at all (Supplementary Figure S7). These results confirm that an aromatic side chain (Phe or Trp) is required to fill the hydrophobic pocket on i/TIF34 and indicate that the contacts of Y677 and R678 with D207 and D224, respectively, are redundant (see more biochemical evidence further below).

In a similar fashion, specific substitutions of D207 and D224 (alone or in combination), or L222 of i/TIF34, generated in a plasmid copy of *TIF34-HA* encoding HA-tagged i/TIF34, were tested for growth defects in a *tif34Δ* strain. In agreement with the aforementioned results, individual *D207K* and *D224K* substitutions produce no effects; however, the combined *D207K D224K* (dubbed *DD/KK* herein) mutant displays a severe Ts^- phenotype (Figure 3B). Finally, both charge substitutions of L222 in *L222D* or *L222K*, which probably drastically disturb the L222-containing hydrophobic pocket or perhaps even the entire local structure around blades 5 and 6 (Figure 2C and D), also impart severe Ts^- and Slg^- phenotypes (Figure 3B; summarized in 3C).

Impairment of the contact between b/PRT1 and i/TIF34 eliminates association of i/TIF34 and g/TIF35 from the rest of eIF3 *in vivo*

To further test whether the mutations under study impair a direct contact between b/PRT1 and i/TIF34 proteins we introduced three single-Ala-substitution mutations into full length b/PRT1, synthesized and radiolabeled the resulting mutant proteins *in vitro* and tested their binding affinities towards i/TIF34 and g/TIF35 fused with the GST moiety. As shown in Figure 4A, all three completely eliminate binding of b/PRT1 specifically to i/TIF34 but not to g/TIF35. Similarly, both single D/K substitutions and the *DD/KK* double mutation of i/TIF34, the latter of which was chosen for further analysis, abolished binding of [^{35}S]-labeled i/TIF34 to GST-b/PRT1 but not to GST-g/TIF35 (Figure 4B and data not shown).

Next we wished to demonstrate the effect of our mutations on the association of i/TIF34 with the rest of eIF3 *in vivo*. Towards this end we analyzed formation of the entire eIF3-containing MFC (see our model in Figure 4C) in yeast cells by Ni^{2+}-chelation chromatography using His_8-tagged *PRT1* as bait. As reported previously (13), a fraction of a/TIF32, j/HCR1, eIF2, eIF5 and eIF1 co-purified specifically with wt b/PRT1-His but not with its untagged version (Figure 5A, lanes 4–6 versus 1–3). The *prt1-W674A* mutation of one of the two contacts between i/TIF34 and b/PRT1 severely diminishes (by >90%) association of i/TIF34, and in contrast to the above *in vitro* experiments, also that of g/TIF35 with the MFC, whereas *prt1-W674F* shows no effects (Figures 5A and B, lanes 7–9 versus 10–12). This concurs well with our genetic data (Figure 3A). In addition, the overall integrity of the MFC also seems to be modestly affected. Similarly, the *tif34-DD/KK* mutation of the other contact also severely reduces binding of i/TIF34 and g/TIF35 to the purified b/PRT1-His complex (Figures 5C and D, lanes 9–12 versus 5–8). Importantly, overexpressing His_8-tagged *TIF35* as bait in the background of *tif34-DD/KK* further supported these novel observations as g/TIF35-His practically failed to pull down any of the MFC components with the exception of i/TIF34 (Supplementary Figure S8A). The fact that the *DD/KK* mutation does not affect the mutual interaction between i/TIF34 and g/TIF35 *in vivo* is in perfect agreement with our *in vitro* binding data (Figure 4B). Together these results strongly suggest that binding of i/TIF34 with b/PRT1, in addition to the direct g/TIF35–b/PRT1 interaction, is a necessary prerequisite for stable eIF3-association of g/TIF35 *in vivo* indicating that the observed growth phenotypes are a direct consequence of the loss of the essential i/TIF34–g/TIF35 mini-module from the rest of eIF3. Hence the fact that the individual

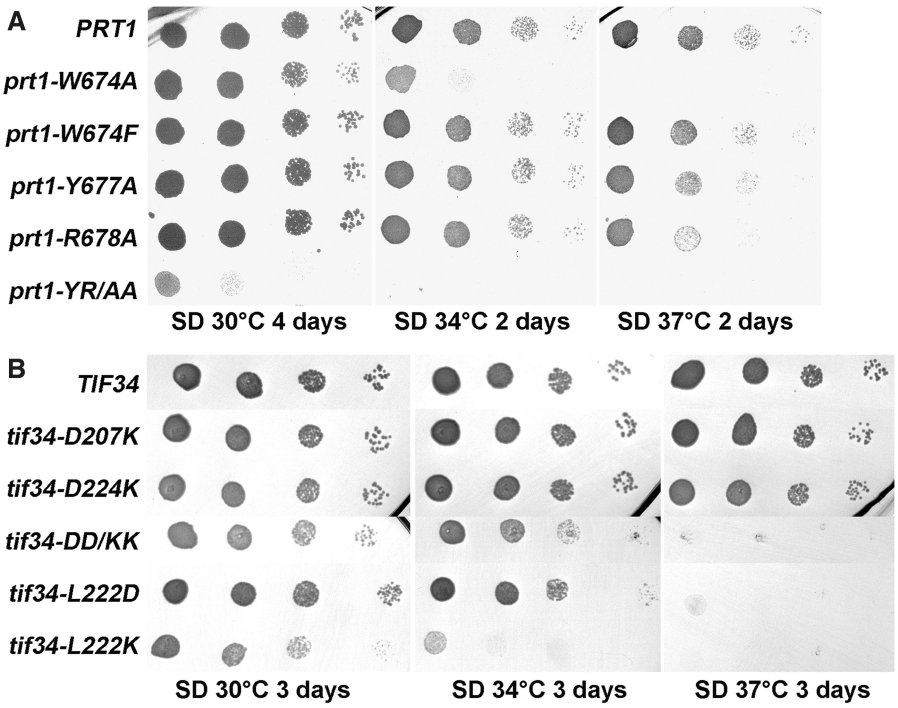

C

PRT1 mutations	30°C	34°C	37°C
W674A	WT	Slg$^-$	severe Ts$^-$
W674F	WT	WT	WT
Y677A	WT	WT	WT
R678A	WT	WT	mild Slg$^-$
Y677A R678A	severe Slg$^-$	severe Ts$^-$	severe Ts$^-$
Y677A R678D		lethal	
***TIF34* mutations**			
D207K	WT	WT	mild Slg$^-$
D224K	WT	WT	WT
D207K D224K	WT	Slg$^-$	severe Ts$^-$
L222D	WT	Slg$^-$	severe Ts$^-$
L222K	Slg$^-$	severe Slg$^-$	severe Ts$^-$

Figure 3. Phenotypic and biochemical analysis of i/TIF34 and b/PRT1 mutations that disrupt subunit interactions. (**A**) The *prt1-W674A* and *-YR/AA* but not *-W674F* mutations produce severe slow growth and temperature sensitive phenotypes. The YAH06 (*prt1Δ*) strain was transformed with the corresponding plasmids carrying individual mutant alleles and the resident pCR52 (*PRT1,URA3*) covering plasmid was evicted on 5-FOA. The resulting strains were then spotted in four serial 10-fold dilutions on SD medium and incubated at 30, 34 and 37°C. (**B**) The *tif34-DD/KK, -L222D* and *L222K* mutations produce severe slow growth and temperature sensitive phenotypes. The H450 (*tif34Δ*) strain was transformed with the corresponding plasmids carrying individual mutant alleles and the resident YEp-i/TIF34-U (*TIF34, URA3*) covering plasmid was evicted on 5-FOA. The resulting strains were then spotted in four serial 10-fold dilutions on SD medium and incubated at 30, 34 and 37°C. (**C**) Summary of phenotypes of mutations analyzed in this study.

prt1-Y677A, *prt1-R678A*, *tif34-D207K* and *tif34-D224K* mutations diminish the b/PRT1–i/TIF34 interaction *in vitro* (Figure 4) yet produce no significant growth phenotypes (Figure 3) can be explained by proposing that their impact *in vivo* is largely overcome by a stabilization effect of simultaneous binding of g/TIF35 to i/TIF34 and b/PRT1 in the context of the entire eIF3 complex, as was observed (Supplementary Figure S8B and C). In other words, their aforementioned redundancy is dependent on the presence of g/TIF35 *in vivo*. Indeed, this effect is not powerful enough in the case of more deleterious double mutations. Since we had confirmation that genetic and molecular defects of both *prt1-W674A* and *tif34-DD/KK* mutations have the same nature, we decided to focus our further analysis on the latter.

Disruption of the b/PRT1–i/TIF34 interaction prevents 40S-binding of the i/TIF34–g/TIF35 mini-module and selectively affects stability of pre-initiation complexes *in vivo*

We showed previously that a partial eIF3 subcomplex containing a/TIF32 and c/NIP1, and eIF5, but lacking

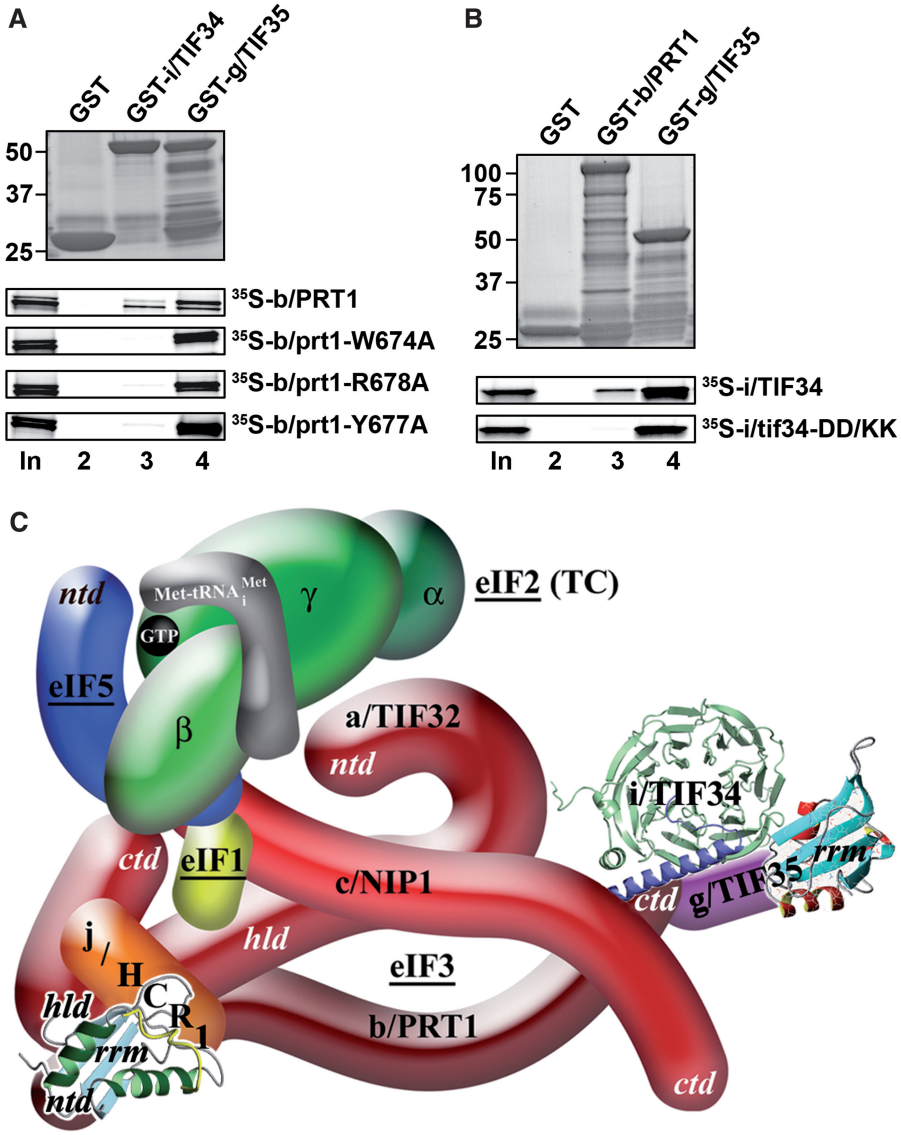

Figure 4. The *tif34-DD/KK* mutation impairs the direct interaction between i/TIF34 and b/PRT1 *in vitro* and the revised 3D model of eIF3 in the MFC. (**A**) The *prt1-W674A*, *-Y677A*, and *-R678A* mutations impair the direct interaction between b/PRT1 and i/TIF34 *in vitro*. Full-length i/TIF34 (lane 3) and g/TIF35 (lane 4) fused to GST, and GST alone (lane 2), were tested for binding to ^{35}S-labeled wt b/PRT1 and its mutant derivatives; 10% of input amounts added to each reaction is shown in lane 1 (In). (**B**) Full-length b/PRT1 (lane 3) and g/TIF35 (lane 4) fused to GST, and GST alone (lane 2), were tested for binding to ^{35}S-labeled wt i/TIF34 and the *DD/KK* mutant derivative. (**C**) A revised 3D model of eIF3 and its associated eIFs in the MFC (based on the data from (9); *ntd*, N-terminal domain; *ctd*, C-terminal domain; *hld*, HCR1-like domain; *rrm*, RNA recognition motif; TC, ternary complex). The NMR structure of the interaction between the RRM of human eIF3b (green and light blue) and the N-terminal peptide of human eIF3j (yellow) (12), the NMR structure of the C-terminal RRM of human eIF3g (red and sky-blue) (5), and the X-ray structure of the yeast i/TIF34–b/PRT1 complex (this study), were used to replace the original schematic representations of the corresponding molecules.

the b/PRT1, i/TIF34 and g/TIF35 subunits, still interacted with the 40S ribosomes *in vivo* (albeit with ~2-fold reduced affinity compared to wt 5-subunit eIF3), whereas the b/PRT1–i/TIF34–g/TIF35 subcomplex lacking the N-terminal RRM of b/PRT1 did not (13,37). Hence given that mutating the contact residues between b/PRT1 and i/TIF34 strongly impairs association of i/TIF34 and g/TIF35 with eIF3 in the MFC (Figure 5), it could be consequently expected that the ribosome occupancy of only i/TIF34 and g/TIF35 gets impaired. To examine this, we measured binding of selected eIF3 subunits and other MFC components to 40S subunits by formaldehyde cross-linking followed by high velocity sedimentation in sucrose gradients, as this method provides the best available approximation of the native composition of 43S/48S pre-initiation complexes *in vivo* (38). In accord with our prediction, we observed a relative ~90% decrease in the amounts of i/TIF34 and g/TIF35 associated with 40S subunits in whole-cell extracts (WCEs) obtained from the *tif34-DD/KK* cells grown at the semipermissive temperature (Figure 6A, '43–48S' lanes). Surprisingly, rather significant reductions in

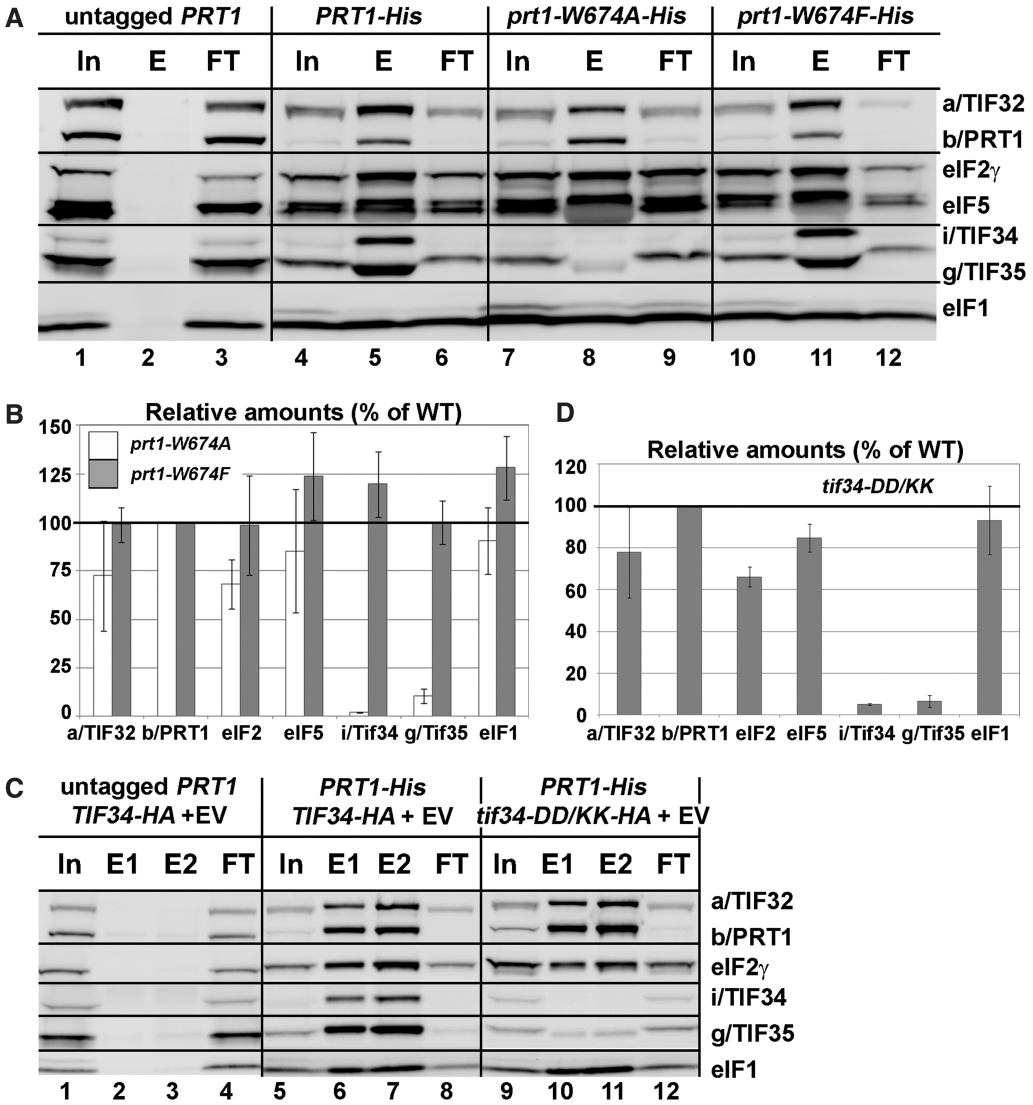

Figure 5. Disrupting the b/PRT1–i/TIF34 interaction eliminates association of the i/TIF34-g/TIF35 mini-module from the MFC *in vivo*. (**A** and **B**) WCEs prepared from YAH06 (*prt1Δ*) bearing untagged b/PRT1 (lanes 1–3), 8xHis-tagged b/PRT1 (lanes 4–6), and two of its mutant derivatives (lanes 7–9 and 10–12) were incubated with Ni^{2+} agarose and the bound proteins were eluted and subjected to western blot analysis with the antibodies indicated in each row. (In) lanes contained 5% of the input WCEs; (E) lanes contained 100% of eluate from the resin; (FT) lanes contained 5% of the flow through. (**B**) The Western signals for indicated proteins in the E fractions of the wt *PRT1-His* and its mutants were quantified, normalized for the amounts of the wt b/PRT1 in these fractions and plotted in the histogram as percentages of the corresponding values calculated for the wt b/PRT1. (**C** and **D**) WCEs were prepared from YAH12 (*prt1Δ tif34Δ*) bearing untagged *PRT1* and wt *TIF34* (lanes 1–4) and from YAH11 (*prt1Δ tif34Δ*) bearing 8xHis-tagged *PRT1* and either wt *TIF34* plus empty vector (lanes 5–8) or mutant *tif34-DD/KK* plus empty vector (lanes 9–12) and analyzed analogously to (A and B).

40S-binding (~40%) were also observed for other eIF3 subunits and eIF5, whereas binding of eIF2 (TC) and eIF1 was reduced only marginally (~20%). The lack of an increase in abundance of unbound eIF3 and eIF5 factors in the *tif34-DD/KK* gradients, which might have been expected given the pronounced loss of these proteins from the PICs, is attributed to an increased instability of eIFs defective to properly bind to 40S relative to those tightly bound in PICs during sedimentation. This phenomenon was also observed by us and others in the past (39–41). Quantification of input lanes ruled out a possibility of an increased proteolysis of eIF3 and eIF5 in the living cells as well as in the WCEs even after prolonged incubation on ice (Figure 6A). We conclude that the physical detachment of i/TIF34 and g/TIF35 from the rest of eIF3 not only prevents their binding to the 40S ribosome but also significantly weakens 40S-association of the remaining a/TIF32-b/PRT1-c/NIP1 subcomplex and eIF5. Remarkably, these findings thus may suggest that the mutant cells contain a subpopulation of PICs containing only eIF1 and the TC (see further below).

Detachment of the i/TIF34–g/TIF35 mini-module from eIF3 dramatically increases leaky scanning over the AUG start site producing a severe Gcn$^-$ phenotype

To elucidate the functional consequences of this PIC-assembly defect, we employed the translational

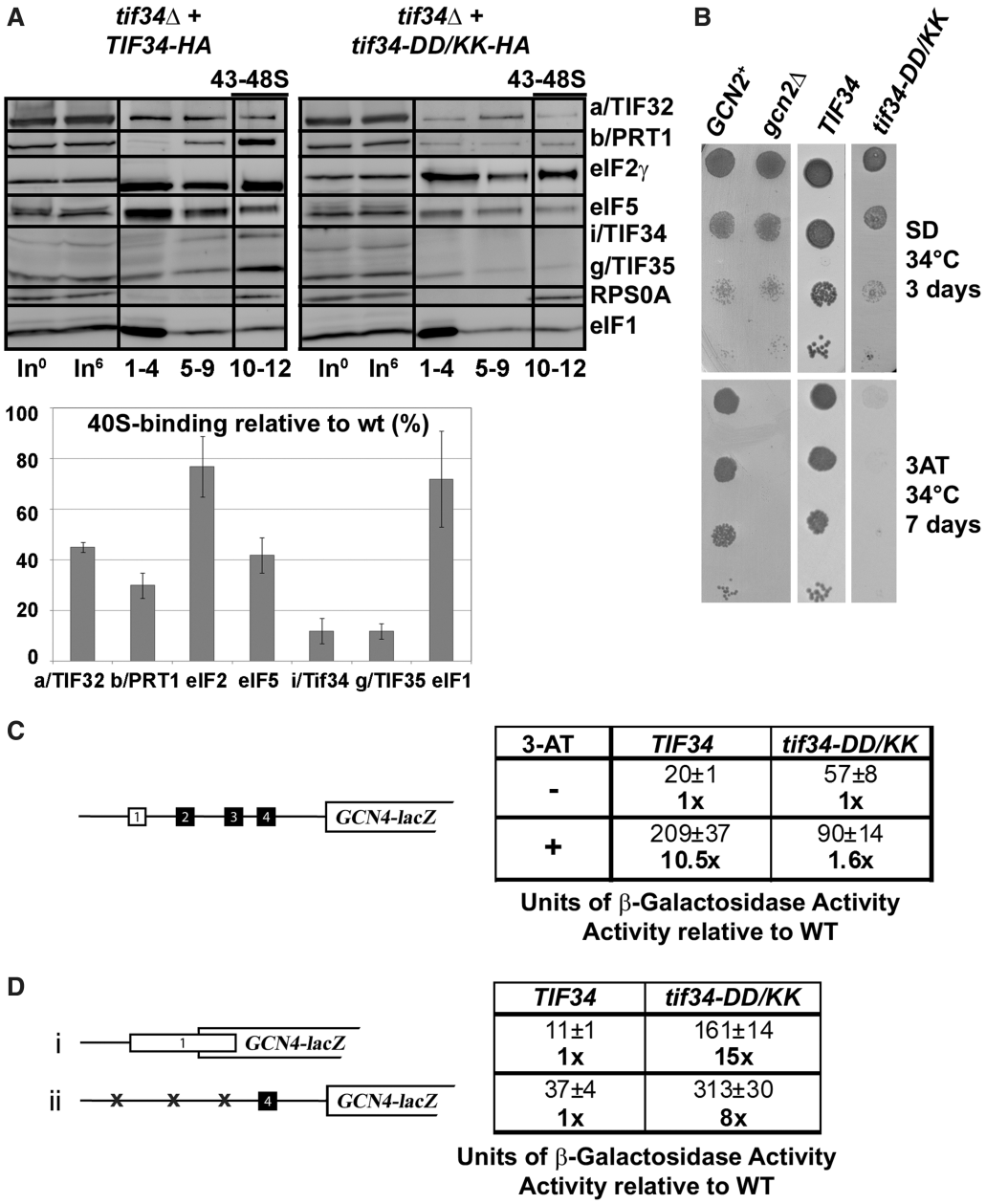

Figure 6. Disruption of the b/PRT1–i/TIF34 interaction prevents 40S-binding of the i/TIF34–g/TIF35 mini-module and dramatically increases leaky scanning over the AUG start site producing a severe Gcn$^-$ phenotype. (**A**) Physical detachment of i/TIF34 and g/TIF35 from the rest of eIF3 selectively affects stability of pre-initiation complexes *in vivo*. Transformants of H450 (*tif34Δ*) bearing wt or mutant *i/TIF34-HA* were grown in SD medium at 34 C to an OD_{600} of approximately 1.5 and cross-linked with 2% HCHO prior to harvesting. WCEs were prepared, separated on a 7.5–30% sucrose gradient by centrifugation at 41 000 rpm for 5 h and subjected to western blot analysis (note that the anti-RPS0A antibodies were generated in this study; see Supplementary Data). Fractions 1–4, 5–9, and 10–12 (43–48S) were pooled; lanes 'In^{0}' and 'In^{6}' show samples of the input WCEs (5%) that were processed immediately before (h0) or after (h6) incubation for 6 h on ice, mimicking the duration of the HCHO fractionation experiment to document the stability of the factors of interest in WCEs. Proportions of the 40S-bound proteins relative to the amount of 40S subunits were calculated using NIH ImageJ from three independent experiments. The resulting values obtained with the wt strain were set to 100% and those obtained with mutant strains were expressed as percentages of the wt (SDs are given). This experiment was repeated seven times with similar results. (**B**) *tif34-DD/KK* imparts the Gcn$^-$ phenotype. H417 (*GCN2*), H418 (*gcn2Δ*) and H450 (*tif34Δ*) bearing wt or mutant *i/TIF34-HA* were spotted in four serial 10-fold dilutions on SD (upper panel) or SD containing 30 mM 3-AT (lower panel) and then incubated at 34°C for 3 and 7 days, respectively. (**C**) *tif34-DD/KK* severely prevents derepression of *GCN4-lacZ* upon starvation. The H450 strains as in panel A were transformed with the *GCN4-lacZ* reporter p180 and grown in SD medium at 34°C to an OD_{600} of approximately 1. The β-galactosidase activities were measured in the WCEs and expressed in units of nmol of *O*-nitrophenyl-β-D-galactopyranoside hydrolyzed per minute per mg of protein. To induce *GCN4-lacZ* expression, strains were grown in minimal medium to an OD_{600} approximately 0.5 and then treated with 10 mM 3-AT for 6 h. The table gives mean values and standard deviations obtained from at least six independent measurements with three independent transformants, and activities with 3-AT-induction relative to those without induction. (**D**) Detachment of the i/TIF34–g/TIF35 mini-module from eIF3 provokes unusually severe leaky scanning defect. The H450 strains as in (A) were transformed with the *GCN4-lacZ* reporter plasmids pM226 (i) and plig102-3 (ii) and analyzed as in (C). The table gives activities in mutant relative to wt cells.

control mechanism of *GCN4*, which depends on four short upstream open reading frames (uORFs) found in its mRNA leader and has been adapted to serve as an experimental tool for monitoring various translational steps [reviewed in (42)]. The expression of *GCN4*, a transcriptional activator of many biosynthetic genes, is delicately regulated in a nutrient-dependent manner by the GCN2 kinase. Under nutrient-replete conditions the kinase is inactive and the *GCN4* expression is repressed. Upon amino-acid starvation, GCN2 becomes activated and derepresses *GCN4* synthesis by reducing the steady state levels of the TC. Mutants defective in the TC formation and/or its recruitment to the 40S subunit mimic starvation conditions and constitutively derepress *GCN4* even under nutrient-replete conditions, producing the Gcd$^-$ phenotype. Conversely, mutants that fail to derepress *GCN4* under starvation conditions provoke the Gcn$^-$ phenotype, which signals defects in the steps following assembly of 48S PICs, such as processivity of scanning, AUG recognition or subunit joining (42).

In accord with the nearly wt levels of 40S-bound TC (Figure 6A), *tif34-DD/KK* did not display the Gcd$^-$ phenotype; however, it did impart the severe Gcn$^-$ phenotype characterized by a failure to grow in the presence of 3-aminotriazole (3-AT) at 34°C (Figure 6B, column 4; 3-AT is an inhibitor of histidine biosynthetic genes.) Using the wt *GCN4-lacZ* reporter plasmid we indeed confirmed almost an absolute failure to derepress *GCN4* in response to 3-AT in the *DD/KK* cells (Figure 6C). The fact that the *tif34-DD/KK* cells sport the Gcn$^-$ phenotype as severe as the deletion of *GCN2* by itself (Figure 6B, column 2) suggests that the *DD/KK* mutation deregulates *GCN4* translational control by a dramatic impairment of one or more initiation steps following the TC recruitment.

To investigate this, we decided to employ the *GCN4-lacZ* reporter constructs with specific modifications in the *GCN4* mRNA leader, which have been successfully used in the past to reveal malfunctioning in scanning processivity, scanning rates, stringency of AUG selection or in subunit joining (12,39,40,43). Defects in recognition of the AUG start codon resulting in so-called leaky scanning can be identified with two *GCN4-lacZ* constructs: one where the first uORF (uORF1) is elongated and overlaps the beginning of *GCN4* (Figure 6D, constructs i); the other where only the last uORF (uORF4), non-permissive for reinitiation (44,45), is preserved in the mRNA leader of *GCN4-lacZ* (Figure 6D, construct ii). Only those ribosomes that skip (leaky scan) AUGs of the corresponding uORFs in both constructs may initiate on *GCN4-lacZ*, thereby producing an increase in β-galactosidase activity. Accordingly, both *tif34-DD/KK* and *prt1-W674A* show an unusually robust increase (up to 15-fold) of expression from both of these constructs (Figure 6D and Supplementary Figure S8D). Surprisingly, further analysis of other potential defects described above did not reveal any clearly distinguishable defects (see 'Discussion' section). Taken together these results strongly suggest that stable association of the i/TIF34–g/TIF35 mini-module with the rest of eIF3 stabilizes binding of eIF3 and eIF5 to the PICs to ensure their proper assembly required for stringent AUG recognition.

Increased gene dosage of *TIF35* suppresses growth and leaky scanning defects of the *i/tif34-DD/KK* mutant by preventing formation of aberrant PICs

Given the close interdependence of both small eIF3 subunits in terms of their stability and incorporation into the eIF3 complex it may be possible to suppress some of the observed phenotypes of *tif34-DD/KK* by increasing the gene dosage of *TIF35*. Accordingly, overexpressing *TIF35* significantly suppressed its growth deficiency (Figure 7A), unexpectedly, however, it did not strengthen association of i/TIF34 and g/TIF35 with b/PRT1-His in the MFC (Figure 7B, lanes 5–8 versus 1–4 and versus Figure 5C, lanes 9–12; these experiments were carried out at the same time and are summarized in the quantification plot of Figure 7B). Instead, it repeatedly decreased the amounts of eIF5, and mainly of eIF2 and eIF1 co-purifying with the rest of eIF3 suggesting that the increased dosage of g/TIF35 destabilized formation of the MFC *in vivo*. Sequestration of eIF2 and eIF1 in a separate complex by excess of g/TIF35 in cells could explain this unexpected phenomenon; however, was not observed (Supplementary Figure S8A). Hence, the molecular details of this mechanism are at present unknown to us. Most importantly, whereas it had no impact on the amounts of the 40S-bound eIF3 subunits and eIF5 when compared to wt and *i/tif34-DD/KK* cells bearing an empty vector, high dosage of g/TIF35 significantly decreased the amounts of eIF2 (~2-fold) and evened the eIF1 amounts to wt levels (Figure 7C, compare 43–48S fractions and the quantification plot summarizing results from Figures 6A and 7C). (Increased amounts of g/TIF35 in the ribosomal fractions are caused by trailing of the large excess of this protein through sucrose gradients and thus are not significant.) Importantly, the fact that the eIF2 levels actually matched those of eIF3 and eIF5 suggests that destabilization of the MFC in turn prevents formation of the aberrant TC-containing PICs. We therefore propose that the presence of aberrant PICs in the cell interferes with the canonical initiation process and significantly contributes to the observed growth defects associated with the loss of the i/TIF34–g/TIF35 mini-module from the rest of eIF3.

Hence it is likely that the robustly increased tendency to leaky scan initiating AUGs in *tif34-DD/KK* (Figure 6D) comes from malfunctioning of these erroneous PICs during the AUG recognition process. In strong support of this assumption, high dosage g/TIF35 fully suppressed the severe leaky scanning defect of the *DD/KK* mutant as well as its Gcn$^-$ phenotype (Figure 8A and B). These findings also argue that this unusually severe leaky scanning defect is actually the primary cause of the Gcn$^-$ phenotype in the mutant cells. To our knowledge, this type of a direct causal dependence has not been observed before.

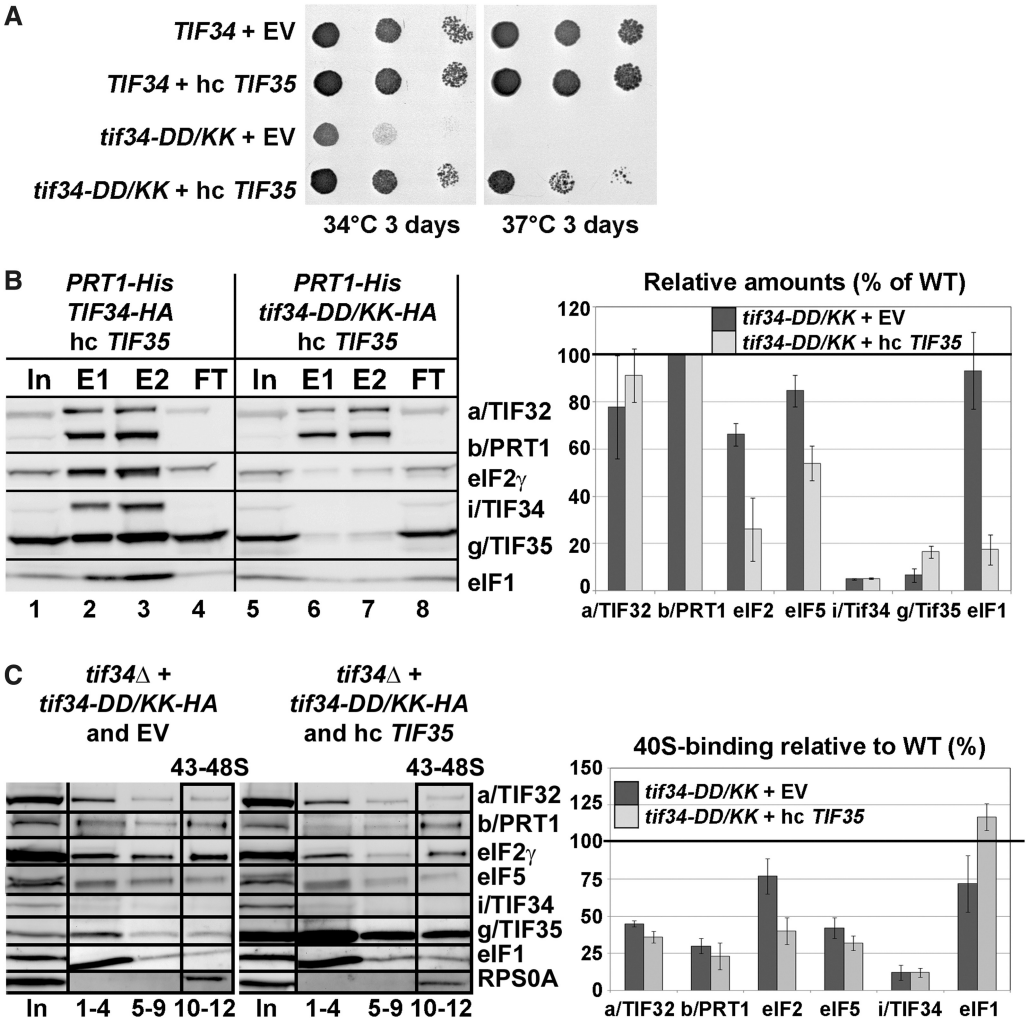

Figure 7. Increased gene dosage of *TIF35* partially suppresses growth defects of *tif34-DD/KK* mutant by preventing formation of the aberrant PICs. (**A**) High copy expression of *TIF35* partially suppresses growth phenotypes of *DD/KK*. The H450 strains as in Figure 6A were transformed with empty vector or hc *TIF35* and spotted in three serial 10-fold dilutions on SD medium and incubated at 34°C and 37°C for 3 days. (**B**) High dosage of g/TIF35 destabilizes formation of the MFC *in vivo*. The YAH12 (*prt1Δ tif34Δ*) strains as in Figure 5C were transformed with hc *TIF35* and subjected to Ni^{2+}-chelation chromatography as described in Figure 5A. The histogram shown on the right combines data from Figure 5C and D and this panel; the data were obtained in parallel experiments carried out at the same time. (**C**) High dosage of g/TIF35 prevents formation of aberrant TC-containing PICs *in vivo*. The H450 transformants as in (A) were subjected to formaldehyde cross-linking as described in Figure 6A. Proportions of the 40S-bound proteins relative to the amount of 40S subunits are shown in the histogram on the right. The resulting values obtained with the wt strain were set to 100% and those obtained with the *DD/KK* strain transformed with empty vector or high copy *TIF35* were expressed as percentages of the former (SDs are given).

Increased gene dosage of *SUI1* (eIF1) selectively suppresses the Gcn$^-$ and leaky scanning phenotypes of the *tif34-DD/KK* mutant

Initiation factors eIF1, eIF1A and eIF5 are considered to be the key controllers of the start selection process in eukaryotes (46). To examine their effect in the background of our leaky scanning *DD/KK* mutant, we overexpressed them individually in the *DD/KK* mutant strain while scoring for suppression of its Gcn$^-$ phenotype on 3-AT plates. Interestingly, overexpressing eIF1 but not eIF1A and eIF5 markedly suppressed the Gcn$^-$ but not the Slg$^-$ phenotype of *DD/KK* (Figures 8A and data not shown). To test whether this pronounced effect requires stable PIC association of eIF1, we examined eIF1 mutants with either severely weakened (*sui1*^{Q84P}, *sui1*^{D83G}, *sui1*$^{93\text{-}97}$) or wt (*sui1*^{G107R}) PIC affinity (41,47) for their ability to suppress the Gcn$^-$ phenotype. Out of these mutants, only high copy (hc) *sui1*^{G107R} with wt PIC affinity was capable of nearly wt Gcn$^-$ phenotype suppression (Figure 8A, right-hand panel). Hence, in order to suppress the *DD/KK* mutant, eIF1 must be capable of stable 40S-binding. Accordingly, high dosage of wt eIF1 as well as sui1^{G107R} also considerably suppressed the leaky scanning defect (Figure 8B). As expected, overexpressing eIF1A and eIF5 had no effect (data not shown). These experiments thus further support the idea that the leaky scanning defect is the main contributor to the failure of mutant cells to induce *GCN4* expression under starvation conditions.

In contrast to increased dosage of g/TIF35, which destabilized formation of the MFC *in vivo* (Figure 7B),

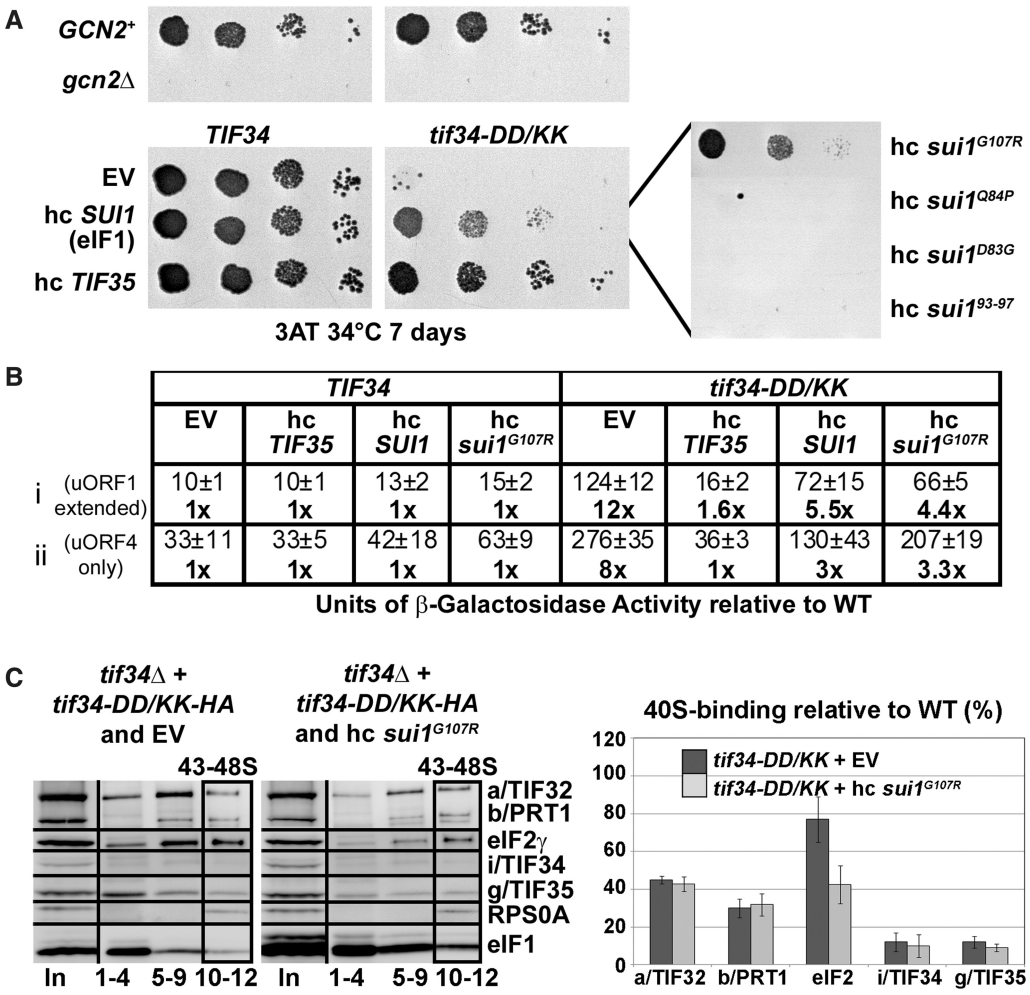

Figure 8. Increased gene dosage of *TIF35*, *SUI1* (eIF1), and its mutant allele $sui1^{G107R}$ suppresses the Gcn$^-$ phenotype of *tif34-DD/KK* as well as its severe leaky scanning defect; and high copy $sui1^{G107R}$ disrupts aberrant PICs *in vivo*. (**A**) The H450 strains as in Figure 6A were transformed with empty vector, hc *SUI1* (eIF1) or its mutant alleles, and with hc *TIF35*, respectively, spotted in four serial 10-fold dilutions on 3-AT containing SD media and tested for growth at 34°C for 7 days. (**B**) The strains as in (A) were further transformed with constructs shown in Figure 6D and analyzed as described in there. (**C**) High dosage of sui1^{G107R} disrupts the aberrant TC-containing PICs *in vivo*. The H450 transformants as in panel A were subjected to formaldehyde cross-linking as described in Figure 6A. Proportions of the 40S-bound proteins relative to the amount of 40S subunits are shown in the histogram on the right. The resulting values obtained with the wt strain were set to 100% and those obtained with the *DD/KK* strain transformed with empty vector or hc $sui1^{G107R}$ were expressed as percentages of the former (SDs are given).

Ni^{2+}-chelation experiments from WCE of the *tif34-DD/KK* cells overexpressing either wt eIF1 or $sui1^{G107R}$ repeatedly showed no further destabilization of the MFC integrity in the mutant cells (data not shown). However, we did observe a clear negative effect of overexpressing $sui1^{G107R}$ on the amount of TC associated with 40S subunits in the *DD/KK* mutant *in vivo* reminiscent of that displayed by hc *TIF35* (Figure 8C compare with Figure 7C). Interestingly, no similar TC reduction was detected in cells overexpressing wt eIF1 (data not shown).

DISCUSSION

In this study we show that residues 654–700 of b/PRT1 are sufficient for i/TIF34 binding and present, to our knowledge, the first atomic-resolution structure of the interaction between two essential core eIF3 subunits. Our structure reveals that the two major contacts between i/TIF34 and b/PRT1(654–700) occur on the bottom side of the i/TIF34 β-propeller through conserved residues in blades 5 and 6. Disrupting the first contact between D207 and D224 of i/TIF34 and the corresponding Y677 and R678 of b/PRT1 produces lethal or Ts$^-$ phenotypes and severely diminishes MFC- and 40S-association of i/TIF34, and also that of g/TIF35, *in vivo* (Figures 3–6). Importantly, it also destabilizes binding of the rest of eIF3 and eIF5 to the 40S subunit (Figure 6). Likewise, disrupting the second contact between W674 of b/PRT1 and the hydrophobic pocket of i/TIF34 confers essentially the same phenotypes (Figures 3–5, Supplementary Figure S8D, and data not shown). Together these results clearly indicate that both contacts between b/PRT1 and i/TIF34 critically stabilize association of the i/TIF34–g/TIF35 mini-module with the rest of eIF3, in close co-operation with those contacts that g/TIF35 makes with both subunits. This in turn ensures efficient loading of these

two small eIF3 subunits onto the 40S where they are subsequently required for proper assembly of the 48S PICs.

Several important intermolecular bridges between yeast eIF3 and the solvent-exposed side of the 40S ribosome were previously identified, including those between the NTD of a/TIF32 and the small ribosomal protein RPS0A, the a/TIF32-CTD and helices 16–18 of 18S rRNA and RPS2 and RPS3, and the CTD of j/HCR1 and RPS2 (12,37,44,48). Note that both RPS2 and 3 are situated near the mRNA entry pore (Figure 9, upper panel). Besides them, the CTD of c/NIP1 and the b/PRT1-RRM were also shown to critically contribute to the eIF3 affinity for the 40S subunit; however, their binding partners remain to be identified (12,37). Whether or not the remaining eIF3 subunits in i/TIF34 and g/TIF35 likewise participate in this functionally crucial eIF3-ribosome binding activity remained unclear until now. On the one hand a partial subcomplex composed of i/TIF34, g/TIF35 and b/PRT1 lacking its N-terminal RRM showed zero 40S-binding affinity *in vivo* (9). On the other hand, another subcomplex comprising c/NIP1, the critical N-terminal half of a/TIF32, and eIF5 showed a substantial affinity for the 40S subunits *in vivo*, though not as strong as that of the wt 6-subunit eIF3 (37). Based on these findings and the data presented here, we propose that whereas the major and essential driving force of the 40S-binding affinity of yeast eIF3 lies in the three largest subunits, as proposed earlier (37), i/TIF34 and g/TIF35 provide complementary 40S-binding activity that is required for stabilization of the entire 48S PICs. It is therefore conceivable that the proper establishment of all intermolecular bridges between eIF3 and the 40S ribosome is needed to ensure precise positioning of eIF3 on the small subunit and thereby flawless functioning of eIF3 not only in formation of 43S and 48S PICs, but also in the subsequent initiation steps.

This last notion resonates with our findings that the *DD/KK* mutation produces severe Gcn$^-$ phenotype owing to the robustly increased skipping of the AUG start codon (Figure 6). It is assumed that this so-called leaky scanning phenotype results from an inability of the 48S PIC to switch from the open/scanning-conducive conformation of the 40S head region to the closed/scanning-arrested one that occurs upon AUG recognition and is strictly regulated by eIFs 1 and 1A (reviewed in (46)). The conformational change upon scanning arrest is characterized by dissolution of the contact between RPS3 and helix 16 of 18S rRNA and reformation of the helix18–helix34-RPS3 connection designated as the latch on the mRNA entry channel (49). Interestingly, the leaky scanning phenotype was also observed with mutations disrupting the web of interactions among the a/TIF32-CTD, the b/PRT1-RRM and j/HCR1 located most likely below the mRNA entry channel (12,48) (Figure 9, lower panel). Likewise, g/TIF35 was recently found to interact with RPS3 and RPS20, two subunits located above the mRNA entry channel (5) (Figure 9). This advocates that both termini of b/PRT1 and their associated eIF3 subunits can influence the precision and/or timing of this critical conformational transition upon AUG start codon

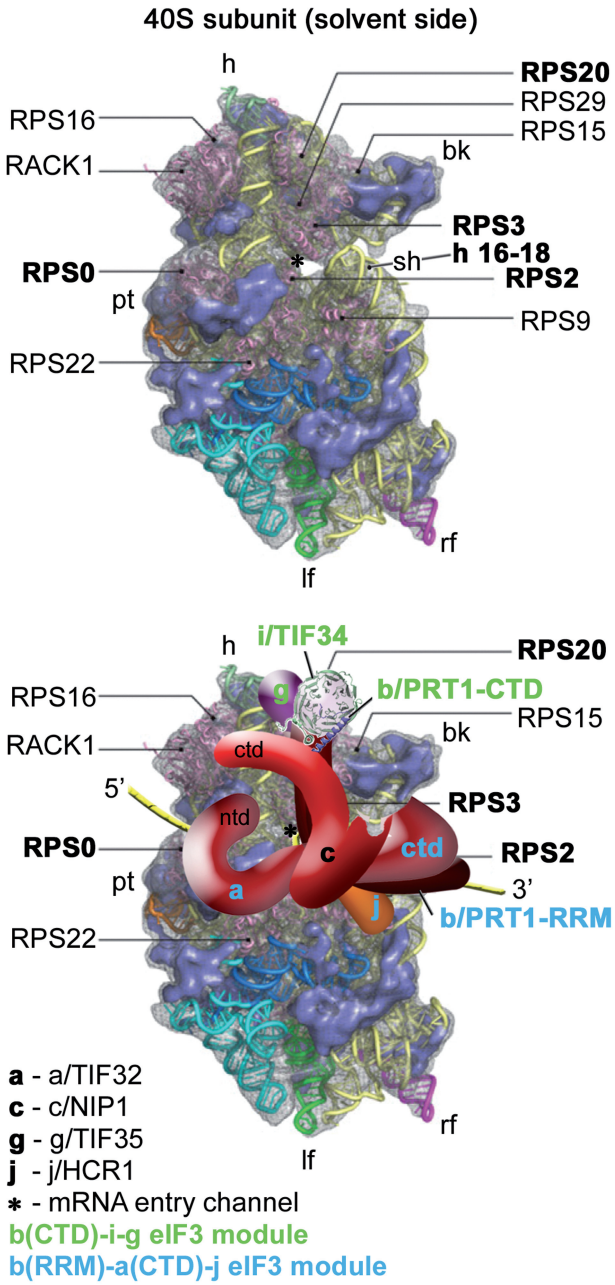

Figure 9. A model of two eIF3 modules bound to the opposite termini of the scaffold b/PRT1 subunit situated near the mRNA entry channel of the 40S subunit. (Upper panel) The Cryo-EM reconstruction of the 40S subunit is shown from the solvent side with ribosomal RNA represented as tubes. Ribosomal proteins, with known bacterial homologs and placement, are shown as pink cartoons and labeled (adapted from (57)). Positions of RPS0, 2, 3 and 20 and 18S rRNA helices 16–18 are highlighted in bold. The mRNA entry channel is designated by an asterisk. (Lower panel) Hypothetical location of *S. cerevisiae* eIF3 on the back side of the 40S subunit based on the data presented in this study and elsewhere, including the interactions between RPS0 and a/TIF32-NTD; RPS2 and j/HCR1; RPS2 and 3 and a/TIF32-CTD; helices 16-18 of 18S rRNA and a/TIF32-CTD; and RPS3 and 20 and g/TIF35 (see text for details). The schematic representations of b/PRT1-CTD and i/TIF34 were replaced with the X-ray structure as in Figure 4C. Two eIF3 modules represented by the b/PRT1-CTD–i/TIF34–g/TIF35 and the b/PRT1-RRM–a/TIF32-CTD–j/HCR1 are color-coded in green and blue, respectively. The yellow lines represent mRNA.

recognition (see our model in Figure 9, lower panel). We envisage three functional consequences of our mutants that could explain the leaky scanning as well as growth defects.

First, the lack of i/TIF34 and g/TIF35 may change the overall conformation and/or orientation of the rest eIF3 on the ribosome in a way that interferes with dynamics of the latch closing upon start codon recognition, allowing the 40S ribosome to skip the authentic AUG codon and continue scanning downstream. The aforementioned fact that g/TIF35 interacts with RPS20 and mainly with RPS3, which is one of the main components of the 'latch mechanism' (5), is consistent with this hypothesis. If true, the scaffold b/PRT1 subunit would serve to connect two eIF3 modules at each of its termini as indicated in Figure 9 (a/TIF32-CTD–j/HCR1 at the N-terminal RRM, and i/TIF34–g/TIF35 at the C-terminal α-helix) that would work together and with c/NIP1 (39) and other eIFs (46) to fine-tune the AUG selection process.

The second contributor to the leaky scanning phenotype might originate from defects in the interaction of the PICs with mRNA in the background of the disrupted interactions between eIFs. It is evident now that eIF3 is crucial for productive mRNA recruitment (50,51) and there is also evidence that eIF3 directly interacts with mRNA (5,44,52). This might suggest that changes in how eIF3 interacts with the PICs could negatively affect the way the mRNA interacts with the mRNA binding channel having an ultimate impact on fidelity of start codon recognition.

The third contribution could arise from our finding that breaking the contact between b/PRT1 and i/TIF34 subunits leads to accumulation of erroneous PICs containing the TC and eIF1 (Figure 6A), the amounts of which can be reduced by overexpressing *TIF35* (Figure 7C) or *sui1*^{G107R} (Figure 8C). The fact that high dosage of g/TIF35 suppresses the Gcn$^-$ and partially also the Slg$^-$ phenotypes of *tif34-DD/KK* but paradoxically does not better the assembly of the MFC and 48S PICs indicates that the presence of these aberrant complexes has a dominant negative effect on the initiation process reducing the overall fitness of mutant cells. Given the lack of any precedent for these repeatedly observable effects, we can only hypothesize that such forms of aberrant PICs would originate from simultaneous binding of all eIFs associated around eIF3 in the MFC to the ribosome followed by rapid dissociation of the unstably bound eIF3 (since lacking the i/TIF34–g/TIF35 mini-module) and eIF5 (eIF5 is known to bind to eIF3 very tightly (3)). It is assumed that the MFC has to undergo a relatively extensive rearrangement when it associates with the 40S subunit (37), as eIFs 1, 2, and most probably also 5 occur on the 40S interface side, whereas eIF3 binds to the solvent-exposed side [reviewed in (2)]. Hence we can stipulate that eIF3 and eIF5 preferentially fall off during this rearrangement period. We further stipulate that the resulting TC-eIF1-rich PICs would have the TC locked in a conformation conducive to scanning but incompatible with initiation (the so-called the P^{out} conformation of the TC), as recently described for some eIF1A mutants (53), and as such they would be skipping the AUG start codons with dramatically increased frequency, as observed with our mutants. How to explain the paradox mentioned above? We propose that the increased dosage of g/TIF35 completely eliminates the MFC-driven PIC assembly pathway that is considered to be the most efficient way of the PIC formation (1). As a consequence, PICs in the mutant cells overexpressing *g/TIF35* must form solely by a less efficient yet still fully functional stochastic association of individual eIFs with the 40S ribosome, reminiscent of the bacterial initiation reaction, with no need for ribosomal rearrangement.

The fact that high dosage of sui1^{G107R} also reduced amounts of TC-containing PICs in *tif34-DD/KK* (Figure 8C) but, in contrast to high copy *TIF35*, did not further destabilize the MFC in the mutant cells suggests a different molecular mechanism of suppression. In the light of earlier observations with reconstituted translational systems showing that mammalian eIF1 disrupts aberrantly formed PICs *in vitro* (54), we could speculate that an increased dosage of eIF1 disrupts the aberrant PICs directly also *in vivo*. In support, we found that the *sui1*^{G107R} mutant, which in contrast to other *sui1* mutants decreases the fidelity of start codon recognition without increasing the rate of eIF1 release from the PICs, suppressed the Gcn$^-$ and leaky scanning phenotypes of the *DD/KK* mutant like wt eIF1 (Figure 8A and B). These results imply that the eIF1 effect in *DD/KK* cells requires its stable physical presence on the 40S ribosome, where it could directly manipulate the aberrant PICs. However, at odds with this scenario, overexpression of wt eIF1 had no impact on the amounts of the 40S-bound TC in *tif34-DD/KK*. Hence at present we cannot offer any satisfactory explanation for this rather intriguing observation.

The aforementioned paradox that overexpressing *TIF35* significantly suppresses the growth defect of the *tif34-DD/KK* mutant without rescuing the 40S association of eIF3 and eIF5 may also evoke a notion that the yeast cells can grow at wt rates with only a relatively small fraction (~40%) of the normal amounts of eIF3, eIF2 and eIF5 bound to 40S PICs. While we indeed cannot rule out this possibility, we think that in reality the 40S-binding of all factors in the living cells is most likely not as dramatically affected as we see in our cross-linking experiments, where the effect of a weaker 40S-association might get magnified by a mechanical breakage of cells and all other *in vitro* manipulations.

Finally, it should also be noted that we recently generated and analyzed two specific mutations in i/TIF34 and g/TIF35, neither of which had any effects on eIF3 and PIC assembly, that produced a severe slow scanning defect and significantly reduced processivity of scanning through stable secondary structures (5). Neither of these scanning phenotypes was, however, found associated with the *W674A* and *DD/KK* mutations analyzed here. This is not surprising, since the latter mutations affect translation by destabilizing the MFC and PIC formation, while the former mutations, which have no assembly defects, primarily disrupt eIF3 functions downstream of the 48S PIC assembly. This is consistent with the dual role of eIF3 as a central hub required for

mRNA binding to the 43S PIC (48,50,51) as well as a crucial player in scanning and AUG recognition (5,12,39). It will now be intriguing to investigate the binding determinants of g/TIF35 in a partial subcomplex with i/TIF34 and b/PRT1-CTD and their interactions with the 40S subunit using the powerful combination of structural, genetic and biochemical approaches in order to continue replacing the *hic sunt leones* on our illustrative model of eIF3 with real structures as presented in Figure 4C.

ACCESSION CODES

Structure factors and coordinates for the i/TIF34-b/PRT1(654-700) complex have been deposited in the Protein Data Bank under accession code 3zwl.

SUPPLEMENTARY DATA

Supplementary Data are available at NAR Online: Supplementary Tables 1–5, Supplementary Figures 1–9, Supplementary Methods, Supplementary References [58–64].

ACKNOWLEDGEMENTS

We are thankful to Jon Lorsch, Monica Liu and Phil Evans for critical reading of the manuscript and to an unknown reviewer for his insightful comments. We are indebted to Phil Evans and Gerhard Reitmayr for help with diffraction data analysis and Python scripting. We also gratefully acknowledge members of Lukavsky, Valášek, Neuhaus, Nagai and Krásný laboratories for numerous discussions.

FUNDING

The Wellcome Trust grant (090812/B/09/Z); Howard Hughes Medical Institute, and Inst. Research Concept (AV0Z50200510 to L.S.V.); the Medical Research Council and HFSP (RGP0024/2008 to P.J.L.); EMBO Long-term fellowship (to D.D.). Funding for open access charge: The Wellcome Trust grant (090812/B/09/Z).

Conflict of interest statement. None declared.

REFERENCES

1. Hinnebusch,A.G. (2006) eIF3: a versatile scaffold for translation initiation complexes. *Trends Biochem Sci.*, **31**, 553–562.
2. Jackson,R.J., Hellen,C.U.T. and Pestova,T.V. (2010) The mechanism of eukaryotic translation initiation and principles of its regulation. *Nat. Rev. Mol. Cell Biol.*, **11**, 113–127.
3. Phan,L., Schoenfeld,L.W., Valášek,L., Nielsen,K.H. and Hinnebusch,A.G. (2001) A subcomplex of three eIF3 subunits binds eIF1 and eIF5 and stimulates ribosome binding of mRNA and $tRNA_i^{Met}$. *EMBO J.*, **20**, 2954–2965.
4. Naranda,T., Kainuma,M., McMillan,S.E. and Hershey,J.W.B. (1997) The 39-kilodalton subunit of eukaryotic translation initiation factor 3 is essential for the complex's integrity and for cell viability in *Saccharomyces cerevisiae*. *Mol. Cell. Biol.*, **17**, 145–153.
5. Cuchalová,L., Kouba,T., Herrmannová,A., Danyi,I., Chiu,W.-l. and Valášek,L. (2010) The RNA recognition motif of eukaryotic translation initiation factor 3g (eIF3g) is required for resumption of scanning of posttermination ribosomes for reinitiation on GCN4 and together with eIF3i stimulates linear scanning. *Mol. Cell. Biol.*, **30**, 4671–4686.
6. Masutani,M., Sonenberg,N., Yokoyama,S. and Imataka,H. (2007) Reconstitution reveals the functional core of mammalian eIF3. *EMBO J.*, **26**, 3373–3383.
7. Fraser,C.S., Lee,J.Y., Mayeur,G.L., Bushell,M., Doudna,J.A. and Hershey,J.W. (2004) The j-subunit of human translation initiation factor eIF3 is required for the stable binding of eIF3 and its subcomplexes to 40S ribosomal subunits in vitro. *J. Biol. Chem.*, **279**, 8946–8956.
8. Zhou,M., Sandercock,A.M., Fraser,C.S., Ridlova,G., Stephens,E., Schenauer,M.R., Yokoi-Fong,T., Barsky,D., Leary,J.A., Hershey,J.W. *et al.* (2008) Mass spectrometry reveals modularity and a complete subunit interaction map of the eukaryotic translation factor eIF3. *Proc. Natl Acad. Sci. USA*, **105**, 18139–18144.
9. Valášek,L., Nielsen,K.H. and Hinnebusch,A.G. (2002) Direct eIF2-eIF3 contact in the multifactor complex is important for translation initiation in vivo. *EMBO J.*, **21**, 5886–5898.
10. Asano,K., Phan,L., Anderson,J. and Hinnebusch,A.G. (1998) Complex formation by all five homologues of mammalian translation initiation factor 3 subunits from yeast *Saccharomyces cerevisiae*. *J. Biol. Chem.*, **273**, 18573–18585.
11. ElAntak,L., Tzakos,A.G., Locker,N. and Lukavsky,P.J. (2007) Structure of eIF3b RNA recognition motif and its interaction with eIF3j: structural insights into the recruitment of eIF3b to the 40 S ribosomal subunit. *J. Biol. Chem.*, **282**, 8165–8174.
12. ElAntak,L., Wagner,S., Herrmannová,A., Karásková,M., Rutkai,E., Lukavsky,P.J. and Valášek,L. (2010) The indispensable N-terminal half of eIF3j co-operates with its structurally conserved binding partner eIF3b-RRM and eIF1A in stringent AUG selection. *J. Mol. Biol.*, **396**, 1097–1116.
13. Valášek,L., Phan,L., Schoenfeld,L.W., Valášková,V. and Hinnebusch,A.G. (2001) Related eIF3 subunits TIF32 and HCR1 interact with an RNA recognition motif in PRT1 required for eIF3 integrity and ribosome binding. *EMBO J.*, **20**, 891–904.
14. Marintchev,A. and Wagner,G. (2005) Translation initiation: structures, mechanisms and evolution. *Q. Rev. Biophys.*, **37**, 197–284.
15. Dodd,R.B., Allen,M.D., Brown,S.E., Sanderson,C.M., Duncan,L.M., Lehner,P.J., Bycroft,M. and Read,R.J. (2004) Solution structure of the Kaposi's sarcoma-associated Herpesvirus K3 N-terminal domain reveals a novel E2-binding C4HC3-type RING domain. *J. Biol. Chem.*, **279**, 53840–53847.
16. Muchmore,S.W., Sattler,M., Liang,H., Meadows,R.P., Harlan,J.E., Yoon,H.S., Nettesheim,D., Chang,B.S., Thompson,C.B., Wong,S.-L. *et al.* (1996) X-ray and NMR structure of human Bcl-xL, an inhibitor of programmed cell death. *Nature*, **381**, 335–341.
17. Szymczyna,B.R., Taurog,R.E., Young,M.J., Snyder,J.C., Johnson,J.E. and Williamson,J.R. (2009) Synergy of NMR, computation, and X-ray crystallography for structural biology. *Structure*, **17**, 499–507.
18. Leslie,A. (2006) The integration of macromolecular diffraction data. *Acta Cryst.Section D*, **62**, 48–57.
19. Evans,P. (2006) Scaling and assessment of data quality. *Acta Cryst. Section D*, **62**, 72–82.
20. French,S. and Wilson,K. (1978) On the treatment of negative intensity observations. *Acta Cryst Section A*, **34**, 517–525.
21. Collaborative Computational Project,N. (1994) The CCP4 suite: programs for protein crystallography. *Acta Crystallogr. D Biol Crystallogr.*, **50**, 760–763.
22. de La Fortelle,E. and Bricogne,G. (1997) Maximum-likelihood heavy-atom parameter refinement for multiple isomorphous replacement and multiwavelength anomalous diffraction methods. *Methods Enzymol.*, **276**, 472–494.
23. Kelley,L.A. and Sternberg,M.J.E. (2009) Protein structure prediction on the Web: a case study using the Phyre server. *Nat. Protocols*, **4**, 363–371.
24. McCoy,A.J., Grosse-Kunstleve,R.W., Storoni,L.C. and Read,R.J. (2005) Likelihood-enhanced fast translation functions. *Acta Cryst. Section D*, **61**, 458–464.

25. Zhang,K.Y., Cowtan,K. and Main,P. (1997) Combining constraints for electron-density modification. *Methods Enzymol.*, **277**, 53–64.
26. Cowtan,K. (2006) The Buccaneer software for automated model building. 1. Tracing protein chains. *Acta Cryst. Section D*, **62**, 1002–1011.
27. Emsley,P. and Cowtan,K. (2004) Coot: model-building tools for molecular graphics. *Acta Cryst. Section D*, **60**, 2126–2132.
28. Murshudov,G.N., Vagin,A.A. and Dodson,E.J. (1997) Refinement of macromolecular structures by the maximum-likelihood method. *Acta Cryst. Section D*, **53**, 240–255.
29. Davis,I.W., Leaver-Fay,A., Chen,V.B., Block,J.N., Kapral,G.J., Wang,X., Murray,L.W., Arendall,W.B. III, Snoeyink,J., Richardson,J.S. *et al.* (2007) MolProbity: all-atom contacts and structure validation for proteins and nucleic acids. *Nucleic Acids Res.*, **35**, W375–383.
30. Coyle,S.M., Gilbert,W.V. and Doudna,J.A. (2009) Direct Link between RACK1 function and localization at the ribosome in vivo. *Mol. Cell. Biol.*, **29**, 1626–1634.
31. Li,D. and Roberts,R. (2001) Human genome and diseases: WD-repeat proteins: structure characteristics, biological function, and their involvement in human diseases. *Cell. Mol. Life Sci.*, **58**, 2085–2097.
32. Jennings,B.H., Pickles,L.M., Wainwright,S.M., Roe,S.M., Pearl,L.H. and Ish-Horowicz,D. (2006) Molecular recognition of transcriptional repressor motifs by the WD domain of the groucho/TLE corepressor. *Mol. Cell*, **22**, 645–655.
33. Oliver,A.W., Swift,S., Lord,C.J., Ashworth,A. and Pearl,L.H. (2009) Structural basis for recruitment of BRCA2 by PALB2. *EMBO Rep.*, **10**, 990–996.
34. ter Haar,E., Harrison,S.C. and Kirchhausen,T. (2000) Peptide-in-groove interactions link target proteins to the $\hat{I}^2$-propeller of clathrin. *Proc. Natl Acad. Sci. USA*, **97**, 1096–1100.
35. Krissinel,E. and Henrick,K. (2007) Inference of macromolecular assemblies from crystalline state. *J. Mol. Biol.*, **372**, 774–797.
36. Gallivan,J.P. and Dougherty,D.A. (1999) Cation-pi interactions in structural biology. *Proc. Natl Acad. Sci. USA*, **96**, 9459–9464.
37. Valášek,L., Mathew,A., Shin,B.S., Nielsen,K.H., Szamecz,B. and Hinnebusch,A.G. (2003) The yeast eIF3 subunits TIF32/a and NIP1/c and eIF5 make critical connections with the 40S ribosome in vivo. *Genes Dev.*, **17**, 786–799.
38. Valášek,L., Szamecz,B., Hinnebusch,A.G. and Nielsen,K.H. (2007) In vivo stabilization of preinitiation complexes by formaldehyde cross-linking. *Methods Enzymol.*, **429**, 163–183.
39. Valášek,L., Nielsen,K.H., Zhang,F., Fekete,C.A. and Hinnebusch,A.G. (2004) Interactions of eukaryotic translation initiation factor 3 (eIF3) subunit NIP1/c with eIF1 and eIF5 promote preinitiation complex assembly and regulate start codon selection. *Mol. Cell. Biol.*, **24**, 9437–9455.
40. Fekete,C.A., Mitchell,S.F., Cherkasova,V.A., Applefield,D., Algire,M.A., Maag,D., Saini,A.K., Lorsch,J.R. and Hinnebusch,A.G. (2007) N- and C-terminal residues of eIF1A have opposing effects on the fidelity of start codon selection. *EMBO J.*, **26**, 1602–1614.
41. Nanda,J.S., Cheung,Y.-N., Takacs,J.E., Martin-Marcos,P., Saini,A.K., Hinnebusch,A.G. and Lorsch,J.R. (2009) eIF1 controls multiple steps in start codon recognition during eukaryotic translation initiation. *J. Mol. Biol.*, **394**, 268–285.
42. Hinnebusch,A.G. (2005) Translational regulation of GCN4 and the general amino acid control of yeast. *Annu. Rev. Microbiol.*, **59**, 407–450.
43. Nielsen,K.H., Szamecz,B., Valasek,L., Jivotoskaya,A., Shin,B.S. and Hinnebusch,A.G. (2004) Functions of eIF3 downstream of 48S assembly impact AUG recognition and GCN4 translational control. *EMBO J.*, **23**, 1166–1177.
44. Szamecz,B., Rutkai,E., Cuchalova,L., Munzarova,V., Herrmannova,A., Nielsen,K.H., Burela,L., Hinnebusch,A.G. and Valášek,L. (2008) eIF3a cooperates with sequences 5′ of uORF1 to promote resumption of scanning by post-termination ribosomes for reinitiation on GCN4 mRNA. *Genes Dev.*, **22**, 2414–2425.
45. Munzarová,V., Pánek,J., Gunišová,S., Dányi,I., Szamecz,B. and Valášek,L.S. (2011) Translation reinitiation relies on the interaction between eIF3a/TIF32 and progressively folded cis-acting mRNA elements preceding short uORFs. *PLoS Genet.*, **7**, e1002137.
46. Mitchell,S.F. and Lorsch,J.R. (2008) Should I stay or should i go? Eukaryotic translation initiation factors 1 and 1a control start codon recognition. *J. Biol. Chem.*, **283**, 27345–27349.
47. Cheung,Y.N., Maag,D., Mitchell,S.F., Fekete,C.A., Algire,M.A., Takacs,J.E., Shirokikh,N., Pestova,T., Lorsch,J.R. and Hinnebusch,A.G. (2007) Dissociation of eIF1 from the 40S ribosomal subunit is a key step in start codon selection in vivo. *Genes Dev.*, **21**, 1217–1230.
48. Chiu,W.-L., Wagner,S., Herrmannova,A., Burela,L., Zhang,F., Saini,A.K., Valasek,L. and Hinnebusch,A.G. (2010) The C-terminal region of eukaryotic translation initiation factor 3a (eIF3a) promotes mRNA recruitment, scanning, and, together with eIF3j and the eIF3b RNA recognition motif, selection of AUG start codons. *Mol. Cell. Biol.*, **30**, 4415–4434.
49. Passmore,L.A., Schmeing,T.M., Maag,D., Applefield,D.J., Acker,M.G., Algire,M.A., Lorsch,J.R. and Ramakrishnan,V. (2007) The eukaryotic translation initiation factors eIF1 and eIF1A induce an open conformation of the 40S ribosome. *Mol. Cell*, **26**, 41–50.
50. Mitchell,S.F., Walker,S.E., Algire,M.A., Park,E.-H., Hinnebusch,A.G. and Lorsch,J.R. (2010) The 5′-7-Methylguanosine Cap on eukaryotic mRNAs serves both to stimulate canonical translation initiation and to block an alternative pathway. *Mol. Cell*, **39**, 950–962.
51. Jivotovskaya,A., Valášek,L., Hinnebusch,A.G. and Nielsen,K.H. (2006) Eukaryotic translation initiation factor 3 (eIF3) and eIF2 can promote mRNA binding to 40S subunits independently of eIF4G in yeast. *Mol. Cell. Biol.*, **26**, 1355–1372.
52. Pisarev,A.V., Kolupaeva,V.G., Yusupov,M.M., Hellen,C.U.T. and Pestova,T.V. (2008) Ribosomal position and contacts of mRNA in eukaryotic translation initiation complexes. *EMBO J.*, **27**, 1609–1621.
53. Saini,A.K., Nanda,J.S., Lorsch,J.R. and Hinnebusch,A.G. (2010) Regulatory elements in eIF1A control the fidelity of start codon selection by modulating tRNAiMet binding to the ribosome. *Genes Dev.*, **24**, 97–110.
54. Pestova,T.V., Borukhov,S.I. and Hellen,C.U.T. (1998) Eukaryotic ribosomes require initiation factors 1 and 1A to locate initiation codons. *Nature*, **394**, 854–859.
55. Baker,N.A., Sept,D., Joseph,S., Holst,M.J. and McCammon,J.A. (2001) Electrostatics of nanosystems: Application to microtubules and the ribosome. *Proc. Natl Acad. Sci. USA*, **98**, 10037–10041.
56. Dolinsky,T.J., Czodrowski,P., Li,H., Nielsen,J.E., Jensen,J.H., Klebe,G. and Baker,N.A. (2007) PDB2PQR: expanding and upgrading automated preparation of biomolecular structures for molecular simulations. *Nucleic Acids Res.*, **35**, W522–W525.
57. Taylor,D.J., Devkota,B., Huang,A.D., Topf,M., Narayanan,E., Sali,A., Harvey,S.C. and Frank,J. (2009) Comprehensive molecular structure of the eukaryotic ribosome. *Structure*, **17**, 1591–1604.
58. Kuzmic,P. (2009) DynaFit–a software package for enzymology. *Methods in Enzymology*, **467**, 247–280.
59. Kuzmic,P. (1996) Program DYNAFIT for the analysis of enzyme kinetic data: Application to HIV proteinase. *Analyt. Biochem.*, **237**, 260–273.
60. Nielsen,K.H. and Valášek,L. (2007) In vivo deletion analysis of the architecture of a multi-protein complex of translation initiation factors. *Methods Enzymol.*, **431**, 15–32.
61. Grant,C.M., Miller,P.F. and Hinnebusch,A.G. (1994) Requirements for intercistronic distance and level of eIF-2 activity in reinitiation on GCN4 mRNA varies with the downstream cistron. *Mol. Cell. Biol.*, **14**, 2616–2628.
62. Cigan,A.M., Foiani,M., Hannig,E.M. and Hinnebusch,A.G. (1991) Complex formation by positive and negative translational regulators of *GCN4*. *Mol. Cell. Biol.*, **11**, 3217–3228.
63. Smith,D.B. and Johnson,K.S. (1988) Single-step purification of polypeptides expressed in *Escherichia coli* as fusions with glutathione S-transferase. *Gene*, **67**, 31–40.
64. Gietz,R.D. and Sugino,A. (1988) New yeast-*Escherichia coli* shuttle vectors constructed with in vitro mutagenized yeast genes lacking six-base pair restriction sites. *Gene*, **74**, 527–534.

Functional characterization of the role of the N-terminal domain of the c/Nip1 subunit of eukaryotic initiation factor 3 (eIF3) in AUG recognition.

Karásková M.*, Gunišová S.*, Herrmannová A.*, Wagner S., Munzarová V., Valášek L.

J Biol Chem. 2012 Aug 17;287(34):28420-34. doi: 10.1074/jbc.M112.386656. Epub 2012 Jun 20.
PMID: 22718758;

*These authors contributed equally to this work

Translation initiation in eukaryotes starts with assembly of the 48S PIC near the 7-methylguanosine cap. The PIC then scans the 5'UTR of the mRNA until it recognizes the first AUG start codon. The start codon selection is a key step of translation initiation as it sets the reading frame for decoding. Initiation factors eIF1A, eIF1, eIF2 and eIF5 were identified previously as crucial for ensuring high fidelity of AUG recognition. In addition, eIF3 was also shown to participate in this process, probably by coordinating functions of other eIFs and by promoting their association with 40S subunits. In this respect, the c/NIP1-NTD seems to be especially important as it makes direct contacts with eIF1 and eIF5 and indirectly it also interacts with eIF2. Previously, the N-terminal 160 amino acids of c/NIP1 were subjected to the clustered 10-alanine mutagenesis and several regions (called boxes) were identified as important for the 43S PIC assembly and/or AUG selection.

Specific mutations that reduce the stringency of start codon recognition and allow increased utilization of near-cognate codons (UUG or AUU) produce the Sui$^-$ phenotype (suppressor of *i*nitiation codon mutation); mutations that affect formation of 43S PIC by reducing the rate of the TC recruitment produce Gcd$^-$ phenotype (general control derepressed).

In this study we investigated the dual role of the c/NIP1-NTD in TC recruitment and AUG selection. We randomly mutated the previously identified boxes using degenerate oligonucleotides and the fusion PCR technique. We constructed mutant libraries, screened them for Sui$^-$ and Gcd$^-$ phenotypes and isolated five mutants with strong defects. These mutants fell into three major classes that affect either TC recruitment, stringency of AUG recognition or both. We also pinpointed specific residues involved in these functions.

Furthermore, we determined the key binding sites for eIF5 and eIF1 within the c/NIP1-CTD. eIF5 binds to the extreme C-terminus of c/NIP1 (residues 1-45) and that this interaction is important for the PIC formation. eIF1 binds to the following region of

c/NIP1-CTD (residues 60-137) and impairment of this interaction results in reduced stringency of AUG selection.

⌘ *Author's Choice*

THE JOURNAL OF BIOLOGICAL CHEMISTRY VOL. 287, NO. 34, pp. 28420–28434, August 17, 2012

Functional Characterization of the Role of the N-terminal Domain of the c/Nip1 Subunit of Eukaryotic Initiation Factor 3 (eIF3) in AUG Recognition*

Received for publication, May 30, 2012, and in revised form, June 19, 2012 Published, JBC Papers in Press, June 20, 2012, DOI 10.1074/jbc.M112.386656

Martina Karásková[1], Stanislava Gunišová[1], Anna Herrmannová[1], Susan Wagner, Vanda Munzarová, and Leoš Shivaya Valášek[2]

From the Laboratory of Regulation of Gene Expression, Institute of Microbiology Academy of Sciences of the Czech Republic, Videnska 1083, Prague 4, 142 20, the Czech Republic

Background: AUG recognition is promoted by several initiation factors (eIFs).
Results: eIF5 interacts with the extreme N terminus of eIF3c/Nip1 to promote pre-initiation complex assembly, and eIF1 binds the region that immediately follows.
Conclusion: eIF1 binding to c/Nip1 is equally important for its 40 S ribosome recruitment and AUG selection.
Significance: Understanding start codon selection that sets the reading frame for decoding is key in gene expression studies.

In eukaryotes, for a protein to be synthesized, the 40 S subunit has to first scan the 5′-UTR of the mRNA until it has encountered the AUG start codon. Several initiation factors that ensure high fidelity of AUG recognition were identified previously, including eIF1A, eIF1, eIF2, and eIF5. In addition, eIF3 was proposed to coordinate their functions in this process as well as to promote their initial binding to 40 S subunits. Here we subjected several previously identified segments of the N-terminal domain (NTD) of the eIF3c/Nip1 subunit, which mediates eIF3 binding to eIF1 and eIF5, to semirandom mutagenesis to investigate the molecular mechanism of eIF3 involvement in these reactions. Three major classes of mutant substitutions or internal deletions were isolated that affect either the assembly of pre-initiation complexes (PICs), scanning for AUG, or both. We show that eIF5 binds to the extreme c/Nip1-NTD (residues 1–45) and that impairing this interaction predominantly affects the PIC formation. eIF1 interacts with the region (60–137) that immediately follows, and altering this contact deregulates AUG recognition. Together, our data indicate that binding of eIF1 to the c/Nip1-NTD is equally important for its initial recruitment to PICs and for its proper functioning in selecting the translational start site.

Translation is a fundamental process contributing to the regulation of gene expression, normal developmental processes, and occurrence of disease. It can be divided into initiation, elongation, termination, and ribosome recycling with the initiation phase serving as a target of the most regulatory pathways (for a review, see Ref. 1). Undoubtedly, the start codon selection is the key step of this phase and in fact of translation in general as it sets the reading frame for decoding. Initiation at an incorrect codon will produce a completely miscoded protein, wasting valuable resources of the cell and creating a potentially toxic peptide. In contrast to prokaryotic cells, the mRNAs of which posses a Shine-Dalgarno sequence that ensures a direct placement of the start codon into the ribosomal P-site, eukaryotic ribosomes have to search a 5′-untranslated region (UTR) of an mRNA for the start codon by a successive movement called scanning. During this process, ribosomes have to read and respond to a variety of integrated yet not well understood signals that orchestrate the AUG recognition. These signals originate from mutual molecular and functional interactions between mRNA and ribosomes with a number of proteins called eukaryotic translation initiation factors (eIFs) such as eIF1A, eIF1, eIF2 (in the form of the eIF2·Met-tRNA$_i^{Met}$·GTP ternary complex (TC)[3]), and eIF5.

Upon initial binding of the latter factors to the 40 S small ribosomal subunit stimulated by the multisubunit eIF3 complex, eIFs 1 and 1A serve to stabilize a specific conformation of the 40 S head relative to its body that opens the mRNA binding channel for mRNA recruitment to form the 48 S pre-initiation complex (PIC). That requires dissolving the latch formed by helices 18 and 34 of 18 S rRNA and establishing a new interaction between Rps3 and helix 16 (2). This so-called open/scanning-conducive conformation with the anticodon of Met-tRNA$_i^{Met}$ not fully engaged in the ribosomal P-site to prevent premature engagement with putative start codons is then maintained during scanning for the AUG start codon in an ATP-dependent process (for reviews, see Refs. 3 and 4). During this search, eIF2 partially hydrolyzes its GTP with the help of the GTPase accelerating factor eIF5. Prior to start codon recognition, the "gate-keeping" function of eIF1 prevents the release of the resultant phosphate ion producing both GTP- and GDP·P$_i$-bound states of the factor possibly in equilibrium (5). Encoun-

* This research was supported by The Wellcome Trust Grants 076456/Z/05/Z and 090812/B/09/Z and Czech Science Foundation Grant 305/10/0335.
⌘ *Author's Choice*—Final version full access.
[1] These authors contributed equally to this work.
[2] To whom correspondence should be addressed. Tel.: 420-241-062-288; Fax: 420-241-062-665; E-mail: valasekl@biomed.cas.cz.

[3] The abbreviations used are: TC, ternary complex; NTD, N-terminal domain; PIC, pre-initiation complex; MFC, multifactor complex; CTD, C-terminal domain; SD, synthetic defined medium; YPD, yeast extract-peptone-dextrose medium; WCE, whole-cell extract; 3-AT, 3-aminotriazole; uORF, upstream ORF; sc, single copy; hc, high copy.

ter of the AUG start codon induces a reciprocal conformational switch of the 48 S PIC to the closed/scanning-arrested form stabilized by a functional interaction between eIF1A and eIF5 (6) with the initiator Met-tRNA fully accommodated in the P-site (7). This irreversible reaction serves as the decisive step in stalling the entire machinery at the AUG start codon and is triggered by displacement or dissociation of eIF1 (8) possibly promoted by eIF1A and eIF5 and subsequent release of free P_i. In short, eIF1 and eIF1A (via its C-terminal tail) antagonize the codon-anticodon interactions in the P-site by blocking the full accommodation of initiator tRNA in the P-site in a manner that is overcome efficiently by the action of the N-terminal tail of eIF1A and eIF5 upon establishment of a perfect AUG-anticodon duplex in an optimal AUG context (for reviews, see Refs. 3 and 4).

Specific mutations that reduce the stringency of start codon recognition in budding yeast, allowing increased utilization of near-cognate codons (UUG or AUU), produce the Sui$^-$ phenotype (suppressor of initiation codon mutation). Mutations with the opposite effect of lowering UUG initiation in the presence of a given Sui$^-$ mutation impart the Ssu$^-$ phenotype (suppressor of Sui$^-$). Defects in AUG selection can also be identified by measuring the efficiency of initiation at the AUG of uORF1 in *GCN4* mRNA in a well established *in vivo GCN4-lacZ* reporter system (for example, see Refs. 9 and 10).

Besides the aforementioned factors, there is an increasing number of reports suggesting that the multifunctional eIF3 complex also significantly contributes to the regulation of AUG recognition (9–13). First of all, yeast eIF3 plays a critical role in productive mRNA recruitment (14, 15) and directly interacts with mRNA (16–18), suggesting that the way the mRNA interacts with the mRNA binding channel during scanning for AUG can be influenced by eIF3. In addition, yeast eIF3 is composed of six subunits (a/Tif32, b/Prt1, c/Nip1, i/Tif34, g/Tif35, and j/Hcr1), two of which directly interact with eIF1, TC, or eIF5 in the multifactor complex (MFC) (Fig. 1) (for a review, see Ref. 4). Particularly intriguing in this respect is the N-terminal domain (NTD) of c/Nip1 that makes direct contacts with eIFs 1 and 5 and via the latter also associates with the TC (19, 20). Indeed, several important segments (designated as Boxes) within the c/Nip1-NTD were identified previously; mutations of these segments impaired stringency of the start codon selection and produced either Sui$^-$ or Ssu$^-$ phenotypes in a manner intensified or suppressible by increased gene dosage of eIF5 or eIF1 (11). As could be expected, some of the identified mutations also affected assembly of the PICs. Furthermore, increased frequency of skipping the AUG of uORF1 in the *GCN4-lacZ* reporter (a leaky scanning phenotype) was observed with mutations disrupting the web of mutual interactions among the members of an eIF3 module composed of the RNA recognition motif in the NTD of b/Prt1 and j/Hcr1 and the C-terminal domain (CTD) of a/Tif32 (Fig. 1) (9, 10). The robust leaky scanning phenotype also accompanies perturbed interactions within the other eIF3 module formed by the extreme CTD of b/Prt1 and by i/Tif34 and g/Tif35 (Fig. 1) (13). Interestingly, both modules are thought to reside near the 40 S mRNA entry channel with g/Tif35 and the a/Tif32-CTD directly interacting with the Rps3 "latch" component (9, 10). Based on these observations, we recently proposed that the scaffold b/Prt1 subunit serves to connect both eIF3 modules at each of its termini to work together with c/Nip1 and other eIFs to fine-tune the AUG selection process (13).

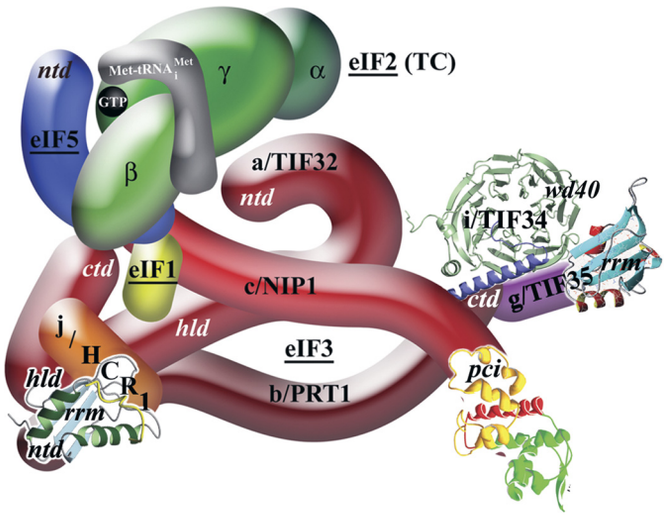

FIGURE 1. **A three-dimensional model of eIF3 and its associated eIFs in the MFC (adapted from Ref. 13).** *ntd*, N-terminal domain; *ctd*, C-terminal domain; *hld*, Hcr1-like domain; *rrm*, RNA recognition motif; *pci*, PCI domain. The NMR structure of the interaction between the RNA recognition motif of human eIF3b (*green* and *light blue*) and the N-terminal peptide of human eIF3j (*yellow*) (9), the NMR structure of the C-terminal RNA recognition motif of human eIF3g (*red* and *sky blue*) (18), the x-ray structure of the yeast i/Tif34·b/Prt1-CTD complex (13), and the three-dimensional homology model of the c/Nip1-CTD (31) were used to replace the original schematic representations of the corresponding molecules.

In this study, we subjected the aforementioned segments of the c/Nip1-NTD to semirandom mutagenesis to pinpoint critical residues that either promote the assembly of PICs (by screening for the Gcd$^-$ (general control derepressed) phenotype) or more importantly ensure stringent selection of the AUG start codon (by screening for the Sui$^-$ phenotype). Strikingly, we were able to separate the effects of distinct amino acid substitutions within a short 8-residue segment on the manifestation of either of the latter phenotypes, suggesting that the c/Nip1-NTD promotes both initiation reactions independently of each other at least to a certain degree. Based on our findings, we propose a model suggesting that not only the productive recruitment of eIF1 to 40 S ribosomes but also its proper functioning during the AUG recognition process depends on its contact with the stretch of amino acid residues 60–137 of the c/Nip1-NTD.

EXPERIMENTAL PROCEDURES

Construction of Yeast Strains and Plasmids—HMJ04 and HMJ06 were generated by introducing YCpMJ-MET-Nip1-W into HLV04 and HKN06 (11), respectively. The original pNIP1$^+$ (*c/NIP1 URA3*) covering plasmid was evicted on SD plates containing 5-fluoro-orotic acid.

To create HMJ08, H2880 (21) was first transformed with YCpNIP1-His-L to cover for the deletion of *NIP1* that was made in the next step by introducing the SacI-SphI fragment carrying the *nip1*Δ::*hisG-URA3-hisG* integration cassette from pLV10 (11). The uracil auxotrophy was regained by growing the cells on SD plates containing 5-fluoro-orotic acid. The resulting

TABLE 1
Yeast strains used in this study

Strain	Genotype	Source or Ref.
HMJ04	*MATα trp1 leu2-3,–112 ura3-52 his4-303*[*ATT*] *SUI1 nip1*Δ *GCN2* YCpMJ-Met-NIP1-W (*MET3-NIP1 TRP1*)	This study
HMJ06	*MATa trp1 leu2-3,–112 ura3-52 nip1*Δ *gcn2*Δ YCpMJ-Met-NIP1-W (*MET3-NIP1 TRP1*)	This study
HMJ08	*MATa, trp1 leu2-3,–112 ura3-52 nip1*Δ YCpNIP1-His-U (*NIP1-His URA3*)	This study
HLV04	*MATα trp1 leu2-3,–112 ura3-52 his4-303*[*ATT*] *SUI1 nip1*Δ *GCN2* pNIP1$^+$ (*NIP1 URA3*)	11
HKN06	*MATa trp1 leu2-3,–112 ura3-52 nip1*Δ *gcn2*Δ pNIP1$^+$ (*NIP1 URA3*)	11
TD301-8D	*MATα leu2-3,–112 ura3-52 his4-303*[*ATT*] *sui1-1*	11
H2880	*MAT*a *trp1 leu2-3,–112 ura3-52*	21
H2881	*MAT*a *trp1 leu2-3,–112 ura3-52 gcn2*Δ	21

strain was subsequently transformed with YCpNIP1-His-U, and the leucine auxotrophy was regained by growing the cells in liquid medium containing leucine and selecting for those that lost the YCpNIP1-His-L plasmid on SD ± leucine plates producing HMJ08.

YCpMJ-MET-NIP1-W was constructed by inserting the 2618-bp BamHI-HindIII fragment from pGAD-NIP1 (22) into YCplac22MET-W (23) digested by BamHI-HindIII.

YCpNIP1-Box12-WW was made by fusion PCR using the template YCpNIP1-His-L and two sets of primers (JKNIP1Mut and MJreversV111WV112W; LV22ext and MJ111WW) in the first PCR. The PCR products thus obtained were mixed in 1:1 ratio, and the second PCR was performed using primers JKNIP1Mut and LV22ext. The resulting PCR product (631 bp) was cut with AvaI-XbaI and inserted into AvaI-XbaI-digested YCpNIP1-His-help3 (11).

The following plasmids were created essentially the same as those described above with the exception of the primer sets (containing the degenerate oligonucleotides) that were used in the first PCRs: YCpNIP1-Box12-SPW (JKNIP1Mut and LV12C-1XR; LV22ext and LVBOX12C-1X), YCpNIP1-Box12-WWPW (JKNIP1Mut and LV12C-3XR; LV22ext and LVBOX12C-3X), YCpNIP1-GAP^{85} (JKNIP1Mut and LV12C-2XR; LV22ext and LVBOX12C-2X), YCpNIP1-GAP^{92} (JKNIP1Mut and LV12C-4XR; LV22ext and LVBOX12C-4X), and YCpNIP1-Box15-2 (JKNIP1Mut and LV15C-2XR; LV22ext and LVBOX15C-2X).

YEpNIP1-GAP^{85}, -GAP^{92}, and -Box15-2 were constructed by inserting the 2887-bp HindIII-PstI fragments from the corresponding single copy plasmids described above into YEplac181 digested with HindIII-PstI. pT7-NIP1-N270, pT7-NIP1-N-Box12-SPW, pT7-NIP1-N-Box12-WWPW, pT7-NIP1-N-Box12-WW, pT7-NIP1-N-Box15-2, pT7-NIP1-N-GAP^{85}, and pT7-NIP1-N-GAP^{92} were all made by inserting the NdeI-HindIII-digested PCR product obtained with primers JKNIP1Mut and LVRN270 using the templates YCpNIP1-His-L, YCpNIP1-Box12-SPW, YCpNIP1-Box12-WWPW, YCpNIP1-Box12-WW, YEpNIP1-Box15-2, YEpNIP1-GAP^{85}, and YEpNIP1-GAP^{92}, respectively, into NdeI-HindIII-digested pT7-7.

pT7-NIP1-N-Δ46/137 and pT7-NIP1-N-Δ60 were created by inserting the NdeI-BamHI-digested PCR product obtained using the template YCpNIP1-His-L and the set of primers MJNIP1_46–137 and MJNIP1_46–137rev or MJNIP1_61–205 and MJNIP1_61–205rev, respectively, into NdeI-BamHI-digested pT7-7. Lists of all yeast strains and plasmids can be found in Tables 1 and 2, respectively; a list of all PCR primers will be provided upon request.

Yeast Biochemical Methods—GST pulldown experiments with GST fusions and *in vitro* synthesized ^{35}S-labeled polypeptides (see Table 2 for vector descriptions) were conducted as described in Fig. 5. Ni^{2+} chelation chromatography of eIF3 complexes containing His_8-tagged c/Nip1 from yeast whole-cell extracts (WCEs) and Western blot analysis were conducted as described in detail previously (24). In short, WCEs were incubated at 4 °C overnight with 15 μl of 50% Ni^{2+}-Sepharose 6 Fast Flow (GE Healthcare) suspended in 300 μl of buffer A (20 mM Tris-HCl (pH 7.5), 100 mM KCl, 5 mM $MgCl_2$, 0.5 mM β-mercaptoethanol, 1 mM phenylmethylsulfonyl fluoride, 20 mM imidazole, 10% (v/v) glycerol, 1 EDTA-free complete Protease Inhibitor Mix tablets (Roche)) followed by washing and elution. Polysome profile analysis and 2% HCHO cross-linking followed by WCE preparation and fractionation of extracts for analysis of pre-initiation complexes were carried out as described previously (24). β-Galactosidase assays were conducted as described (25).

RESULTS

Semirandom Mutagenesis of the Selected Segments of the N-terminal Domain of the c/Nip1 Subunit of eIF3—The c/Nip1-NTD mediates eIF3 interactions with eIFs 1 and 5 and indirectly with eIF2 (20). By subjecting the N-terminal 160 amino acids of c/Nip1 to the clustered 10-alanine mutagenesis, we showed previously that these c/Nip1 interactions stimulate the assembly of the 43 S PICs and somehow coordinate the functions of eIF1 and eIF5 in stringent AUG selection (11). To understand the molecular mechanism of the c/Nip1 involvement in these functions and also to identify specific residues that are critical for them, we randomly mutated selected groups of conserved residues within the previously identified clustered 10-alanine mutagenesis c/nip1-Box mutations 6R, 12, and 15 (Fig. 2*A*) (20) using degenerate oligonucleotides and the fusion PCR technique. Degenerate oligonucleotides were designed to substitute a given group of amino acid residues with degenerate codons NNN where the N nucleotide was synthesized with a mixture of A, C, G, and T, each at 25% of the total. This way we constructed nine mutant libraries containing random amino acid residues at selected sites within each group derived from the latter three Boxes (Fig. 2*A*). These mutant libraries were then separately introduced into two different yeast strains (both deleted for chromosomal *NIP1* and carrying a wild-type (WT) *NIP1* allele under the control of *MET3* promoter) and screened for the Sui^- and Gcd^- phenotypes indicative of a relaxed stringency of AUG recognition (strain HMJ04) or of a defect in 43 S PIC assembly (strain HMJ06), respectively, in the

TABLE 2
Plasmids used in this study

Plasmid	Description	Source of Ref.
YCplac111	Single copy cloning vector, *LEU2*	43
YEplac181	High copy cloning vector, *LEU2*	43
YEplac195	High copy cloning vector, *URA3*	43
YCplac22MET-W	Single copy cloning vector with conditional *MET3* promoter, *TRP1* plasmid from YCplac22	K. Nasmyth
YCpMJ-MET-NIP1-W	Single copy *NIP1* under *MET3* promoter, *TRP1* plasmid from YCplac22	This study
YCpNIP1-His-U	Single copy *NIP1-His*, *Ura3* plasmid from YCplac33	20
YEpNIP1-His-U	High copy *NIP1-His*, *Ura3* plasmid from YEplac195	20
YCpNIP1-His-L	Single copy *NIP1-His*, *Leu2* plasmid from YCplac111	20
YEpNIP1-His-L	High copy *NIP1-His*, *Ura3* plasmid from YEplac181	20
YCpNIP1-Box12-SPW	Single copy *NIP1-His* containing K113S/K116P/K118W substitutions in Box12, *LEU2* plasmid from YCplac111	This study
YCpNIP1-Box12-WWPW	Single copy *NIP1-His* containing V111W/V112W/K116P K118W substitutions in Box12, *LEU2* plasmid from YCplac111	This study
YCpNIP1-Box12-WW	Single copy *NIP1-His* containing V111W/V112W substitutions in Box12, *LEU2* plasmid from YCplac111	This study
YCpNIP1-GAP^{85}	Single copy *NIP1-His* containing deletion of 85 residues (Val^{60}-Asn^{144}), *LEU2* plasmid from YCplac111	This study
YCpNIP1-GAP^{92}	Single copy *NIP1-His* containing deletion of 92 residues (Asp^{46}-Asn^{137}), *LEU2* plasmid from YCplac111	This study
YCpNIP1-Box15-2	Single copy *NIP1-His* containing I142V/E145W/F146T/D147L/I149R substitutions in Box15, *LEU2* plasmid from YCplac111	This study
YEpNIP1-GAP^{85}	High copy *NIP1-His* containing deletion of 85 residues (Val^{60}-Asn^{144}), *LEU2* plasmid from YEplac181	This study
YEpNIP1-GAP^{92}	High copy *NIP1-His* containing deletion of 92 residues (Asp^{46}-Asn^{137}), *LEU2* plasmid from YEplac181	This study
YEpNIP1-Box15-2	High copy *NIP1-His* containing I142V/E145W/F146T/D147L/I149R substitutions in Box15, *LEU2* plasmid from YEplac181	This study
pLV10	*nip1*Δ::*hisG*::*URA3*::*hisG* (*NIP1* disruption *hisG* cassette)	11
p367	Low copy *URA3* vector containing *HIS4-ATG-lacZ* fusion	44
p391	Low copy *URA3* vector containing *HIS4-TTG-lacZ* fusion	44
P2041	Low copy *URA3* vector containing *HIS4-ATT-lacZ* fusion, 3rd codon replaced with *TTA*	44
p180 (YCp50-GCN4-lacZ)	Low copy *URA3* vector containing wild-type *GCN4* leader	45
YEpTIF5-U	High copy *TIF5-FLAG*, *URA3* plasmid from YEplac195	11
YEpSUI1-U	High copy *SUI1*, *URA3* plasmid from YEplac195	11
p1780-IMT	High copy *SUI2*, *SUI3*, *GCD11*, *IMT4*, *URA3* plasmid from YEp24	30
pGEX-TIF5	*GST-TIF5* fusion plasmid from pGEX-4T-1	46
pGEX-SUI1	*GST-SUI1* fusion plasmid from pGEX-5X-3	11
pT7-NIP1-N270	*NIP1* (1–270) ORF under T7 promoter	This study
pT7-NIP1-N-Box12-SPW	*NIP1* (1–270) ORF containing K113S/K116P K118W substitutions in Box12 under T7 promoter	This study
pT7-NIP1-N-Box12-WWPW	*NIP1* (1–270) ORF containing V111W/V112W/K116P/K118W substitutions in Box12 under T7 promoter	This study
pT7-NIP1-N-Box12-WW	*NIP1* (1–270) ORF containing V111W V112W substitutions in Box12 under T7 promoter	This study
pT7-NIP1-N-GAP^{85}	*NIP1* (1–270) ORF containing deletion of 85 residues (Val^{60}-Asn^{144}) under T7 promoter	This study
pT7-NIP1-N-GAP^{92}	*NIP1* (1–270) ORF containing deletion of 92 residues (Asp^{46}-Asn^{137} under T7 promoter	This study
pT7-NIP1-N-Box15-2	*NIP1* (1–270) ORF containing I142V/E145W/F146T/D147L/I149R substitutions in Box15 under T7 promoter	This study
pT7-NIP1-N-Δ46/137	*NIP1* ORF (amino acid residues 46–137) under T7 promoter	This study
pT7-NIP1-N-Δ60	*NIP1* ORF (amino acid residues 61–205) under T7 promoter	This study

presence of methionine, which shuts off expression of the WT gene.

Mutations that relax the stringency of translational start site selection in yeast (so-called Sui$^-$ mutations) were isolated by selecting for growth on medium lacking histidine in a *his4-303* genetic background where the start codon of the *HIS4* gene has been mutated and instead its third coding triplet (UUG) is used to initiate *HIS4* translation (26). In other words, such mutations suppress histidine auxotrophy of the WT *his4-303* cells, turning their His$^-$ into a His$^+$ phenotype. Mutations that affect formation of 43 S PICs by reducing the rate of the TC recruitment (so called Gcd$^-$ mutations) were isolated by their ability to constitutively derepress *GCN4* translation in cells lacking the kinase Gcn2, which makes them resistant to the inhibitor of histidine biosynthesis, 3-aminotriazole (3-AT). Gcn4 is a transcriptional activator of amino acid biosynthetic genes whose expression is under tight translational control via four short upstream ORFs (uORFs) occurring in its leader mRNA. The *gcn2*Δ cells in which translational activation of *GCN4* is eliminated fail to grow on 3-AT-containing medium (for more details, see Ref. 27).

Approximately 10,000 clones from each library were screened individually for the His$^+$ and 3-AT^{Res} phenotypes. Altogether, five mutants with strong phenotypes were isolated, two of which fall in the Box12 group and one that falls in the Box15 group (Fig. 2*B*). In addition to those, a few other mutations in the latter Boxes were also identified; however, given their less pronounced phenotypes, we did not characterize them any further. Similarly, no mutations with strong phenotypes were found in the Box6R group; hence, we stopped working with this group at this point. Although not programmed intentionally, two large internal deletions of 85 (GAP^{85}) and 92 (GAP^{92}) residues impinging into the region between Asp^{46} and Asn^{144} of the c/Nip1-NTD also resulted from this mutagenic procedure (Fig. 2*B*). All mutant phenotypes were corroborated to be plasmid-born by retransformation of isolated plasmid DNAs into the *nip1*Δ strains carrying the WT *NIP1 URA3* covering plasmid that was subsequently evicted by plasmid shuffling. As shown in Fig. 2, *C* and *D* (summarized in Fig. 2*B*), three major classes of mutant substitutions were identified, imparting either (*a*) only the Sui$^-$ phenotype (c/nip1-Box12-SPW (Fig. 2*C*, *lane 3*)), (*b*) only the Gcd$^-$ phenotype (c/nip1-Box15-2 (Fig. 2*D*, *lane 7*)), or (*c*) both combined (c/nip1-Box12-WWPW and both GAP mutants (Fig. 2, *C* and *D*, *lanes 4–6*, respectively)). All of these mutations also resulted in a slow growth (Slg$^-$) phenotype of different strengths as illustrated by their varying effects on translation initiation rates estimated by measuring the polysome:monosome ratios (summarized in Fig. 2*B*).

Our finding that no Sui$^-$ mutations were detected in the Box15 group is consistent with the fact that the original c/nip1-Box15 also displayed only the Gcd$^-$ phenotype (11). In con-

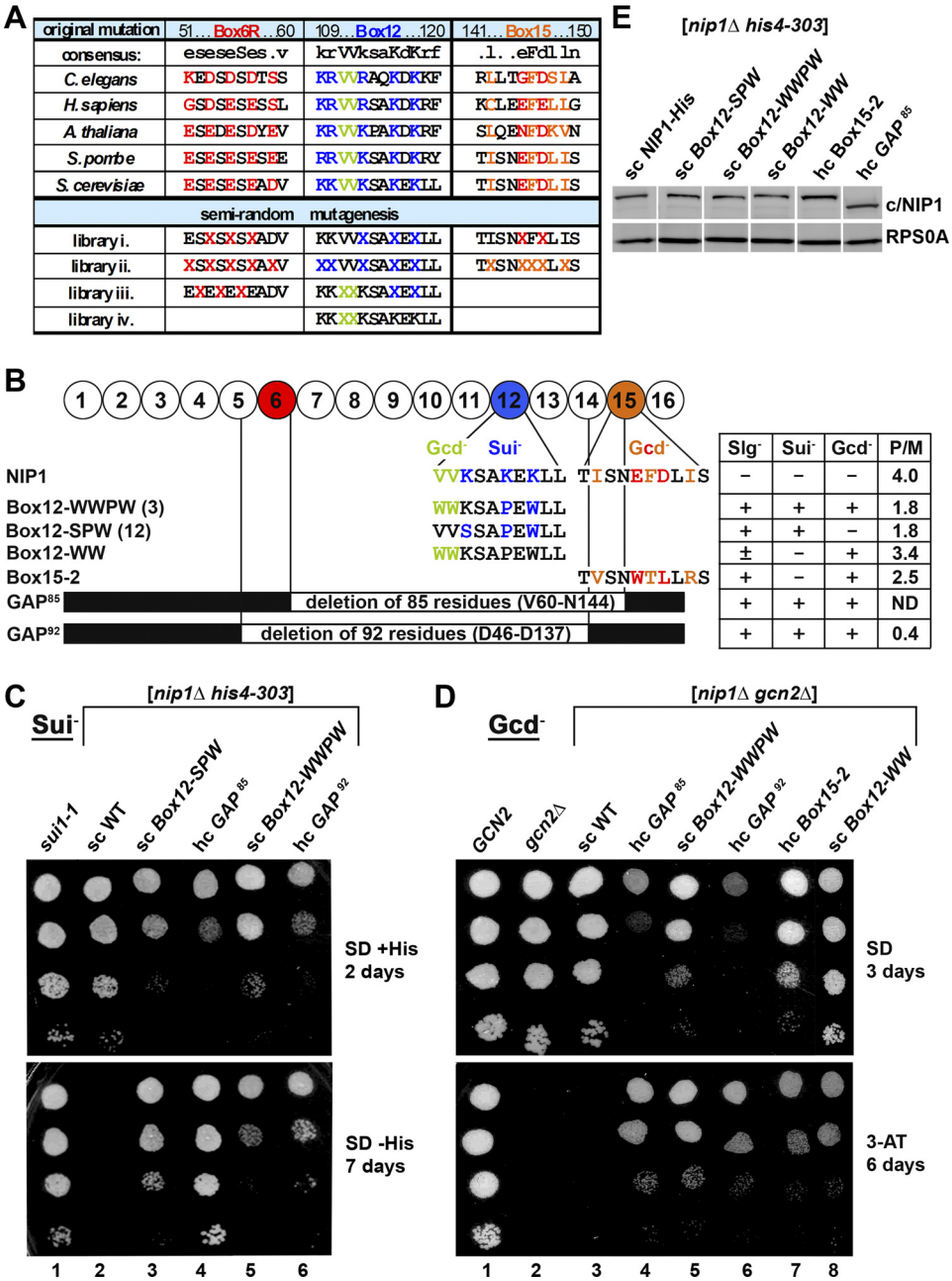

FIGURE 2. **Semirandom mutagenesis of the preselected segments (Boxes) of the extreme NTD of c/Nip1 yields mutants displaying either Sui$^-$ or Gcd$^-$ phenotypes alone or in combination.** *A*, amino acid sequence alignment of the Boxes of interest from the c/Nip1-NTD of *Saccharomyces cerevisiae* with that of other species. The amino acid sequence of *S. cerevisiae* c/Nip1 (accession number P32497.2 UniProtKB/Swiss-Prot) between residues 1 and 160 was aligned with its *Caenorhabditis elegans* (accession number A8WWU0.1 UniProtKB/Swiss-Prot), *Homo sapiens* (accession number Q99613.1 UniProtKB/Swiss-Prot), *Arabidopsis thaliana* (accession number AAC83464.1 GenBank), and *Schizosaccharomyces pombe* (accession number CAB11485.2 GenBank) homologues using ClustalW; only the sequences corresponding to the Boxes of interest are shown. Highly conserved residues are color-coded. Altogether, nine mutant libraries containing random amino acid residues at selected, color-coded sites marked with "*X*" and grouped together individually for each Box are indicated. *B*, schematic representation of the first 160 amino acid residues of c/Nip1 shown as *numbered circles* (Boxes 1–16), each of which is composed of 10 consecutive residues. Three Boxes of interest are color-coded, and the sequences and phenotypes of the mutants derived from the semirandom mutagenesis are given below the schematic. Two internal deletions that were unintentionally generated by this mutagenic procedure are also shown with the deleted residues indicated. A table to the *right* of the schematic summarizes phenotypes associated with individual mutations including Slg$^-$, Sui$^-$, Gcd$^-$, and the polysome/monosome (*P/M*) ratios (averaged values of replicate experiments are given; S.E. values ranged between 5 and 15% and are not shown). *C*, the c/Nip1 mutants producing the Sui$^-$ phenotype indicative of a defect in AUG recognition. The HLV04 (*nip1Δ his4-303*) strain was transformed with the corresponding sc or hc plasmids carrying WT *NIP1* and its mutant alleles, and the resident pNIP1$^+$ (*NIP1, URA3*) covering plasmid was evicted on 5-fluoro-orotic acid. The resulting strains and the parental control strain TD301-8D (*NIP1 sui1-1 his4-303*) were then spotted in four serial 10-fold dilutions on SD medium containing histidine (*upper panel*) or lacking histidine (*lower panel*) and incubated at 30 °C for 2 (*upper panel*) or 7 days (*lower panel*). *D*, the c/Nip1 mutants producing the Gcd$^-$ phenotype indicative of a defect in the assembly of the PICs. The HKN06 (*nip1Δ gcn2Δ*) strain was transformed with the corresponding sc or hc plasmids carrying WT *NIP1* and its mutant alleles, and the resident pNIP1$^+$ (*NIP1, URA3*) covering plasmid was evicted on 5-fluoro-orotic acid. The resulting transformants and isogenic strains H2880 (*GCN2*) (*lane 1*) and H2881 (*gcn2Δ*) (*lane 2*) transformed with empty vector were spotted in four serial dilutions on SD (*upper panel*) or SD medium containing 30 mM 3-AT (*lower panel*) and incubated at 30 °C for 3 and 6 days, respectively. *E*, Western blot analysis of the WCEs derived from the indicated strains described in *C* using antibodies raised against c/Nip1 and Rps0A.

trast, whereas the original c/nip1-Box12 mutation produced merely the mild Sui$^-$ phenotype, our semirandom substitutions of Box12 impart strong Sui$^-$ as well as Gcd$^-$ phenotypes. Perhaps the most striking observation, however, is the fact that whereas the deletion of the first 160 residues is lethal (11) the internal deletions of 84 or 91 residues are not lethal and resulted "only" in severe Slg$^-$, Sui$^-$, and Gcd$^-$ phenotypes. Because the protein levels of Box15-2 and both GAP mutants in a single copy (sc) number were found partially reduced when compared with those of the WT c/Nip1, we generated high copy number versions of these three alleles. High copy (hc) expression increased their protein levels by ~2-fold and more or less matched the sc expression of the WT c/Nip1 (Fig. 2*E*). Importantly, because there was no qualitative difference in the mutant phenotypes between the sc and hc expressions of the latter alleles (data not shown), we decided to use their hc versions throughout the rest of the study.

Dissection of Effects of the Specific c/Nip1-Box12 Residues on Phenotypes Indicating Impaired Formation of PICs Versus AUG Selection—We noted that substitution of three Box12 lysines (113, 116, and 118) by Ser, Pro, and Trp in c/nip1-Box12-SPW produced merely the Sui$^-$ phenotype, whereas substitution of two preceding highly conserved valines (111 and 112) by tryptophans in combination with K116P and K118W in c/nip1-Box12-WWPW produced both the Sui$^-$ and Gcd$^-$ phenotypes (Fig. 2, *B–D*). The fact that both mutants contain K116P and K118W substitutions might thus suggest that these two also highly conserved lysines specifically contribute to the stringency of AUG selection, whereas Val^{111} and Val^{112} participate in assembly of the PICs. To test that, we separated the V111W and V112W double substitution from K116P and K118W by producing two individual c/nip1-Box12-WW and c/nip1-Box12-PW mutant alleles, which were then tested for Sui$^-$ and Gcd$^-$ phenotypes as described above. Strikingly, in accord with our prediction, c/nip1-Box12-WW imparts the severe Gcd$^-$ phenotype but not Sui$^-$ (Fig. 2*D*, *lane 8*). At odds with our prediction, the c/nip1-Box12-PW mutant showed no apparent phenotype (data not shown). Thus, we propose that whereas the two consecutive valines (Val^{111} and Val^{112}) somehow promote recruitment of the TC to the small ribosomal subunit all three consecutive lysines (Lys^{113}, Lys^{116}, and Lys^{118}) are critically required for proper detection of the AUG start codon. In support, one of the "weaker" Box12 mutants that was isolated in our initial screen but not analyzed further carried substitutions of exactly these three lysines (K113Y, K116H, and K118H) and displayed the Sui$^-$ but not Gcd$^-$ phenotype (data not shown).

To demonstrate that the Sui$^-$ phenotype is indeed caused by increased selection of the UUG triplet as the start site and that our Sui$^-$ mutants increase initiation rates at near-cognate codons in general, we examined expression of matched *HIS4-lacZ* reporters containing UUG or AUU *versus* AUG start codons (Fig. 3*A*). Previously, we reported that the original c/nip1-Box12 10-Ala substitution increased the UUG/AUG and AUU/AUG initiation ratios by ~3- and 5-fold, respectively (11). In comparison, all three Sui$^-$ mutants (12-SPW, -WWPW, and GAP^{85}) generated here conferred a much more dramatic increase in the UUG/AUG initiation ratio (from 12- to 29-fold) and a similar increase in the AUU/AUG initiation ratio

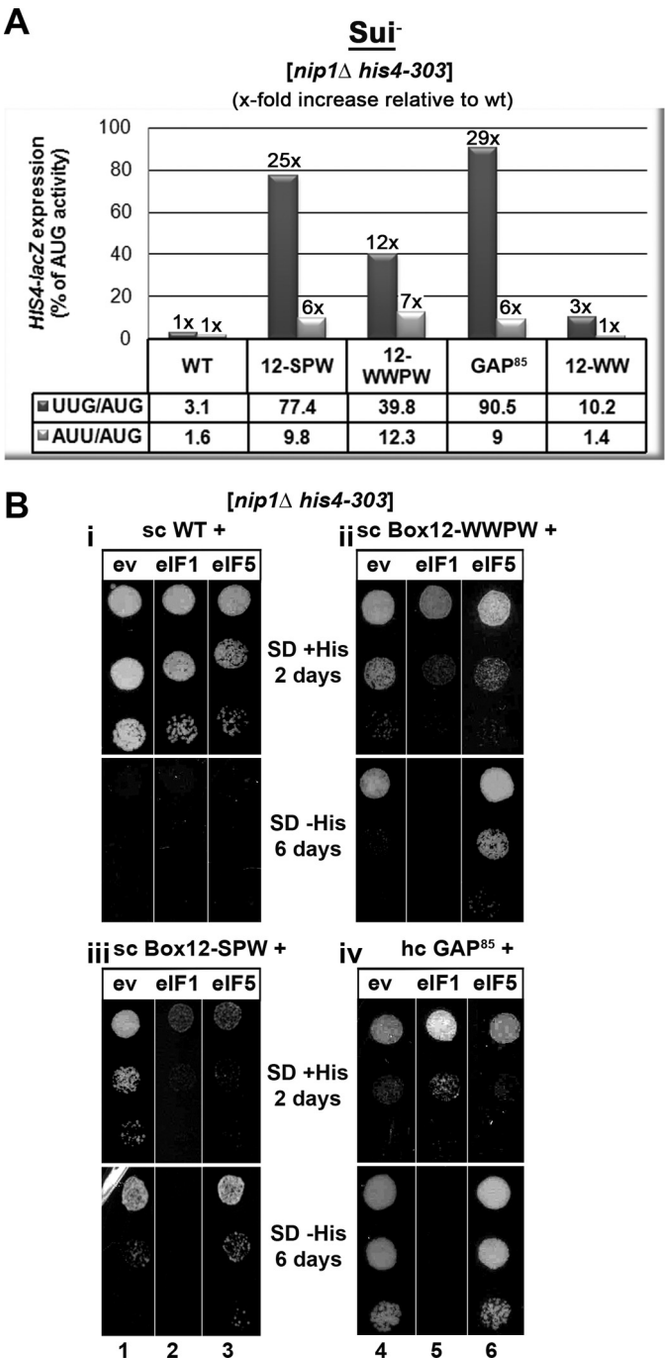

FIGURE 3. **High dosage suppressor analysis of the c/Nip1-NTD Sui$^-$ mutants by the selected eIFs known to participate in the AUG recognition process.** *A*, quantification of Sui$^-$ phenotypes. Strains from Fig. 2*C* were transformed with *HIS4-lacZ* reporters with AUG (p367), UUG (p391), or AUU (p2042), respectively, and grown in SD medium supplemented with His and Trp at 30 °C, and β-galactosidase activities were measured in WCEs. The mean percentages of the UUG or AUU initiation rates relative to those of AUG and an *x*-fold increase over the WT c/Nip1 were calculated from three experiments with six independent transformants. *B*, genetic effects of high copy expression of the indicated eIFs on selected Sui$^-$ mutants of c/Nip1. Strains from Fig. 2*C* were transformed with either empty vector (*ev*; *lanes 1* and *4*) or the corresponding plasmids overexpressing *SUI1* (*eIF1*; *lanes 2* and *5*) or *TIF5* (*eIF5*; *lanes 3* and *6*), respectively, and the resulting transformants were spotted in three serial dilutions on SD medium containing histidine (*upper panels i* and *ii*) or lacking histidine (*lower panels iii* and *iv*) and incubated at 30 °C for 2 (*upper panels i* and *ii*) or 6 days (*lower panels iii* and *iv*).

(~6-fold), indicating a strong preference for selecting UUG over the AUU as the false start site. As expected, the "Gcd$^-$-only" Box12-WW mutant showed little to no increase in both ratios.

High Dosage Suppressor Analysis of the c/Nip1-NTD Sui$^-$ Mutants by Selected eIFs Known to Participate in the AUG Recognition Process—We showed previously that the Sui$^-$ phenotype of the original *Box12* mutation was suppressed by overexpressing WT eIF1 despite the fact that at the same time its Slg$^-$ phenotype was exacerbated (11). In contrast, overproduction of eIF5 had an intensifying effect on both Sui$^-$ and Slg$^-$ phenotypes of *nip1-Box12*. To examine genetic interactions between our new Sui$^-$ mutants and these key players in the AUG recognition pathway, we transformed the *nip1-Box12* mutants and *nip1-GAP^{85}* with hc vectors overexpressing eIF1 or eIF5 and scored the resulting transformants for growth in the presence or absence of histidine (Fig. 3*B*).

In analogy with our original data, overexpressing eIF1 reduced the growth rate of both *Box12* mutants in the presence of histidine and suppressed their Sui$^-$ phenotype in its absence (Fig. 3*B*, *panels ii* and *iii*, *lanes 5* and *2*). Because the reduced growth rate of both mutants on His+ medium somewhat complicates our conclusion regarding the suppression of the Sui$^-$ defect, we measured the UUG/AUG and AUU/AUG ratios in *WWPW* and *SPW* mutants bearing either empty vector or hc eIF1. We found that overexpression of eIF1 reduced the latter ratios in the *SPW* mutant by ~44 and 40%, respectively, and in the *WWPW* mutant by ~30 and 33%, respectively. These findings clarify that the eIF1-mediated suppression is significant but not full. Interestingly, high dosage eIF1 also suppressed the Sui$^-$ phenotype of *nip1-GAP^{85}*; however, it did not worsen but improved its Slg$^-$ phenotype (*panel iv*, *lane 5*), indicating that in this particular mutant the eIF1 suppression effect is more potent. Overexpression of eIF5 surprisingly had no significant effect on the *GAP^{85}* mutant (*panel iv*, *lane 6*), whereas it exacerbated the Sui$^-$ but not Slg$^-$ phenotype of *Box12-WWPW* (*panel ii*, *lane 6*). It is worth reiterating that these two mutants are not only Sui$^-$ but also display the Gcd$^-$ phenotype, which may contribute to the observed genetic interactions that differ from the original "Sui$^-$-only" *Box12* mutant. Consistently, overexpressing eIF5 in the Sui$^-$-only *nip1-Box12-SPW* allele had an intensifying effect on both its Slg$^-$ and Sui$^-$ phenotypes (*panel iii*, *lane 3*). The intensifying effect on the Sui$^-$ phenotype is inferred from the fact that it reduced growth on His+ but not on His− medium. It should be mentioned that neither of these Sui$^-$ mutants conferred a significant Ssu$^-$ phenotype when combined with dominant negative Sui$^-$ alleles of eIF5 (in *SUI5^{G31R}*) or *SUI3* (a subunit of eIF2; in *SUI3^{S264Y}*) (data not shown). Taken together, it is evident that each of these three Sui$^-$ mutants impairs the AUG selection process in a more or less different way (see "Discussion").

The nip1-Box15-2, -Box12-WW, and -Box12-WWPW Mutants Affect Recruitment of the TC to the PICs in a Manner Partially Reversible by Overexpressing TC—The NTD of c/Nip1 indirectly interacts with the TC via their common binding partner eIF5 and thus promotes its recruitment to the 40 S ribosomes (11, 19, 20). As hinted above, an inability to recruit and/or stably anchor the TC to the PICs constitutively derepresses the otherwise tightly controlled expression of *GCN4* under non-starvation conditions, producing the Gcd$^-$ phenotype even in the absence of the Gcn2 kinase. Mutants having such a mechanistic defect in the *gcn2*Δ background are commonly characterized by having their Gcd$^-$ defect suppressible by overexpression of the TC as an increased cellular concentration of TC offsets the defect in its recruitment. The failure of hc TC to suppress the Gcd$^-$ phenotype suggests a more complex defect(s) in the *GCN4* regulation, the nature of which has not been understood so far.

To determine which of our newly generated *NIP1* mutants affect the TC loading to the PICs as the rate-limiting defect, we introduced them with either empty vector or hc TC and tested the resulting transformants for growth in the presence of 3-AT. As shown in Fig. 4*A*, hc TC significantly suppressed the Gcd$^-$ phenotypes of the *nip1-Box12-WW* and *-Box15-2* mutants and to a smaller degree perhaps that of *-Box12-WWPW* but not that of the *GAP^{85}* mutant, although it did partially suppress its slow growth defect. Importantly, increased TC dosage also suppressed, in fact almost fully, the Slg$^-$ phenotype of *Box15-2*, strongly indicating that the TC recruitment is the dominating defect in this mutant.

To quantify the Gcd$^-$ phenotypes of all Gcd$^-$ mutants and to confirm or exclude its suppression by hc TC in *WWPW* and *GAP^{85}*, we assayed expression of a *GCN4-lacZ* reporter containing all four uORFs in the mRNA leader under non-starvation conditions (Fig. 4*B*). As expected, the WT *gcn2*Δ *NIP1$^+$* strain showed constitutively low *GCN4-lacZ* expression irrespective of the presence of either empty vector or hc TC, whereas all four mutations bearing an empty vector displayed significantly increased derepression of *GCN4-lacZ* expression in the *gcn2*Δ background after normalizing for their effects on the expression of an incontrollable *GCN4-lacZ* construct lacking all four uORFs (Fig. 4*B*). These results thus confirm that all of our Gcd$^-$ mutants do diminish translational repression of *GCN4* imposed by its uORFs as expected. Measuring the β-galactosidase activities in the presence of hc TC also confirmed moderate (by ~30%) suppression of the *WWPW* Gcd$^-$ defect and no suppression of that displayed by the *GAP^{85}* mutant (Fig. 4*B*). Together, these results clearly imply that the impaired TC recruitment and thus the proper assembly of the PICs are to a varying degree one of the rate-limiting defects in all but one of our Gcd$^-$ mutants.

The Extreme N Terminus of c/Nip1 Interacts with eIF5, the Segment That Immediately Follows Binds eIF1, and nip1-Box12-SPW Increases Binding Affinity of the c/Nip1-NTD for eIF1 in Vitro—Having analyzed all newly generated mutations by genetic means, we next sought to investigate molecular effects of the semirandom substitutions as well as internal deletions of the c/Nip1-NTD on binding affinities toward its direct binding partners in eIF1 and eIF5. We began by examining the effects of both GAP deletions on *in vitro* binding of ^{35}S-labeled c/Nip1-NTD (residues 1–270) to GST-eIF5 or GST-eIF1 fusions produced in *Escherichia coli* (Fig. 5*A*). Although this assay is more qualitative than quantitative in its nature, it has been reliably used in the past to provide rough estimates of altered binding affinities of mutant proteins (for example, see Refs. 9–13, 20, 24, and 28–30). In agreement with previous results, the WT c/Nip1-NTD polypeptide bound specifically to

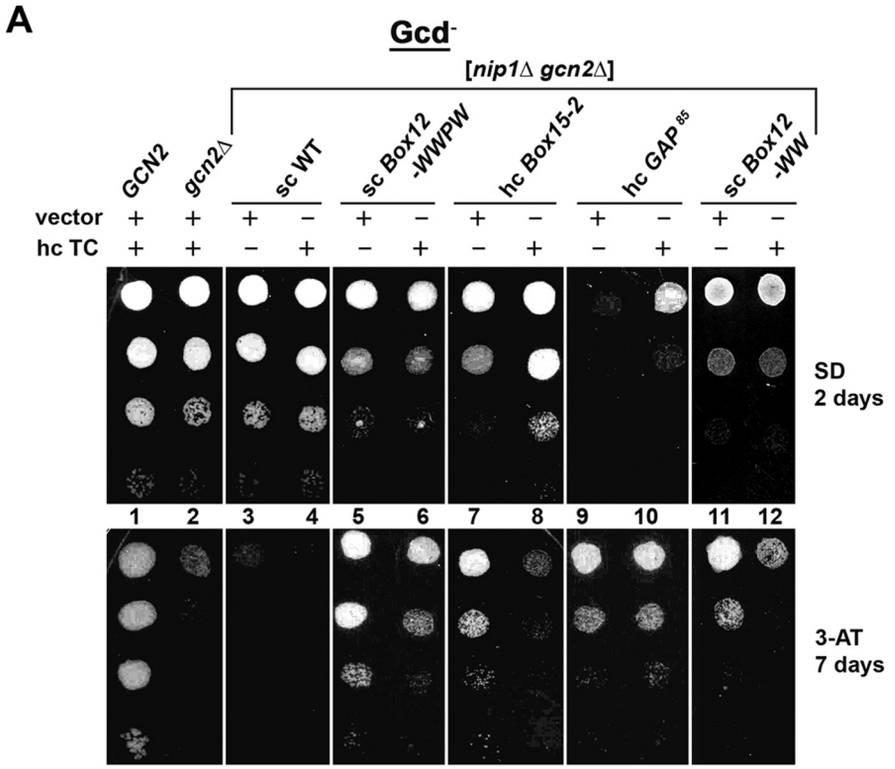

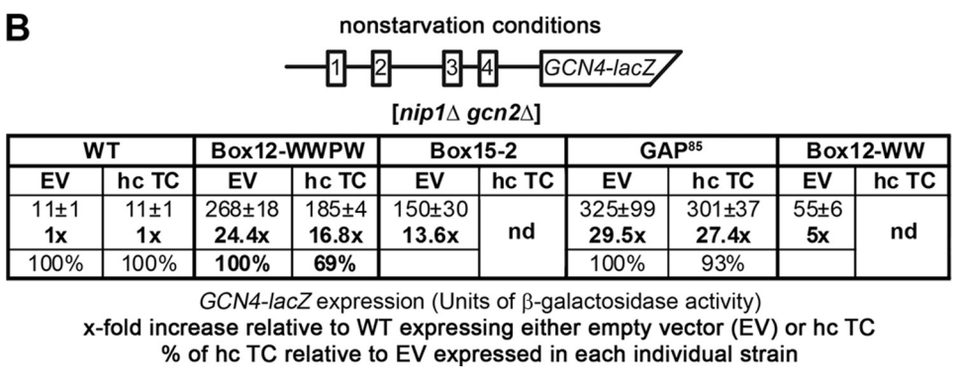

WT		Box12-WWPW		Box15-2		GAP85		Box12-WW	
EV	hc TC	EV	hc TC	EV	hc TC	EV	hc TC	EV	hc TC
11±1 **1x**	11±1 **1x**	268±18 **24.4x**	185±4 **16.8x**	150±30 **13.6x**	nd	325±99 **29.5x**	301±37 **27.4x**	55±6 **5x**	nd
100%	100%	**100%**	**69%**			100%	93%		

GCN4-lacZ expression (Units of β-galactosidase activity)
x-fold increase relative to WT expressing either empty vector (EV) or hc TC
% of hc TC relative to EV expressed in each individual strain

FIGURE 4. **The c/nip1-Boxes 12-WWPW, 12-WW, and 15-2 impair *GCN4* translational control (produce the Gcd⁻ phenotype) in the canonical manner suppressible by overexpressing the TC.** *A*, strains from Fig. 2*D* were transformed with either empty vector or all three subunits of eIF2 + *IMT4* (*TC*) on a high copy plasmid. The resulting transformants and isogenic strains H2880 (*GCN2*) and H2881 (*gcn2*Δ) transformed with empty vector were spotted in four serial dilutions on SD medium (*upper panel*) or SD medium containing 30 mM 3-AT (*lower panel*) and incubated at 30 °C for 2 and 7 days, respectively. *B*, quantification of the Gcd⁻ phenotypes with or without the hc TC effect. Selected *nip1*Δ strains from *A* were further transformed with p180 containing the *GCN4-lacZ* fusion with all four uORFs present (shown as a schematic above the plot) and grown in minimal medium for 6 h, and the β-galactosidase activities were measured in the WCEs and expressed in units of nmol of *o*-nitrophenyl-β-D-galactopyranoside hydrolyzed/min/mg of protein. The mean values and standard deviations obtained from at least six independent measurements with three independent transformants, the *x*-fold increases in activities of the mutant strains relative to the corresponding WT expressing either empty vector (*EV*) or hc TC, and percentages of hc TC activities relative to empty vector activities in each individual strain (indicating the extent of the hc TC suppression effect) are given in the histogram. *nd*, not done.

GST-eIF5 and GST-eIF1 but not to GST alone (Fig. 5*B*). Strikingly, both GAP deletions (Δ60–144 and Δ46–137) completely eliminated binding to eIF1 but not to eIF5 (*lane 3 versus lane 4*). In fact, binding to eIF5 was even strengthened perhaps because of the fact that the eIF5-binding site in the remaining c/Nip1 polypeptide was more ideally exposed for the interaction. In any case, given that the minimal c/Nip1 fragment required and sufficient for WT binding to both eIF1 and eIF5 is 156 residues (19), these results strongly suggest that the extreme N-terminal 45 residues constitute the binding site for eIF5, whereas the segment encompassing residues 60–137 represents the eIF1-binding site (Fig. 5*A*). In support, removal of the first 60 residues (in Δ60) or expressing the internal "GAP^{92}" segment (in Δ45/137) had the opposite effect; *i.e.* it eliminated binding to eIF5 but not to eIF1 (*lane 4 versus lane 3*). In an effort to directly demonstrate that the first 45 residues are sufficient for the interaction with eIF5, we created pT7 constructs expressing only the first 45 or 60 N-terminal residues of c/Nip1; however, they did not yield stable proteins. Taken together, these data suggest that the molecular nature of defects displayed by both GAPs is associated with the loss of eIF1 binding to the c/Nip1-NTD. This is consistent with the fact that hc eIF1 suppressed the Sui⁻ phenotype and partially suppressed Slg⁻ phenotype of GAP^{85} (Fig. 3*B*, *panel iv*). Further analysis of binding affinities

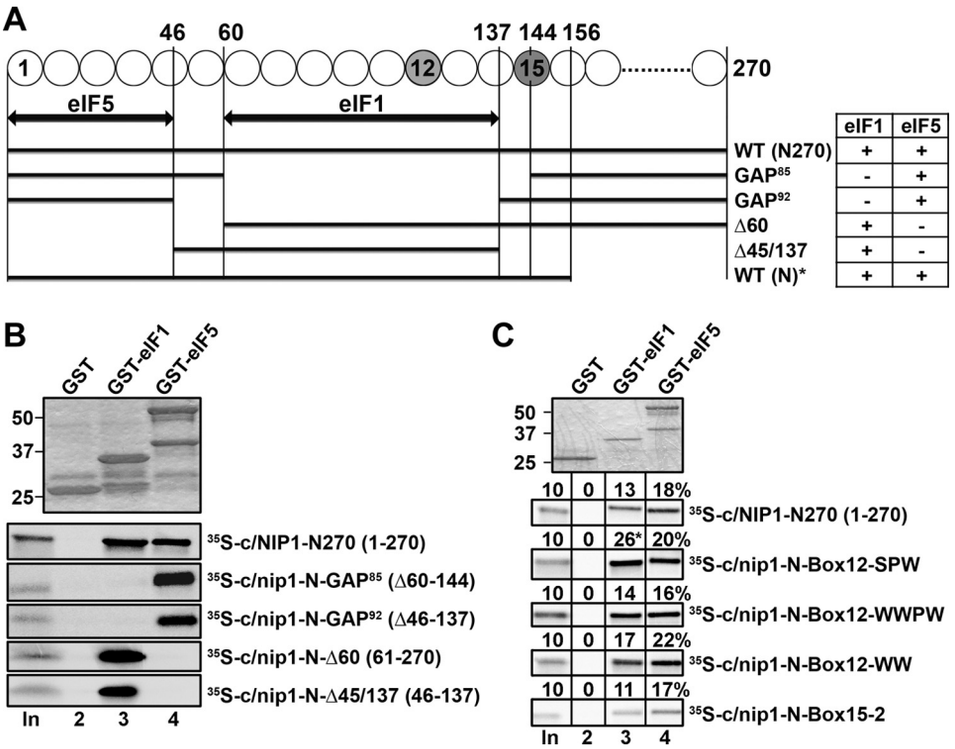

FIGURE 5. **The extreme N terminus of c/Nip1 interacts with eIF5, the segment that immediately follows binds eIF1, and *nip1-Box12-SPW* increases binding affinity of the c/Nip1-NTD for eIF1 *in vitro*.** *A*, schematic as in Fig. 2*B* showing the minimal binding segments (as *arrows*) of the c/Nip1-NTD for eIFs 1 and 5. The *lines* beneath the *arrows* depict the ^{35}S-labeled segments of the c/Nip1-NTD used in the binding assays of *B* with the amino acid end points and clone designations indicated. The binding of each c/Nip1 construct to GST-eIF1 or -eIF5 is summarized in the table on the *right*. Data from the WT (*(N)**) construct were taken from Ref. 19 for comparison purposes only. *B*, eIF1 and eIF5 fused to GST (*lanes 3* and *4*) or GST alone (*lane 2*) was expressed in *E. coli*, immobilized on glutathione-Sepharose beads, and incubated with the ^{35}S-labeled c/Nip1 segments indicated to the *right* of the *lower panels* at 4 °C for 2 h. The beads were washed three times with phosphate-buffered saline, and bound proteins were separated by SDS-PAGE. Gels were first stained with GelCode Blue Stain Reagent (Pierce) (*top panel*) followed by autoradiography (*bottom panels*). *Lane 1* shows 10% of the input (*In*) amounts. *C*, same as in *B* except that the semirandom mutations of c/Nip1-Boxes are under study. The amount of each ^{35}S-labeled c/Nip1 polypeptide bound to each GST fusion protein was quantified and is expressed above the corresponding panel as a percentage of the input (three independent measurements were made, and the outputs were averaged with the S.E. ranging between 3 and 11%).

of semirandom Box mutants did not reveal any specific changes with the exception of Box12-SPW, which showed a reproducible ~2-fold increase in binding to eIF1 (Fig. 5*C*, *third panel*, *lane 3* with *asterisk*) (see also below). Note that Box12 falls in the eIF1 binding region, whereas Box15 lies further downstream.

nip1-GAP^{85} Completely Diminishes Whereas nip1-Box12-SPW Modestly Increases the Amount of eIF1 Associated with the MFC in Vivo—To test whether our mutations affect binding of c/Nip1 to eIFs 1 and 5 and the TC in the context of the entire eIF3, we analyzed the *in vivo* composition of the MFC in cells expressing the individual His$_8$-tagged *NIP1* mutant alleles by Ni^{2+} chelation chromatography. As reported previously (11), a fraction of a/Tif32, i/Tif34, g/Tif35, eIF2, eIF5, and eIF1 co-purified specifically with WT c/Nip1-His but not with its untagged version (Fig. 6*A*, *lane 5 versus lane 2*). Although neither of the mutations affects the extreme N-terminal binding site for eIF5, *Box15-2* and *GAP^{85}* reduced *in vivo* association of mutant eIF3 with eIF5 by more than 60% (*lanes 17* and *20*). In addition, *Box12-WWPW* also lowered the eIF3 binding affinity for eIF5 but to a smaller extent (by ~30%) (*lane 11*). This is most probably an indirect effect arising from the overall changes of the c/Nip1-NTD fold in the context of the entire eIF3/MFC. As eIF5 mediates an indirect contact between eIF2 and the c/Nip1-NTD (19, 20), dramatic reductions in eIF2 association with the rest of MFC were also observed in these three mutant strains in a remarkable proportional accord with the extent of the eIF5 loss. In perfect agreement, all these *NIP1* mutant alleles impart severe Gcd$^-$ phenotypes (Fig. 2*D*), strongly suggesting that impaired TC loading to the PICs represents one of their functional defects in translation. Interestingly, another Gcd$^-$ mutant, *Box12-WW*, showed virtually WT levels of eIF5 associated with the rest of eIF3 but significantly reduced amounts of eIF2 (*lane 14*). These results suggest that its TC binding defect mechanistically differs from those of the other three mutants (see "Discussion" for more details). In contrast, *Box12-SPW*, which is the only mutant allele that does not produce the Gcd$^-$ phenotype, showed WT levels of both eIF5 and eIF2 (Fig. 6*A*, *lane 8*). This Sui$^-$ mutant, however, did display a modest increase in the eIF1 amounts associated with the MFC, consistent with our *in vitro* binding data presented in Fig. 5*C*. It should be noted here that despite numerous repetitions the experimental error for eIF1 remained relatively high in this particular experiment. Nevertheless, because the increase in eIF1 recovery averaged out to ~20% relative to WT, we propose that *Box12-SPW* slightly but specifically increases the binding affinity of the c/Nip1-NTD for eIF1 both *in vitro* and *in vivo*. Conversely, eIF1 binding was completely diminished by *GAP^{85}*

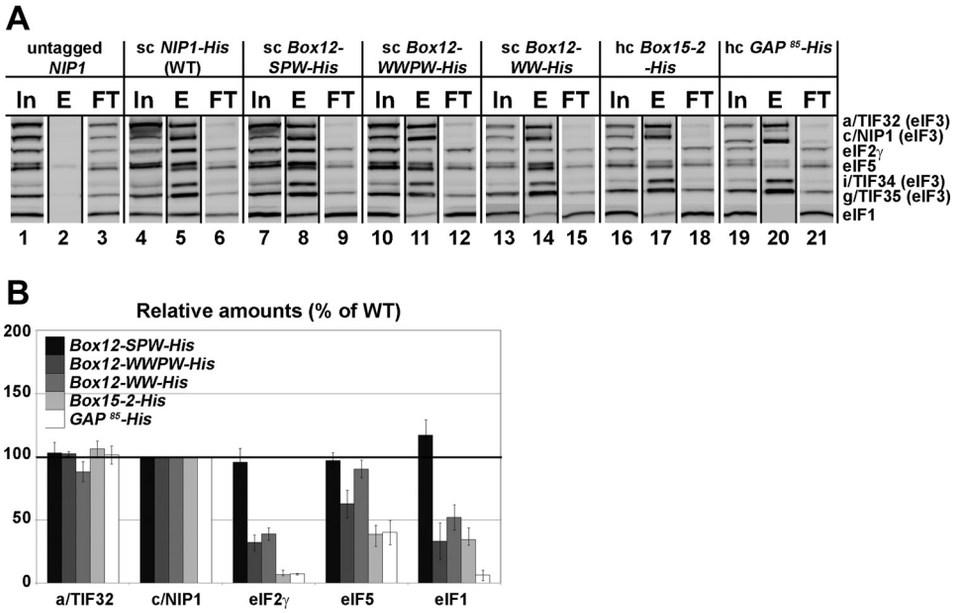

FIGURE 6. **The semirandom mutations of c/Nip1-Boxes selectively affect composition of the MFC *in vivo*.** *A*, WCEs prepared from the selected strains described in Fig. 2*C* were incubated with Ni^{2+}-Sepharose, and the bound proteins were eluted and subjected to Western blot analysis with the antibodies indicated in each *row*. *In*, lanes contained 5% of the input WCEs; *E*, lanes contained 100% of the eluate from the resin (a typical recovery is ~10% of the input for the WT); *FT*, lanes contained 5% of the flow-through from 100% input that did not bind to the resin (the limiting factor in this experiment). *B*, the Western signals for the indicated proteins in the eluate fractions of the WT *NIP1-His* and its mutants were quantified, normalized for the amounts of the WT c/Nip1 in these fractions, and plotted in the histogram as percentages of the corresponding values calculated for the WT c/Nip1; S.D. values are given.

(Fig. 6*A*, *lane 20*) as expected because this mutant has the eIF1-binding site deleted. Finally, eIF1 binding in the remaining three Box mutants (12-WWPW, 12-WW, and 15-2) was also reduced but to a much smaller degree than in the case of the GAP^{85} mutant. Taking our *in vitro* binding data into account (Fig. 5*C*), we think that these reductions are not a result of impaired direct binding between eIF1 and the NTD of c/Nip1 but rather an indirect consequence of changes in the arrangement of the assembly of the eIFs around the mutant c/Nip1-NTD.

The c/Nip1-NTD Mutants Generally Reduce 40 S Subunit Association of eIF3 and eIF5 in Vivo but Have Varying Effects on eIF1 and TC Recruitment to the 43–48 S PICs—All results described so far suggest that the three identified classes of the c/Nip1-NTD mutants that we generated have a varying impact on the composition of the 43–48 S PICs, the analysis of which would greatly help with the explanation of their molecular defects. To address this issue, we measured binding of selected eIF3 subunits and other MFC components to 40 S subunits by formaldehyde cross-linking followed by high velocity sedimentation in sucrose gradients (24). This method provides the best available approximation of the native composition of 43–48 S pre-initiation complexes *in vivo*. As shown in Fig. 7, *A–C* (*left panels*), we observed the expected co-sedimentation of a proportion of eIF3, eIF2, eIF5, and eIF1 with the 40 S species in the WCEs derived from WT cells. In the case of the class "a" *Box12-SPW* mutant, we observed a relative ~50% decrease in the amounts of selected eIF3 subunits (c/Nip1, i/Tif34, and g/Tif35) and eIF5 associated with 40 S subunits (Fig. 7*A*, *right panel*), indicating that this mutation destabilizes eIF3 and its tightly bound partner eIF5 (28) on the ribosome *in vivo* perhaps by increasing their dissociation rates as suggested previously for some other eIF3 mutants (13, 31). In contrast, eIF2 levels remained practically unchanged, which nicely correlates with the fact that this mutant does not impart the Gcd^- phenotype. Importantly and in accord with our binding data mentioned above, we reproducibly detected significantly increased amounts of eIF1 in the 40 S subunit-containing fractions (note the peak of the eIF1 signal in the 40S subunit-containing fractions that is apparent only in the panel showing the *SPW* mutant). Hence, we propose that tighter binding of eIF1 to the c/Nip1-NTD somehow prevents eIF1 from properly functioning in the AUG start codon selection process, producing the severe Sui^- phenotype (see "Discussion" for our model).

The class "b" *WWPW* mutant imparting both the Sui^- and Gcd^- phenotypes reduced 40 S subunit binding of eIF3 to a similar extent and that of eIF5 to an even greater extent than did *Box12-SPW* (Fig. 7*B*, *right panel*). Here, the reduction in eIF5 on the 40 S ribosome might be attributed either to the reduced amount of eIF5 in the affinity-purified MFC and/or to the decrease in 40 S subunit-associated eIF3; we cannot rule out either of these possibilities. In accord with its Gcd^- phenotype and in contrast to *Box12-SPW*, it also significantly reduced the eIF2 levels on the ribosome. Another striking difference between *WWPW* and *SPW* mutants is that the former also markedly reduced the 40 S subunit-associated amounts of eIF1. These results thus imply that (i) the nature of the Sui^- defect differs between these two mutants and (ii) the character of the *WWPW* Sui^- defect conspicuously resembles so-called class "i" mutations in *SUI1* encoding eIF1 (3). Class i Sui^- mutations weaken eIF1 association with PICs, and their Sui^- phenotype can be partially suppressed by their own overexpression; in accord, the Sui^- defect of *WWPW* is also partially suppressible

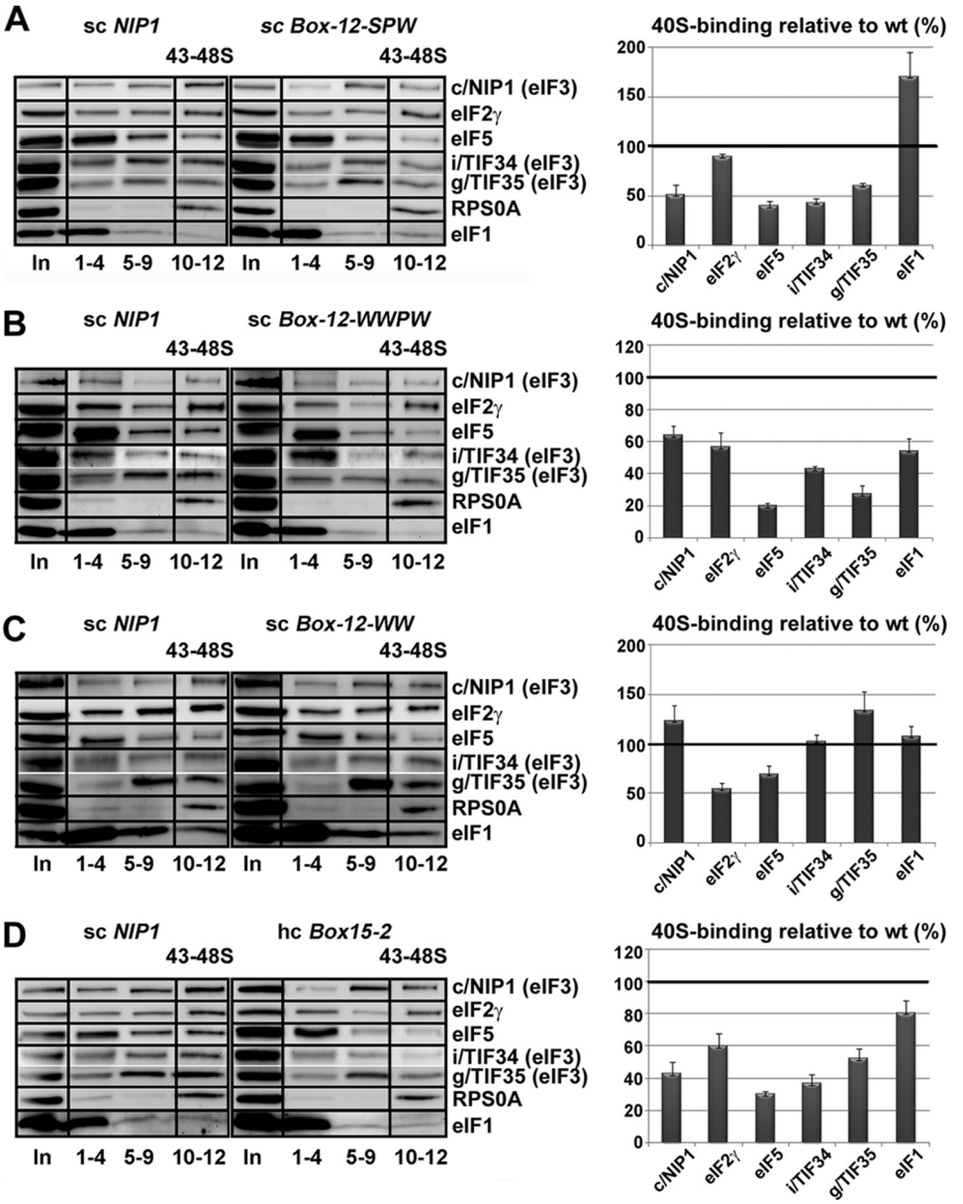

FIGURE 7. **The c/Nip1-NTD mutants generally reduce 40 S subunit association of eIF3 and eIF5 *in vivo* but have varying effects on eIF1 and TC recruitment to the 43–48 S PICs.** *A–D*, selected strains described in Fig. 2, *C* and *D*, were grown in YPD medium at 30 °C to an A_{600} of ~1.5 and cross-linked with 2% HCHO prior to harvesting. WCEs were prepared, separated on a 7.5–30% sucrose gradient by centrifugation at 41,000 rpm for 5 h, and subjected to Western blot analysis. Fractions 1–4, 5–9, and 10–12 (43–48 S) were pooled, and 5% of each pooled sample was loaded on the gel; *lane* "*In*" shows 5% input. Proportions of the 40 S subunit-bound proteins relative to the amount of 40 S subunits were calculated using Quantity One software (Bio-Rad) from at least three independent experiments. The resulting values obtained with the WT strain were set to 100%, and those obtained with mutant strains were expressed as percentages of the WT in the histograms on the *right* (S.D. values are given).

by hc eIF1 (Fig. 3). Intuitively, the same results could be also expected with another class b mutant, GAP^{85}, which completely removes the eIF1-binding site (Fig. 5) and practically eliminates eIF1 from the MFC *in vivo* (Fig. 6). Despite numerous attempts, however, the results were not satisfactorily conclusive because they suffered from huge experimental error. We think the most probable reason for this is the extremely long doubling time of the large internal deletion of this mutant that makes it very hard to work with when compared with other, not so slow growing mutants. Nevertheless, our *in vitro* and *in vivo* binding as well as hc eIF1 suppression data strongly suggest that GAP^{85} also causes the Sui$^-$ phenotype by weakening the eIF1 binding to PICs in a manner partially suppressible by hc eIF1.

The class "c" *WW* mutant, which still falls in the original Box12 segment, imparts only the Gcd$^-$ phenotype in a manner partially suppressible by hc TC (Fig. 4) and as such was expected to reduce mainly the eIF2 amounts on the 40 S ribosome. As shown in Fig. 7*C*, besides eIF2, we also found decreased amounts of eIF5 but not eIF3 and eIF1. Interestingly and in accord with our binding data showing a significant loss of eIF2 but not eIF5 from the MFC *in vivo* (Fig. 6), 40 S ribosome binding of eIF2 was more severely impaired than that of eIF5. This is significant because in all other Gcd$^-$ mutants examined in this

work eIF5 association with PICs was always more impaired than that of eIF2. These results seem to indicate that the *WW* mutant impairs eIF2 recruitment by a different mechanism than via the destabilization of eIF5 binding to the c/Nip1-NTD in the MFC, which is the only way that we have seen so far (see "Discussion" for further details). These results also suggest that the "PW" but not the "WW" part of the *WWPW* mutant is responsible for the weakened eIF3 binding to PICs *in vivo*.

Finally, another representative class c mutant, *Box15-2*, reduced binding of eIF3 and eIF5 with 40 S species (Fig. 7*D*, *right panel*), indicating that this part of the NTD of c/Nip1 also is required for stable incorporation of eIF3 and eIF5 into the PICs. Importantly, consistent with the Gcd$^-$ only phenotype of this mutant, 40 S subunit-associated amounts of eIF2 (TC) were also significantly reduced in contrast to eIF1, the binding of which was affected only modestly.

DISCUSSION

In this report, we added great detail into our understanding of the dual role of the NTD of c/Nip1 in TC recruitment and AUG selection, delineated its binding sites for eIF1 and eIF5, and pinpointed specific residues involved in both of these functions. First, we showed that the extreme N-terminal 45 residues of the c/Nip1-NTD in the GST-GAP^{92} construct, which practically lacks the rest of the originally defined minimal eIF5-binding segment (in residues 1–156; Ref. 19), are sufficient for binding to eIF5 *in vitro*, whereas their removal completely abrogates it (Fig. 5). These findings clearly imply that the tip of the c/Nip1 protein is the direct mediator of eIF3 control over the eIF5 function(s) on the ribosome. This is consistent with our earlier observations that two 10-Ala substitution mutants (*Box2* and *Box4*) falling directly in this region preferentially reduced association of the c/Nip1-NTD with eIF5 *versus* eIF1 *in vitro* and accordingly lowered eIF5 occupancy in native PICs (11). Interestingly, similar *in vivo* but not *in vitro* effects were also observed with the original *Box6R* mutation, although the mutated region lies outside of the minimal eIF5-binding domain defined here (11). Likewise, neither of our newly generated mutations occurs in this domain and thus shows no impairment of eIF5 binding *in vitro* (Fig. 5), but most of mutations reduce eIF5 amounts in the MFC *in vivo* (Fig. 6). In addition, we observed that the minimal eIF5-binding domain lacking the eIF1-binding site that immediately follows shows much stronger affinity for eIF5 than the entire N-terminal segment (Fig. 5). To accommodate these findings, we propose that the c/Nip1-NTD, which is not involved in any eIF3 intersubunit interactions, adopts a dynamic fold that undergoes a relatively large restructuring when eIF3 associates with other eIFs in the MFC. This could play an important role when the MFC contacts the 40 S subunit and eIF3 and its other components (all in contact with the c/Nip1-NTD) must find their attachment sites on both sides of the ribosome (see our model below). If true, one can envisage that even mutations lying outside of the defined c/Nip1-binding sites for eIFs 1 and 5 might have a marked impact on the folding of the rest of the NTD and could prevent association of eIF1 and/or eIF5 with the MFC indirectly, for example due to spatial constraints.

Also, the c/Nip1-NTD internal deletions (Δ60–144 in *GAP^{85}* and Δ46–137 in *GAP^{92}*) completely eliminated association of eIF1 with the NTD *in vitro* and with eIF3 in the MFC *in vivo* (Figs. 5 and 6 and data not shown), and the missing fragments showed WT binding to eIF1 *in vitro* (Fig. 5 and data not shown). This clearly suggests that the segment spanning residues 60–137 is responsible for eIF1 recruitment to the MFC and via MFC to the 40 S ribosome. Interestingly, neither of our *Box12* mutations reduced eIF1 binding *in vitro*, indicating that the region from 111 to 120 is not the most critical determinant of the c/Nip1-eIF1 interaction. The absolute loss of contact between eIF1 and the c/Nip1-NTD that dominates in the *GAP* mutants produced very severe Slg$^-$ and Sui$^-$ phenotypes partially and fully suppressible, respectively, by high copy eIF1 (Fig. 3). Conversely, overexpressing eIF5 showed no effect on either phenotype. Intuitively, these results suggest that the rate-limiting defect in both GAPs should be the loading of eIF1 to the PIC and/or the lack of the eIF1-c/Nip1-NTD contact therein. The former would be reminiscent of the class i *sui1* mutations that specifically reduce the eIF1/Sui1 amounts in the PICs and produce the Sui$^-$ phenotype in a manner partially suppressible by their own overexpression (3, 8). Although the aforementioned technical difficulties prevented us from showing this directly, we posit that the eIF1 recruitment to the ribosome is one of the major defects displayed by this mutant in addition to its failure to properly promote TC assembly with the PICs (in a manner not suppressible by hc TC, which we cannot explain). In many ways, a similar but certainly not completely identical molecular effect also underlies a Sui$^-$ defect of the largest semirandom *Box12-WWPW* mutant. It markedly reduced amounts of the MFC- and PIC-bound eIF1 *in vivo* but not *in vitro* (Figs. 5- 7), and its Sui$^-$ but not Slg$^-$ phenotype was partially suppressible by high copy eIF1 by the principle of mass action (Fig. 3).

The class a (Sui$^-$-only) mutant *Box12-SPW* is a variant of the *WWPW* mutation within Box12 lacking the first two Trp substitutions of Val^{111} and Val^{112} (shown to produce the canonical Gcd$^-$ phenotype on their own; see below) but having an extra substitution of Lys^{113} by serine. It is intriguing that such a short stretch of residues, apparently not even directly contacting eIF1, contains two distinct sets of residues that are involved in two mutually distinguishable processes. Although the Sui$^-$ phenotype of the *SPW* mutant was also partially suppressible by hc eIF1 as in the case of *GAP^{85}* and *WWPW* (Fig. 3), our biochemical experiments clearly suggest that the molecular effects of its Sui$^-$ defect significantly differ from the latter two. We think that it is because *GAP^{85}* and *WWPW* also impair a step preceding the AUG selection, in particular the TC recruitment, which must undoubtedly greatly influence the normal progress of all following steps. In this respect, the *SPW* effect on AUG selection can be considered the most direct.

The *SPW* mutation surprisingly increased the affinity of the c/Nip1-NTD for eIF1 *in vitro* (Fig. 5) and to a certain degree *in vivo* in the context of the entire MFC (Fig. 6). In addition, perhaps as a result of this, it also markedly increased the steady state levels of eIF1 in the PICs while reducing the overall amounts of eIF3 and eIF5 (Fig. 7). To explain these effects, we propose the following model. If we presume that the c/Nip1-

NTD delivers eIF1 to the back side of the 40 S ribosome from which it has to relocate to the P-site area on the interface side (32) (see our model below), tighter binding of eIF1 to the SPW mutant could shift the equilibrium between eIF1 bound near the P-site toward eIF1 bound to eIF3, which is known to reside on the back side of the 40 S ribosome (4). (The existence of two eIF1-binding sites on the ribosome (one on eIF3 and the other near the P-site) was also recently proposed by A. Hinnebusch (3).) This could at least partially account for the Sui$^-$ phenotype of *SPW* by altering the proper positioning of eIF1 for stringent AUG selection. In other words, because of the increased affinity of the mutant c/Nip1-NTD for eIF1, the *SPW* mutation would interfere with the eIF1 gatekeeping role at the P-site either by preventing its stable binding therein and/or by evoking its premature dissociation/displacement at near-cognate start codons. Both defects would be mitigated by eIF1 overexpression as was observed. However, this "altered distribution/improper positioning" model would still not explain the fact that the occupancy of eIF1 is increased in native PICs. One way to account for this elevated eIF1 occupancy would be to propose that a second consequence of the *SPW* mutation is to delay eIF1 dissociation from the 40 S ribosome specifically at AUG codons in the manner described previously for the "class ii" Sui$^-$ mutant in *SUI1* represented by *sui1-G107R*, which produces the Sui$^-$ defect by slowing not accelerating the release of eIF1 from 48 S PICs (33). Indeed, HCHO cross-linking analysis of *G107R* showed that this mutation also reduces the amounts of eIF3 and eIF5 associated with the PICs *in vivo* while producing a slight increase in the eIF1 amounts. In fact, this second defect would not only explain the observed higher occupancy of eIF1 in bulk PICs (which are dominated by AUG initiation events), but in addition, it would also be expected to contribute to the *SPW* Sui$^-$ phenotype by reducing initiation specifically at AUG codons.

Finally, the three mutations *Box12-WW*, *12-WWPW*, and *Box15-2* produced canonical Gcd$^-$ phenotypes suppressible by overexpressing the TC in cells lacking protein kinase Gcn2 (Fig. 4), providing strong genetic evidence that they decrease the rate of TC binding to 40 S ribosomes and thus deregulate *GCN4* translational control. Accordingly, they significantly decreased the eIF2/TC levels in both the MFC (Fig. 6) and the PIC *in vivo* (Fig. 7). Increased dosage of the TC also fully suppressed the Slg$^-$ phenotype of the *Box15-2* mutant, suggesting that the TC recruitment is the rate-limiting defect in these cells and residues Ile^{142}, Glu^{145}, Phe^{146}, Asp^{147}, and Ile^{149} are critically required for this c/Nip1 role. Although we did not attempt to dissect the individual effects of these five residues any further, we assume that they are all required because of the following facts. Two mutant libraries of the original Box15, each containing ~10,000 clones, were screened. One library contained mutations in only two of these five residues (E145*X* and D147*X*), and no Gcd$^-$ mutants (not even weak ones) were identified. The other library contained mutations in all five residues, and only one of ~10,000 transformants showed a strong Gcd$^-$ phenotype. In contrast to *Box15-2*, the Slg$^-$ phenotype of the *WW* mutant was not suppressed, indicating that the molecular nature of its defect differs to some degree. Indeed, whereas *Box15-2* also markedly decreased the eIF5 levels in the MFC, the *WW* mutation had a negligible effect if any (Fig. 6). To explain this difference, we propose that although *Box15-2* affects the c/Nip1-NTD fold in such a way that primarily impedes the eIF5 attachment to its tip in the context of the MFC *Box12-WW* allows Nip1-NTD-eIF5-CTD binding but changes the overall orientation of the eIF5-CTD in the MFC so that it can no longer contact the β-subunit of eIF2 to promote efficient TC recruitment to 40 S ribosomes. It is also noteworthy that in contrast to all other mutants the *WW* mutation did not destabilize eIF3 binding to the ribosome. Hence, it seems that the former effect and the latter lack of effect are the unique characteristics of the "V111W/V112W" substitutions because the "parental" WWPW mutant showed biochemical effects similar to those of *Box15-2*.

Based on these results, we propose the following model. The fact that the NTD of c/Nip1 interacts simultaneously with eIF1 and the CTD of eIF5 (19, 20) and via the latter with the β-subunit of the TC makes the c/Nip1-NTD one of the most critical domains ensuring the functions of the MFC in recruiting the latter factors to the 43 S PIC and regulating their contributions to the start codon selection process thereon. It has been shown that disrupting mutual interactions among individual components of the yeast MFC significantly reduces translation initiation rates by affecting not only the steps of the PIC assembly but also the subsequent postassembly events (9–12, 14, 15, 18, 20, 21, 29). This not only suggests that the MFC-driven pathway of PIC assembly ensures the efficiency of the whole initiation process but also that the postassembly persistence of at least some contacts among the MFC components is required for smooth scanning through the 5′-UTR of the mRNA and proper AUG recognition. There is increasing evidence that the major eIF3 body contacts the solvent side of the 40 S subunit in proximity to mRNA at both the entry and exit channel pores (9, 10, 13, 18, 22, 34). However, some of its domains, including the c/Nip1-NTD, were proposed to reach out under the 40 S beak toward the ribosomal A-site (11, 22). Although it is not known where the eIF5-CTD resides, the very recent analysis of 40 S ribosome-associated eIF2 suggested that the eIF2γ-bound eIF2β faces the A-site (35), indicating that the CTD of eIF5 also occurs somewhere in this area. The modeled eIF2β location would be consistent with the proposed placement of the CTD of the a/Tif32 subunit of eIF3 (22) that directly interacts with this eIF2 subunit in the MFC (20). If true, this could mean that the MFC-established c/Nip1-NTD-eIF5-CTD and a/Tif32-CTD-eIF2β contacts also remain preserved in the scanning PICs. In such a case, the latter two eIF3 domains would be ideally positioned to actively contribute to the regulation of AUG selection via their contacts with eIF2 and eIF5. Indeed, mutations in the a/Tif32-CTD and its interacting partner j/Hcr1 were shown to markedly increase the frequency of skipping the AUG start site, producing the leaky scanning phenotype (9, 10). In contrast, the binding site of eIF1 in the eIF1·40 S ribosome complex lacking all other eIFs was mapped close to the ribosomal P-site in the interface platform area (32, 36). In addition, eIF1 appears to bind to the ribosome via the same surface that also contacts the c/Nip1-NTD (36, 37). Hence,

unlike the eIF2β and the eIF5-CTD interactions, the eIF1 contact with the c/Nip1-NTD on the ribosome must be undoubtedly given up at a certain point of initiation.

Taken together, we propose that upon MFC binding to the ribosome the c/Nip1-NTD together with the a/Tif32-CTD accommodate eIF1, the eIF5-CTD, and the eIF2β-NTD near the A-site. Whereas the latter two domains remain bound in this area, eIF1 is subsequently transferred to its "scanning-competent" position near the P-site. This transfer could be a part of a large conformational rearrangement of the 40 S head that is triggered by eIFs 1 and 1A and that opens up the mRNA binding channel for mRNA recruitment (2). We think that this particular process is slowed down in our gain-of-function *SPW* mutant because of its increased affinity for eIF1, resulting in the severe Sui$^-$ defect.

Based on biophysical studies conducted with a yeast *in vitro* reconstituted system using eIFs 1, 1A, and 5 and TC but not eIF3, eIF1 was proposed to be ejected from PICs upon AUG recognition to "open the gate" for the subsequent P_i release, resulting in scanning arrest (38). Premature loss of eIF1 from the scanning PICs in numerous mutants is also generally considered to be the major cause of the Sui$^-$ phenotype (8). An interesting alternative scenario to the "ejection model" is that eIF1 upon AUG recognition triggers a reciprocal conformational rearrangement from the open to closed states, and instead of being directly ejected, it drifts back to the c/Nip1-NTD in the A-site. Although there is no direct evidence for this option with the exception of the fact that addition of eIF3 to reconstituted PICs in the system of Lorsch and co-workers (38), while having no effect on the rate constant for eIF1 dissociation, reduces the extent of eIF1 dissociation from reconstituted PICs, we think it has an important physiological relevance as follows. i) The c/Nip1-NTD could control timing and dynamics of the eIF1 shuffling between its two positions on the ribosome depending on the immediate scanning status, *i.e.* on a conformational state of the ribosome. ii) Holding on to eIF1 by eIF3 post-initiation could speed up the reinitiation process after translation of short uORFs. eIF3 critically promotes reinitiation by staying 80 S ribosome-bound during the first elongation cycles to stabilize the 40 S subunit on mRNA after termination on a short uORF (17, 39, 40). In the next step, the 40 S subunit must resume scanning to locate the next AUG of a downstream ORF. Intuitively, to be able to resume scanning, it is very likely that conformational changes similar to those occurring in the newly formed 48 S PIC also must occur in the mRNA-bound post-termination 40 S complex (39). Hence, having eIF1 already present could make the transition from post-termination to scanning complex faster and thus more efficient. iii) eIF3 together with eIFs 1 and 1A was proposed to greatly stimulate a ribosomal recycling step following termination (41). If eIF1 is ejected in a complex with eIF3 post-initiation as eIF5 is with eIF2 prior to subunit joining (42), the eIF3·eIF1 complex could in turn directly participate in recycling at one end of the translational cycle and serve as a nucleation center for the new round of MFC formation at the other end. Certainly, more experiments are needed to support or exclude these possibilities.

Acknowledgments—We are thankful to Alan G. Hinnebusch and the members of the Valášek and Krásný laboratories for helpful comments, to Jan Kosla for help with preparation of the c/Nip1 mutagenesis, and to Olga Krydová for technical and administrative assistance. We are also indebted to an unknown reviewer whose insightful comments greatly improved the quality of this work.

REFERENCES

1. Sonenberg, N., and Hinnebusch, A. G. (2009) Regulation of translation initiation in eukaryotes: mechanisms and biological targets. *Cell* **136,** 731–745
2. Passmore, L. A., Schmeing, T. M., Maag, D., Applefield, D. J., Acker, M. G., Algire, M. A., Lorsch, J. R., and Ramakrishnan, V. (2007) The eukaryotic translation initiation factors eIF1 and eIF1A induce an open conformation of the 40S ribosome. *Mol. Cell* **26,** 41–50
3. Hinnebusch, A. G. (2011) Molecular mechanism of scanning and start codon selection in eukaryotes. *Microbiol. Mol. Biol. Rev.* **75,** 434–467
4. Valášek, L. S. (2012) 'Ribozoomin'—translation initiation from the perspective of the ribosome-bound eukaryotic initiation factors (eIFs). *Curr. Protein Pept. Sci.* **13,** 305–330
5. Algire, M. A., Maag, D., and Lorsch, J. R. (2005) P_i release from eIF2, not GTP hydrolysis, is the step controlled by start-site selection during eukaryotic translation initiation. *Mol. Cell* **20,** 251–262
6. Maag, D., Algire, M. A., and Lorsch, J. R. (2006) Communication between eukaryotic translation initiation factors 5 and 1A within the ribosomal pre-initiation complex plays a role in start site selection. *J. Mol. Biol.* **356,** 724–737
7. Saini, A. K., Nanda, J. S., Lorsch, J. R., and Hinnebusch, A. G. (2010) Regulatory elements in eIF1A control the fidelity of start codon selection by modulating $tRNA_i^{Met}$ binding to the ribosome. *Genes Dev.* **24,** 97–110
8. Cheung, Y. N., Maag, D., Mitchell, S. F., Fekete, C. A., Algire, M. A., Takacs, J. E., Shirokikh, N., Pestova, T., Lorsch, J. R., and Hinnebusch, A. G. (2007) Dissociation of eIF1 from the 40S ribosomal subunit is a key step in start codon selection *in vivo*. *Genes Dev.* **21,** 1217–1230
9. Elantak, L., Wagner, S., Herrmannová, A., Karásková, M., Rutkai, E., Lukavsky, P. J., and Valásek, L. (2010) The indispensable N-terminal half of eIF3j/HCR1 cooperates with its structurally conserved binding partner eIF3b/PRT1-RRM and with eIF1A in stringent AUG selection. *J. Mol. Biol.* **396,** 1097–1116
10. Chiu, W. L., Wagner, S., Herrmannová, A., Burela, L., Zhang, F., Saini, A. K., Valásek, L., and Hinnebusch, A. G. (2010) The C-terminal region of eukaryotic translation initiation factor 3a (eIF3a) promotes mRNA recruitment, scanning, and, together with eIF3j and the eIF3b RNA recognition motif, selection of AUG start codons. *Mol. Cell. Biol.* **30,** 4415–4434
11. Valásek, L., Nielsen, K. H., Zhang, F., Fekete, C. A., and Hinnebusch, A. G. (2004) Interactions of eukaryotic translation initiation factor 3 (eIF3) subunit NIP1/c with eIF1 and eIF5 promote preinitiation complex assembly and regulate start codon selection. *Mol. Cell. Biol.* **24,** 9437–9455
12. Nielsen, K. H., Valásek, L., Sykes, C., Jivotovskaya, A., and Hinnebusch, A. G. (2006) Interaction of the RNP1 motif in PRT1 with HCR1 promotes 40S binding of eukaryotic initiation factor 3 in yeast. *Mol. Cell. Biol.* **26,** 2984–2998
13. Herrmannová, A., Daujotyte, D., Yang, J. C., Cuchalová, L., Gorrec, F., Wagner, S., Dányi, I., Lukavsky, P. J., and Valásek, L. S. (2012) Structural analysis of an eIF3 subcomplex reveals conserved interactions required for a stable and proper translation pre-initiation complex assembly. *Nucleic Acids Res.* **40,** 2294–2311
14. Mitchell, S. F., Walker, S. E., Algire, M. A., Park, E. H., Hinnebusch, A. G., and Lorsch, J. R. (2010) The 5′-7-methylguanosine cap on eukaryotic mRNAs serves both to stimulate canonical translation initiation and to block an alternative pathway. *Mol. Cell* **39,** 950–962
15. Jivotovskaya, A. V., Valásek, L., Hinnebusch, A. G., and Nielsen, K. H. (2006) Eukaryotic translation initiation factor 3 (eIF3) and eIF2 can promote mRNA binding to 40S subunits independently of eIF4G in yeast. *Mol. Cell. Biol.* **26,** 1355–1372

16. Pisarev, A. V., Kolupaeva, V. G., Yusupov, M. M., Hellen, C. U., and Pestova, T. V. (2008) Ribosomal position and contacts of mRNA in eukaryotic translation initiation complexes. *EMBO J.* **27,** 1609–1621
17. Szamecz, B., Rutkai, E., Cuchalová, L., Munzarová, V., Herrmannová, A., Nielsen, K. H., Burela, L., Hinnebusch, A. G., and Valásek, L. (2008) eIF3a cooperates with sequences 5′ of uORF1 to promote resumption of scanning by post-termination ribosomes for reinitiation on GCN4 mRNA. *Genes Dev.* **22,** 2414–2425
18. Cuchalová, L., Kouba, T., Herrmannová, A., Dányi, I., Chiu, W. L., and Valásek, L. (2010) The RNA recognition motif of eukaryotic translation initiation factor 3g (eIF3g) is required for resumption of scanning of post-termination ribosomes for reinitiation on GCN4 and together with eIF3i stimulates linear scanning. *Mol. Cell. Biol.* **30,** 4671–4686
19. Asano, K., Clayton, J., Shalev, A., and Hinnebusch, A. G. (2000) A multifactor complex of eukaryotic initiation factors, eIF1, eIF2, eIF3, eIF5, and initiator $tRNA^{Met}$ is an important translation initiation intermediate *in vivo*. *Genes Dev.* **14,** 2534–2546
20. Valásek, L., Nielsen, K. H., and Hinnebusch, A. G. (2002) Direct eIF2-eIF3 contact in the multifactor complex is important for translation initiation *in vivo*. *EMBO J.* **21,** 5886–5898
21. Nielsen, K. H., Szamecz, B., Valásek, L., Jivotovskaya, A., Shin, B. S., and Hinnebusch, A. G. (2004) Functions of eIF3 downstream of 48S assembly impact AUG recognition and GCN4 translational control. *EMBO J.* **23,** 1166–1177
22. Valásek, L., Mathew, A. A., Shin, B. S., Nielsen, K. H., Szamecz, B., and Hinnebusch, A. G. (2003) The yeast eIF3 subunits TIF32/a, NIP1/c, and eIF5 make critical connections with the 40S ribosome *in vivo*. *Genes Dev.* **17,** 786–799
23. Valásek, L., Trachsel, H., Hasek, J., and Ruis, H. (1998) Rpg1, the *Saccharomyces cerevisiae* homologue of the largest subunit of mammalian translation initiation factor 3, is required for translational activity. *J. Biol. Chem.* **273,** 21253–21260
24. Nielsen, K. H., and Valásek, L. (2007) *In vivo* deletion analysis of the architecture of a multiprotein complex of translation initiation factors. *Methods Enzymol.* **431,** 15–32
25. Grant, C. M., and Hinnebusch, A. G. (1994) Effect of sequence context at stop codons on efficiency of reinitiation in GCN4 translational control. *Mol. Cell. Biol.* **14,** 606–618
26. Donahue, T. (2000) in *Translational Control of Gene Expression* (Sonenberg, N., Hershey, J. W. B., and Mathews, M. B., eds) pp. 487–502, Cold Spring Harbor Laboratory Press, Cold Spring Harbor, NY
27. Hinnebusch, A. G. (2005) Translational regulation of GCN4 and the general amino acid control of yeast. *Annu. Rev. Microbiol.* **59,** 407–450
28. Phan, L., Schoenfeld, L. W., Valásek, L., Nielsen, K. H., and Hinnebusch, A. G. (2001) A subcomplex of three eIF3 subunits binds eIF1 and eIF5 and stimulates ribosome binding of mRNA and $tRNA_i^{Met}$. *EMBO J.* **20,** 2954–2965
29. Yamamoto, Y., Singh, C. R., Marintchev, A., Hall, N. S., Hannig, E. M., Wagner, G., and Asano, K. (2005) The eukaryotic initiation factor (eIF) 5 HEAT domain mediates multifactor assembly and scanning with distinct interfaces to eIF1, eIF2, eIF3, and eIF4G. *Proc. Natl. Acad. Sci. U.S.A.* **102,** 16164–16169
30. Asano, K., Krishnamoorthy, T., Phan, L., Pavitt, G. D., and Hinnebusch, A. G. (1999) Conserved bipartite motifs in yeast eIF5 and eIF2Bepsilon, GTPase-activating and GDP-GTP exchange factors in translation initiation, mediate binding to their common substrate eIF2. *EMBO J.* **18,** 1673–1688
31. Kouba, T., Rutkai, E., Karásková, M., and Valášek, L. S. (2012) The eIF3c/NIP1 PCI domain interacts with RNA and RACK1/ASC1 and promotes assembly of translation preinitiation complexes. *Nucleic Acids Res.* **40,** 2683–2699
32. Rabl, J., Leibundgut, M., Ataide, S. F., Haag, A., and Ban, N. (2011) Crystal structure of the eukaryotic 40S ribosomal subunit in complex with initiation factor 1. *Science* **331,** 730–736
33. Nanda, J. S., Cheung, Y. N., Takacs, J. E., Martin-Marcos, P., Saini, A. K., Hinnebusch, A. G., and Lorsch, J. R. (2009) eIF1 controls multiple steps in start codon recognition during eukaryotic translation initiation. *J. Mol. Biol.* **394,** 268–285
34. Kouba, T., Danyi, I., Munzarová, V., Vlčková, V., Cuchalová, L., Neueder, A., Milkereit, P., and Valášek, L. S. (2012) Small ribosomal protein RPS0 stimulates translation initiation by mediating 40S-binding of eIF3 via its direct contact with the eIF3a/TIF32 subunit. *PLoS One*, **7,** e40464
35. Shin, B. S., Kim, J. R., Walker, S. E., Dong, J., Lorsch, J. R., and Dever, T. E. (2011) Initiation factor eIF2γ promotes eIF2-GTP-Met-$tRNA_i^{Met}$ ternary complex binding to the 40S ribosome. *Nat. Struct. Mol. Biol.* **18,** 1227–1234
36. Lomakin, I. B., Kolupaeva, V. G., Marintchev, A., Wagner, G., and Pestova, T. V. (2003) Position of eukaryotic initiation factor eIF1 on the 40S ribosomal subunit determined by directed hydroxyl radical probing. *Genes Dev.* **17,** 2786–2797
37. Reibarkh, M., Yamamoto, Y., Singh, C. R., del Rio, F., Fahmy, A., Lee, B., Luna, R. E., Ii, M., Wagner, G., and Asano, K. (2008) Eukaryotic initiation factor (eIF) 1 carries two distinct eIF5-binding faces important for multifactor assembly and AUG selection. *J. Biol. Chem.* **283,** 1094–1103
38. Maag, D., Fekete, C. A., Gryczynski, Z., and Lorsch, J. R. (2005) A conformational change in the eukaryotic translation preinitiation complex and release of eIF1 signal recognition of the start codon. *Mol. Cell* **17,** 265–275
39. Munzarová, V., Pánek, J., Gunišová, S., Dányi, I., Szamecz, B., and Valášek, L. S. (2011) Translation reinitiation relies on the interaction between eIF3a/TIF32 and progressively folded cis-acting mRNA elements preceding short uORFs. *PLoS Genet.* **7,** e1002137
40. Pöyry, T. A., Kaminski, A., and Jackson, R. J. (2004) What determines whether mammalian ribosomes resume scanning after translation of a short upstream open reading frame? *Genes Dev.* **18,** 62–75
41. Pisarev, A. V., Hellen, C. U., and Pestova, T. V. (2007) Recycling of eukaryotic posttermination ribosomal complexes. *Cell* **131,** 286–299
42. Jennings, M. D., and Pavitt, G. D. (2010) eIF5 has GDI activity necessary for translational control by eIF2 phosphorylation. *Nature* **465,** 378–381
43. Gietz, R. D., and Sugino, A. (1988) New yeast-*Escherichia coli* shuttle vectors constructed with *in vitro* mutagenized yeast genes lacking six-base pair restriction sites. *Gene* **74,** 527–534
44. Cigan, A. M., Pabich, E. K., and Donahue, T. F. (1988) Mutational analysis of the HIS4 translational initiator region in *Saccharomyces cerevisiae*. *Mol. Cell. Biol.* **8,** 2964–2975
45. Mueller, P. P., and Hinnebusch, A. G. (1986) Multiple upstream AUG codons mediate translational control of GCN4. *Cell* **45,** 201–207
46. Phan, L., Zhang, X., Asano, K., Anderson, J., Vornlocher, H. P., Greenberg, J. R., Qin, J., and Hinnebusch, A. G. (1998) Identification of a translation initiation factor 3 (eIF3) core complex, conserved in yeast and mammals, that interacts with eIF5. *Mol. Cell. Biol.* **18,** 4935–4946

5. DISCUSSION

5.1 Structural analysis of eIF3 subcomplexes

eIF3 is the most complex initiation factor composed of six different subunits in yeast *Saccharomyces cerevisiae*, all of which have corresponding orthologues in mammalian eIF3 containing thirteen different subunits. The structural complexity is well illustrated by its elaborate subunit-subunit interaction web, which has been mapped in great detail for yeast eIF3 and its associated eIFs (Valášek et al., 2002). To better understand to all functions of individual interactions among eIF3 subunits more detailed information at the molecular level would be required.

In our work (Elantak et al., 2010) we obtained first structural information about an interaction between two eIF3 subunits. Using NMR spectroscopy, we determined the solution structure of interaction between human eIF3j (heIF3j) and human eIF3b (heIF3b). We showed that heIF3j is held via its N-terminal acidic motif (NTA) centered by conserved tryptophan residue in a hydrophobic pocket formed by helix α1 loop5 of the heIF3b-RRM. We then mutated the corresponding residues in its yeast orthologues and showed that the critical determinants of the j/HCR1-b/PRT1-RRM interaction are evolutionary conserved. Furthermore we found that disrupting this interaction by mutations in b/PRT1-RRM strongly affects association of eIF3 with 40S while mutations in j/HCR1-NTA showed no such defect. Finally, mutations in both j/HCR1-NTA and b/PRT1-RRM produced leaky scanning phenotype that indicates a defect in AUG recognition.

Our results suggest that the interaction between j/HCR1 and b/PRT1-RRM is required for proper recognition of the AUG start codon. It is not surprising, as j/HCR1 was shown to interact with the constituents of the mRNA entry channel that govern the conformational switch of the 40S ribosome upon AUG recognition. We proposed that j/HCR1 in cooperation with b/PRT1-RRM acts in a way that would prompt the switch to scanning arrested conformation when the start codon enters the P-site, thus preventing leaky scanning. Furthermore, as only mutations in b/PRT1-RRM affected

the 40S binding of eIF3, we proposed that this activity is independent on the b/PRT1-j/HCR1 contact and that b/PRT1-RRM forms an important intermolecular bridge between eIF3 and 40S subunit.

In our next structural study (Herrmannová et al., 2011) we focused on the C-terminus of b/PRT1 and its interaction with i/TIF34. We reported the 2.2 Å resolution crystal structure of the complex between the yeast seven-bladed β-propeller i/TIF34 and C-terminal α-helix of b/PRT1. The interaction is mediated by two major contacts, which we subjected to mutational analysis. Disrupting the b/PRT1-i/TIF34 interaction by site-specific mutations resulted in severe growth phenotypes and eliminated i/TIF34 and also g/TIF35 from eIF3 and MFC *in vivo*. Interestingly, the loss of i/TIF34-g/TIF35 minimodule from eIF3 affected 40S binding of remaining eIF3 subunits and also eIF5, which led to accumulation of aberrant PICs containing only eIF1 and TC that were defective in AUG recognition and produced severe leaky scanning phenotype. The growth and leaky scanning phenotype was almost fully suppressible by overexpression of g/TIF35 and partially also by eIF1.

Based on these results we proposed that i/TIF34-g/TIF35 minimodule provides additional 40S-binding activity that is necessary for stabilization of 48S PICs as the loss of this minimodule leads to formation of aberrant 48S PICs lacking eIF3 and eIF5. Furthermore we argued that the severe leaky scanning phenotype results from incompetence of these aberrant PICs to switch to scanning arrested conformation. Overexpression of g/TIF35 suppressed the leaky scanning but unexpectedly did not improve association of the minimodule with the MFC. Instead, it destabilized formation of the MFC *in vivo*. This led us to a hypothesis that overexpression of g/TIF35 prevents the formation of these aberrant PICs by eliminating the MFC-driven pathway in favor of less effective but fully functional „stochastic“ pathway of the PIC formation, where eIFs bind to the 40S not in a higher order super complex (such as the MFC) but individually (see Figure 1).

To conclude, our results clearly illustrate the importance of structural studies on eIF3 as well as a detailed analysis of its subunit-subunit interactions. The ultimate goal of our lab is to achieve a high-resolution structure of the entire eIF3, which would greatly extend our knowledge of eIF3 functions on the molecular level.

5.2 Functional characterization of eIF3 subunits

Another important long term goal of the laboratory is to characterize and assign functions to individual subunits of the eIF3 complex. In (Cuchalová et al., 2010) we focused on previously only poorly characterized two small eIF3 subunits (g/TIF35 and i/TIF34), which are essential for viability of the yeast cells (Hanachi et al., 1999; Naranda et al., 1997). However, quite surprisingly, detailed biochemical analysis carried out with purified eIF3 subcomplexes showed that the trimeric complex of a/TIF32-b/PRT1-c/NIP1 promoted the 48S PIC formation and stimulated translation *in vitro* as efficiently as the wild-type five subunit complex, suggesting that g/TIF35 and i/TIF34 are dispensable for two key functions of eIF3 in translation initiation (Phan et al., 2001). On the other hand, we showed that elimination of g/TIF35 and i/TIF34 from the MFC leads to accumulation of aberrant 48S PICs *in vivo* that severely impair the initiation rates (Herrmannová et al., 2011).

To resolve this paradox, we performed a site-directed mutagenesis of the RRM of g/TIF35 and generated the g/tif35-KLF mutation (Cuchalová et al., 2010). The *g/tif35-KLF* mutation had no impact on RNA-binding affinity, on the integrity of the MFC, or on formation of the 43S PICs, but it markedly reduced rates of translation initiation and decreased the processivity of scanning through stable secondary structures. Furthermore, it displayed a strong Gcn$^-$ phenotype resulting from inability of post-termination 40S subunits at uORF1 of *GCN4* to resume scanning for reinitiation downstream as further discussed in chapter 5.4. Similarly, a mutation in i/TIF34 called *i/tif34-Q258R* had no effect on MFC integrity but displayed the strong Gcn$^-$ phenotype owing to the markedly impaired rate of scanning.

Taken together, the essential character of both small eIF3 subunits might be explained by proposing that the loss of their stimulatory effects on linear scanning predominantly affects translation of a subset of specific mRNAs. For example mRNAs encoding tightly regulated genes such as those involved in cell cycle regulation or signal transduction have often long 5'UTRs that are rich in secondary structures (Kozak, 2005; van der Velden and Thomas, 1999). Their efficient translation thus may depend on scanning-stimulating functions of g/TIF35 and i/TIF34. If it cannot be provided, these often essential genes might not get sufficiently expressed, which in turn results in

lethality. This proposal is consistent with previous findings that specific mutations in i/TIF34 deregulate progression through the cell cycle and affect mating (Verlhac et al., 1997). By the same token, overexpression of human eIF3i leads to cell size increase, proliferation enhancement, cell-cycle progression and anchorage-independent growth, and therefore is often observed in carcinomas (Ahlemann et al., 2006).

In our other study (Elantak et al., 2010) we functionally characterized the only nonessential subunit of eIF3, j/HCR1. We showed that the N-terminal half of j/HCR1 is indispensable and sufficient to fulfill all functions of j/HCR1 needed to support the wild-type growth of yeast cells and that the deletion of j/HCR1 or j/HCR1-NTD leads to a strong leaky scanning phenotype indicative of a defect in AUG recognition. The latter result indicates that j/HCR1 stays 40S-bound even after mRNA recruitment at least to the point of AUG recognition, in disagreement with some previous proposals, and thus may contribute to the stabilization of the properly formed PICs at the start codon. A similar role in pausing scanning upon establishment of a correct initiation codon-anticodon base-pairing was proposed for eIF1A (Fekete et al., 2007). In agreement with this proposal we observed that the leaky scanning phenotype of the j/HCR1 deletion is partially suppressible by overexpression of eIF1A but not of eIF1. As j/HCR1 interacts with the constituents of the mRNA entry channel that govern the conformational switch of the 40S ribosome upon AUG recognition, we proposed that j/HCR1 cooperation with the b/PRT1-RRM acts in a way that would prompt the switch to scanning arrested conformation when the start codon enters the P-site, thus preventing leaky scanning.

Having found that j/HCR1 and its binding partner the b/PRT1-RRM play an important role in proper AUG start codon selection (Elantak et al., 2010), we wished to investigate the cellular functions of their mutual binding partner – the a/TIF32-CTD. We did that in (Chiu et al., 2010), where we generated several site-specific mutations in the a/TIF32-CTD and found out that they reduced recruitment of mRNA to native 40S subunits and impaired processivity of scanning *in vivo*. In addition, they also affected the AUG start codon recognition, as the a/TIF32-CTD binding partners b/PRT1-RRM and j/HCR1. In particular, mutations in the a/TIF32-CTD produced moderate increase in leaky scanning and suppressed the ability of dominant Sui$^-$ mutations in eIF5, eIF2β and eIF1A to increase initiation from the UUG codon, thus producing a strong Ssu$^-$ phenotype. Analogous mutations, conferring both leaky scanning and Ssu$^-$ phenotypes, were previously described for eIF1A and it was proposed that such mutations destabilize the closed conformation of the 48S PIC (Fekete et al., 2007). Hence the fact

that the a/TIF32-CTD interacts with components of the 40S subunit located near the mRNA entry channel (Chiu et al., 2010; Valášek et al., 2003) suggests that the a/TIF32-CTD can modulate the mRNA entry channel latch in a way influencing the transition from open to closed PIC conformation. Interestingly, the mutations in the a/TIF32-CTD also produce phenotypes suggesting the opposite effect of destabilizing the open conformation of the PIC, as they reduce the processivity of scanning. These seemingly opposite effects can be explained by proposing that the mutations in the a/TIF32-CTD reduce the rate or extent of switching in both directions between the fully open and fully closed conformations of the PIC.

Finally, the proximity of the a/TIF32-CTD to the mRNA entry channel might also explain its ability to promote mRNA recruitment as it could serve as an extension of the mRNA binding channel. The similar function was already suggested for mammalian eIFa and eIF3d (Pisarev et al., 2008).

In our most recent study (Karásková et al., 2012) we focused on the N-terminal domain of the c/NIP1 subunit of eIF3. This domain was already characterized previously and it was shown to mediate eIF3 interactions with eIF1 and eIF5 (Valášek et al., 2002), stimulate the assembly of the 43S PICs and somehow coordinate the functions of eIF1 and eIF5 in stringent AUG selection (Valášek et al., 2004). In order to understand the molecular mechanism of the c/NIP1-NTD involvement in these functions in great detail, and also to identify specific residues that are critical for them, we embarked on a comprehensive genetic and biochemical study of this important domain.

We subjected several previously identified segments of the c/NIP1-NTD to semi-random mutagenesis and identified three major classes of mutants that affected either the TC recruitment (c/nip1-BOX15-2) or AUG selection (c/nip1-BOX12-SPW) or both (c/nip1-BOX12-WWPW, GAP^{85} and GAP^{92}).

Interestingly, substitution of three BOX12 lysines (113, 116 and 118) in c/nip1-BOX12-SPW produced only the Sui^- phenotype, while substitution of two preceding valines (111 and 112) and lysines (116 and 118) in c/nip1-BOX12-WWPW produced both the Sui^- and the Gcd^- phenotype. We then separated the two consecutive valines in c/nip1-BOX12-WW, and indeed observed only the Gcd^- phenotype. Thus, we proposed that the valines somehow promote recruitment of the TC to the small ribosomal subunit, while the lysines are required for proper detection of the AUG start codon. It is

intriguing that such a short stretch of residues contains two distinct sets of residues that are involved in two mutually distinguishable processes.

The absolute loss of contact between the c/NIP1-NTD and eIF1 in mutants with internal deletions of residues 60-144 or 46-137 (GAP^{85} and GAP^{92}) produced the severe Sui^- phenotype suppressible by overexpression of eIF1. This resembles the class I *sui1* mutations that specifically reduce eIF1 amounts in the PICs and produce the Sui^- phenotype that is partially suppressible by their own overexpression (Cheung et al., 2007).

Finally, we showed that residues Ile142, Glu145, Phe146, Asp147 and Ile149 are critically required for the TC recruitment as mutations in these residues (in c/nip1-BOX15-2) produced canonical Gcd^- phenotype suppressible by overexpression of the TC, and decreased levels of the TC in PICs *in vivo*.

We also delineated binding sites for eIF1 and eIF5 within the c/NIP1-NTD. In particular, the residues 1-45 are sufficient for binding of eIF5 *in vitro* and the binding site for eIF1 immediately follows (residues 60-137). Interestingly, we observed that the minimal eIF5-binding domain lacking the eIF1-binding site shows much stronger affinity for eIF5 than the entire N-terminal segment. We thus proposed that the c/NIP1-NTD, which is not interacting with any other eIF3 subunits, adopts a dynamic fold that undergoes a relatively large restructuring when eIF3 associates with other eIFs in the MFC. This could play an important role when the MFC contacts the 40S subunit and eIF3 and its other components must find their attachment sites on both sides of the ribosome.

Taken together, we proposed that upon the MFC binding to the ribosome the c/NIP1-NTD binds near the A-site where it delivers eIF1 and eIF5 (Valášek et al., 2003; Valášek et al., 2004). Whereas eIF5 remains bound in this area, eIF1 is subsequently transferred to its scanning competent position near the P-site (Rabl et al., 2011). This transfer could be part of a large conformational rearrangement of the 40S head that is triggered by eIF1 and eIF1A and that opens up the mRNA binding channel for mRNA recruitment (Passmore et al., 2007).

5.3 Newly identified eIF3 binding sites on 40S ribosome

Recently, several crystal structures of the eukaryotic ribosome were solved, revealing partial structures and positions of all 33 small ribosomal proteins (RPSes) and 18S rRNA (Ben-Shem et al., 2011; Rabl et al., 2011). The structure of the 40S subunit can be divided into the traditional hallmark features of the small bacterial ribosomal subunit, comprising the head, platform, body, beak, shoulder, right foot and left foot (Ben-Shem et al., 2010)

To better understand the role of eIF3 in the assembly of the PICs, a systematic effort was dedicated to mapping the binding sites of eIF3 on the 40S ribosome (Figure 3.). We previously identified the a/TIF32-NTD as an important intermolecular bridge between eIF3 and the 40S subunit interacting with the small ribosomal protein RPS0A located on the ribosomal solvent side near the mRNA exit channel (Kouba et al., 2012a; Valášek et al., 2003). In addition, it was also shown that the extreme CTD of a/TIF32 becomes critical for 40S binding in the presence of a mutant form of eIF5 that interferes with the integrity of the MFC, as it contacts helices 16-18 of 18S rRNA (Valášek et al., 2003). Recently, we showed that the PCI domain of the c/NIP1-CTD interacts with blades 1-3 of the small ribosomal protein RACK1/ASC1 located on the head of the 40S subunit above the mRNA exit channel (Kouba et al., 2012b).

We further extended the knowledge on eIF3 whereabouts on the ribosome in (Elantak et al., 2010), where we showed that the C-terminal half of j/HCR1 specifically interacts with RPS2 and RPS23, both constituents of the mRNA entry channel. These interactions were dependent on the intact KERR motif in the j/HCR1-CTD. Interestingly RPS2 and RPS23 are on the opposite sides of the mRNA entry channel, RPS2 on the solvent and RPS23 on the interface side of the ribosome near the ribosomal A-site (see further below).

In accordance with these results, we then identified contacts between the a/TIF32-CTD, a binding partner of j/HCR1, and RPS2 and RPS3 (Chiu et al., 2010). Interestingly, ribosomal proteins RPS2 and RPS3 are together with helices 16-18 of 18S rRNA all constituents of the mRNA entry channel. Furthermore, we also found new interactions between g/TIF35 and RPS3 and RPS20 that were not affected by the previously described g/tif35-KLF mutation (Cuchalová et al., 2010).

Taken together our results strongly suggest that eIF3 is located on the solvent-exposed side of the 40S ribosome, as was already proposed by others for mammalian eIF3 (Pisarev et al., 2008; Siridechadilok et al., 2005; Srivastava et al., 1992). The fact that the a/TIF32-CTD, j/HCR1, and g/TIF35 all bind to the components of the mRNA entry channel that remodels during the switch from open to closed conformation of the 40S ribosome implies that their functions in scanning as well as the AUG selection process most probably stem from making these contacts. Interestingly, j/HCR1 was also shown to occur on the other, interface side of the mRNA entry channel, thanks to its interaction with RPS23 and hydroxyl radical probing (Fraser 2007). This may suggest that j/HCR1 either protrudes the mRNA entry channel and contacts both of its sides, or more likely that it can bind to two distinct binding sites depending on its current role in the translation process. In addition to j/HCR1, the c/NIP1-NTD was also proposed to contact the interface side by protruding under the beak area and reaching to the ribosomal A-site (Valášek et al., 2003; Valášek et al., 2004).

5.4 Resumption of scanning is mediated by eIF3

Reinitiation (REI) is a gene-specific translational control mechanism used to regulate expression of specific proteins such as transcription factors or proto-oncogenes in response to different environmental stimuli (Kozak, 2005). Ribosomes initiate in the usual way at the first AUG start codon, but when they reach the termination codon, the 40S subunit remains bound to the mRNA, resumes scanning and after binding a new ternary complex (TC) initiates again at the downstream AUG. As REI depends on rebinding of TC, it can be delicately regulated by changes in the eIF2-GTP levels (Hinnebusch, 2005).

One well studied example of translational control using REI is the yeast *GCN4* gene. The *GCN4* mRNA encodes a transcriptional activator of mainly amino acid biosynthetic genes and contains four short upstream open reading frames (uORFs) in its leader sequence. Most ribosomes translate the first REI-permissive uORF1 and after termination about half of them resume scanning downstream. During non-starvation conditions when levels of TC are high, the rescanning ribosomes acquire new TC

rapidly and reinitiate at one of the next three uORFs, which REI-nonpermissive. However, under starvation conditions the TC levels are low and rescanning ribosomes have to travel a longer distance until they acquire the new TC. This increases the chance of bypassing all three REI-nonpermissive uORFs and reaching the start codon of *GCN4* (Hinnebusch, 2005).

The mechanism of reinitiation is still far from being comprehensively understood. There are indications that REI might be dependent on the post-initiation presence of eIF4G on the 40S ribosomal subunit (Pöyry et al., 2004) and a series of our recent studies clearly suggest that eIF3 is critically required for the progress of REI (Cuchalová et al., 2010; Munzarová et al., 2011; Szamecz et al., 2008).

In the publication (Szamecz et al., 2008), we first truncated the extreme NTD of a/TIF32 by 200 resides (in *a/tif32-Δ8*) and observed that it blocked the induction of the *GCN4* expression by previously unknown mechanism. It interfered with a step following termination at the stop codon of uORF1. Subsequently we detected a genetic interaction between the a/tif32-Δ8 mutation and mutations (deletions or substitutions) in sequences 5‘ of uORF1 in a way that the negative impact of the a/tif32-Δ8 on REI was almost eliminated by these mutations upstream of uORF1. These results thus strongly suggested that the a/TIF32-NTD promotes REI by interacting with the 5‘ sequences of uORF1, which we named the a/TIF32-NTD-responsive site (eIF3a-RS). In addition, we also showed that the efficiency of REI conferred by the eIF3a-RS strictly depends on its proper positioning relative to the 40S mRNA exit channel. We concluded that the interaction between the a/TIF32-NTD and the eIF3a-RS upstream of uORF1 stabilizes association of the post-termination 40S subunit with mRNA and thereby promotes efficient resumption of scanning and REI downstream from uORF1. This is further supported by the fact that the a/TIF32-NTD interacts directly with RPS0A, as mentioned above, which is located near the 40S mRNA exit channel (Spahn et al., 2001). These results were further confirmed and extended in the following study of my colleagues (Munzarová et al., 2011), where four distinct REI-promoting elements were identified within the originally described eIF3a-RS upstream of uORF1, two of which were shown to operate in the a/TIF32-NTD dependent manner.

These intriguing results thus suggest that eIF3 stays bound to the 40S ribosome even after subunit joining and travels with elongating 80S ribosomes for several

elongation cycles before it highly likely progressively dissociates and reappears back as late as during the termination event (Beznosková et al., 2013).

The a/TIF32 does not seem to be the only subunit of eIF3 directly involved in the REI mechanism. In our other study (Cuchalová et al., 2010), we described a mutant in the g/TIF35-RRM, called g/tif35-KLF, that also showed a strong Gcn$^-$ phenotype. This phenotype was clearly caused by the inability of 40S ribosomes to resume scanning after termination at uORF1 of *GCN4* mRNA and thus strongly resembled the Gcn$^-$ phenotype of the a/tif32-Δ8. However, detailed genetic analysis revealed that the g/TIF35-RRM and the a/TIF32-NTD ensure efficient resumption of scanning by different molecular mechanism, which in case of the g/TIF35-RRM still remains to be elucidated.

To conclude, we showed that eIF3, and namely its a/TIF32-NTD and g/TIF35-RRM, critically promotes efficient REI in yeast. In agreement with our results, eIF3g has also been shown to play an important role in REI in plants (Park et al., 2001), and mammalian eIF3 was identified as a key factor required for REI on mRNA of feline calicivirus (Pöyry et al., 2007).

6. CONCLUSIONS

This work significantly contributes to our understanding of the function of eIF3 in translation initiation as well as of its location on 40S ribosome and brings new structural insights into interactions between its subunits.

We contributed to the ultimate goal of resolving the structure of the eIF3 complex as whole by our partial structural studies showing molecular details of two important contacts between given eIF3 subunits.

We identified several novel contacts between eIF3 and the 40S ribosome that allowed us to better predict its position on the solvent side of the 40S subunit.

Finally, we characterized functions of several eIF3 subunits, or their particular domains, genetically and biochemically and showed that: i) j/HCR1, the b/PRT1-RRM and the a/TIF32-CTD play a direct role in AUG recognition *in vivo*; ii), the c/NIP1-NTD also critically promotes AUG recognition and the TC recruitment by modulating the functions of eIF1 and eIF5; iii) the a/TIF32-CTD stimulates mRNA recruitment; iv) g/TIF35, i/TIF34 and the a/TIF32-CTD stimulate rate and processivity of scanning; and finally v) the a/TIF32-NTD and g/TIF35 enable resumption of scanning of post-termination 40S ribosomes for reinitiation downstream.

7. REFERENCES

Ahlemann, M., Zeidler, R., Lang, S., Mack, B., Münz, M. and Gires, O. (2006). Carcinoma-associated eIF3i overexpression facilitates mTOR-dependent growth transformation. *Mol. Carcinog.* **45**, 957–67.

Algire, M. A., Maag, D. and Lorsch, J. R. (2005). Pi release from eIF2, not GTP hydrolysis, is the step controlled by start-site selection during eukaryotic translation initiation. *Mol. Cell* **20**, 251–62.

Asano, K., Phan, L., Anderson, J. and Hinnebusch, A. G. (1998). Complex formation by all five homologues of mammalian translation initiation factor 3 subunits from yeast Saccharomyces cerevisiae. *J. Biol. Chem.* **273**, 18573–85.

Asano, K., Clayton, J., Shalev, A. and Hinnebusch, A. G. (2000). A multifactor complex of eukaryotic initiation factors, eIF1, eIF2, eIF3, eIF5, and initiator tRNA(Met) is an important translation initiation intermediate in vivo. *Genes Dev.* **14**, 2534–46.

Barthelme, D., Dinkelaker, S., Albers, S.-V., Londei, P., Ermler, U. and Tampé, R. (2011). Ribosome recycling depends on a mechanistic link between the FeS cluster domain and a conformational switch of the twin-ATPase ABCE1. *Proc. Natl. Acad. Sci. U. S. A.* **108**, 3228–33.

Ben-Shem, A., Jenner, L., Yusupova, G. and Yusupov, M. (2010). Crystal structure of the eukaryotic ribosome. *Science* **330**, 1203–9.

Ben-Shem, A., Garreau de Loubresse, N., Melnikov, S., Jenner, L., Yusupova, G. and Yusupov, M. (2011). The structure of the eukaryotic ribosome at 3.0 Å resolution. *Science* **334**, 1524–9.

Beznosková, P., Cuchalová, L., Wagner, S., Shoemaker, C. J., Gunišová, S., von der Haar, T. and Valášek, L. S. (2013). Translation Initiation Factors eIF3 and HCR1 Control Translation Termination and Stop Codon Read-Through in Yeast Cells. *PLoS Genet.* **9**, e1003962.

Cuchalová, L., Kouba, T., Herrmannová, A., Dányi, I., Chiu, W. and Valásek, L. (2010). The RNA recognition motif of eukaryotic translation initiation factor 3g (eIF3g) is required for resumption of scanning of posttermination ribosomes for reinitiation on GCN4 and together with eIF3i stimulates linear scanning. *Mol. Cell. Biol.* **30**, 4671–86.

Dennis, M. D., Person, M. D. and Browning, K. S. (2009). Phosphorylation of plant translation initiation factors by CK2 enhances the in vitro interaction of multifactor complex components. *J. Biol. Chem.* **284**, 20615–28.

ElAntak, L., Tzakos, A. G., Locker, N. and Lukavsky, P. J. (2007). Structure of eIF3b RNA recognition motif and its interaction with eIF3j: structural insights into

the recruitment of eIF3b to the 40 S ribosomal subunit. *J. Biol. Chem.* **282**, 8165–74.

Elantak, L., Wagner, S., Herrmannová, A., Karásková, M., Rutkai, E., Lukavsky, P. J. and Valásek, L. (2010). The indispensable N-terminal half of eIF3j/HCR1 cooperates with its structurally conserved binding partner eIF3b/PRT1-RRM and with eIF1A in stringent AUG selection. *J. Mol. Biol.* **396**, 1097–116.

Erickson, F. L. and Hannig, E. M. (1996). Ligand interactions with eukaryotic translation initiation factor 2: role of the g-subunit. *EMBO J.* **15**, 6311–6320.

Fekete, C. A., Mitchell, S. F., Cherkasova, V. A., Applefield, D., Algire, M. A., Maag, D., Saini, A. K., Lorsch, J. R. and Hinnebusch, A. G. (2007). N- and C-terminal residues of eIF1A have opposing effects on the fidelity of start codon selection. *EMBO J.* **26**, 1602–14.

Greenberg, J. R., Phan, L., Gu, Z., DeSilva, A., Apolito, C., Sherman, F., Hinnebusch, A. G. and Goldfarb, D. S. (1998). Nip1p associates with 40S ribosomes and the Prt1p subunit of eIF3 and is required for efficient translation initiation. *J Biol Chem* **273**, 23485–23494.

Gu, Z., Moerschell, R. P., Sherman, F. and Goldfarb, D. S. (1992). NIP1, a gene required for nuclear transport in yeast. *Proc Natl Acad Sci USA* **89**, 10355–10359.

Hanachi, P., Hershey, J. W. B. and Vornlocher, H. P. (1999). Characterization of the p33 subunit of eukaryotic translation initiation factor-3 from Saccharomyces cerevisiae. *J Biol Chem* **274**, 8546–8553.

Herrmannová, A., Daujotyte, D., Yang, J.-C., Cuchalová, L., Gorrec, F., Wagner, S., Dányi, I., Lukavsky, P. J. and Shivaya Valásek, L. (2011). Structural analysis of an eIF3 subcomplex reveals conserved interactions required for a stable and proper translation pre-initiation complex assembly. *Nucleic Acids Res.*

Hinnebusch, A. G. (2005). Translational regulation of GCN4 and the general amino acid control of yeast. *Annu. Rev. Microbiol.* **59**, 407–50.

Hinnebusch, A. G. and Lorsch, J. R. (2012). The mechanism of eukaryotic translation initiation: new insights and challenges. *Cold Spring Harb. Perspect. Biol.* **4**,.

Hinnebusch, A. G., Dever, T. E. and Asano, K. A. (2007). Mechanism of translation initiation in the yeast Saccharomyces cerevisiae. In *Translational Control in biology and medicine* (ed. Sonenberg, N., Mathews, M., and Hershey, J. W. B.), pp. 225–268. Cold Spring Harbor, NY.: Cold Spring Harbor Laboratory Press.

Hofmann, K. and Bucher, P. (1998). The PCI domain: a common theme in three multi-protein complexes. *Trends Biochem. Sci.* **23**, 204–205.

Cheung, Y.-N., Maag, D., Mitchell, S. F., Fekete, C. A., Algire, M. A., Takacs, J. E., Shirokikh, N., Pestova, T., Lorsch, J. R. and Hinnebusch, A. G. (2007).

Dissociation of eIF1 from the 40S ribosomal subunit is a key step in start codon selection in vivo. *Genes Dev.* **21**, 1217–30.

Chiu, W.-L., Wagner, S., Herrmannová, A., Burela, L., Zhang, F., Saini, A. K., Valásek, L. and Hinnebusch, A. G. (2010). The C-terminal region of eukaryotic translation initiation factor 3a (eIF3a) promotes mRNA recruitment, scanning, and, together with eIF3j and the eIF3b RNA recognition motif, selection of AUG start codons. *Mol. Cell. Biol.* **30**, 4415–34.

Iost, I., Dreyfus, M. and Linder, P. (1999). Ded1p, a DEAD-box protein required for translation initiation in Saccharomyces cerevisiae, is an RNA helicase. *J Biol Chem* **274**, 17677–17683.

Jivotovskaya, A., Valášek, L., Hinnebusch, A. G. and Nielsen, K. H. (2006). Eukaryotic translation initiation factor 3 (eIF3) and eIF2 can promote mRNA binding to 40S subunits independently of eIF4G in yeast. *Mol Cell Biol* **26**, 1355–1372.

Kapp, L. D. and Lorsch, J. R. (2004). GTP-dependent recognition of the methionine moiety on initiator tRNA by translation factor eIF2. *J. Mol. Biol.* **335**, 923–36.

Karásková, M., Gunišová, S., Herrmannová, A., Wagner, S., Munzarová, V., Valášek, L. S., Gunisová, S. and Valásek, L. S. (2012). Functional Characterization of the Role of the N-terminal Domain of the c/Nip1 Subunit of Eukaryotic Initiation Factor 3 (eIF3) in AUG Recognition. *J. Biol. Chem.* **287**, 28420–34.

Keierleber, C., Wittekind, M., Qin, S. L. and McLaughlin, C. S. (1986). Isolation and characterization of PRT1, a gene required for the initiation of protein biosynthesis in Saccharomyces cerevisiae. *Mol. Cell. Biol.* **6**, 4419–24.

Khoshnevis, S., Neumann, P. and Ficner, R. (2010a). Crystal structure of the RNA recognition motif of yeast translation initiation factor eIF3b reveals differences to human eIF3b. *PLoS One* **5**,.

Khoshnevis, S., Gross, T., Rotte, C., Baierlein, C., Ficner, R. and Krebber, H. (2010b). The iron-sulphur protein RNase L inhibitor functions in translation termination. *EMBO Rep.* **11**, 214–9.

Khoshnevis, S., Hauer, F., Milón, P., Stark, H. and Ficner, R. (2012). Novel insights into the architecture and protein interaction network of yeast eIF3. *RNA* **18**, 2306–19.

Kouba, T., Dányi, I., Gunišová, S., Munzarová, V., Vlčková, V., Cuchalová, L., Neueder, A., Milkereit, P. and Valášek, L. S. (2012a). Small Ribosomal Protein RPS0 Stimulates Translation Initiation by Mediating 40S-Binding of eIF3 via Its Direct Contact with the eIF3a/TIF32 Subunit. *PLoS One* **7**, e40464.

Kouba, T., Rutkai, E., Karásková, M. and Valášek, L. S. (2012b). The eIF3c/NIP1 PCI domain interacts with RNA and RACK1/ASC1 and promotes assembly of translation preinitiation complexes. *Nucleic Acids Res.* **40**, 2683–99.

Kovarik, P., Hašek, J., Valášek, L. and Ruis, H. (1998). RPG1: an essential gene of saccharomyces cerevisiae encoding a 110-kDa protein required for passage through the G1 phase. *Curr Genet* **33**, 100–109.

Kozak, M. (1978). How do eucaryotic ribosomes select initiation regions in messenger RNA? *Cell* **15**, 1109–1123.

Kozak, M. (1986). Point mutations define a sequence flanking the AUG initiator codon that modulates translation by eukaryotic ribosomes. *Cell* **44**, 283–292.

Kozak, M. (2005). Regulation of translation via mRNA structure in prokaryotes and eukaryotes. *Gene* **361**, 13–37.

Lomakin, I. B. and Steitz, T. A. (2013). The initiation of mammalian protein synthesis and mRNA scanning mechanism. *Nature* **500**, 307–11.

Lorsch, J. R. and Dever, T. E. (2010). Molecular view of 43 S complex formation and start site selection in eukaryotic translation initiation. *J. Biol. Chem.* **285**, 21203–7.

Marintchev, A. and Wagner, G. (2005). Translation initiation: structures, mechanisms and evolution. *Q. Rev. Biophys.* **37**, 197–284.

Mitchell, S. F., Walker, S. E., Algire, M. A., Park, E.-H., Hinnebusch, A. G. and Lorsch, J. R. (2010). The 5'-7-Methylguanosine Cap on Eukaryotic mRNAs Serves Both to Stimulate Canonical Translation Initiation and to Block an Alternative Pathway. *Mol. Cell* **39**, 950–962.

Munzarová, V., Pánek, J., Gunišová, S., Dányi, I., Szamecz, B. and Valášek, L. S. (2011). Translation reinitiation relies on the interaction between eIF3a/TIF32 and progressively folded cis-acting mRNA elements preceding short uORFs. *PLoS Genet.* **7**, e1002137.

Naranda, T., Kainuma, M., McMillan, S. E. and Hershey, J. W. B. (1997). The 39-kilodalton subunit of eukaryotic translation initiation factor 3 is essential for the complex's integrity and for cell viability in Saccharomyces cerevisiae. *Mol Cell Biol* **17**, 145–153.

Nielsen, K. H., Szamecz, B., Valasek A., L. J., Shin, B. S. and Hinnebusch, A. G. (2004). Functions of eIF3 downstream of 48S assembly impact AUG recognition and GCN4 translational control. *EMBO J.* **23**, 1166–1177.

Nielsen, K. H., Valášek, L., Sykes, C., Jivotovskaya, A. and Hinnebusch, A. G. (2006). Interaction of the RNP1 motif in PRT1 with HCR1 promotes 40S binding of eukaryotic initiation factor 3 in yeast. *Mol Cell Biol* **26**, 2984–2998.

Park, H. S., Himmelbach, A., Browning, K. S., Hohn, T. and Ryabova, L. A. (2001). A plant viral "reinitiation" factor interacts with the host translational machinery. *Cell* **106**, 723–33.

Passmore, L. A., Schmeing, T. M., Maag, D., Applefield, D. J., Acker, M. G., Algire, M. A., Lorsch, J. R. and Ramakrishnan, V. (2007). The eukaryotic translation initiation factors eIF1 and eIF1A induce an open conformation of the 40S ribosome. *Mol. Cell* **26**, 41–50.

Pavitt, G. D., Ramaiah, K. V. A., Kimball, S. R. and Hinnebusch, A. G. (1998). eIF2 independently binds two distinct eIF2B subcomplexes that catalyze and regulate guanine-nucleotide exchange. *Genes Dev.* **12**, 514–526.

Pestova, T. V and Kolupaeva, V. G. (2002). The roles of individual eukaryotic translation initiation factors in ribosomal scanning and initiation codon selection. *Genes Dev.* **16**, 2906–2922.

Pestova, T. V, Lomakin, I. B., Lee, J. H., Choi, S. K., Dever, T. E. and Hellen, C. U. T. (2000). The joining of ribosomal subunits in eukaryotes requires eIF5B. *Nature* **403**, 332–335.

Pestova, T. V, Lorsch, J. R. and Hellen, C. U. T. (2007). The mechanism of translation initiation in eukaryotes. In *Translational Control in biology and medicine* (ed. Sonenberg, N., Mathews, M., and Hershey, J. W. B.), pp. 87–128. Cold Spring Harbor, NY.: Cold Spring Harbor Laboratory Press.

Phan, L., Schoenfeld, L. W., Valásek, L., Nielsen, K. H. and Hinnebusch, a G. (2001). A subcomplex of three eIF3 subunits binds eIF1 and eIF5 and stimulates ribosome binding of mRNA and tRNA(i)Met. *EMBO J.* **20**, 2954–65.

Pick, E., Hofmann, K. and Glickman, M. H. (2009). PCI complexes: Beyond the proteasome, CSN, and eIF3 Troika. *Mol. Cell* **35**, 260–4.

Pisarev, A. V, Hellen, C. U. T. and Pestova, T. V (2007). Recycling of eukaryotic posttermination ribosomal complexes. *Cell* **131**, 286–99.

Pisarev, A. V, Kolupaeva, V. G., Yusupov, M. M., Hellen, C. U. T. and Pestova, T. V (2008). Ribosomal position and contacts of mRNA in eukaryotic translation initiation complexes. *EMBO J.* **27**, 1609–21.

Pisarev, A. V, Skabkin, M. A., Pisareva, V. P., Skabkina, O. V, Rakotondrafara, A. M., Hentze, M. W., Hellen, C. U. T. and Pestova, T. V (2010). The role of ABCE1 in eukaryotic posttermination ribosomal recycling. *Mol. Cell* **37**, 196–210.

Pisareva, V. P., Pisarev, A. V, Komar, A. A., Hellen, C. U. T. and Pestova, T. V (2008). Translation initiation on mammalian mRNAs with structured 5'UTRs requires DExH-box protein DHX29. *Cell* **135**, 1237–50.

Pöyry, T. A. A., Kaminski, A. and Jackson, R. J. (2004). What determines whether mammalian ribosomes resume scanning after translation of a short upstream open reading frame? *Genes Dev.* **18**, 62–75.

Pöyry, T. A. A., Kaminski, A., Connell, E. J., Fraser, C. S. and Jackson, R. J. (2007). The mechanism of an exceptional case of reinitiation after translation of a long ORF reveals why such events do not generally occur in mammalian mRNA translation. *Genes Dev.* **21**, 3149–62.

Querol-Audi, J., Sun, C., Vogan, J. M., Smith, M. D., Gu, Y., Cate, J. H. D. and Nogales, E. (2013). Architecture of Human Translation Initiation Factor 3. *Structure*.

Rabl, J., Leibundgut, M., Ataide, S. F., Haag, A. and Ban, N. (2011). Crystal structure of the eukaryotic 40S ribosomal subunit in complex with initiation factor 1. *Science* **331**, 730–6.

Rogers Jr., G. W., Richter, N. J. and Merrick, W. C. (1999). Biochemical and kinetic characterization of the RNA helicase activity of eukaryotic initiation factor 4A. *J Biol Chem* **274**, 12236–12244.

Saini, A. K., Nanda, J. S., Lorsch, J. R. and Hinnebusch, A. G. (2010). Regulatory elements in eIF1A control the fidelity of start codon selection by modulating tRNA(i)(Met) binding to the ribosome. *Genes Dev.* **24**, 97–110.

Shoemaker, C. J. and Green, R. (2011). Kinetic analysis reveals the ordered coupling of translation termination and ribosome recycling in yeast. *Proc. Natl. Acad. Sci. U. S. A.* **108**, E1392–8.

Singh, C. R., He, H., Ii, M., Yamamoto, Y. and Asano, K. (2004). Efficient incorporation of eukaryotic initiation factor 1 into the multifactor complex is critical for formation of functional ribosomal preinitiation complexes in vivo. *J. Biol. Chem.* **279**, 31910–31920.

Siridechadilok, B., Fraser, C. S., Hall, R. J., Doudna, J. A. and Nogales, E. (2005). Structural roles for human translation factor eIF3 in initiation of protein synthesis. *Science* **310**, 1513–5.

Sokabe, M., Fraser, C. S. and Hershey, J. W. B. (2012). The human translation initiation multi-factor complex promotes methionyl-tRNAi binding to the 40S ribosomal subunit. *Nucleic Acids Res.* **40**, 905–13.

Spahn, C. M., Beckmann, R., Eswar, N., Penczek, P. A., Sali, A., Blobel, G. and Frank, J. (2001). Structure of the 80S ribosome from Saccharomyces cerevisiae--tRNA-ribosome and subunit-subunit interactions. *Cell* **107**, 373–86.

Srivastava, S., Verschoor, A. and Frank, J. (1992). Eukaryotic initiation factor 3 does not prevent association through physical blockage of the ribosomal subunit-subunit interface. *J. Mol. Biol.* **220**, 301–304.

Szamecz, B., Rutkai, E., Cuchalová, L., Munzarová, V., Herrmannová, A., Nielsen, K. H., Burela, L., Hinnebusch, A. G. and Valásek, L. (2008). eIF3a cooperates with sequences 5' of uORF1 to promote resumption of scanning by post-termination ribosomes for reinitiation on GCN4 mRNA. *Genes Dev.* **22**, 2414–25.

Unbehaun, A., Borukhov, S. I., Hellen, C. U. T. and Pestova, T. V (2004). Release of initiation factors from 48S complexes during ribosomal subunit joining and the link between establishment of codon-anticodon base-pairing and hydrolysis of eIF2-bound GTP. *Genes Dev.* **18**, 3078–93.

Valásek, L. S. (2012). "Ribozoomin"--translation initiation from the perspective of the ribosome-bound eukaryotic initiation factors (eIFs). *Curr. Protein Pept. Sci.* **13**, 305–30.

Valásek, L., Hasek, J., Trachsel, H., Imre, E. M. and Ruis, H. (1999). The Saccharomyces cerevisiae HCR1 gene encoding a homologue of the p35 subunit of human translation initiation factor 3 (eIF3) is a high copy suppressor of a temperature-sensitive mutation in the Rpg1p subunit of yeast eIF3. *J. Biol. Chem.* **274**, 27567–72.

Valásek, L., Phan, L., Schoenfeld, L. W., Valásková, V. and Hinnebusch, A. G. (2001a). Related eIF3 subunits TIF32 and HCR1 interact with an RNA recognition motif in PRT1 required for eIF3 integrity and ribosome binding. *EMBO J.* **20**, 891–904.

Valásek, L., Hasek, J., Nielsen, K. H. and Hinnebusch, A. G. (2001b). Dual function of eIF3j/Hcr1p in processing 20 S pre-rRNA and translation initiation. *J. Biol. Chem.* **276**, 43351–60.

Valášek, L., Trachsel, H., Hašek, J. and Ruis, H. (1998). Rpg1, the Saccharomyces cerevisiae homologue of the largest subunit of mammlian translation initiation factor 3, is required for translational activity. *J. Biol. Chem.* **273**, 21253–21260.

Valášek, L., Nielsen, K. H. and Hinnebusch, A. G. (2002). Direct eIF2-eIF3 contact in the multifactor complex is important for translation initiation in vivo. *EMBO J.* **21**, 5886–5898.

Valášek, L., Mathew, A., Shin, B. S., Nielsen, K. H., Szamecz, B. and Hinnebusch, A. G. (2003). The yeast eIF3 subunits TIF32/a, NIP1/c, and eIF5 make critical connections with the 40S ribosome in vivo. *Genes Dev.* **17**, 786–799.

Valášek, L., Nielsen, K. H., Zhang, F., Fekete, C. A. and Hinnebusch, A. G. (2004). Interactions of Eukaryotic Translation Initiation Factor 3 (eIF3) Subunit NIP1/c with eIF1 and eIF5 Promote Preinitiation Complex Assembly and Regulate Start Codon Selection. *Mol. Cell. Biol.* **24**, 9437–9455.

Van der Velden, A. W. and Thomas, A. A. M. (1999). The role of the 5' untranslated region of an mRNA in translation regulation during development. *Int. J. Biochem. Cell Biol.* **31**, 87–106.

Verlhac, M.-H., Chen, R.-H., Hanachi, P., Hershey, J. W. B. and Derynck, R. (1997). Identification of partners of TIF34, a component of the yeast eIF3 complex, required for cell proliferation and translation initiation. *EMBO J.* **16**, 6812–6822.

Walker, S. E., Zhou, F., Mitchell, S. F., Larson, V. S., Valasek, L., Hinnebusch, A. G. and Lorsch, J. R. (2013). Yeast eIF4B binds to the head of the 40S ribosomal subunit and promotes mRNA recruitment through its N-terminal and internal repeat domains. *RNA* **19**, 191–207.

Weisser, M., Voigts-Hoffmann, F., Rabl, J., Leibundgut, M. and Ban, N. (2013). The crystal structure of the eukaryotic 40S ribosomal subunit in complex with eIF1 and eIF1A. *Nat. Struct. Mol. Biol.* **20**, 1015–7.

Yamamoto, Y., Singh, C. R., Marintchev, A., Hall, N. S., Hannig, E. M., Wagner, G. and Asano, K. (2005). The eukaryotic initiation factor (eIF) 5 HEAT domain mediates multifactor assembly and scanning with distinct interfaces to eIF1, eIF2, eIF3, and eIF4G. *Proc. Natl. Acad. Sci. U. S. A.* **102**, 16164–9.

Yu, Y., Marintchev, A., Kolupaeva, V. G., Unbehaun, A., Veryasova, T., Lai, S.-C., Hong, P., Wagner, G., Hellen, C. U. T. and Pestova, T. V (2009). Position of eukaryotic translation initiation factor eIF1A on the 40S ribosomal subunit mapped by directed hydroxyl radical probing. *Nucleic Acids Res.* **37**, 5167–82.

Zhou, M., Sandercock, A. M., Fraser, C. S., Ridlova, G., Stephens, E., Schenauer, M. R., Yokoi-Fong, T., Barsky, D., Leary, J. A., Hershey, J. W., et al. (2008). Mass spectrometry reveals modularity and a complete subunit interaction map of the eukaryotic translation factor eIF3. *Proc. Natl. Acad. Sci. U. S. A.* **105**, 18139–44.